

University of Nebraska - Lincoln

DigitalCommons@University of Nebraska - Lincoln

---

Engineering Mechanics Dissertations & Theses

Mechanical & Materials Engineering, Department  
of

12-2018

# Evaluation of Deformable Posts in the ZOI and Rigid Posts in Stiff Soil

Thomas Ammon

University of Nebraska - Lincoln, tammon3@gmail.com

Follow this and additional works at: <http://digitalcommons.unl.edu/engmechdiss>



Part of the [Applied Mechanics Commons](#), and the [Structural Engineering Commons](#)

---

Ammon, Thomas, "Evaluation of Deformable Posts in the ZOI and Rigid Posts in Stiff Soil" (2018). *Engineering Mechanics Dissertations & Theses*. 46.

<http://digitalcommons.unl.edu/engmechdiss/46>

This Article is brought to you for free and open access by the Mechanical & Materials Engineering, Department of at DigitalCommons@University of Nebraska - Lincoln. It has been accepted for inclusion in Engineering Mechanics Dissertations & Theses by an authorized administrator of DigitalCommons@University of Nebraska - Lincoln.

EVALUATION OF DEFORMABLE POSTS IN THE ZOI AND RIGID POSTS IN  
STIFF SOIL

by

Thomas J. Ammon

A THESIS

Presented to the Faculty of  
The Graduate College at the University of Nebraska  
In Partial Fulfillment of Requirements  
For the Degree of Master of Science

Major: Mechanical Engineering and Applied Mechanics

Under the Supervision of Professor Cody Stolle

Lincoln, Nebraska

December, 2018

# EVALUATION OF DEFORMABLE POSTS IN THE ZOI AND RIGID POSTS IN STIFF SOIL

Thomas J. Ammon, M.S.

University of Nebraska, 2018

Advisor: Cody Stolle

Debris fences are commonly used by states, in conjunction with a concrete parapet, to protect railway tracks. Their use limits the intrusion of debris that could damage tracks or clutter rail lines. Due to a lack of previously crash-tested systems, the safety performance of such designs are largely unknown. The Iowa Department of Transportation (DOT) desired that researchers at the Midwest Roadside Safety Facility (MwRSF) design a crashworthy debris fence mounted on top of a concrete parapet to meet the *Manual for Assessing Safety Hardware* (MASH) TL-3 crash test conditions. Part I of this thesis details the literature review and design of a crashworthy debris fence.

Part II of this thesis details the results and analysis of 17 bogie tests that were conducted in support of the development of a non-proprietary barrier. These dynamic tests were conducted to evaluate the effectiveness of the modified Midwest Guardrail System (MGS) in both strong and weak soils. The bogie tests were conducted using steel tubes with varying cross-section geometries, embedment depths, and two different soil types. These parameters were investigated to evaluate their importance on the overall post-soil interaction forces.

## **ACKNOWLEDGEMENTS**

I would first like to thank my advisor Dr. Cody Stolle and the Midwest Roadside Safety Facility (MwRSF) for allowing me to continue my education. The knowledge and experienced I have gained at MwRSF have been a blessing, and I will forever be grateful.

Next, I want to thank both of my parents for instilling a work ethic in me from a young age that has allowed me to be successful in the classroom and during working hours.

I would like to extend a thank you to the graduate students and full-time staff at MwRSF, including test site personnel for conducting the live bogie tests. I really enjoyed working with everyone as both an undergraduate and graduate student.

Finally, I would like to thank the Department of State and Iowa Department of Transportation for funding the work that I have completed.

## TABLE OF CONTENTS

ACKNOWLEDGEMENTS .....	iii
TABLE OF CONTENTS.....	iv
LIST OF FIGURES .....	viii
LIST OF TABLES .....	xiii
1 INTRODUCTION .....	1
PART I.....	1
2 INTRODUCTION – DEBRIS FENCE .....	1
2.1 Background and Problem Statement.....	1
2.2 Research Objectives.....	2
3 DEBRIS FENCE LITERATURE REVIEW .....	4
3.1 State Designs.....	4
3.1.1 California .....	7
3.1.2 Delaware .....	10
3.1.3 Florida .....	14
3.1.4 Idaho .....	18
3.1.5 Indiana.....	20
3.1.6 Iowa.....	22
3.1.7 Kansas .....	24
3.1.8 Maryland .....	27
3.1.9 Minnesota.....	32
3.1.10 Nebraska .....	35
3.1.11 New Jersey.....	39
3.1.12 New York.....	41
3.1.13 Oregon.....	43
3.1.14 Texas .....	46
3.1.15 Wisconsin.....	49
3.2 Full-Scale Crash Test (TTI Test No. 42070-6).....	51
3.2.1 System and Testing Details.....	51
3.2.2 Test Results .....	56
3.3 Minnesota Combination Traffic-Bicycle Bridge Rail.....	59
3.4 Caltrans Barrier Mounted Sign and Signpost .....	63
3.5 Real-World Crashes .....	65
3.5.1 Ohio Vandal Protection Fence Crash.....	65
3.5.2 NASS Crash Data .....	66
3.6 Zone of Intrusion.....	69
3.6.1 Guidelines for Attachments to Bridge Rails and Median Barriers ..	69
3.6.2 Zone of Intrusion Study .....	71
3.6.4 Signs on Concrete Median Barriers .....	72

	v
3.7 Lincoln Nebraska Fence Examples.....	73
3.7.1 Aesthetic Debris Fence .....	73
3.7.2 Combination Rail and Pedestrian Fence .....	80
3.8 Design Standards .....	81
3.8.1 Iowa Chain-Link Fence Standards.....	81
3.8.2 Union Pacific and BNSF Standards.....	84
<b>4 DESIGN AND ANALYSIS – DEBRIS FENCE.....</b>	<b>85</b>
4.1 Overview.....	85
4.2 Debris Fence Design Objectives.....	85
4.3 Parapet Selection.....	87
4.4 Loading Conditions.....	91
4.4.1 Lateral Impact Loading.....	92
4.4.2 Longitudinal Impact Loading .....	95
4.4.3 Front Wind Loading.....	98
4.4.4 Back Wind loading .....	102
4.4.5 Dead Load.....	105
4.5 Post Selection Based on Wind Load.....	106
4.5.1 Iowa Wind Spacing and Sizing Requirements.....	107
4.5.2 Selection of Parameters and Pipe Sizing .....	108
4.6 Minimum Design for Wind Loading .....	110
4.6.1 Dynamic Pressure .....	110
4.6.2 Projected Area.....	111
4.6.3 Drag Coefficient.....	111
4.6.4 Maximum Wind Loading.....	113
4.7 Design of Members for Flexure.....	114
4.8 Design of Members for Shear.....	115
4.9 Verification of Design for Wind Loading.....	116
4.9.1 Front Wind Loading.....	116
4.9.2 Back Wind Loading .....	118
4.10 Estimation of Impact Force to Yield Posts .....	119
<b>5 ADDITIONAL PRELIMINARY DEBRIS FENCE COMPONENT DESIGNS.....</b>	<b>122</b>
5.1 Overview.....	122
5.2 Longitudinal Stiffeners .....	122
5.3 Clamp Spacing and Design.....	125
<b>Part I.....</b>	<b>126</b>
<b>6 SUMMARY CONCLUSIONS AND RECOMMENDATIONS .....</b>	<b>126</b>
<b>PART II.....</b>	<b>128</b>
<b>7 INTRODUCTION – POST SOIL INTERACTION FORCES.....</b>	<b>128</b>
7.1 Background.....	128
7.2 Research Objectives.....	128

	vi
7.3 Scope.....	129
7.4 Equipment and Instrumentation.....	138
7.4.1 Bogie Vehicles.....	138
7.4.2 Test Vehicle.....	139
7.4.3 Accelerometers.....	140
7.4.4 Retroreflective Optic Speed Trap.....	140
7.4.5 Digital Photography.....	141
7.5 End of Test Determination.....	141
7.6 Data Processing.....	142
8 EFFECT OF PARAMETER VARIATION ON POST-SOIL FORCES.....	143
8.1 Introduction and Motivation.....	143
8.2 Post Width.....	143
8.2.1 48-in. Embedment in Weak Soil.....	143
8.2.2 72-in. Embedment in Weak Soil.....	146
8.2.3 96-in. Embedment in Weak Soil.....	148
8.2.4 48-in. Embedment in Strong Soil.....	150
8.2.5 72-in. Embedment in Strong Soil.....	152
8.2.6 Post Width Discussion.....	154
8.3 Embedment Depth.....	156
8.3.1 4-in. Width in Weak Soil.....	156
8.3.2 6-in. Width in Weak Soil.....	162
8.3.3 8-in. Width in Weak Soil.....	166
8.3.4 6-in. Width in Strong Soil.....	170
8.3.5 8-in. Width in a Strong Soil.....	172
8.3.6 Embedment Depth Discussion.....	174
8.4 Soil Type.....	176
8.4.1 6-in. Width in a 48-in Embedment.....	176
8.4.1 6-in. Width in a 72-in. Embedment.....	179
8.4.2 8-in. Width in a 48-in. Embedment.....	181
8.4.3 8-in. Width in a 72-in. Embedment.....	183
8.4.4 Soil Discussion.....	185
8.5 Dimensionless Number Study.....	186
8.5.1 Purpose and Motivation.....	186
8.5.2 Buckingham Pi Theorem.....	186
8.5.3 Derivation of Dimensionless Groups.....	188
8.5.4 Dimensionless Graph.....	190
9 SUMMARY, CONCLUSIONS, AND RECOMMENDATIONS.....	193
10 REFERENCES.....	196
11 APPENDICES.....	199
Appendix A. Lateral Impact.....	200
Appendix B. <a href="#">Longitudinal Impact</a> .....	205
Appendix C. Front Wind Loading.....	210

	vii
Appendix D. Back Wind Loading.....	216
Appendix E. Dead Load .....	222
Appendix F. Chain Link Area Determination.....	225
Appendix G. Material Specifications .....	228
Appendix H. Bogie Test Results .....	241
Appendix I. Filtering Study.....	276
11.1 Background.....	277
11.2 Research Objectives.....	277
11.3 Scope.....	277
11.4 Methods.....	278
11.5 Square Wave Pulses.....	278
11.5.1 Square Wave Discussion.....	283
11.6 Sawtooth Wave Pulse .....	283
11.6.1 Sawtooth Wave Discussion.....	289
11.7 Triangle Wave Pulses .....	289
11.8 Triangle Wave Discussion .....	295



## LIST OF FIGURES

Figure 1. California Concrete Barrier [2] .....	8
Figure 2. Chain Link Railing [2].....	9
Figure 3. Delaware Bridge Safety Fence, Type 1 [3] .....	11
Figure 4. Delaware Bridge Safety Fence, Connection Details [3].....	12
Figure 5. Delaware Bridge Safety Fence, Type 2 [3] .....	13
Figure 6. Florida Bridge Fencing Over Railroad, Sheet 1 [4] .....	15
Figure 7. Florida Bridge Fencing Over Railroad, Sheet 2 [4] .....	16
Figure 8. Florida Bridge Fencing Over Railroad, Sheet 3 [4] .....	17
Figure 9. Idaho Protective Fence for Combination Rail and Parapet [5].....	19
Figure 10. Indiana Bridge Railing Pedestrian Fence [6].....	21
Figure 11. Iowa Protection Fence Design [7] .....	23
Figure 12. Kansas Railroad Protective Fence for Shoulders Less than 6 ft [8] .....	25
Figure 13. Kansas Railroad Protective Fence for Shoulders Greater than 6 ft [8] .....	26
Figure 14. Maryland Type I Chain Link Safety Fence [9] .....	28
Figure 15. Maryland Type I Chain Link Safety Fence [9] .....	29
Figure 16. Maryland Type II Chain Link Safety Fence [9] .....	30
Figure 17. Maryland Type II Chain Link Safety Fence [9] .....	31
Figure 18. Minnesota Concrete Parapet Type P-1 [10] .....	33
Figure 20. Nebraska Closed Concrete Rail Bridge Deck [11].....	36
Figure 21. Nebraska Railroad Protection Fence Details [11] .....	37
Figure 22. Nebraska Fence Details with an Alternate Post Attachment [11] .....	38
Figure 23. New Jersey Curved Chain Link Fence [12] .....	40
Figure 24. New York Pedestrian Fencing on Concrete Barrier and Parapet [13].....	42
Figure 29. Wisconsin Chain Link Fence Details [16].....	50
Figure 30. Vandal Protection Fence Details [17].....	53
Figure 31. Pretest Parapet and Fence Details [17].....	54
Figure 32. Pretest Fence and Connection Details [17] .....	55
Figure 33. Post-test Fence Damage [17].....	57
Figure 34. Summary of Test Results [17].....	58
Figure 35. Minnesota Combination Traffic-Bicycle Bridge Rail Design Details ....	60
Figure 36. Minnesota Combination Traffic-Bicycle Bridge Rail Design Details ....	61
Figure 37. Tension Cable Taper and Rail Design.....	62
Figure 38. Barrier Mounted Sign Test Article .....	64
Figure 39. Barrier Mounted Sign Vehicle Impact .....	64
Figure 40. Valley View Vandal Protection Fence Crash [21] .....	66
Figure 41. View of Barrier at Point of Impact [22] .....	67
Figure 42. Vehicle Damage [22].....	67
Figure 43. Point of Impact [23].....	68
Figure 44. Vehicle Damage [23].....	69
Figure 45. Aesthetic Debris Fence Bridge Rail Details .....	75
Figure 46. Aesthetic Debris Fence Bridge Parapet and Placement Details .....	76
Figure 47. Aesthetic Debris Fence Details .....	77
Figure 48. Aesthetic Debris Fence Overview .....	78

Figure 49. Aesthetic Design Missing Panels .....	78
Figure 50. Aesthetic Design Missing Panel .....	79
Figure 51. Aesthetic Design Broken Screws .....	79
Figure 52. Lincoln Pedestrian Fence .....	80
Figure 53. TL-4 Bridge Rail .....	89
Figure 54. TL-4 Bridge Rail Rebar Placement .....	90
Figure 55. Comparison of TL-4 Barriers .....	91
Figure 56. Lateral Impact Loading Configuration .....	93
Figure 57. Shear and Moment Diagrams for Lateral Impact .....	95
Figure 58 Longitudinal Impact Loading Configuration.....	96
Figure 59. Shear and Moment Diagrams for Longitudinal Impact.....	98
Figure 60. Front Wind Loading Configuration.....	99
Figure 61. Simplified Loading Configuration .....	100
Figure 62 Back Wind Loading Configuration .....	102
Figure 63. Simplified Back Wind Loading.....	103
Figure 64. Dead Load Configuration .....	105
Figure 65. Drag Coefficient vs Reynolds Number for Cylinders [33] .....	112
Figure 66. Front Wind Loading Simplified Configuration.....	117
Figure 67. Back Wind Loading Simplified Configuration .....	118
Figure 68. Lateral Impact Loading Configuration.....	120
Figure 69. Potential Top Rail Isometric Back View.....	124
Figure 70. Potential Top Rail Side View .....	124
Figure 71. Potential Saddle Clamp Design.....	125
Figure 72. Test Matrix, Test Nos. P3G-1 through P3G-23.....	131
Figure 73. Test and Bogie Layout.....	132
Figure 74. Post a1-a3 Details, Test Nos. P3G-1 through P3G-23 .....	133
Figure 75. Post a4-a6 Details, Test Nos. P3G-1 through P3G-23 .....	134
Figure 76. Post a7-a10 Details, Test Nos. P3G-1 through P3G-23 .....	135
Figure 77. Post b1-b3 Details, Test Nos. P3G-1 through P3G-23.....	136
Figure 78. Post b4-b7 Details, Test Nos. P3G-1 through P3G-23.....	137
Figure 79. Rigid-Frame Bogie No. 3 and Guidance Track.....	139
Figure 80. Rigid-Frame Bogie No. 2 and Guidance Track.....	139
Figure 81. Force vs. Displacement for P3G-1 and P3G-2 .....	145
Figure 82. Energy vs. Displacement for P3G-1 and P3G-2.....	145
Figure 83. Force vs. Displacement for P3G-3 and P3G-4 .....	147
Figure 84. Energy vs. Displacement for P3G-3 and P3G-4.....	147
Figure 85. Force vs. Displacement for P3G-5 and P3G-6.....	149
Figure 86. Energy vs. Displacement for P3G-5 and P3G-6.....	149
Figure 87. Force vs. Displacement for P3G-7 and the average of P3G-8 and P3G-17 .....	151
Figure 88. Energy vs. Displacement for P3G-and the average of P3G-8 and P3G-17 .....	151
Figure 89. Force vs. Displacement for P3G-18 and P3G-19 .....	153
Figure 90. Energy vs. Displacement for P3G-18 and P3G-19.....	153
Figure 91. Force vs. Displacement for P3G-13, P3G-14, P3G-22 and P3G-15 .....	160

Figure 92. Energy vs. Displacement for P3G-13, P3G-14, P3G-22, and P3G-15..	160
Figure 93. Force vs. Displacement for P3G-1, P3G-3 and P3G-5.....	165
Figure 94. Energy vs. Displacement for P3G-1, P3G-3, and P3G-5 .....	165
Figure 95. Force vs. Displacement for P3G-2, P3G-4 and P3G-6.....	169
Figure 96. Energy vs. Displacement for P3G-2, P3G-4 and P3G-6 .....	169
Figure 97. Force vs. Displacement for P3G-7 and P3G-18 .....	171
Figure 98. Energy vs. Displacement for P3G-7 and P3G-18.....	171
Figure 99. Force vs. Displacement for the average of P3G-8 and P3G-17 .....	173
Figure 100. Energy vs. Displacement for the Average of P3G-8 and P3G- and P3G- 19.....	173
Figure 101. Average Forces at 15 in. of Deflection vs. Embedment Depth .....	175
Figure 102. Force vs. Displacement for P3G-1 and P3G-7 .....	178
Figure 103. Energy vs. Displacement for P3G-1 and P3G-7.....	178
Figure 104. Force vs. Displacement for P3G-3 and P3G-18 .....	180
Figure 105. Energy vs. Displacement for P3G-3 and P3G-18.....	180
Figure 106. Force vs. Displacement for P3G-2 and the average of P3G-8 and P3G- 17.....	182
Figure 107. Energy vs. Displacement for P3G-2 and the average of P3G-8 and P3G- 17.....	182
Figure 108. Force vs. Displacement for P3G-2 and the average of P3G-8 and P3G- 17.....	184
Figure 109. Energy vs. Displacement for P3G-2 and the average of P3G-8 and P3G- 17.....	184
Figure 110. Dimensionless Diagram (Weak Soil) .....	191
Figure A-1. Lateral Impact Loading Configuration.....	201
Figure A-2. Lateral Impact Shear and Moment Diagrams .....	204
Figure B-1. Longitudinal Impact Loading Configuration.....	206
Figure B-2. Longitudinal Impact Shear and Moment Diagrams .....	209
Figure C-1. Front Wind Loading .....	211
Figure C-2. Front Wind Loading – Simplified Model.....	212
Figure C-3. Simplified Front Wind Loading Shear and Moment Diagrams .....	215
Figure D-1. Back Wind Loading .....	217
Figure D-2. Back Wind Loading – Simplified Model .....	218
Figure D-3. Simplified Back Wind Loading Shear and Moment Diagrams.....	221
Figure E-1. Dead Load Configuration .....	223
Figure F-1. Chain-Link Representation .....	226
Figure G-1. 8-in. Square x $\frac{3}{16}$ -in. Steel Tubes, Test Nos. P3G-1 Through P3G-16 .....	231
Figure G-2. 8-in. x 6-in. x $\frac{3}{16}$ -in. Steel Tube, Test Nos. P3G-1 Through P3G-23	232
Figure G-3. 8-in. x 6-in. x $\frac{3}{16}$ -in. Tubes, Test Nos. P3G-1 through P3G-23 .....	233
Figure G-4. 8-in. x 4-in. x $\frac{3}{16}$ -in. Steel Tubes, Test Nos. P3G-1 through P3G-16	234
Figure G-5. 8-in. Square x $\frac{3}{16}$ -in. Tubes, Test Nos. P3G-1 through P3G-16 .....	235
Figure G-6. Sand, Test Nos. P3G-1 through P3G-23 .....	236
Figure G-7. Sand, Test Nos. P3G-1 through P3G-23 .....	237
Figure G-8. 8-in. x 4-in. x $\frac{3}{8}$ -in. Tube, Test Nos P3G-17 through P3G-23.....	238

Figure G-9. 8-in. x 6-in. x $\frac{3}{8}$ -in. Tube, Test Nos. P3G-17 through P3G-23.....	239
Figure G-10. 8-in. x 8-in. x $\frac{3}{8}$ -in. Tube, Test Nos. P3G-17 through P3G-23.....	240
Figure H-1. Test No. P3G-1 Results (SLICE-1).....	242
Figure H-2. Test No. P3G-1 Results (SLICE-2).....	243
Figure H-3. Test No. P3G-2 Results (SLICE-1).....	244
Figure H-4. Test No. P3G-2 Results (SLICE-2).....	245
Figure H-5. Test No. P3G-3 Results (SLICE-1).....	246
Figure H-6. Test No. P3G-3 Results (SLICE-2).....	247
Figure H-7. Test No. P3G-4 Results (SLICE-1).....	248
Figure H-8. Test No. P3G-4 Results (SLICE-2).....	249
Figure H-9. Test No. P3G-5 Results (SLICE-1).....	250
Figure H-10. Test No. P3G-5 Results (SLICE-2).....	251
Figure H-11. Test No. P3G-6 Results (SLICE-1).....	252
Figure H-12. Test No. P3G-6 Results (SLICE-2).....	253
Figure H-13. Test No. P3G-7 Results (SLICE-1).....	254
Figure H-14. Test No. P3G-7 Results (SLICE-2).....	255
Figure H-15. Test No. P3G-8 Results (SLICE-1).....	256
Figure H-16. Test No. P3G-8 Results (SLICE-2).....	257
Figure H-17. Test No. P3G-13 Results (SLICE-1).....	258
Figure H-18. Test No. P3G-13 Results (SLICE-2).....	259
Figure H-19. Test No. P3G-14 Results (SLICE-1).....	260
Figure H-20. Test No. P3G-14 Results (SLICE-2).....	261
Figure H-21. Test No. P3G-15 Results (SLICE-1).....	262
Figure H-22. Test No. P3G-15 Results (SLICE-2).....	263
Figure H-23. Test No. P3G-16 Results (SLICE-1).....	264
Figure H-24. Test No. P3G-16 Results (SLICE-2).....	265
Figure H-25. Test No. P3G-17 Results (SLICE-1).....	266
Figure H-26. Test No. P3G-17 Results (SLICE-2).....	267
Figure H-27. Test No. P3G-18 Results (SLICE-1).....	268
Figure H-28. Test No. P3G-18 Results (SLICE-2).....	269
Figure H-29. Test No. P3G-19 Results (SLICE-1).....	270
Figure H-30. Test No. P3G-19 Results (SLICE-2).....	271
Figure H-31. Test No. P3G-22 Results (SLICE-1).....	272
Figure H-32. Test No. P3G-22 Results (SLICE-2).....	273
Figure H-33. Test No. P3G-23 Results (SLICE-1).....	274
Figure H-34. Test No. P3G-23 Results (SLICE-2).....	275
Figure I-1. 50 ms. Square Wave Pulse.....	279
Figure I-2. . 25 ms. Square Wave Pulse.....	279
Figure I-3. 15 ms. Square Wave Pulse.....	280
Figure I-4. 10 ms. Square Wave Pulse.....	280
Figure I-5. 7.5 ms. Square Wave Pulse.....	281
Figure I-6. 5 ms. Square Wave Pulse.....	281
Figure I-7. 2.5 ms. Square Wave Pulse.....	282
Figure I-8. 1 ms. Square Wave Pulse.....	282
Figure I-9. 50 ms. Sawtooth Wave Pulse.....	285

Figure I-10. 25 ms. Sawtooth Wave Pulse.....	285
Figure I-11. 15 ms. Sawtooth Wave Pulse.....	286
Figure I-12. 10 ms. Sawtooth Wave Pulse.....	286
Figure I-13. 7.5 ms. Sawtooth Wave Pulse.....	287
Figure I-14. 5 ms. Sawtooth Wave Pulse.....	287
Figure I-15. 2.5 ms. Sawtooth Wave Pulse.....	288
Figure I-16. 1 ms. Sawtooth Wave Pulse.....	288
Figure I-17. 50 ms. Triangle Wave Pulse .....	291
Figure I-18. 25 Triangle Wave Pulse .....	291
Figure I-19. 15 ms. Triangle Wave Pulse .....	292
Figure I-20. 10 ms. Triangle Wave Pulse .....	292
Figure I-21. 7.5 ms. Triangle Wave Pulse .....	293
Figure I-22. 5 ms. Triangle Wave Pulse .....	293
Figure I-23. 2.5 ms. Triangle Wave Pulse .....	294
Figure I-24. 1 ms Triangle Wave Pulse .....	294

## LIST OF TABLES

Table 1. State Standards – Fence Details.....	5
Table 2. State Fence Designs by Percent.....	6
Table 3. State Parapet Attachment Methods by Percent.....	6
Table 4. ZOI Values [24].....	71
Table 5. Lateral Impact Loading Variables.....	93
Table 6. Longitudinal Impact Loading Variables.....	96
Table 7. Front Wind Loading Variables.....	100
Table 8. Back Wind Loading Variables.....	103
Table 9. Variable Definitions.....	106
Table 10. ‘h’ Values.....	108
Table 11. Calculated Vertical Post Spacing.....	109
Table 12. Chain-Link Area Exposed to Wind.....	111
Table 13. Calculated Reynolds Numbers and Drag Coefficients.....	113
Table 14. Maximum Expected Wind Loads.....	113
Table 15. Nominal Plastic Flexural Strength.....	115
Table 16. Front Wind Loading Results.....	117
Table 17. Back Wind Loading Results.....	119
Table 18. Resulting Forces.....	121
Table 19. Test Matrix.....	130
Table 20. P3G-1 and P3G-2 Average Force Comparison– 48-in. Embedment in Weak Soil.....	144
Table 21. P3G-3 and P3G-4 Average Force Comparison – 72-in. Embedment in Weak Soil.....	146
Table 22. P3G-5 and P3G-6 Average Force Comparison – 96-in. Embedment in Weak Soil.....	148
Table 23. P3G-7 and the average of P3G-8 and P3G-17 Average Force Comparison – 48-in. Embedment in Strong Soil.....	150
Table 24. P3G-18 and P3G-19 Average Force Comparison – 72-in. Embedment in Strong Soil.....	152
Table 25. Force Increase from 6-in. to 8-in. Width.....	155
Table 26. Test Nos. P3G-13, P3G-14, P3G-22, and P3G-15 Average Force Values - 4-in. Width in Weak Soil.....	158
Table 27. Test nos. P3G-13 and P3G-15 Force Values- 4-in. Width in Weak Soil.....	158
Table 28. Test nos. P3G-14 and P3G-15 Average Force Values – 4-in. Width in Weak Soil.....	159
Table 29. Expected vs. Actual Force Increase – 4-in. Width in Weak Soil.....	161
Table 30. Test nos. P3G-1 and P3G-3 Average Force Values- 6-in. Width in Weak Soil.....	162
Table 31. Test nos. P3G-1 and P3G-5 Average Force Values- 6-in. Width in Weak Soil.....	163
Table 32. Test nos. P3G-3 and P3G-5 Average Force Values- 6-in. Width in Weak Soil.....	164
Table 33. Expected vs. Actual Force Increase – 6-in. Width in Weak Soil.....	166

Table 34. Test nos. P3G-2 and P3G-4 Average Force Values – 8-in. Width in Weak Soil .....	167
Table 35. Test nos. P3G-2 and P3G-6 Average Force Values – 8-in. Width in Weak Soil .....	167
Table 36. Test nos. P3G-4 and P3G-6 Average Force Values – 8-in. Width in Weak Soil .....	168
Table 37. Expected vs. Actual Force Increase – 8-in. Width in Weak Soil.....	170
Table 38. Test nos. P3G-7 and P3G-18 Average Force Values – 6’’ Width in Strong Soil .....	170
Table 39. Expected vs. Actual Force Increase – 6-in. Width in Strong Soil .....	172
Table 40. The average of Test nos. P3G-8 and P3G-17 and Test no. P3G-19 Average Force Values – 8-in. Width in Strong Soil .....	172
Table 41. Expected vs. Actual Force Increase – 8-in. Width in Strong Soil .....	174
Table 42. Expected vs Actual Force Increase .....	175
Table 43. Test nos. P3G-1 and P3G-7 Average Force Values – 6-in. Width in a 48-in. Embedment .....	177
Table 44. Test nos. P3G-3 and P3G-18 Average Force Values – 6-in. Width in a 72-in. Embedment .....	179
Table 45. Test nos. P3G-2 and the average of P3G-8 and P3G-17 Average Force Values – 8-in. Width in a 48-in. Embedment .....	181
Table 46. Test nos. P3G-4 and P3G-19 Average Force Values – 8-in. Width in a 48-in. Embedment .....	183
Table 47. Force Increase from Weak to Strong Soil.....	185
Table 48. Pi Variables.....	187
Table 49. Dimensionless Groups Values .....	192
Table A-1. Variable Definitions .....	201
Table B-1. Variable Definitions.....	206
Table C-1. Variable Definitions.....	211
Table D-1. Variable Definitions .....	217
Table E-1. Variable Definitions.....	223
Table F-1. Variable Definitions .....	226
Table G-1. Bill of Materials, Test Nos. P3G-1 Through P3G-16.....	229
Table G-2. Bill of Materials, Test Nos. P3G-17 Through P3G-23.....	229
Table 50. Filter Max / Input Max and Filter Slope for Square Waves .....	283
Table I-1. Filter Max / Input Max and Filter Slope for Sawtooth Waves.....	289
Table I-2. Filter Max / Input Max and Filter Slope for Triangle Waves .....	295

## 1 INTRODUCTION

The following thesis is a culmination of two independent topics. The first, consists of the development of vertical posts to be used in a MASH TL-3 compliant debris fence for the Iowa DOT. To limit vehicle interaction, during an impact scenario, these posts need to be flexible enough to yield backwards, but they also need to be rigid enough to withstand maximum anticipated wind loads. This resulted in the selection of 2 $\frac{7}{8}$ -in. outside diameter ASTM F1083 regular grade schedule 40 piping spaced at 8 ft (2.4 m) centers as the vertical posts to be used in this debris fence design.

The second topic in this thesis consists of the analysis of 17 bogie tests completed with rigid posts in soil. During this testing series the post width, embedment depth, and soil type were differentiated to determine the affect each individual parameter had on the overall post-soil interaction forces. This analysis yielded inconclusive results overall, but the post-soil interaction forces did increase as the width, and embedment depth increased, as well as when a stronger soil type was used. Additional testing is recommended to further determine the result of these parameter variations.



## PART I

### 2 INTRODUCTION – DEBRIS FENCE

#### 2.1 Background and Problem Statement

When roadways pass over railway tracks, there is a risk that road debris may fall and damage tracks, clutter rail lines, or potentially cause concerns for train stability and safety. To prevent debris from interfering with train operations, a debris fence may be installed in conjunction with bridge rails on overpasses. In some circumstances, there is limited right-of-way adjacent to the travel lanes, and the fence may be located within a vehicle's Zone of Intrusion (ZOI), which is the lateral extent that a vehicle extends over the top-front face or corner of a barrier during an impact scenario.

The Iowa Department of Transportation (DOT) Office of Rail recently requested that the Midwest Roadside Safety Facility (MwRSF) develop designs for a debris fence, which could be attached to the top of a concrete bridge rail to prevent road debris from falling onto railroad tracks below. However, no debris fence has been crash-tested according to the American Association of State Highways and Transportation Officials (AASHTO) *Manual for Assessing Safety Hardware* (MASH) Test Level 3 (TL-3) specifications [1].

Debris fences attached to bridge rails are subject to two major concerns. If the debris fence is located within the Zone of Intrusion (ZOI), it must not produce excessive occupant compartment deformations, vehicle snag, nor occupant risk due to the presence of stiff beam and post members. However, the fences must be strong enough to withstand live and dead loads from the bridge. It is desirable that, if an impact results in contact

with the fence, the fence be retained on the overpass and not produce additional debris on the tracks below.

Thus, Iowa requested a review and evaluation of existing configurations of pedestrian fence and bridge railing combinations, as well as attachments to the top and sides of concrete barriers, and a recommended debris fence configuration that would likely meet crashworthiness requirements under MASH TL-3 impact conditions.

## **2.2 Research Objectives**

The objective of this research was to determine a parapet and vertical posts to be used in the development of a MASH TL-3 compliant debris fence system attached to a crashworthy concrete bridge parapet design. This design will be used along high-speed roadways and must satisfy safety performance criteria during impact scenarios. In addition, this design must comply with current Iowa DOT Standards for the usage of chain-link fences near the travelled way.

Phase I of the research consisted of a literature review of previously crash-tested fences mounted on concrete parapets and Zone of Intrusion (ZOI) details. In addition, current fence designs used by states were reviewed to compile details regarding fence geometries, key components, and connection details. MwRSF also collected information on debris fence design standards to ensure the design will meet wind load, and dead load requirements.

Phase II of the research effort will consist of the crash testing and evaluation of the proposed debris fence design from Phase I. Prior to executing Phase II, the Iowa DOT and railroad industry will review the proposed design and provide comments and

recommendations as well as determine if full-scale crash testing of the proposed system is desired.

### **3 DEBRIS FENCE LITERATURE REVIEW**

#### **3.1 State Designs**

States through their individual Departments of Transportation are responsible for maintaining design standards for roadside structures, including barriers and barrier attachments. A literature search was conducted to identify standard debris fence designs, also known as vandal protection fences, bridge safety fences, and railroad approach fences. Results of this review are summarized in Tables 1 through 3.

Table 1. State Standards – Fence Details

State	ID	Top of Fence Height (ft)	Fence Design	Parapet Height (in.)	Transition Slope	Vertical Posts					Horizontal Stiffeners					Additional Information or Components		
						Length (in.)	Outside Diameter (in.)	Spacing (ft.)	Vertical Post Attachment to Parapet	Additional Information	Stiffener Quantity	Outside Diameter (in.)	Height Above Parapet to the Center of Rail					
													Rail 1 (in.)	Rail 2 (in.)	Rail 3 (in.)		Rail 4 (in.)	Rail 5 (in.)
California	1	6	Vertical Top Mounted	42	-	73.5	-	5 to 10	Concrete Embedment	HSS Steel (3 in. x 2 in. x 3/16 in.)	-	-	-	-	-	Tension Wire		
Delaware	2	5	Vertical Top Mounted	-	4H : 1V	60.5	2.875	10	Base Plate	-	2	1.66	3	58.5	-	Diagonal Truss Rods		
Delaware	3	7	Curved Top Mounted	-	4H : 1V	74.375	2.875	10	Base Plate	-	4	1.66	3	58.5	69.63	Diagonal Truss Rods		
Florida	4	6	Curved Back Mounted	-	-	Varies	3.5	10	Clamps	-	4	-	-	-	-	Tension Wires		
Idaho	5	-	Angled Top Mounted	-	-	106	-	5 ft to 6 ft 8 in.	Concrete Embedment	HSS Steel (4 in. x 2 in. x 3/16 in.)	5	-	6	32	64	70.75	94	HSS Steel (2 in. x 2 in. x 3/16 in.)
Indiana	6	5 or 6	Vertical Top Mounted	-	-	Varies	2.875	10	Base Plate	-	2	1.66	-	-	-	-	-	
Iowa	7	6	Mounted on Road	-	-	72.75	2.875	-	Road Embedment	-	2	1.66	-	-	-	-	Diagonal Brace Posts	
Kansas	8	6 or 8	Vertical Back Mounted	32-40	-	Varies	2.875	8	Clamps	-	2	1.66	-	-	-	-	-	
Maryland	9	7	Curved Top Mounted	32	-	74.375	2.875	-	Base Plate	-	4	1.66	3	39	58.5	69.63	Diagonal Truss Rods	
Maryland	10	5	Vertical Top Mounted	-	-	60.5	2.875	-	Base Plate	-	2	1.66	3	58.5	-	-	Diagonal Truss Rods	
Minnesota	11	6	Vertical Top Mounted	32-44	-	72	2.875	10	Base Plate	-	1	1.66	-	-	-	-	Tension Wire and Diagonal Brace Posts	
Nebraska	12	6	Vertical Top Mounted	42	9H : 1V	72	3.5	8	Base Plate	-	3	1.66	4	42	72	-	-	
Nebraska	13	7	Vertical Back Mounted	42	-	106.5	3.5	8	Clamps	-	3	1.66	2	45	72	-	-	
New Jersey	14	7	Curved Top Mounted	32	-	75	-	-	Base Plate	HSS Steel (2 in. x 2 in. x 1/4 in.)	4	-	4	32	56	74	-	HSS Steel (1.5 in. x 1.5 in. x 1/8 in.)
New York	15	Varies	Vertical Back Mounted	34-42	-	Varies	2.875	10	Clamps	-	3	1.625	-	-	-	-	-	
Oregon	16	8	Vertical Back Mounted	29	-	120	4	10	Clamps	-	2	1.66	-	-	-	-	-	
Oregon	17	10	Curved Back Mounted	-	-	-	4	10	Clamps	-	4	1.66	-	-	-	-	-	
Texas	18	8	Vertical Back Mounted	-	-	130	4	8	Clamps	-	1	1.66	-	-	-	-	-	Diagonal Truss Rods
Wisconsin	19	8	Angled Top Mounted	32	-	85.5	2.375	8	Base Plate	-	3	1.66	-	-	-	-	-	

Table 2. State Fence Designs by Percent

<b>State Fence Designs</b>				
<b>Vertical Top Mounted</b>	<b>Vertical Back Mounted</b>	<b>Curved Top Mounted</b>	<b>Curved Back Mounted</b>	<b>Angled Top Mounted</b>
33.33%	27.78%	16.67%	11.11%	11.11%

Table 3. State Parapet Attachment Methods by Percent

<b>State Parapet Attachment Methods</b>		
<b>Base Plate</b>	<b>Clamps</b>	<b>Concrete Embedment</b>
50.00%	38.89%	11.11%

### 3.1.1 California

The California Department of Transportation (Caltrans) uses the combination of a vertical-shaped, concrete parapet and a top-mounted, vertical fence to safely keep pedestrian debris away from railroad tracks. The concrete railing used by Caltrans has a height of 40 in. (1,016 mm), and the debris containment fence is mounted 6 in. (152 mm) behind the front face of the parapet. This design is shown in Figure 1 [2].

The debris fence is attached to the top of parapet by anchoring the vertical posts 8 in. (203 mm) into the concrete using a mortar backfill. The rectangular vertical posts extended a total of 6 ft-1½ in. (1.9 m) above the concrete parapet and were placed along the barrier every 5 to 10 ft (1.5 to 3.0 m). The chain-link fabric specified by Caltrans is 6 ft (1.8 m) tall and is made of up a 1-in. (25-mm) diamond-shaped mesh and has a knuckled selvage on the top and bottom of the wire mesh. This mesh is connected to the fence structure by clamping the fence horizontally along the top of the system and vertically at the beginning and end of the parapet. The mesh is additionally connected to the vertical members with vinyl-coated, fabric ties spaced 1 in. (25 mm) apart. This design is shown in Figure 2 [2].







### 3.1.2 Delaware

Delaware DOT uses two different designs for debris fences. The first design is a vertical chain-link fence mounted on top of a parapet and connected to the parapet with a baseplate and four  $\frac{5}{8}$ -in. (16-mm) diameter threaded anchor studs. The chain-link fabric of this system measures 5 ft (1.5 m) in height and contains a 1-in. (25-mm) diamond mesh made out of # 9-gauge wire. The system uses  $2\frac{1}{2}$  -in. (64-mm) nominal diameter pipes spaced in 10 ft (3 m) increments as vertical support posts, two  $1\frac{1}{4}$ -in. (32-mm) nominal diameter pipes as longitudinal stiffeners, and the fence is sloped downward using a  $\frac{3}{8}$ -in. (10-mm) diameter truss rod. Single #9 gauge or double #13 gauge ties are used to connect the wire mesh to the vertical and horizontal members. The fence system is shown in Figure 3, and the mounting and connection details are shown in Figure 4 [3].

The second design used by the state of Delaware is a curved chain-link fence structure mounted on the top of a concrete rail, with a wire mesh height of 7 ft (2.1 m) and using the same base plate as the first system. The sizing and spacing of the vertical members, horizontal stiffeners, and the connection of the wire mesh to the members and stiffeners are the same for both Delaware designs, but a total of four horizontal stiffeners are used in this design. The mounting and connection details are shown in Figure 4, and the fence system is shown in Figure 5 [3].

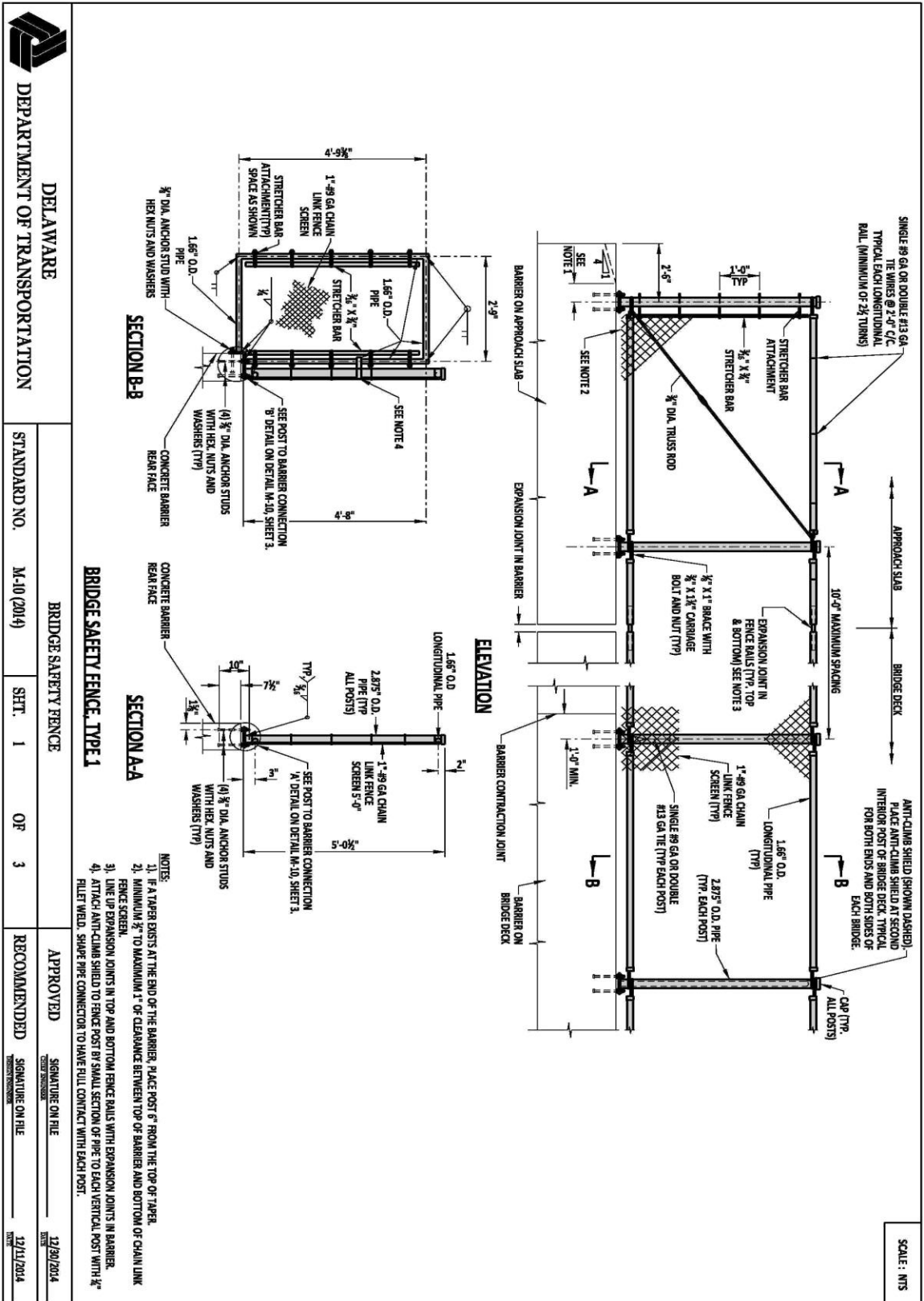


Figure 3. Delaware Bridge Safety Fence, Type 1 [3]





### 3.1.3 Florida

The Florida Department of Transportation (FDOT) uses a curved fence mounted on the back of a concrete parapet to reduce the amount of debris on and around railroad tracks. The FDOT's design standards show that this fence can be used in conjunction with a 36-in. (914-mm) tall, single-slope concrete parapet, but the size and type of barrier can vary [4].

Florida uses a curved chain-link wire mesh fence structure mounted to the back of a concrete parapet for railroad debris protection. Vertical posts are galvanized, schedule 40 tubes, with a 3 in. (76 mm) nominal diameter. There are no structurally-stiff horizontal members, and lateral stiffness is obtained by using four cables wound within the wire mesh fence. Each vertical member is attached to the parapet with two pipe clamps, which are bolted to the concrete parapet with  $\frac{3}{8}$ -in. (10-mm) diameter bolts. The chain-link fabric is composed of a 2-in. (51-mm) diamond mesh that is twisted at the top and has a knuckled selvage at the bottom of the fence. The mesh is connected to the posts and tension cables with wire ties. System drawings and connection details are shown in Figures 6 through 8 [4].

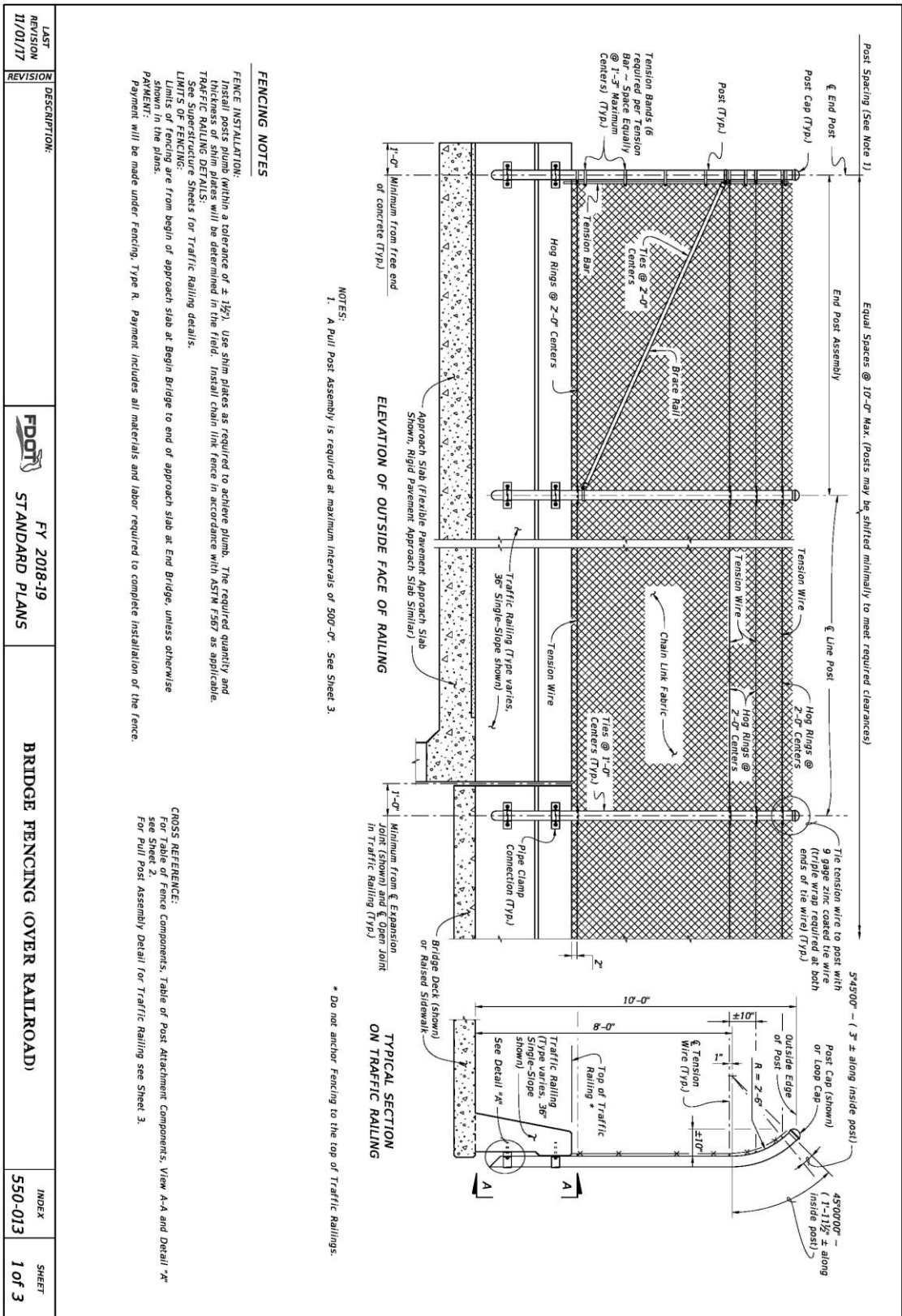
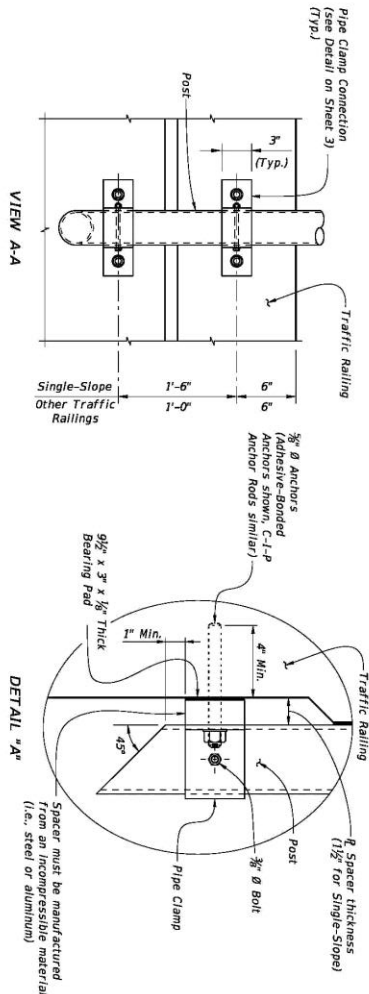


Figure 6. Florida Bridge Fencing Over Railroad, Sheet 1 [4]

TABLE OF CHAIN LINK FENCE COMPONENTS	
COMPONENT	ASTM DESIGNATION
Posts	F1083 Galvanized Steel Pipe - 3" NPS, Schedule 40 Regular Grade
Chain Link Fabric (Chain Link Fabric - top and knurled bottom selvage)	A392 Zinc Coated Steel - 9 gauge (coated wire diameter), Class 2 Coating
	A491 Aluminum Coated Steel - 9 gauge (coated wire diameter)
Tie Wires	F669 Polyvinyl Chloride (PVC) Coated Steel - 9 gauge Class 20
	F626 Zinc Coated Steel Wire - 9 gauge
Brace Bands	F626 12 Gauge (Min. thickness) x 3/8" (Min. width) Steel Bands (beveled or Heavy)
Tension Bars	F626 3/8" (Min. thickness) x 3/8" (Min. width) x 6'-10" (Min. height) Steel Bars
Tension Bands	F626 14 Gauge (Min. thickness) x 3/8" (Min. width) Steel Bands
Miscellaneous Fence Components	F626 Zinc Coated Steel - (Includes post or loop caps, horizontal and brace rail ends, combination rail ends, boulevard clamps and all other miscellaneous fittings & hardware)
Tension Wire	A824 & A817 Type II (Zinc Coated Steel Wire) - 7 gauge, Class 4 Coating
Hog Rings	F626 Type I (Aluminum Coated Steel Wire) - 7 gauge
Brace Rails	F1083 Galvanized Steel Pipe - 1 1/2" NPS, Schedule 40 Regular Grade

TABLE OF POST ATTACHMENT COMPONENTS		
COMPONENT	ASTM DESIGNATION	COMPONENT INFORMATION
Pipe Clamps	A36 or A709 Grade 36	1/2" Steel R
Base Plates	A36 or A709 Grade 36	3/8" Steel R
Shim Plates	A36 or A709 Alloy 6061-T6 or B221 Alloy 6063-T5	Plate thicknesses as required; Holes in shim plates will be 3/8" Ø
Spacers	-	Plate thickness varies based on traffic railing type (See Detail "A")
Pipe Clamp Connection	F1554 grade 36	Hex Head Anchor Rods - 3/8" Ø x 6" (no spacer) or 3/8" Ø x 6" + spacer thickness)
	F1554 grade 36	Hex Head Anchor Rods - 3/8" Ø x 6" (no spacer) or 3/8" Ø x 6" + spacer thickness)
Anchor Rods	A307	3/8" Ø x 4 1/2" Hex Head Bolts for Pipe Clamp Connections to Posts
Nuts	A563	Hex Nuts for Pipe Clamp Connections to Posts
Washers	F436	Flat Washers for Pipe Clamp Connections to Posts
Bearing Pads (Flat Neoprene)	-	In accordance with Specification Section 932 for Auxiliary Structures



**POST ATTACHMENT NOTES**

**ANCHOR RODS, NUTS AND WASHERS:**  
 After the nuts have been tightened, distort the anchor rod threads to prevent removal of the nuts. Coat distorted threads and exposed trimmed ends of anchors with a galvanizing compound in accordance with Specification Section 562.

**CONCRETE:**  
 Embed all nuts, washers, bolts, C-I-P anchor rods, adhesive anchors and framing (posts, internal spacers, C-I-P anchor rods, adhesive anchors, clamps and spacers) in accordance with Specification Section 962. Hot-dip galvanize Fence Framework after fabrication.

**ADHESIVE-BONDED ANCHORS AND DOWELS:**  
 Adhesive Bonding Material Systems for Anchors and Dowels will comply with Specification Section 937 and be installed in accordance with Specification Section 416. Cutting of reinforcing steel is permitted for drilled hole installation.

**WELDING:**  
 All welding will be in accordance with the American Welding Society Structural Welding Code (Steel) ANSI/AWS D1.1 (current edition). Weld metal will be E60XX or E70XX. Nondestructive testing of welds is not required.

**CROSS REFERENCE:**  
 For location of View A-A and Detail "A" see Sheet 1.

LAST REVISION 11/01/17	DESCRIPTION:	FDOT STANDARD PLANS	FY 2018-19	BRIDGE FENCING (OVER RAILROAD)	INDEX 550-013	SHEET 2 of 3
---------------------------	--------------	------------------------	------------	--------------------------------	------------------	-----------------

Figure 7. Florida Bridge Fencing Over Railroad, Sheet 2 [4]





### 3.1.4 Idaho

The Idaho Department of Transportation recommends using an overhanging fence mounted on a parapet to protect pedestrians near the travelled way. The fence posts are directly embedded into the concrete of a vertical 27-in. (686-mm) tall rail system and is placed along the centerline of the 9-in. (229-mm) wide vertical parapet [5].

The combination pedestrian fence system and parapet measure a total of 10 ft-1 in. (3.1 m) in height. The vertical members of the combination system are made out of hollow steel tubes measuring 4 in. x 2 in. x 3/16 in. (102 mm x 51 mm x 5 mm), which are spaced between 5 ft and 6 ft-8 in. (1.5 and 2 m) apart. The fence is 8 ft-7 in. (2.6 m) tall and the upper 3 ft (0.9 m) of the posts are angled at 41 degrees over the roadway. The system uses five horizontal stiffeners made out of 2-in. x 2-in. x 3/16-in. (51-mm x 51-mm x 5-mm) hollow structural steel. There is an additional 2-in. x 2-in. x 3/16 in. (51-mm x 51-mm x 5-mm) horizontal member that is located 15 in. (381 mm) above the parapet, which could mitigate vehicle protrusion from engaging the vertical posts. The members are then connected to a 2-in. (51-mm) square mesh wire fabric with wire ties. Details of this design are shown in Figure 9 [5].

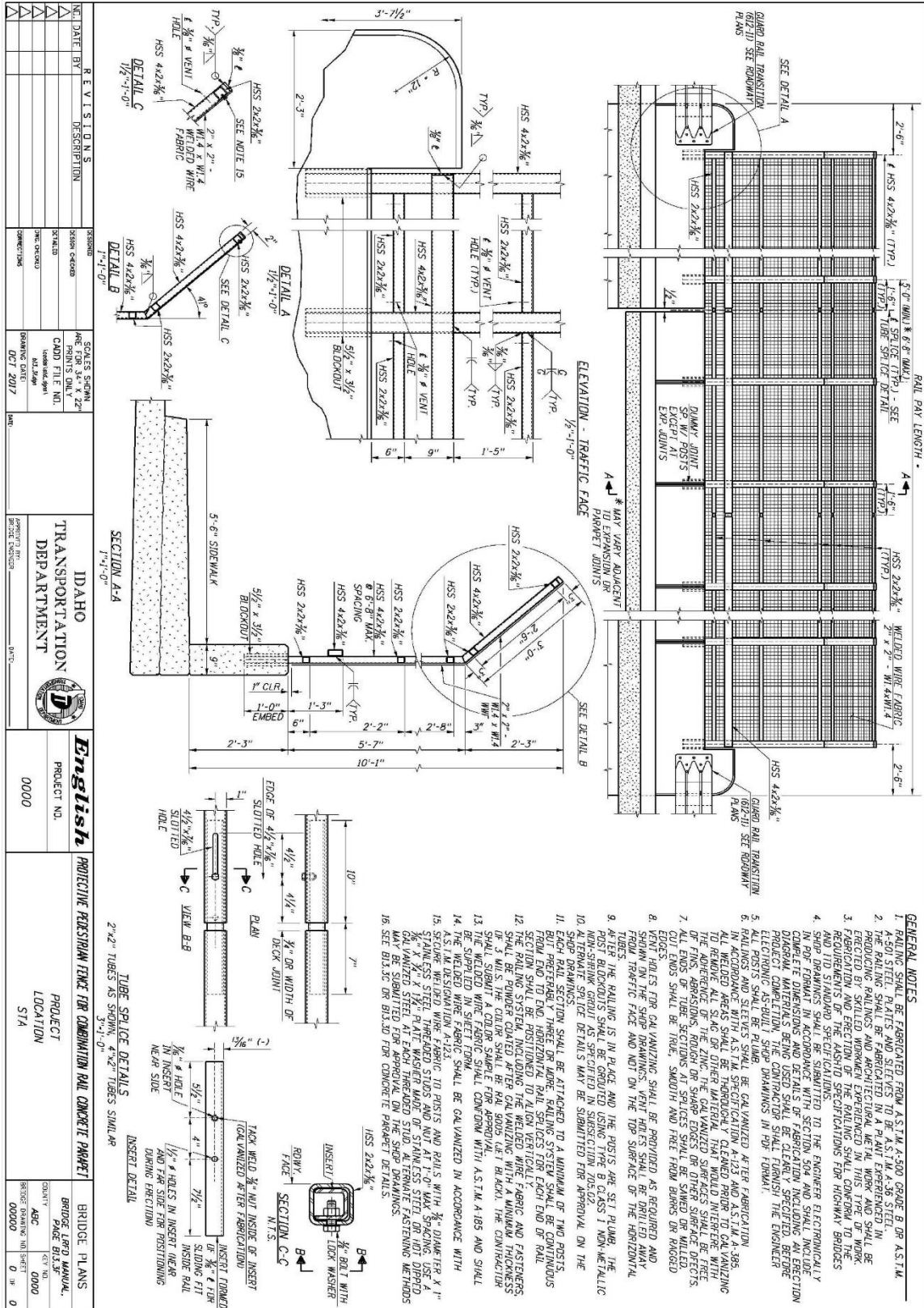


Figure 9. Idaho Protective Fence for Combination Rail and Parapet [5]

### 3.1.5 Indiana

Indiana DOT currently utilizes a vertical pedestrian fence mounted on top of a Type FT or FC safety shape concrete parapet. The fence structure uses 2½-in. (64-mm) nominal diameter steel tube posts spaced 10 ft (3.0 m) on center. These posts are connected to upper and lower horizontal stiffeners with nominal diameters of 1¼ in. (32 mm). The fence can be adjusted for the desired height based on the size of the vertical post and the placement of the horizontal stiffeners. Wire ties are connected to the steel frames spaced at 15 in. (381 mm) intervals or less. The vertical members are then secured to the concrete parapet through a base plate that is connected with four 5⁄8-in. (16-mm) diameter bolts. CAD details are shown in Figure 10 [6].

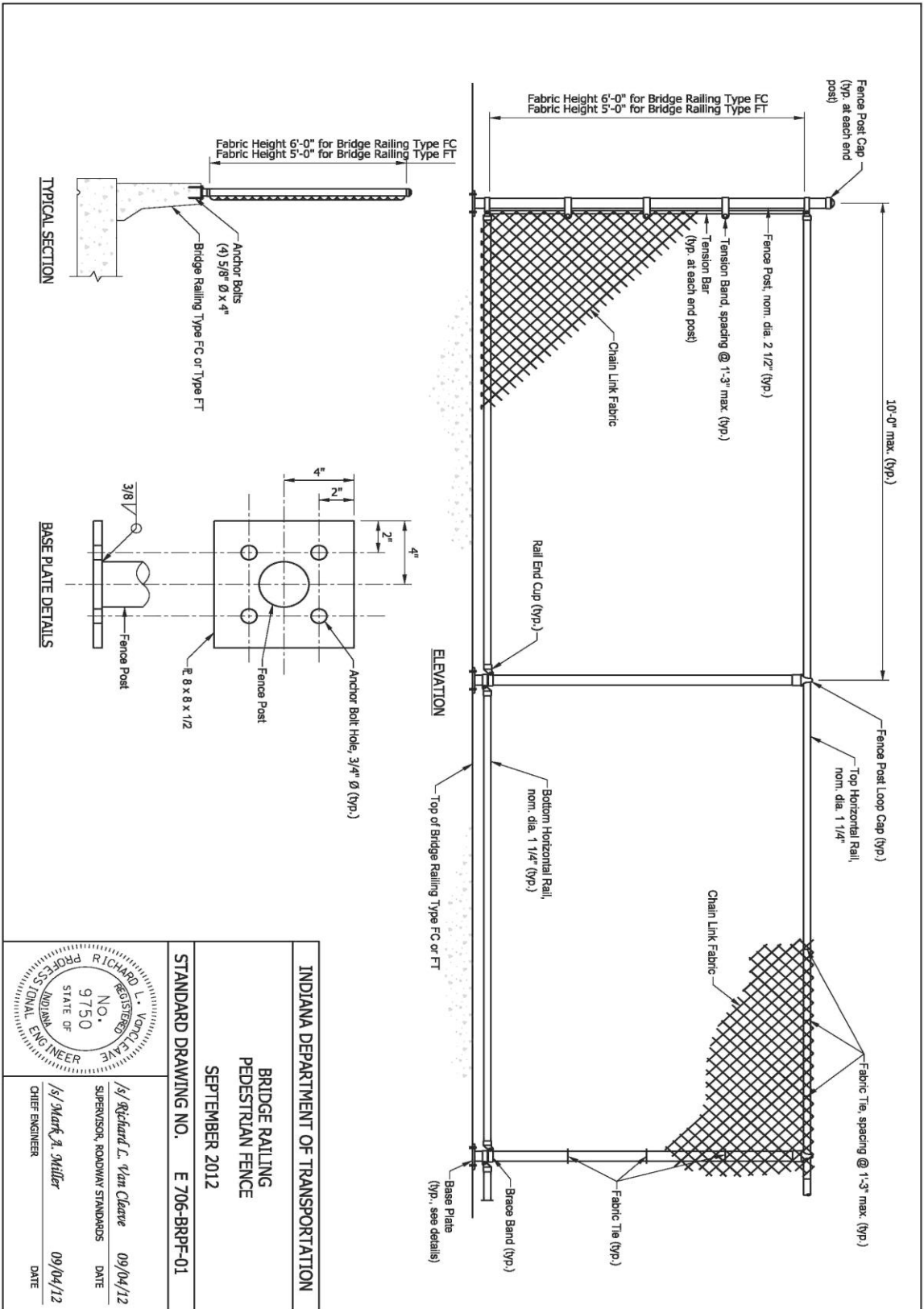


Figure 10. Indiana Bridge Railing Pedestrian Fence [6]

<b>INDIANA DEPARTMENT OF TRANSPORTATION</b> <b>BRIDGE RAILING PEDESTRIAN FENCE</b> <b>SEPTEMBER 2012</b>	
<b>STANDARD DRAWING NO. E 706-BRPF-01</b>	
	/s/ Richard L. VanCleave SUPERVISOR, ROADWAY STANDARDS DATE 09/04/12
/s/ Mark A. Miller CHIEF ENGINEER	DATE 09/04/12

### 3.1.6 Iowa

The Iowa Department of Transportation uses a chain-link fence in conjunction with a pedestrian rail for debris and pedestrian containment purposes. The Iowa design consists of a 6-ft (1.8-m) tall chain-link fence containing a 2-in. (51-mm) diamond mesh, made out of no. 9 wire and has knuckled selvages at the top and bottom of the fence and the 6-ft  $\frac{3}{4}$ -in. (1.8-m) tall vertical tubes with a nominal pipe diameter of  $2\frac{1}{2}$  in. (64 mm) are mounted along the fence. Additionally, the 2-in. (51-mm) nominal diameter tubes were utilized on the bottom of the fence, and  $1\frac{1}{4}$ -in. (32-mm) diameter tubes were used along the top of the fence. The wire mesh was connected to the vertical members by using wire ties or clips spaced every 12 in. (305 mm), and the mesh was connected to the horizontal members using wire ties or clips spaced at 24 in. (610 mm) intervals [7].



### 3.1.7 Kansas

The Kansas Department of Transportation (KDOT) uses two different fences for pedestrian and debris control over railroads, which vary only on height. These fences are mounted to the back of a 35-in. (889-mm) tall, safety-shape concrete parapet [8].

An 8-ft (2.4-m) tall fence is required when the shoulders of the bridge are less than 6 ft (1.8 m) wide, but a 6-ft (1.8-m) tall fence can be used when the bridge shoulders are greater than or equal to 6 ft (1.8 m). The round vertical posts consist of 2½-in. (64-mm) nominal diameter pipes spaced 8 ft (2.4 m) on centers. Two 1¼-in. (32-mm) nominal diameter tubes are used as horizontal stiffeners at the top and bottom of the fence. Additional ⅜-in. (10-mm) diameter threaded rods are used to maintain tension in the mesh. The vertical posts are mounted to the back of the parapet with two pipe clamps and U-bolts, and the base of the each vertical member is connected to a piece of angle iron that is attached to the parapet using a ⅝-in. (16-mm) diameter bolt. The fence is made from 2-in. (51-mm) chain-link fabric that is galvanized or PVC coated, and it contains a knuckled selvage on both the top and bottom of the fence. This wire is then connected to the fence structure with #9 gauge wire ties. The taller design is shown in Figure 12, and the shorter design is shown in Figure 13 [8].



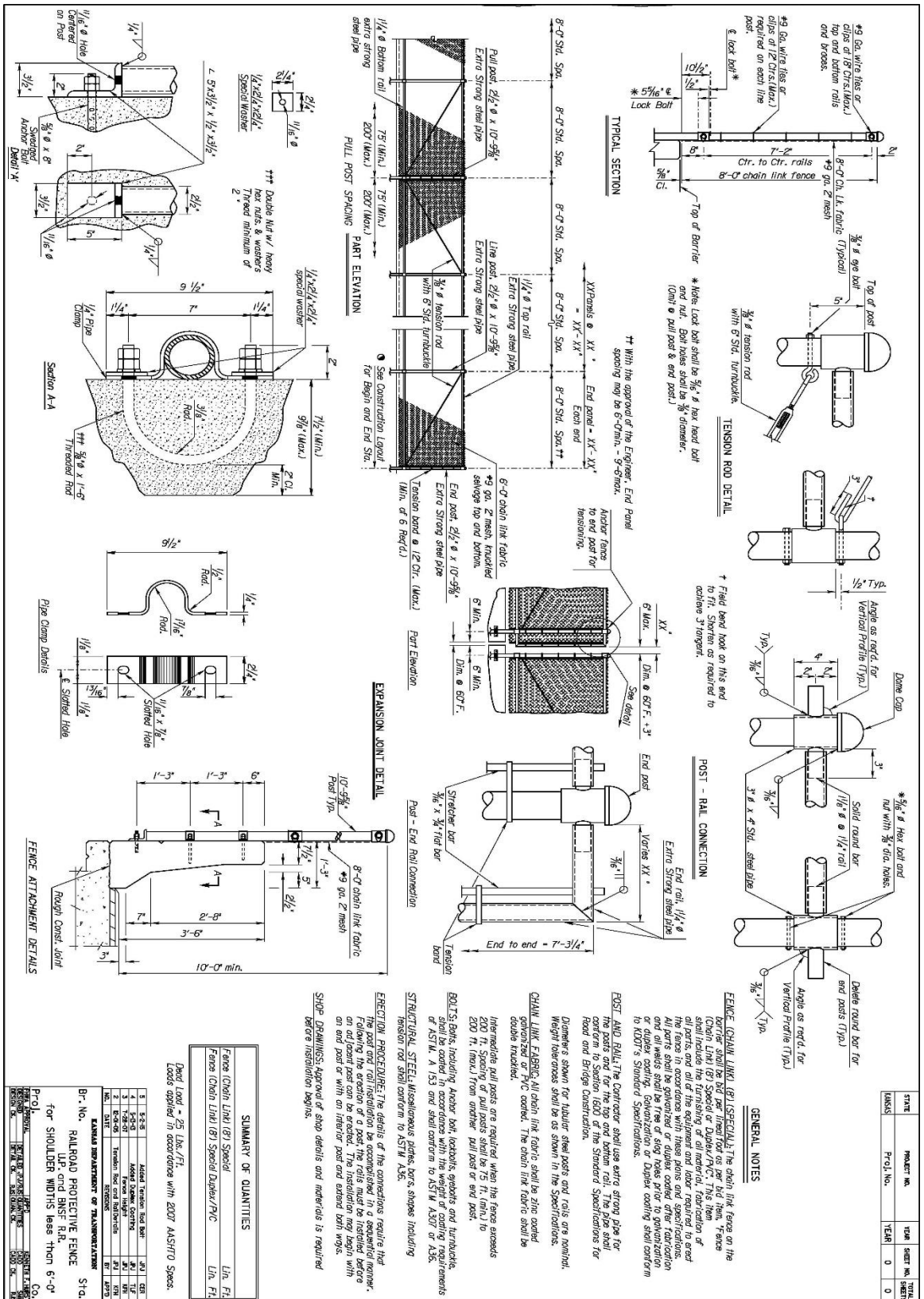


Figure 12. Kansas Railroad Protective Fence for Shoulders Less than 6 ft [8]

STATE	PROJECT NO.	YEAR	SHEET NO.	TOTAL SHEETS
KANSAS	PR-Q No.		0	0

GENERAL NOTES

FENCE (CHAIN LINK) (SEE SPECIFICATIONS) The chain link fence on the border shall be bid per linear foot as per bid item. Fence (Chain Link) (B) Speed or Duplex/PVC. This item shall include the furnishing of all material, fabrication of all parts, and all of the equipment and labor required to erect all parts shall be galvanized or duplex coated after fabrication and all welds shall be free of slag holes prior to galvanization or duplex coating. Galvanization or Duplex coating shall conform to KDOT's Standard Specifications.

POST AND RAIL: The Contractor shall use extra strong pipe for the posts and for the top and bottom rail. The pipe shall conform to Section 1600 of the Standard Specifications for Road and Bridge Construction.

Diameter's shown for tubular steel posts and rails are nominal. Weight tolerances shall be as shown in the Specifications.

CHAIN LINK FABRIC: All chain link fabric shall be zinc coated galvanized or PVC coated. The chain link fabric shall be duplex finished.

Intermediate pull posts are required when the fence exceeds 200 ft. Spacing of pull posts shall be 75 ft. (min.) to 200 ft. (max.) from either pull post or end post.

BOLTS: Bolts, including Anchor Bolt Locknuts, washers and turnbuckle, shall be coated in accordance with the weight of coating requirements of ASTM A 153 and shall conform to ASTM A307 or A36.

STRUCTURAL STEEL: Miscellaneous plates, bars, shapes including tension rod shall conform to ASTM A36.

ERECTOR FORCE/DURE: The details of the connections require that the post and rail installation be accomplished in a sequential manner. An erection force may be needed. The installation sequence begins with an end post or with an interior post and extend both ways.

SHOULDER: Approval of shop details and materials is required before installation begins.

SUMMARY OF QUANTITIES

	Lin.	Flt.
Fence (Chain Link) (B) Speed		
Fence (Chain Link) (B) Special Duplex/PVC		

Draw Load = 25 Lbs./ft.

Loads applied in accordance with 2007 AASHTO Specs.

ESTIMATED QUANTITY OF MATERIALS:

ITEM NO.	DESCRIPTION	AMOUNT	UNIT
1	4" x 4" x 1/2" Post	1	EA
2	4" x 4" x 1/2" Rail	1	EA
3	4" x 4" x 1/2" End Post	1	EA
4	1/2" x 1/2" x 1/4" Turnbuckle	1	EA
5	1/2" x 1/2" x 1/4" Washer	1	EA
6	1/2" x 1/2" x 1/4" Nut	1	EA
7	1/2" x 1/2" x 1/4" Bolt	1	EA
8	1/2" x 1/2" x 1/4" Anchor Bolt	1	EA
9	1/2" x 1/2" x 1/4" Locknut	1	EA
10	1/2" x 1/2" x 1/4" Lockwasher	1	EA
11	1/2" x 1/2" x 1/4" Turnbuckle	1	EA
12	1/2" x 1/2" x 1/4" Washer	1	EA
13	1/2" x 1/2" x 1/4" Nut	1	EA
14	1/2" x 1/2" x 1/4" Bolt	1	EA
15	1/2" x 1/2" x 1/4" Anchor Bolt	1	EA
16	1/2" x 1/2" x 1/4" Locknut	1	EA
17	1/2" x 1/2" x 1/4" Lockwasher	1	EA
18	1/2" x 1/2" x 1/4" Turnbuckle	1	EA
19	1/2" x 1/2" x 1/4" Washer	1	EA
20	1/2" x 1/2" x 1/4" Nut	1	EA
21	1/2" x 1/2" x 1/4" Bolt	1	EA
22	1/2" x 1/2" x 1/4" Anchor Bolt	1	EA
23	1/2" x 1/2" x 1/4" Locknut	1	EA
24	1/2" x 1/2" x 1/4" Lockwasher	1	EA
25	1/2" x 1/2" x 1/4" Turnbuckle	1	EA
26	1/2" x 1/2" x 1/4" Washer	1	EA
27	1/2" x 1/2" x 1/4" Nut	1	EA
28	1/2" x 1/2" x 1/4" Bolt	1	EA
29	1/2" x 1/2" x 1/4" Anchor Bolt	1	EA
30	1/2" x 1/2" x 1/4" Locknut	1	EA
31	1/2" x 1/2" x 1/4" Lockwasher	1	EA
32	1/2" x 1/2" x 1/4" Turnbuckle	1	EA
33	1/2" x 1/2" x 1/4" Washer	1	EA
34	1/2" x 1/2" x 1/4" Nut	1	EA
35	1/2" x 1/2" x 1/4" Bolt	1	EA
36	1/2" x 1/2" x 1/4" Anchor Bolt	1	EA
37	1/2" x 1/2" x 1/4" Locknut	1	EA
38	1/2" x 1/2" x 1/4" Lockwasher	1	EA
39	1/2" x 1/2" x 1/4" Turnbuckle	1	EA
40	1/2" x 1/2" x 1/4" Washer	1	EA
41	1/2" x 1/2" x 1/4" Nut	1	EA
42	1/2" x 1/2" x 1/4" Bolt	1	EA
43	1/2" x 1/2" x 1/4" Anchor Bolt	1	EA
44	1/2" x 1/2" x 1/4" Locknut	1	EA
45	1/2" x 1/2" x 1/4" Lockwasher	1	EA
46	1/2" x 1/2" x 1/4" Turnbuckle	1	EA
47	1/2" x 1/2" x 1/4" Washer	1	EA
48	1/2" x 1/2" x 1/4" Nut	1	EA
49	1/2" x 1/2" x 1/4" Bolt	1	EA
50	1/2" x 1/2" x 1/4" Anchor Bolt	1	EA
51	1/2" x 1/2" x 1/4" Locknut	1	EA
52	1/2" x 1/2" x 1/4" Lockwasher	1	EA
53	1/2" x 1/2" x 1/4" Turnbuckle	1	EA
54	1/2" x 1/2" x 1/4" Washer	1	EA
55	1/2" x 1/2" x 1/4" Nut	1	EA
56	1/2" x 1/2" x 1/4" Bolt	1	EA
57	1/2" x 1/2" x 1/4" Anchor Bolt	1	EA
58	1/2" x 1/2" x 1/4" Locknut	1	EA
59	1/2" x 1/2" x 1/4" Lockwasher	1	EA
60	1/2" x 1/2" x 1/4" Turnbuckle	1	EA
61	1/2" x 1/2" x 1/4" Washer	1	EA
62	1/2" x 1/2" x 1/4" Nut	1	EA
63	1/2" x 1/2" x 1/4" Bolt	1	EA
64	1/2" x 1/2" x 1/4" Anchor Bolt	1	EA
65	1/2" x 1/2" x 1/4" Locknut	1	EA
66	1/2" x 1/2" x 1/4" Lockwasher	1	EA
67	1/2" x 1/2" x 1/4" Turnbuckle	1	EA
68	1/2" x 1/2" x 1/4" Washer	1	EA
69	1/2" x 1/2" x 1/4" Nut	1	EA
70	1/2" x 1/2" x 1/4" Bolt	1	EA
71	1/2" x 1/2" x 1/4" Anchor Bolt	1	EA
72	1/2" x 1/2" x 1/4" Locknut	1	EA
73	1/2" x 1/2" x 1/4" Lockwasher	1	EA
74	1/2" x 1/2" x 1/4" Turnbuckle	1	EA
75	1/2" x 1/2" x 1/4" Washer	1	EA
76	1/2" x 1/2" x 1/4" Nut	1	EA
77	1/2" x 1/2" x 1/4" Bolt	1	EA
78	1/2" x 1/2" x 1/4" Anchor Bolt	1	EA
79	1/2" x 1/2" x 1/4" Locknut	1	EA
80	1/2" x 1/2" x 1/4" Lockwasher	1	EA
81	1/2" x 1/2" x 1/4" Turnbuckle	1	EA
82	1/2" x 1/2" x 1/4" Washer	1	EA
83	1/2" x 1/2" x 1/4" Nut	1	EA
84	1/2" x 1/2" x 1/4" Bolt	1	EA
85	1/2" x 1/2" x 1/4" Anchor Bolt	1	EA
86	1/2" x 1/2" x 1/4" Locknut	1	EA
87	1/2" x 1/2" x 1/4" Lockwasher	1	EA
88	1/2" x 1/2" x 1/4" Turnbuckle	1	EA
89	1/2" x 1/2" x 1/4" Washer	1	EA
90	1/2" x 1/2" x 1/4" Nut	1	EA
91	1/2" x 1/2" x 1/4" Bolt	1	EA
92	1/2" x 1/2" x 1/4" Anchor Bolt	1	EA
93	1/2" x 1/2" x 1/4" Locknut	1	EA
94	1/2" x 1/2" x 1/4" Lockwasher	1	EA
95	1/2" x 1/2" x 1/4" Turnbuckle	1	EA
96	1/2" x 1/2" x 1/4" Washer	1	EA
97	1/2" x 1/2" x 1/4" Nut	1	EA
98	1/2" x 1/2" x 1/4" Bolt	1	EA
99	1/2" x 1/2" x 1/4" Anchor Bolt	1	EA
100	1/2" x 1/2" x 1/4" Locknut	1	EA

FOR SHOULDER WIDTHS LESS THAN 6'-0"

RAILROAD PROTECTIVE FENCE

UP and BNSF R.R.

FOR SHOULDER WIDTHS LESS THAN 6'-0"

RAILROAD PROTECTIVE FENCE

UP and BNSF R.R.

FOR SHOULDER WIDTHS LESS THAN 6'-0"

RAILROAD PROTECTIVE FENCE

UP and BNSF R.R.

FOR SHOULDER WIDTHS LESS THAN 6'-0"

RAILROAD PROTECTIVE FENCE

UP and BNSF R.R.

FOR SHOULDER WIDTHS LESS THAN 6'-0"

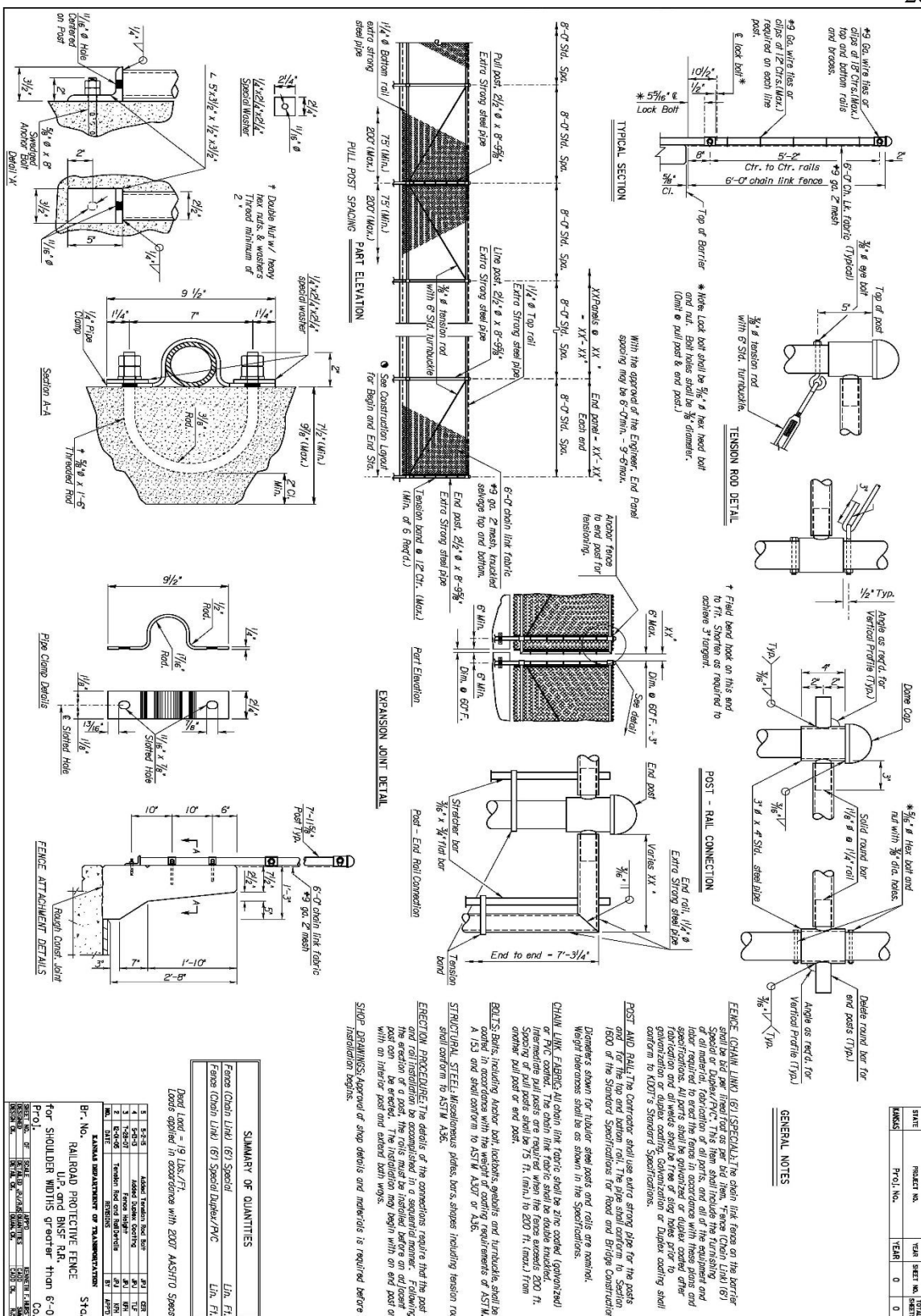


Figure 13. Kansas Railroad Protective Fence for Shoulders Greater than 6 ft [8]

SUMMARY OF QUANTITIES		Lin. Ft.	Sq. Yds.	Sq. Ft.	Sq. Yds.
1	5.5-6	1250	1250	1250	1250
2	5.5-6	1250	1250	1250	1250
3	5.5-6	1250	1250	1250	1250
4	5.5-6	1250	1250	1250	1250
5	5.5-6	1250	1250	1250	1250
6	5.5-6	1250	1250	1250	1250
7	5.5-6	1250	1250	1250	1250
8	5.5-6	1250	1250	1250	1250
9	5.5-6	1250	1250	1250	1250
10	5.5-6	1250	1250	1250	1250
11	5.5-6	1250	1250	1250	1250
12	5.5-6	1250	1250	1250	1250
13	5.5-6	1250	1250	1250	1250
14	5.5-6	1250	1250	1250	1250
15	5.5-6	1250	1250	1250	1250
16	5.5-6	1250	1250	1250	1250
17	5.5-6	1250	1250	1250	1250
18	5.5-6	1250	1250	1250	1250
19	5.5-6	1250	1250	1250	1250
20	5.5-6	1250	1250	1250	1250
21	5.5-6	1250	1250	1250	1250
22	5.5-6	1250	1250	1250	1250
23	5.5-6	1250	1250	1250	1250
24	5.5-6	1250	1250	1250	1250
25	5.5-6	1250	1250	1250	1250
26	5.5-6	1250	1250	1250	1250
27	5.5-6	1250	1250	1250	1250
28	5.5-6	1250	1250	1250	1250
29	5.5-6	1250	1250	1250	1250
30	5.5-6	1250	1250	1250	1250
31	5.5-6	1250	1250	1250	1250
32	5.5-6	1250	1250	1250	1250
33	5.5-6	1250	1250	1250	1250
34	5.5-6	1250	1250	1250	1250
35	5.5-6	1250	1250	1250	1250
36	5.5-6	1250	1250	1250	1250
37	5.5-6	1250	1250	1250	1250
38	5.5-6	1250	1250	1250	1250
39	5.5-6	1250	1250	1250	1250
40	5.5-6	1250	1250	1250	1250
41	5.5-6	1250	1250	1250	1250
42	5.5-6	1250	1250	1250	1250
43	5.5-6	1250	1250	1250	1250
44	5.5-6	1250	1250	1250	1250
45	5.5-6	1250	1250	1250	1250
46	5.5-6	1250	1250	1250	1250
47	5.5-6	1250	1250	1250	1250
48	5.5-6	1250	1250	1250	1250
49	5.5-6	1250	1250	1250	1250
50	5.5-6	1250	1250	1250	1250
51	5.5-6	1250	1250	1250	1250
52	5.5-6	1250	1250	1250	1250
53	5.5-6	1250	1250	1250	1250
54	5.5-6	1250	1250	1250	1250
55	5.5-6	1250	1250	1250	1250
56	5.5-6	1250	1250	1250	1250
57	5.5-6	1250	1250	1250	1250
58	5.5-6	1250	1250	1250	1250
59	5.5-6	1250	1250	1250	1250
60	5.5-6	1250	1250	1250	1250
61	5.5-6	1250	1250	1250	1250
62	5.5-6	1250	1250	1250	1250
63	5.5-6	1250	1250	1250	1250
64	5.5-6	1250	1250	1250	1250
65	5.5-6	1250	1250	1250	1250
66	5.5-6	1250	1250	1250	1250
67	5.5-6	1250	1250	1250	1250
68	5.5-6	1250	1250	1250	1250
69	5.5-6	1250	1250	1250	1250
70	5.5-6	1250	1250	1250	1250
71	5.5-6	1250	1250	1250	1250
72	5.5-6	1250	1250	1250	1250
73	5.5-6	1250	1250	1250	1250
74	5.5-6	1250	1250	1250	1250
75	5.5-6	1250	1250	1250	1250
76	5.5-6	1250	1250	1250	1250
77	5.5-6	1250	1250	1250	1250
78	5.5-6	1250	1250	1250	1250
79	5.5-6	1250	1250	1250	1250
80	5.5-6	1250	1250	1250	1250
81	5.5-6	1250	1250	1250	1250
82	5.5-6	1250	1250	1250	1250
83	5.5-6	1250	1250	1250	1250
84	5.5-6	1250	1250	1250	1250
85	5.5-6	1250	1250	1250	1250
86	5.5-6	1250	1250	1250	1250
87	5.5-6	1250	1250	1250	1250
88	5.5-6	1250	1250	1250	1250
89	5.5-6	1250	1250	1250	1250
90	5.5-6	1250	1250	1250	1250
91	5.5-6	1250	1250	1250	1250
92	5.5-6	1250	1250	1250	1250
93	5.5-6	1250	1250	1250	1250
94	5.5-6	1250	1250	1250	1250
95	5.5-6	1250	1250	1250	1250
96	5.5-6	1250	1250	1250	1250
97	5.5-6	1250	1250	1250	1250
98	5.5-6	1250	1250	1250	1250
99	5.5-6	1250	1250	1250	1250
100	5.5-6	1250	1250	1250	1250

**REVISIONS**

NO.	DATE	BY	DESCRIPTION
1			
2			
3			
4			
5			
6			
7			
8			
9			
10			
11			
12			
13			
14			
15			
16			
17			
18			
19			
20			
21			
22			
23			
24			
25			
26			
27			
28			
29			
30			
31			
32			
33			
34			
35			
36			
37			
38			
39			
40			
41			
42			
43			
44			
45			
46			
47			
48			
49			
50			
51			
52			
53			
54			
55			
56			
57			
58			
59			
60			
61			
62			
63			
64			
65			
66			
67			
68			
69			
70			
71			
72			
73			
74			
75			
76			
77			
78			
79			
80			
81			
82			
83			
84			
85			
86			
87			
88			
89			
90			
91			
92			
93			
94			
95			
96			
97			
98			
99			
100			

**SCALE** 1" = 10'

**PROJECT NO.** 12345

**DATE** 12/15/2023

**BY** J. D. Smith

**CHECKED** M. A. Jones

**APPROVED** K. L. Brown

### 3.1.8 Maryland

Maryland DOT has two standard debris fence designs. The first system has a radial curve at the top of the fence and is mounted on top of a 32-in. (813-mm) tall vertical parapet. The other design is not curved and is mounted on top of an F shape concrete parapet [9].

The radially-curved fence design is shown in Figures 14 and 15. The round vertical posts are 2½ in. (64 mm) nominal diameter, which are welded to base plates. Four ⅝-in. (16-mm) diameter bolts are used to attach the base plate to the top of the parapet. Four 1¼-in. (32-mm) nominal diameter, horizontal tube stiffeners are used for the fence frame. The fence is comprised of a #6 gauge mesh with a 2-in. (51-mm) gap opening connected to the frame with #9 gauge wire or double #13 gauge wire [9].

The vertical fence design is shown in Figures 16 and 17. Vertical posts were 2½-in. (64-mm) nominal diameter pipes welded to base plates and bolted to the top of the parapet with four ⅝-in. (16-mm) bolts. Two 1¼-in. (32-mm) nominal diameter horizontal tube stiffeners are attached to the post with saddle clamps. The fence is constructed with a #6 gauge mesh and a 2-in. (51-mm) gap opening. The chain link is then connected to the vertical and horizontal members of the system with #9 gauge wire or double #13 gauge wire [9].

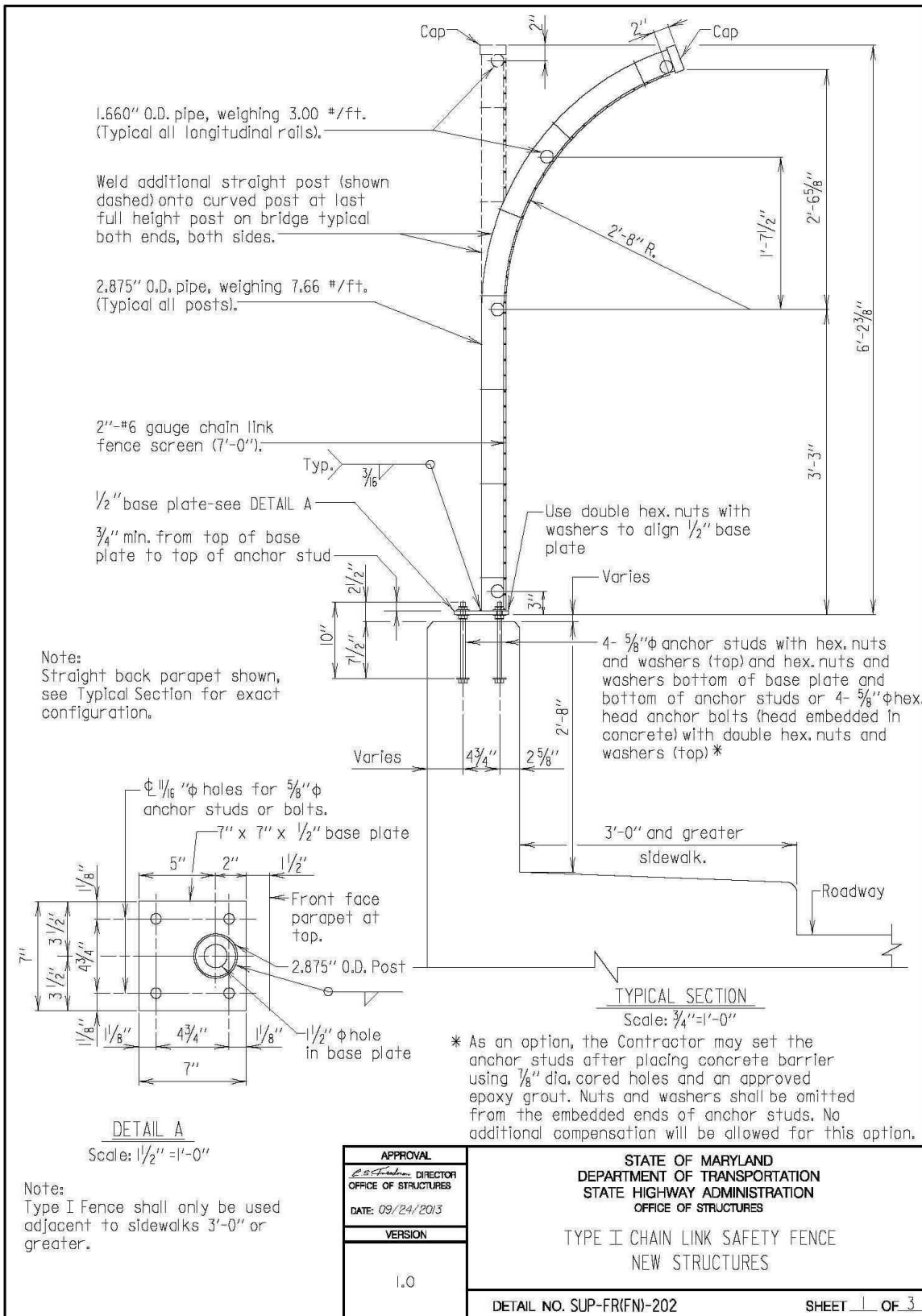


Figure 14. Maryland Type I Chain Link Safety Fence [9]

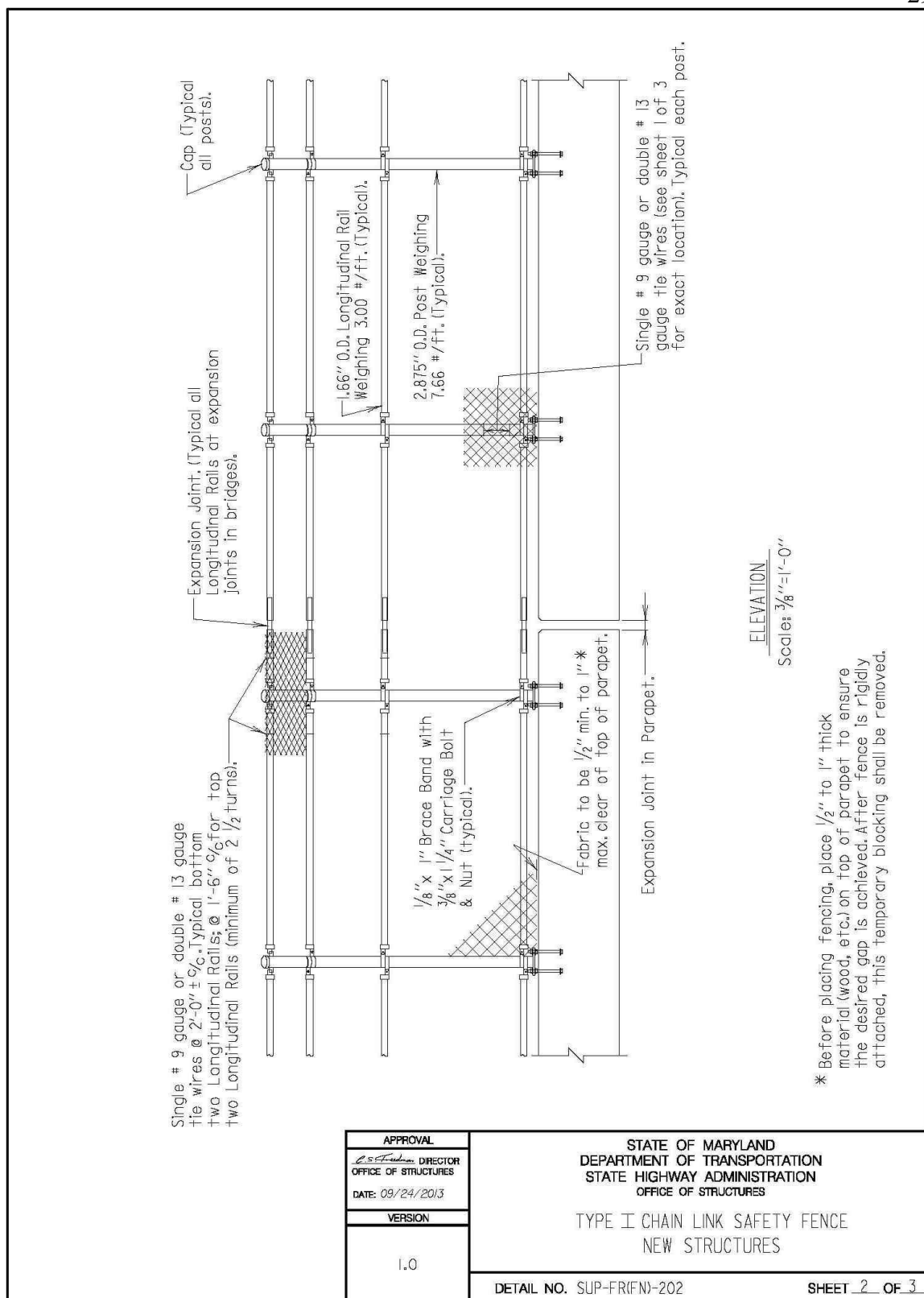


Figure 15. Maryland Type I Chain Link Safety Fence [9]

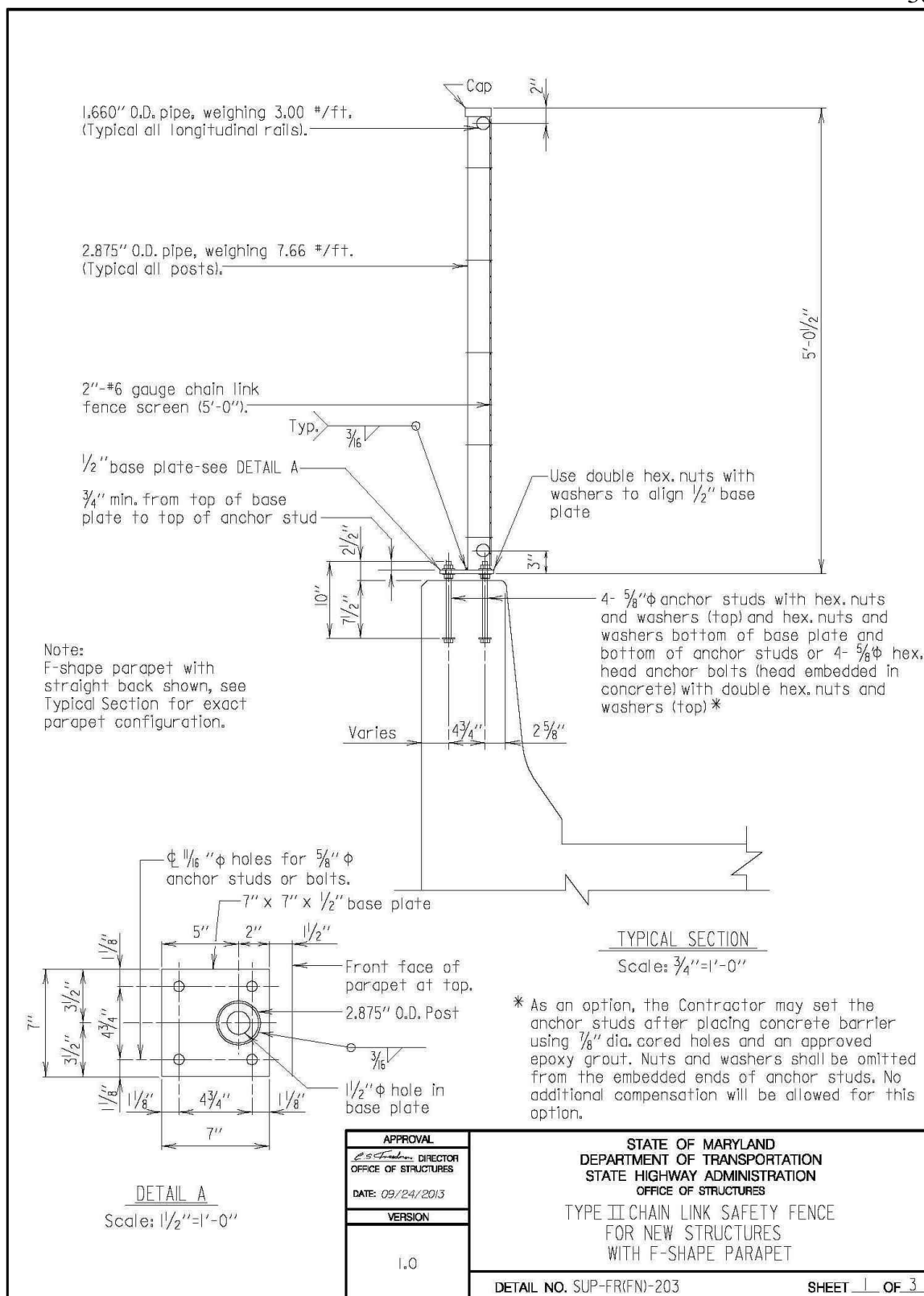


Figure 16. Maryland Type II Chain Link Safety Fence [9]

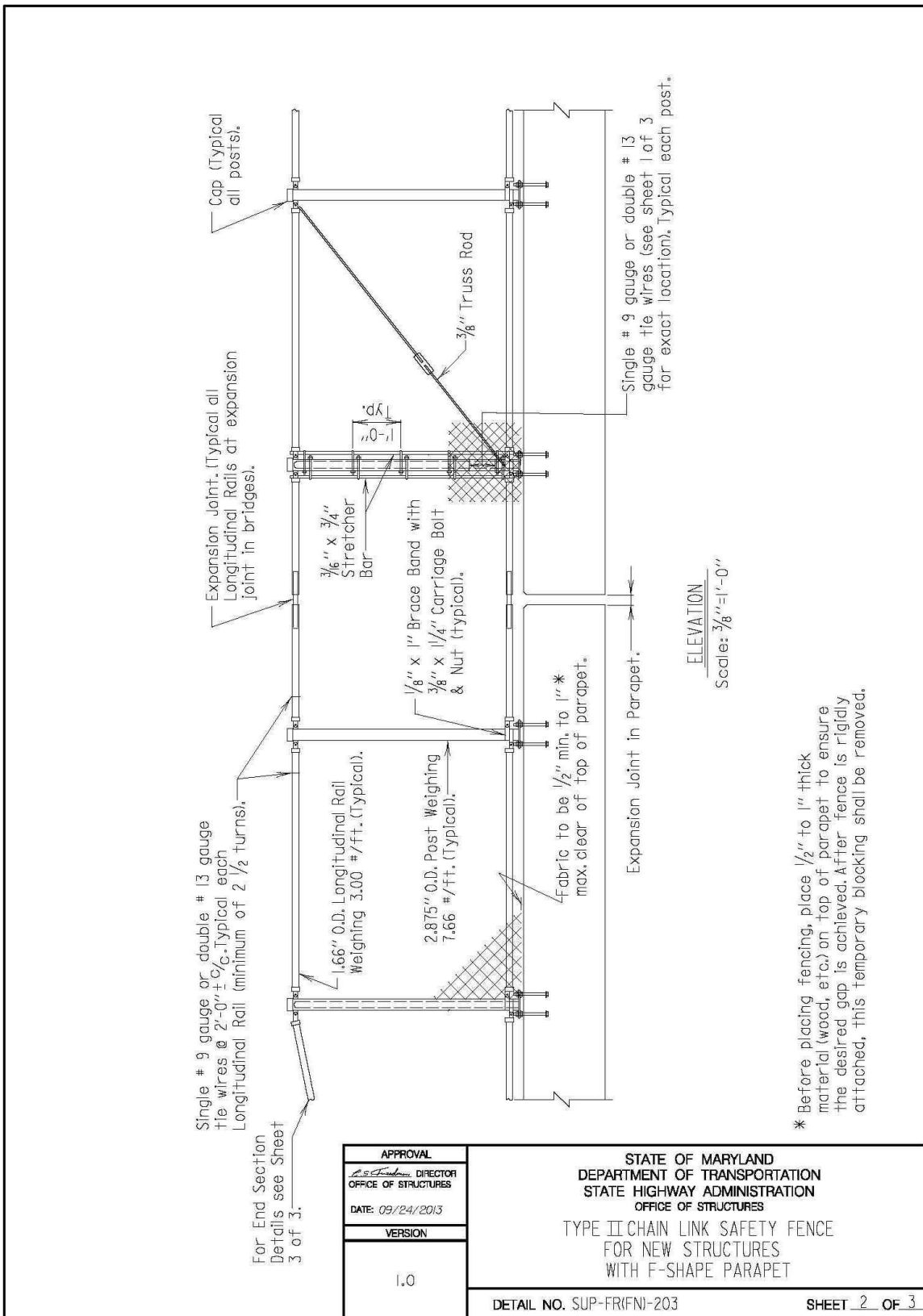


Figure 17. Maryland Type II Chain Link Safety Fence [9]

### 3.1.9 Minnesota

The Minnesota Department of Transportation (MnDOT) uses a debris fence mounted on top of a vertical concrete parapet. The concrete railing that is currently implemented in Minnesota can vary between 32 and 44 in. (813 and 1,118 mm) in height, depending on the application. The top of the parapet measures 15 in. (381 mm) wide, and the front face of the fence is placed at a minimum of 4½ in. (114 mm) away from the front of the concrete parapet, as is shown in Figure 18 [10].

The top-mounted fence structure contains a 6-ft (1.8-m) tall, chain-link wire mesh. Vertical posts, measuring 6ft-1 in. (1.9 m) long, with a nominal diameter of 2½ in. (64 mm), were placed on 10-ft (3.0-m) centers. Cylindrical, 1¼-in. (32-mm) nominal diameter tubes were used as longitudinal stiffeners along the bottom of the mesh and along the top at expansion joints. An additional 7-gauge, galvanized steel tension wire was located at the top of the fence for increased longitudinal support. This wire could also potentially prevent fence elements from falling off the parapet in a high wind loading or impact event. A baseplate is used to connect the vertical posts to the concrete parapet. The wire mesh is connected to the members and tension wire with vinyl coated fabric ties. Additional details are shown in Figure 19 [10].



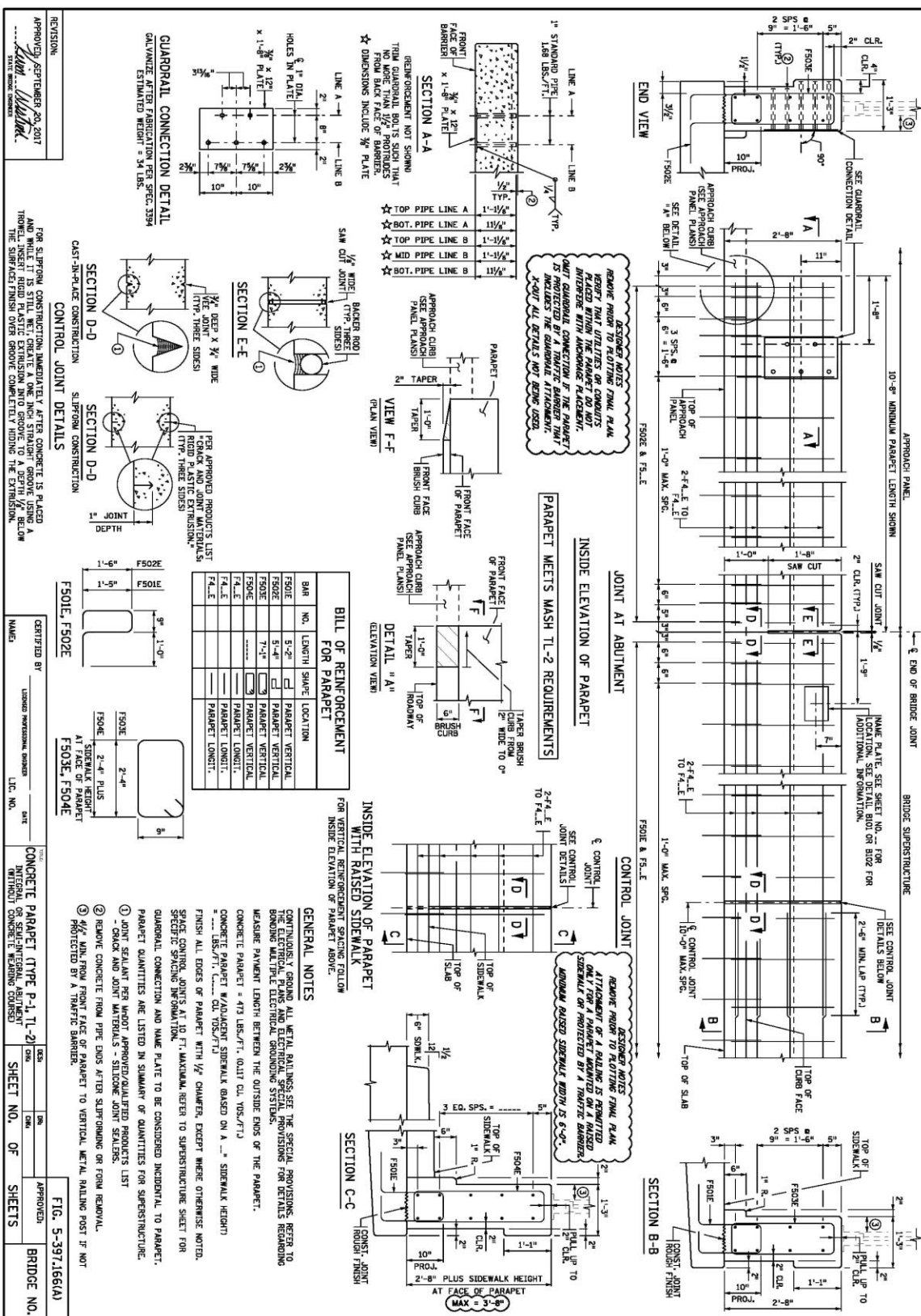


Figure 18. Minnesota Concrete Parapet Type P-1 [10]

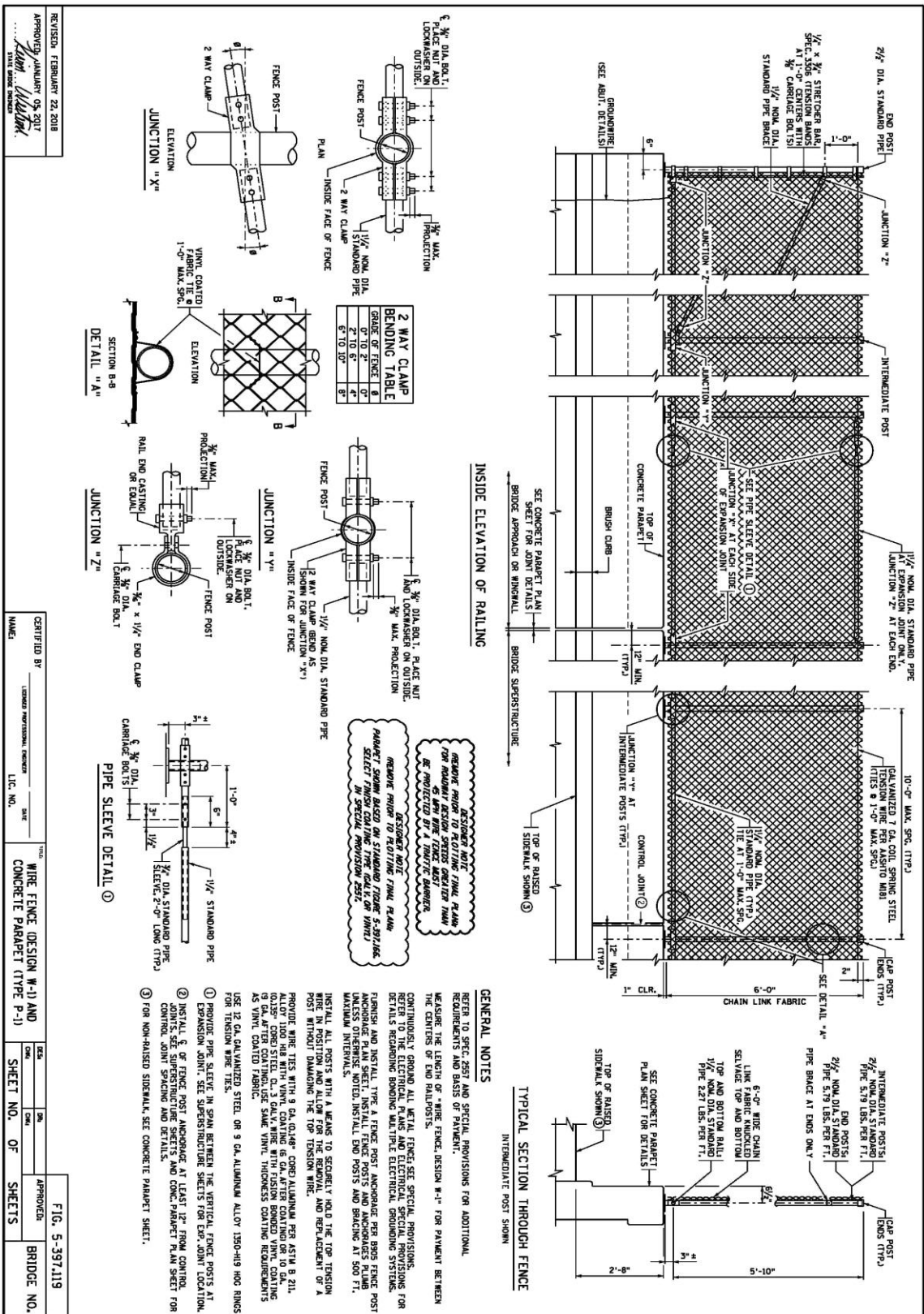


Figure 19. Minnesota Wire Fence Design W-1 [10]

### 3.1.10 Nebraska

The Nebraska Department of Transportation (NDOT) currently utilizes two different fence designs for debris protection over railway overpasses. Both of these fence designs are used in conjunction with a concrete parapet bridge rail. This concrete bridge rail parapet is shown below in Figure 20 [11].

One of the fence designs used by Nebraska contains a vertical 6-ft (1.8-m) tall, galvanized chain-link fence, with knuckled selvage at the top and bottom, mounted to the top of a concrete parapet with a base plate. The fence is placed at the centerline of the parapet, 7 in. (178 mm) back from the front face. Vertical posts, are 6-ft (1.8-m) long cylindrical tubes and are spaced 8 ft (2.4 m) on center along the top of the parapet and have a nominal diameter of 3 in (76 mm). The bottom of the vertical posts are connected to a base plate that is bolted to the top of the concrete parapet using ½-in. (13-mm) diameter U-bolts. This design also contains three, 1¼-in. (32-mm) diameter longitudinal stiffeners extending between the vertical posts. This fence design is shown in Figure 21 [11].

Nebraska also utilizes a back-mounted, 7-ft (2.1-m) tall, debris fence system with galvanized chain-link fence. The vertical posts of the system, measuring 8 ft-10½ in. (2.7 m) in length, are spaced 8 ft (2.4 m) on center and have a nominal diameter of 3 in. (76 mm). The bottom of the post attaches into a bent plate that connects to the parapet through two ½-in. (13-mm) diameter bolts. Three, 1¼-in. (32-mm) pipe stiffeners are used to secure the chain link fabric and provide horizontal support. This fence design is shown in Figure 22 [11].

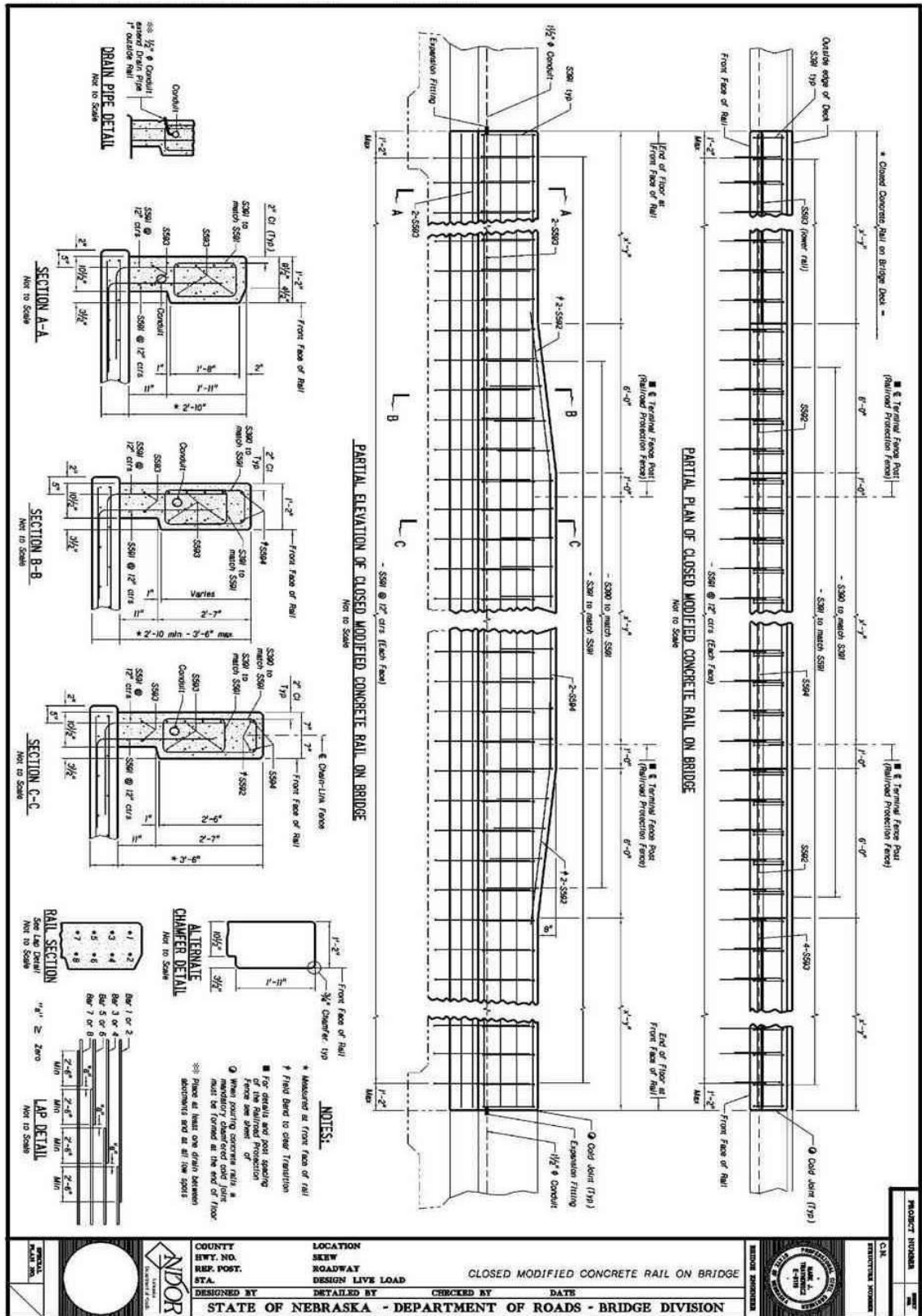


Figure 20. Nebraska Closed Concrete Rail Bridge Deck [11]

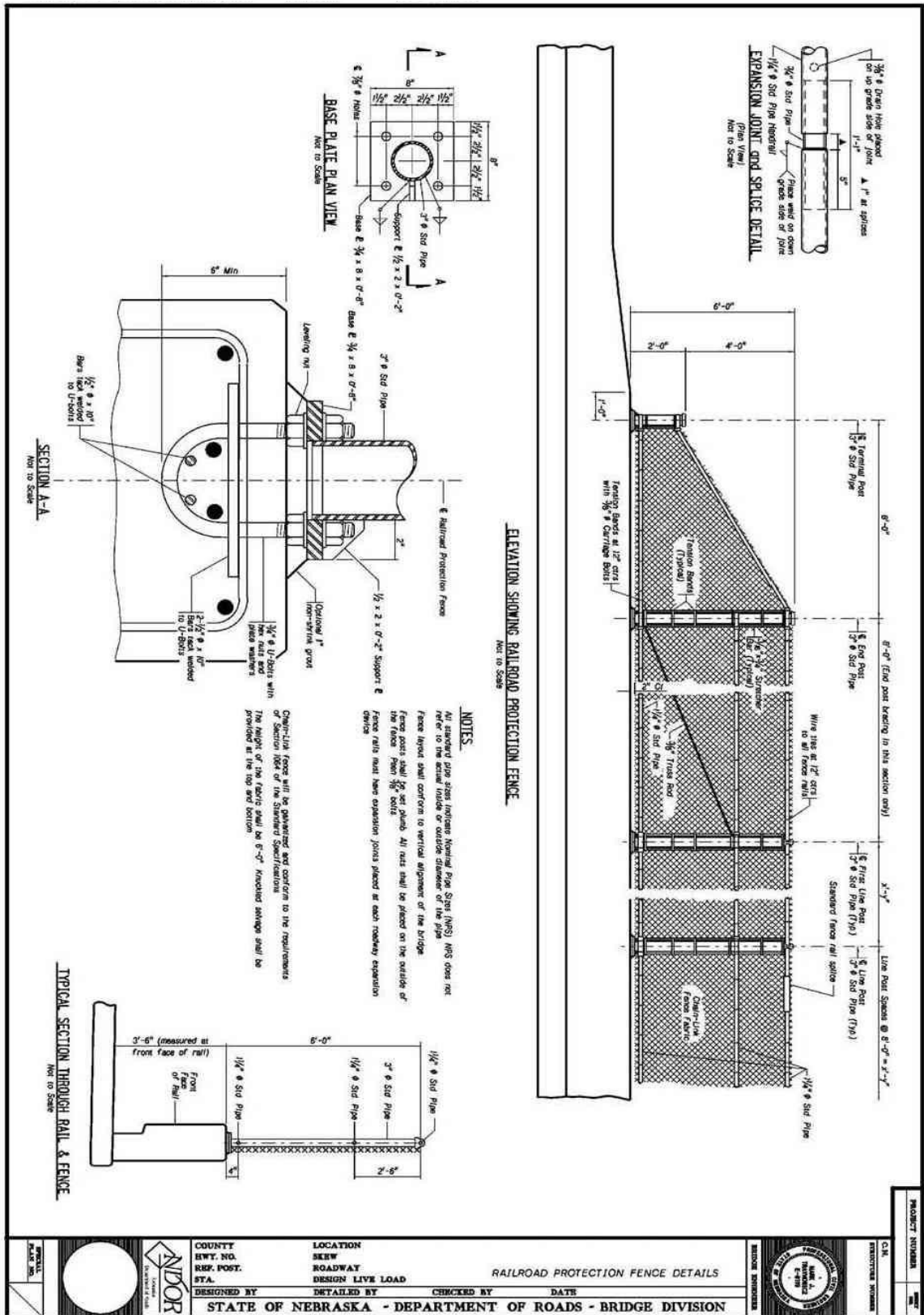


Figure 21. Nebraska Railroad Protection Fence Details [11]



### 3.1.11 New Jersey

New Jersey DOT uses a curved fence mounted on top of a 32-in. (813-mm) tall vertical parapet. The curved fence is constructed using 2-in. (51-mm) square vertical posts and connected with four 1.5-in. (38-mm) square horizontal stiffeners. Each vertical member is connected to a baseplate that is anchored to the parapet using two  $\frac{3}{4}$ -in. (19-mm) diameter corrosion resistant steel bolts. The structural members are connected to a 1-in. (25-mm) gap size diamond mesh with fabric ties spaced every 6 in. (152 mm) for the horizontal stiffeners and every 12 in. (305 mm) for the vertical posts. The geometric details of this design are shown in Figure 23 [12].





### 3.1.12 New York

The New York State Department of Transportation (NYSDOT) uses a vertical fence mounted directly on the back of either a 34-in. (864-mm) tall, safety-shape barrier or a 42-in. (1,067-mm) tall, vertical barrier. The design utilizes 2½-in. (89-mm) nominal diameter pipes spaced in 10 ft (3 m) increments. The posts are attached to the back of the parapet with two clamps and four ¾-in. (10-mm) diameter bolts. Three 1⅝-in. (41-mm) outside diameter horizontal stiffeners are evenly spaced at 2½ ft (0.76 m). The fence uses a 1-in. (25-mm) gap opening, diamond chain-link wire mesh made with 11-gauge wire. The system design is shown in Figure 24 [13].



### 3.1.13 Oregon

Oregon DOT currently utilizes a vertical pedestrian fence mounted on the back of an F-shape concrete bridge rail and a curved pedestrian fence mounted on the back of a vertical bridge rail [14].

Posts in the vertical fence design are 3½-in. (89-mm) nominal diameter tubes spaced 10 ft (3 m) on center. These posts are connected to the backside of the bridge rail with two clamps, which are fastened to the rail with ¾-in. (19-mm) diameter bolts. Two horizontal stiffeners consist of 1 ¼-in. (32-mm) diameter tubes, one located at the top and one located at the bottom. The stiffeners are connected to a 2-in. (51-mm) gap, diamond chain-link fence. This fence design is shown in Figure 25, which is labeled as a Type C Fence Section. Connection details are shown in Figure 26.

The curved fence design contains vertical posts made of 4-in. (102-mm) nominal diameter tubes spaced at a maximum of 10 ft (3 m) apart. These posts are connected to the backside of the bridge rail with two clamps, which are anchored to the concrete with ⅝-in. (16-mm) diameter bolts. Four horizontal stiffeners composed of 1¼-in. (32-mm) diameter tubes are used along the length of the system. The stiffeners are connected to a 2-in. (51-mm) gap, chain-link fence. This fence design is shown in Figure 25, and is labeled as a Type A Fence Section. Connection details are shown in Figure 26 [14].

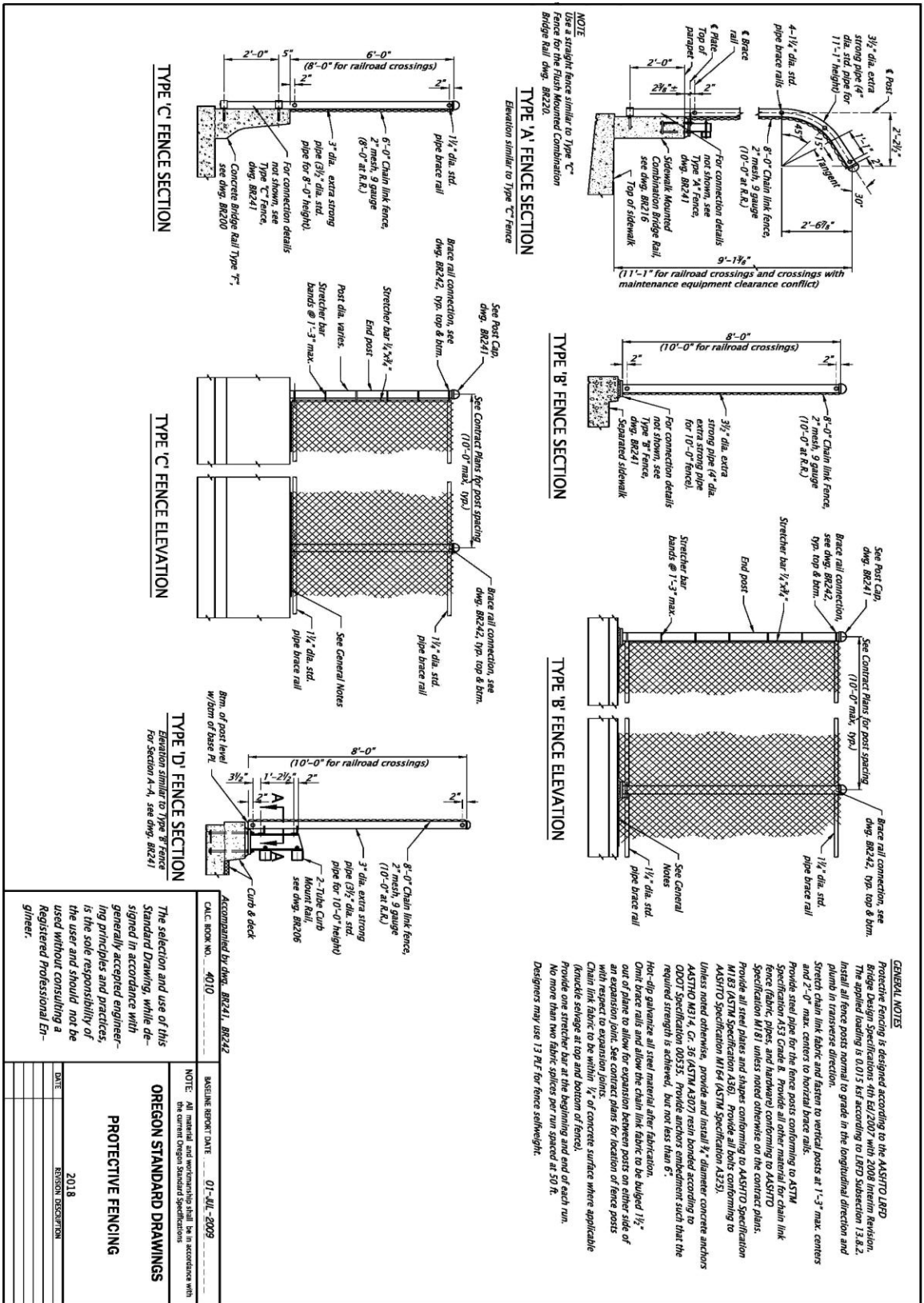


Figure 25. Oregon Pedestrian Fence [14]

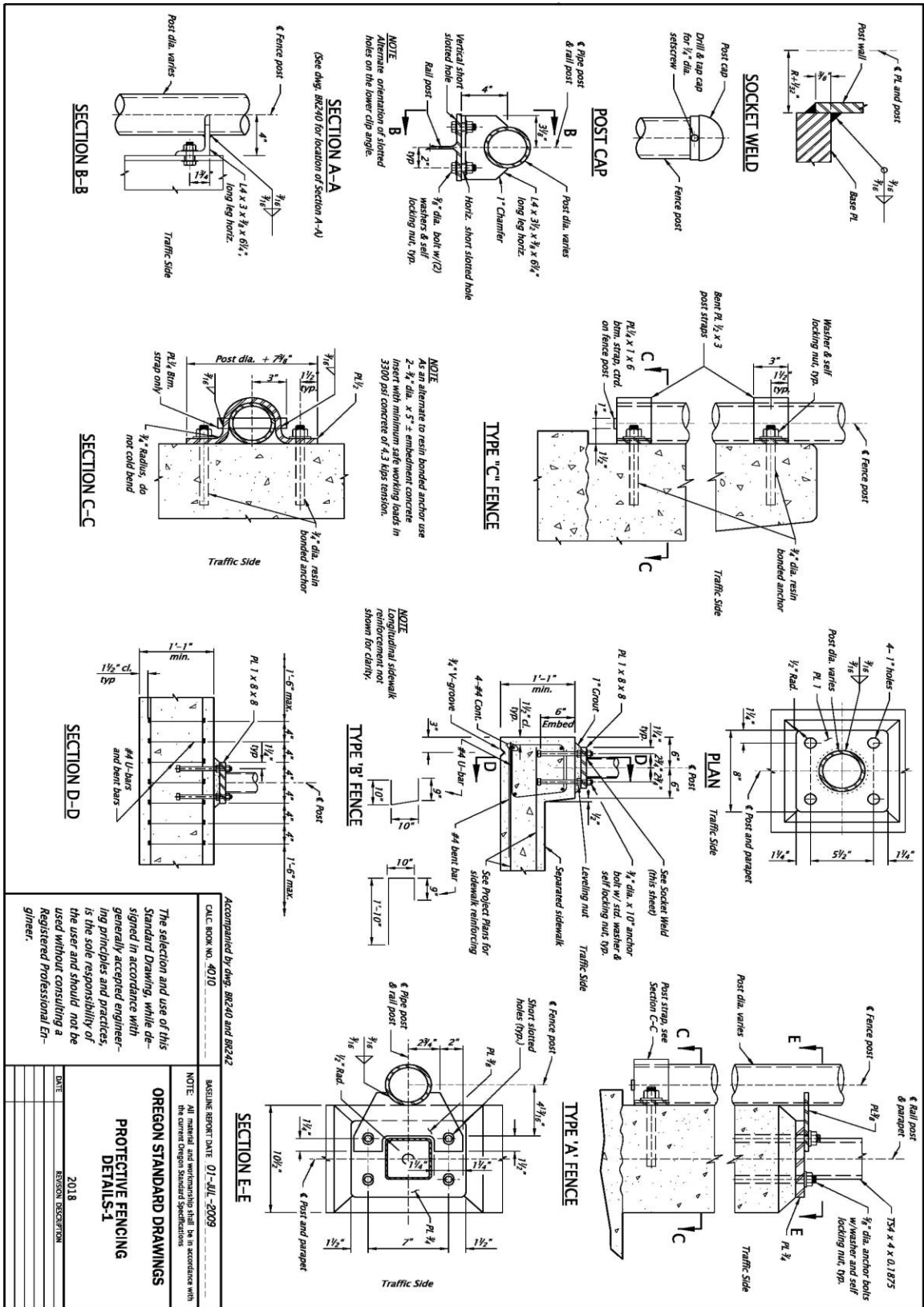


Figure 26. Oregon Protective Fencing Details [14]

### 3.1.14 Texas

The Texas Department of Transportation (TxDOT) utilizes a debris fence mounted to the back of a concrete bridge rail. The Texas T211 vertical concrete parapet or the Texas T551 safety shape concrete parapet are recommended for the debris fence.

Vertical posts consisting of 3½-in. (89-mm) nominal diameter pipes are spaced 8 ft (2.4 m) on center. The vertical posts are connected to the backside of the concrete parapet with a clamp and two ⅝-in. (16-mm) diameter bolts, and a third ⅝-in. (16-mm) diameter bolt attached the post to the barrier directly. One horizontal stiffener is also used, which consists of 1¼-in. (32-mm) nominal diameter pipes threaded through sleeves mounted on the top of the posts. The frame is constructed from 9-gauge steel fabric with a 2-in. (51-mm) diamond gap opening, and it is attached to the posts and stiffeners using 9-gauge steel wire ties. Along the bottom edge of the chain-link fence, a tensioned wire is attached to the fence using wire ties. The debris fence and concrete parapet are shown in Figures 27 and 28 [15].

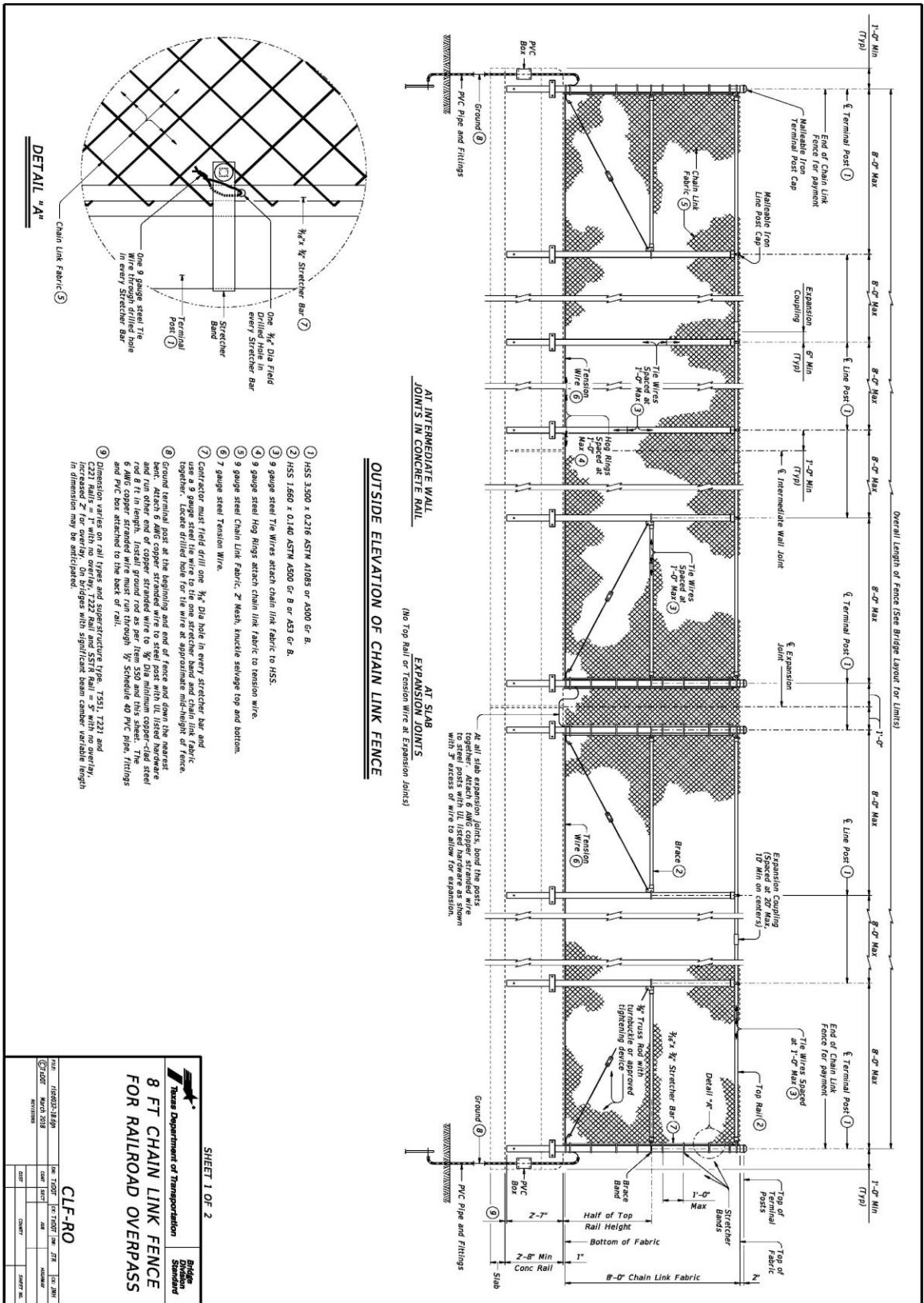


Figure 27. Texas 8 ft Chain Link Fence for Railroad Overpass [15]

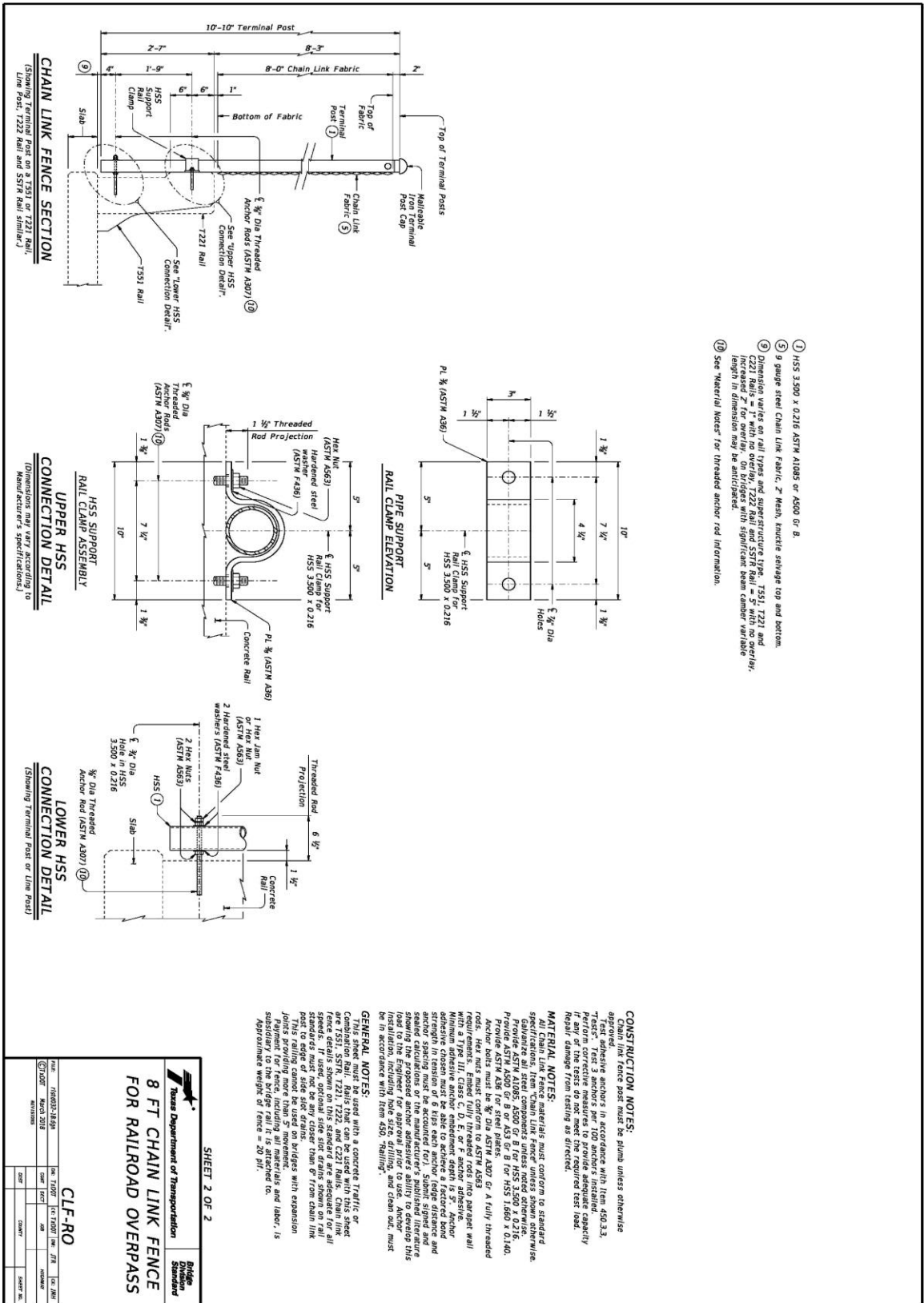


Figure 28. Texas 8 ft Chain Link Fence for Railroad Overpass Details [15]



### 3.1.15 Wisconsin

The Wisconsin DOT utilizes an angled fence mounted on top of a 32-in. (813-mm) tall, vertical concrete parapet. The debris fence is mounted in the middle of the parapet, 3 in. (76 mm) behind its front face.

The vertical posts are composed of 2-in. (51-mm) nominal diameter tubes and are spaced 10 ft (3 m) on centers. The posts are welded to base plates, which are attached to the top of the parapet using two ½-in. (13-mm) diameter anchor bolts. Three 1¼-in. (32-mm) nominal diameter horizontal stiffeners are attached to the vertical posts using saddle clamps. The fence is constructed from 9-gauge, 2-in. (51-mm) gap opening, diamond mesh, chain-link fence attached to the posts and stiffeners with 9-gauge wire ties spaced approximately 12 in. (305 mm) apart. The system and connection details are shown in Figure 29 [16].



### 3.2 Full-Scale Crash Test (TTI Test No. 42070-6)

#### 3.2.1 System and Testing Details

In August of 1995, the Texas Transportation Institute (TTI), located at Texas A&M University (TAMU), published a report titled *Crash Testing and Evaluation of Retrofit Bridge Railings and Transitions* [17]. This research report contained findings from the completion of full-scale crash tests completed at TTI. Test no. 42070-6 was conducted to determine the safety performance of a vandal protection fence mounted on top of a New Jersey concrete barrier [17].

The full-scale crash test was conducted according to the AASHTO *Guide Specifications for Bridge Railings* Performance Level 2 (PL-2) criteria [18]. A 1991 Ford F250 pickup truck with a test inertial weight of 5,397 lb (2,448 kg) impacted the concrete barrier and vandal protection fence at 62.8 mph (101 kph) and at 20.2 degrees approximately 33 ft (10.1 m) downstream from the beginning of the system [17].

The New Jersey barrier used in this full-scale crash test extended 100 ft (30.5 m) in length. The parapet had a height of 32 in. (813 mm), a thickness of 15 in. (381 mm) at the base, and tapering up to a minimum of 6 in. (152 mm) at the top. The barrier was reinforced with eight ½-in. (13-mm) longitudinal bars and multiple ⅝-in. (16-mm) vertical stirrups, spaced at 8-in. (203-mm) increments [17].

A vandal protection fence was connected onto the back of the New Jersey barrier. The fence was 6-ft (1.8-m) tall. Vertical posts were 2½-in. (64 mm) nominal diameter tubes measuring 7.3-ft (2.2-m) long and were spaced 10 ft (3.0 m) on center. Posts were connected to the back of the parapet with two saddle clamps and anchored with ⅝-in. (16-mm) diameter bolts. Between the vertical posts, three horizontal stiffeners were used

to provide shear continuity and had outside diameters of  $1\frac{5}{8}$  in. (41 mm). The horizontal stiffeners were connected to the 1-in. (25-mm) gap, diamond mesh with wire ties. CAD details and pretest photos of the system are shown in Figures 30 through 32 [17].

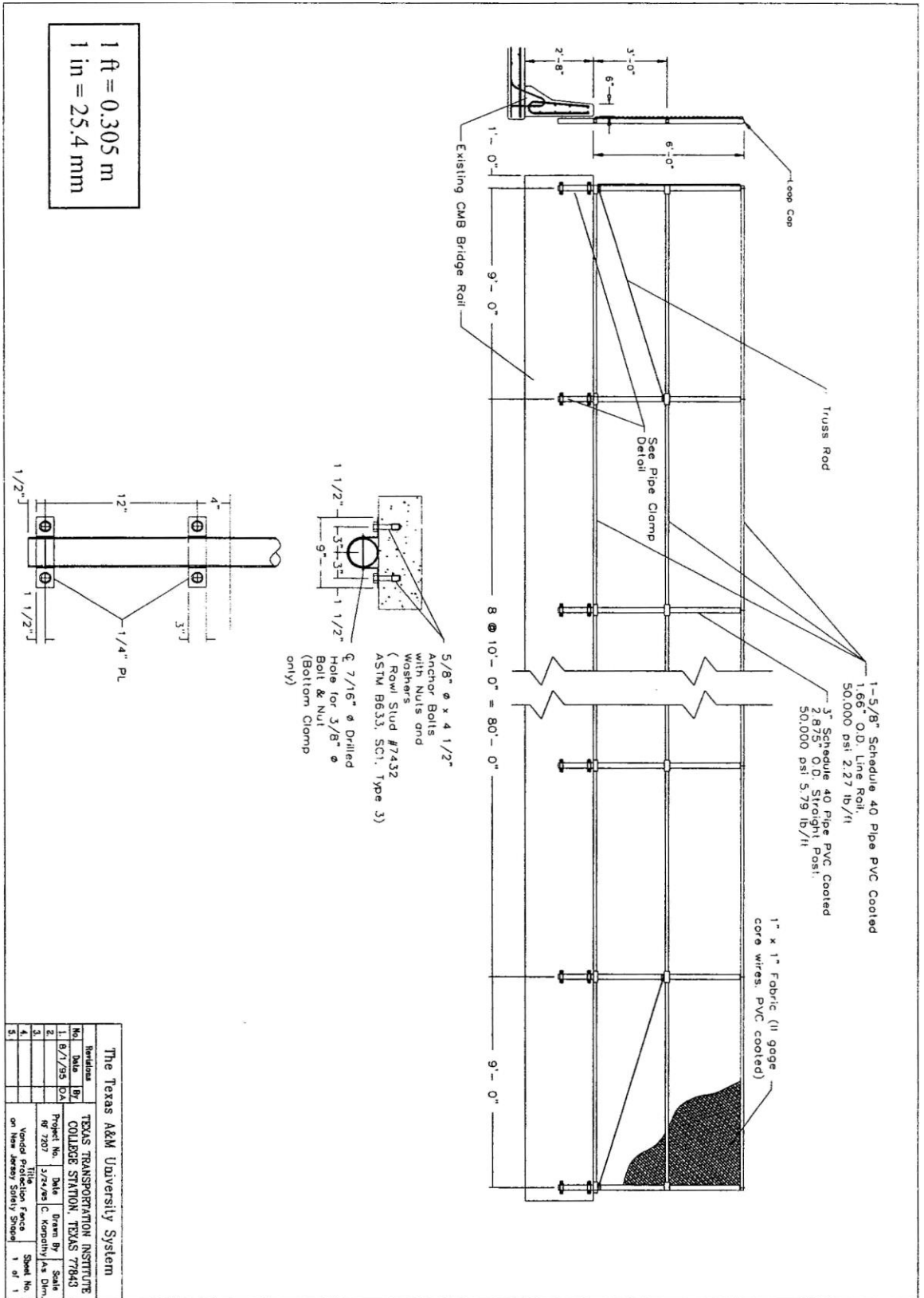


Figure 30. Vandal Protection Fence Details [17]

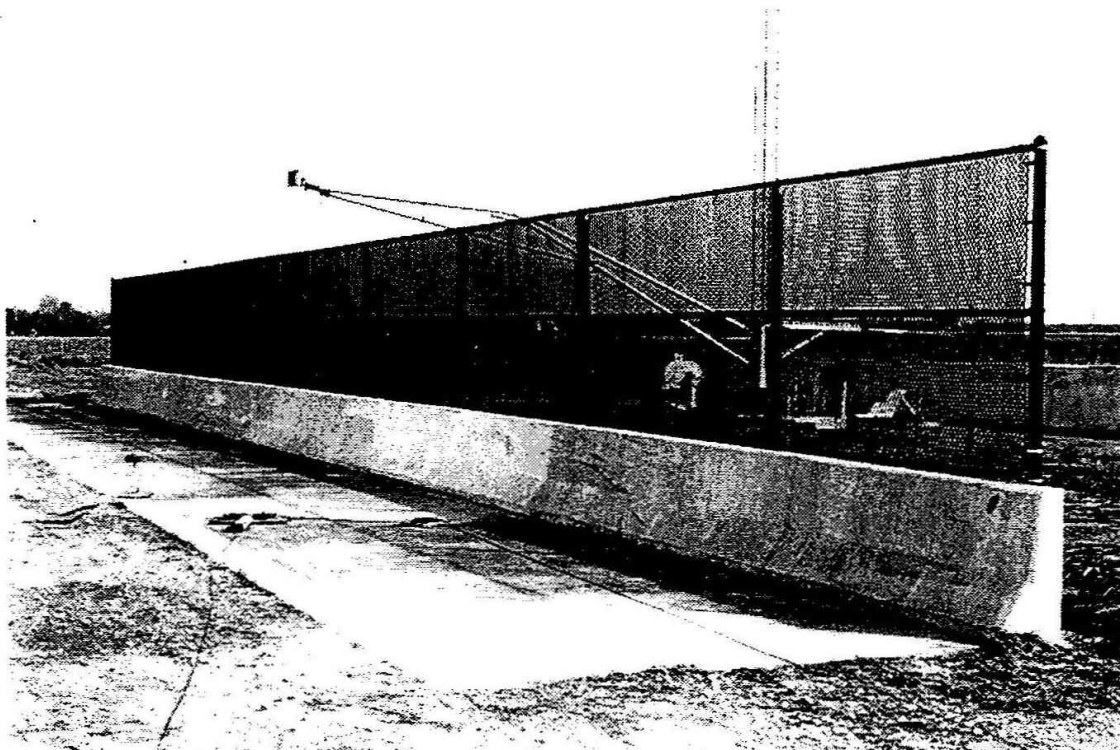
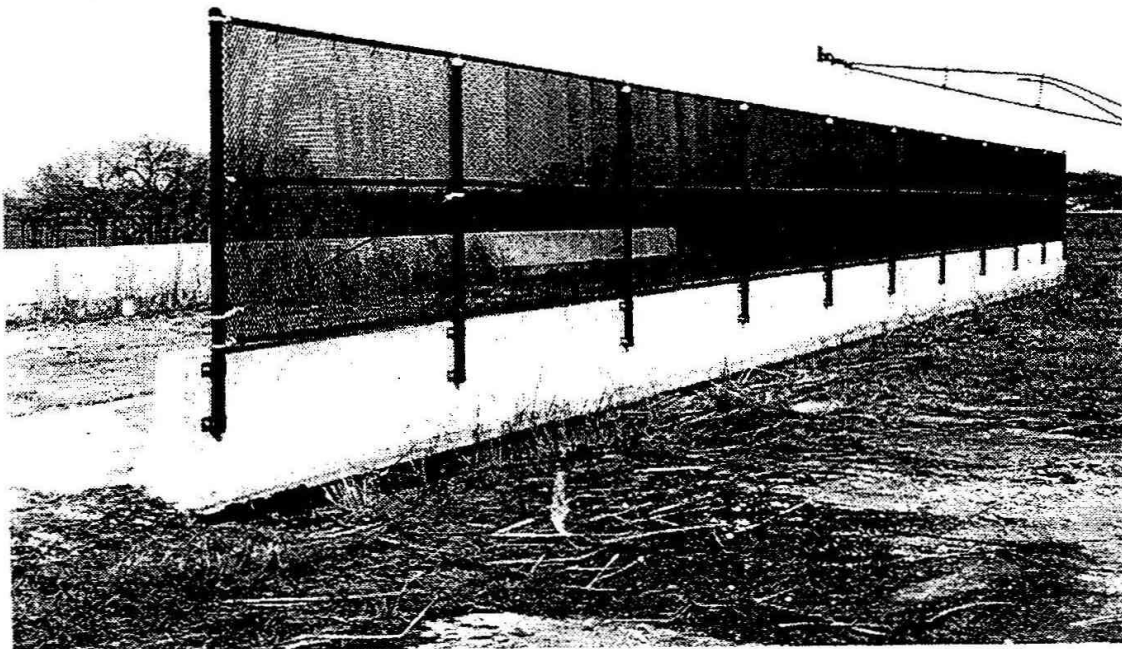


Figure 31. Pretest Parapet and Fence Details [17]

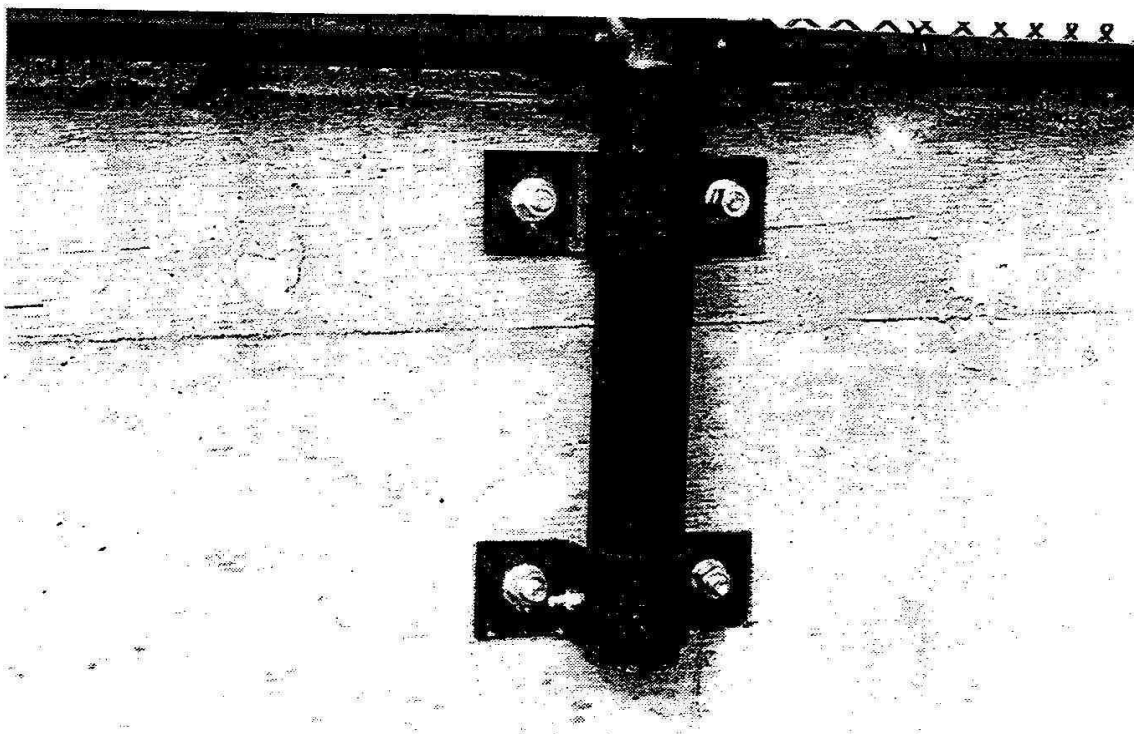
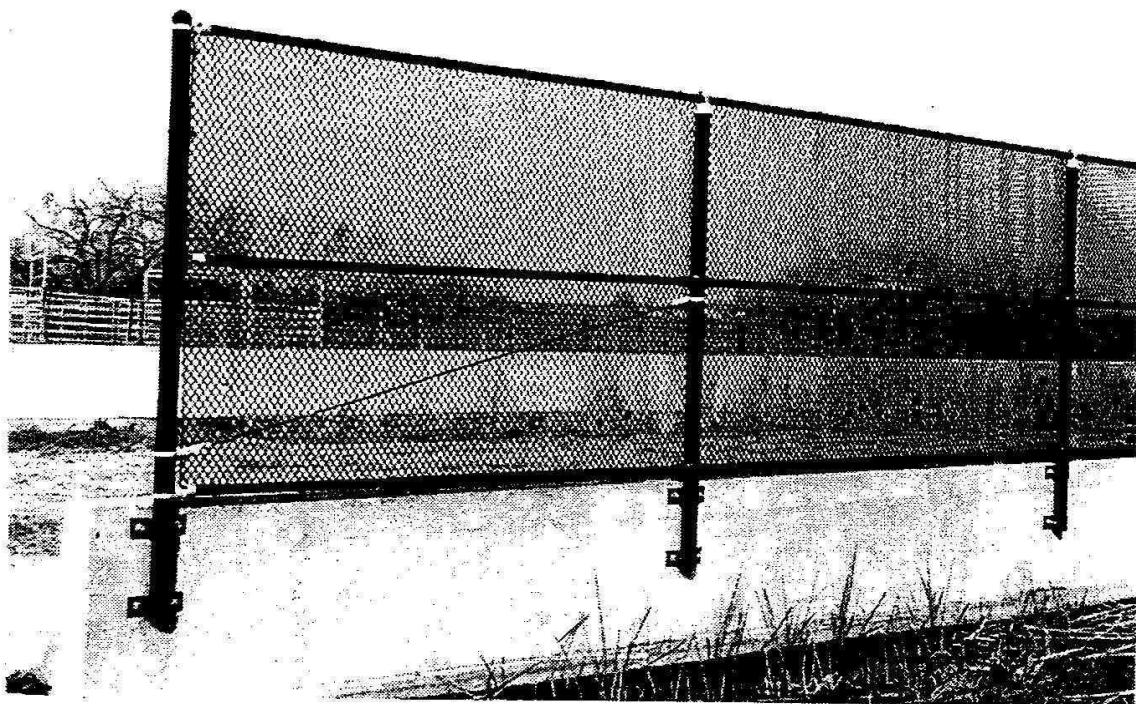


Figure 32. Pretest Fence and Connection Details [17]

### 3.2.2 Test Results

Test no. 42070-6 consisted of a 1991 Ford F-250 pickup truck impacting the New Jersey shape concrete barrier with vandal protection fence at a speed of 62.8 mph (101 kph) and a 20.2 degree angle. All occupant safety risk values were within acceptable limits found in the AASHTO PL-2 standards. The test vehicle was safely redirected and test results were deemed successful. The length of contact spanned 17 ft (5.2 m) downstream from the point of impact, and the test vehicle exited the system at 49.5 mph (80 kph) and at an angle of 4.4 degrees. After the vehicle left the barrier, it came to rest 91 ft (27.7 m) downstream from the initial impact point. Overall, the vehicle received minimal damage, which included bending of the stabilizer bar, floor pan, frame, and front axle on the right side of the vehicle. In addition to this localized bending, the windshield was cracked [17].

The system experienced minimal damage during the full-scale crash test. The lower edge of the chain-link wire was pushed behind the lower horizontal member between post nos. 5 and 6. Also, the middle horizontal member disconnected on the upstream side at post no. 5. Researchers determined that the presence of the fence itself did not result in an adverse safety performance. Post-test damage photos are shown in Figure 33, and a summary of the test results is shown in Figure 34 [17].



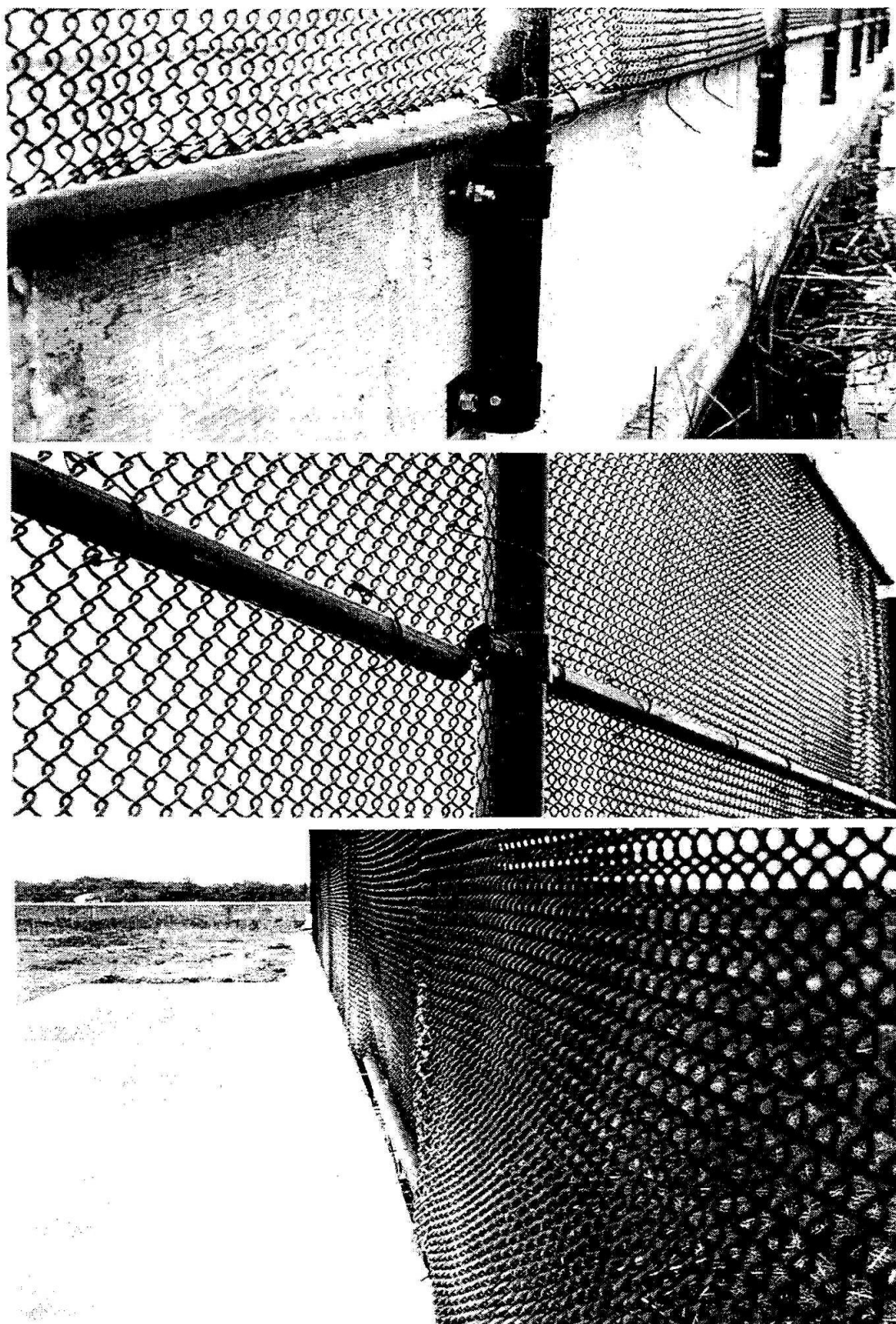


Figure 33. Post-test Fence Damage [17]

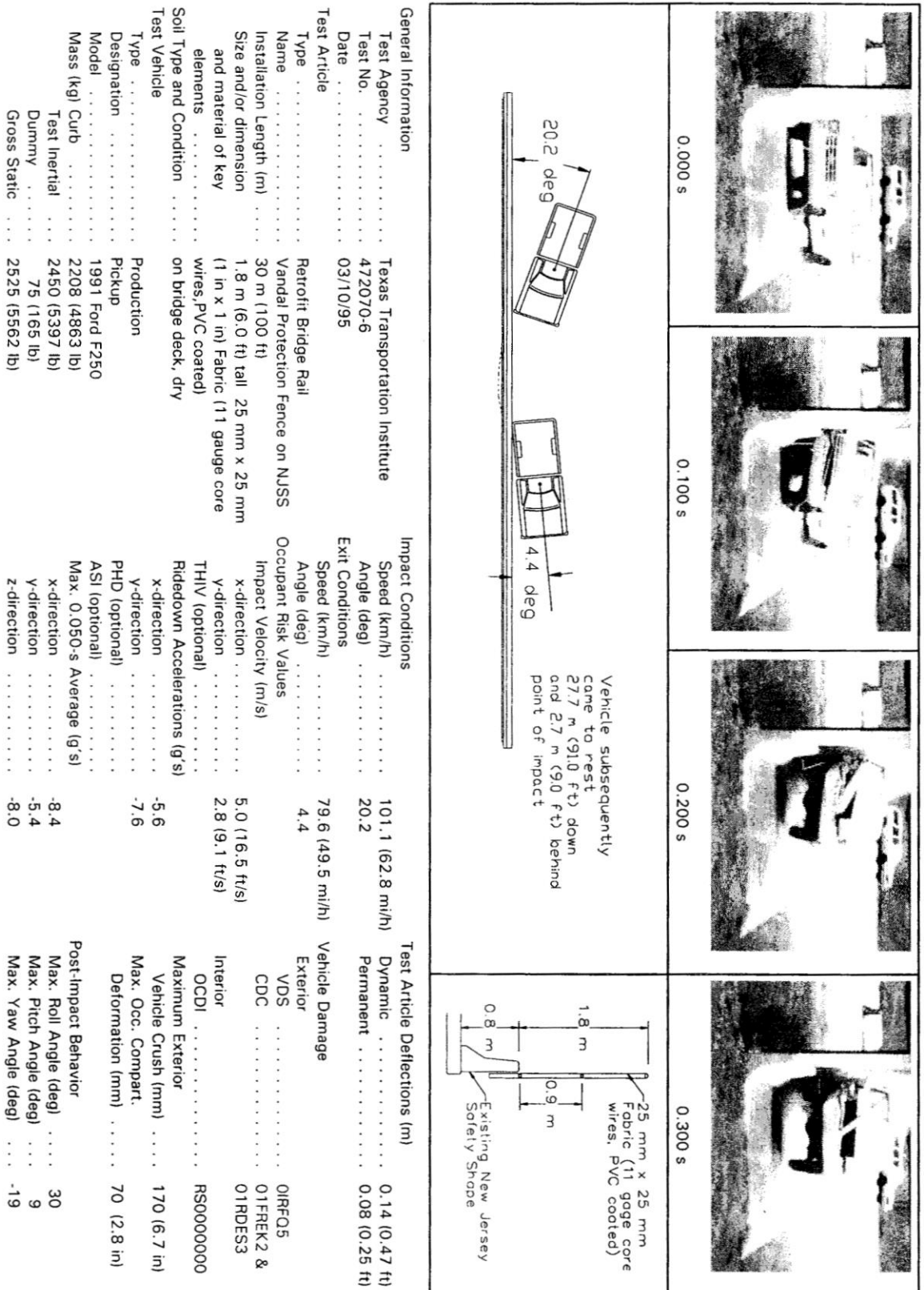


Figure 34. Summary of Test Results [17]

### **3.3 Minnesota Combination Traffic-Bicycle Bridge Rail**

In 1998, Midwest Roadside Safety Facility published a report about the design and crash tests of a bicycle bridge rail for the Minnesota Department of Transportation. Two full-scale crash tests were performed on this design, as shown in Figures 35 through 37, which was deemed acceptable in accordance with requirements dictated by NCHRP Report No. 350 [19].

The test construction included two cables placed within the tubular rails to prevent detachment of large pieces of debris from causing hazardous conditions to vehicles and or behind pedestrians below and/or behind the bridge. The usage of cables to prevent the detachment of large pieces of the bicycle rail structure may be beneficial as a means of containing debris produced during large truck impacts with the debris fence. This idea will need to be utilized with the design; since, there is a very high chance that pieces of the structure will break and fall onto the railway tracks under impact scenarios.

The test construction also tapered the two cables down to the backside of the rail. This configuration allows the cables to be terminated safely and moves the tensioning components to the backside of the rail and farther away from any impacting vehicles.



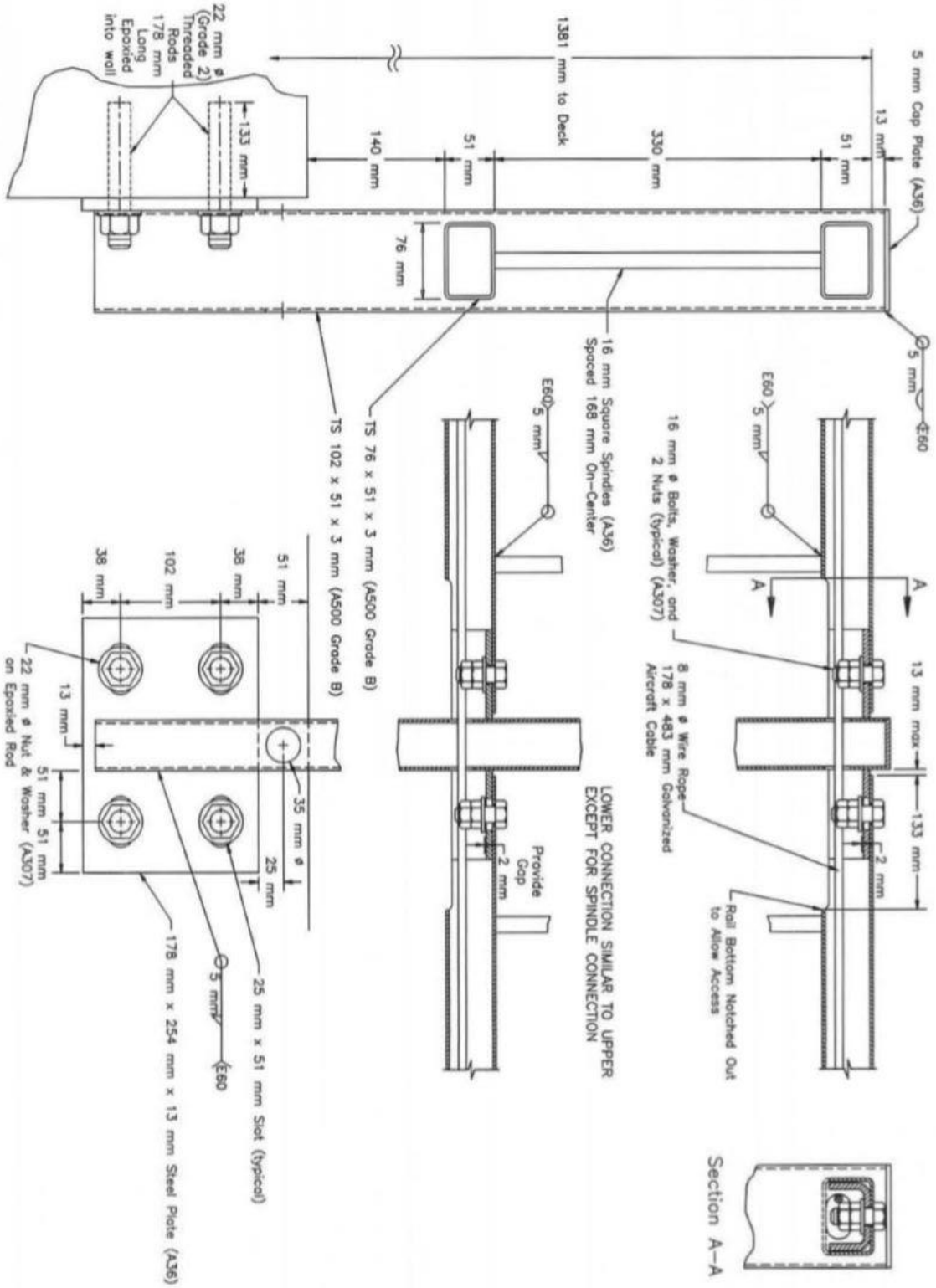


Figure 36. Minnesota Combination Traffic-Bicycle Bridge Rail Design Details



Figure 37. Tension Cable Taper and Rail Design

### 3.4 Caltrans Barrier Mounted Sign and Signpost

In 2011, Caltrans published a report detailing a full-scale crash test of a barrier mounted sign and signpost. One full-scale crash tests were performed on this design, as shown in Figures 38 and 39. The barrier redirected the vehicle but the impact created a high risk to occupants and was not deemed acceptable in accordance with requirements dictated by NCHRP Report No. 350 [20].

The sign post consisted of a 108-in. (2748-mm) tall post with a 4.0-in. (102-mm) outside diameter. The sign configuration consisted of two rectangular 36 in. (914 mm) by 60 in. (1524 mm) panels placed back to back. The post was mounted to the barrier through the usage of a  $\frac{3}{8}$ -in. (10-mm) thick saddle, connected with two 1.0 in. (25 mm) bolts.

The structural adequacy and vehicle trajectory for the test were deemed acceptable but the occupant risk was deemed unacceptable. The hood penetrated the windshield and would have covered the occupants in glass in a real world crash scenario. Additionally, the front grill broke off during the test and would have been a large hazard to the opposing traffic lanes.

This sign and post configuration was well within the impacting vehicles ZOI. This failed test demonstrates the importance of moving any barrier attachments as far out of the ZOI as possible.



Figure 38. Barrier Mounted Sign Test Article



Figure 39. Barrier Mounted Sign Vehicle Impact



### **3.5 Real-World Crashes**

Parapet-mounted fences are common throughout the United States, but because of the lack of previous full scale crash data, their safety performance during real impacts has not been determined. In an attempt to understand the real-world performance of these devices, three different anecdotal vehicular impact events were analyzed.

#### **3.5.1 Ohio Vandal Protection Fence Crash**

An article published on April 5, 2018 describes an impact between a vehicle and a fence mounted on a parapet on the Valley View Bridge in Valley View, Ohio. The impact event began when a vehicle on the bridge lost control and careened across multiple lanes and impacted another vehicle that was heading in the same direction. The second vehicle then was pushed into the bridge and fence system [21].

The vertical posts of the fence were anchored directly into the top of the parapet, and the fence structure extended 10 ft (3 m) above the concrete. One horizontal stiffener was placed in the middle, 5 ft (1.5 m), above the parapet. The article states that it is believed that if the vandal protection fence wouldn't have been there, the vehicle would have most likely plummeted more than 200 ft (70.0 m) off of the bridge. The individual who impacted the barrier was taken to the hospital for minor injuries [21].



Figure 40. Valley View Vandal Protection Fence Crash [21]

### 3.5.2 NASS Crash Data

The National Highway Transportation Traffic Safety Administration (NHTSA) compiles information regarding vehicular crashes within the United States. This resource was used to locate two real-world crashes between motor vehicles and parapet-mounted containment fences.

One such impact event occurred in April 2014 between a motor vehicle and a parapet-mounted fence located in the median. The vehicle was travelling approximately 59.5 mph (95.8 kph) at an angle of 15 degrees when it departed the travelled way and impacted the parapet and fence combination, as shown in Figure 41. The vehicle then careened across the road and impacted another traffic barrier on the other side. During this event, the vehicle did not override the parapet and interact with the fence, which resulted in no vehicle snagging. Overall, the parapet damage was minimal, but the vehicle damage was extensive, as shown in Figure 42, which was concentrated on the front

passenger side of the vehicle. It is believed that damage was related to the second impact event [22].



Figure 41. View of Barrier at Point of Impact [22]

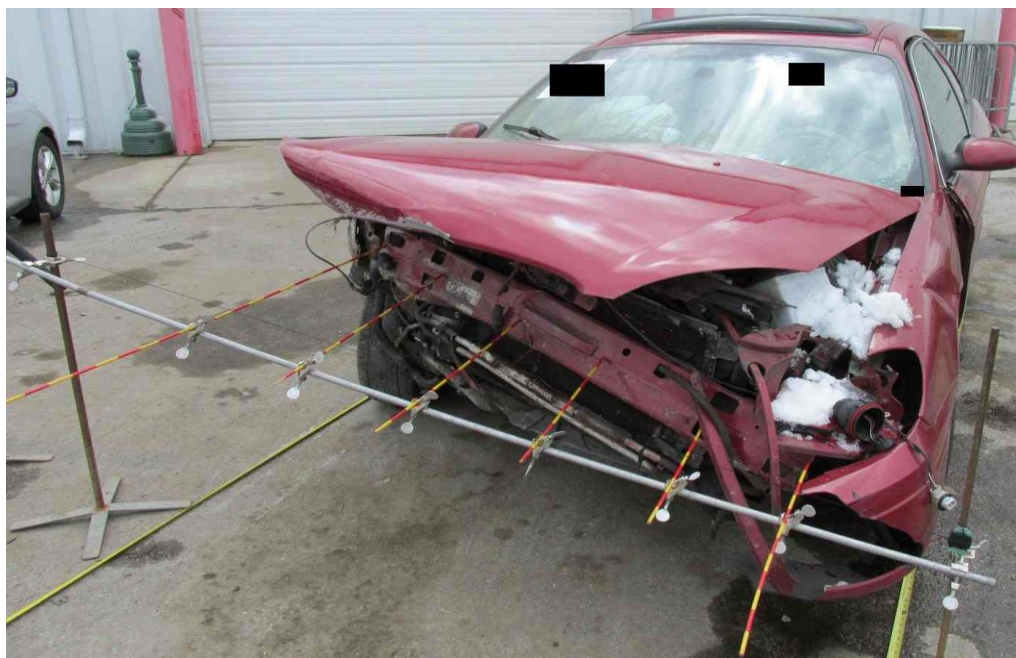


Figure 42. Vehicle Damage [22]

Another event consisted of a crash with a sequence of hazards, where the most severe was a concrete barrier arrangement. Vehicle speed at the point of impact was estimated to be 41 mph (66.0 kph), and the impact angle was 6 degrees with respect to the roadway. Although this non-crashworthy system is not recommended for use on the National Highway System (NHS), it is important to note that no snagging or intrusion occurred into the fence during impact. The vehicle and system damage were minimal, but concrete spalling occurred near one vertical post anchor. The impact location and vehicle damage is shown in Figures 43 and 44 [23].



Figure 43. Point of Impact [23]



Figure 44. Vehicle Damage [23]

### 3.6 Zone of Intrusion

The Zone of Intrusion (ZOI) in roadside safety nomenclature is defined as the lateral extent that a vehicle extends beyond the top-front corner of a barrier during an impact scenario. The ZOI is a very important parameter when attempting to mount items on top of both rigid and non-rigid parapets, because of the potential for the vehicle to extend over a barrier and snag on vertical elements. This snag event can lead to excessive occupant compartment accelerations, projected components, and vehicle redirection into other lanes of traffic.

#### 3.6.1 Guidelines for Attachments to Bridge Rails and Median Barriers

In February 2003, MwRSF published a report titled *Guidelines for Attachments to Bridge Rails and Median Barriers* [24]. This research report quantified ZOI values for

multiple parapet geometries from historical crash test data. This effort was completed by obtaining video and pictures from previous tests and then using video analysis techniques to determine the lateral extent of the vehicle behind the top-front corner of the parapet.

The research team initially hypothesized that the barrier height would relate best to the amount of intrusion, but the test data was too limited to confirm this assumption. Researchers observed that the bumper and bottom portion of the front fender of the pickup truck were typically crushed during rigid barrier impacts, while the engine hood and upper front fender panel generally extended over the top of the barrier. This behavior resulted in the greatest intrusion, generally occurring early in the impact event.

Researchers reviewed crash tests involving rigid barriers ranging from 27<sup>3</sup>/<sub>4</sub> in. (705 mm) to 42 in. (1,067 mm) tall, impacted with pickup trucks and cars. The maximum lateral extents over the top leading edge of the rigid barriers were determined using high-speed video analysis. The ZOI for the pickup truck varied between 8 and 30 in. (203 and 762 mm), and the ZOI for the car varied between 0 and 8 in. (0 and 203 mm), depending on the parapet geometry and attachments. The report notes that if posts are mounted at least 7 in. behind the front face of a rigid barrier, the risk of vehicle snag is greatly reduced, but the authors also noted that offsetting posts to the back of the barrier will not eliminate all of the vehicle snag concerns for all barriers and impact conditions. ZOI values obtained for crash tests on small cars and pickup trucks are shown in Table 4.

Table 4. ZOI Values [24]

Barrier Class	Barrier Name	Barrier Height (in.)	Vehicle	Maximum Intustion (in.)	Vehicle Component
Concrete with Sloped Face	762-mm (30-in.) New Jersey Safety Shape	30	Small Car	6	Hood / Fender
			Pickup	8	Hood / Fender
	Single Slope Concrete Bridge Rail	32	Pickup	12	Hood / Fender
	813-mm (32-in.) F-Shape Bridge Rail	32	Small Car	2	Hood / Fender
			Pickup	8	Hood / Fender
	813-mm (32-in.) New Jersey Safety Shape Bridge Rail	32	Pickup	18	Hood / Fender
813-mm (32-in.) New Jersey Rail	32	Pickup	9	Hood / Fender	
Concrete with Vertical Face	Nebraska Open Concrete Bridge Railing (AASHTO Bridge Guide Specifications)	29	Pickup	16	Hood / Fender
			Pickup	14	Hood / Fender
	813-mm (32-in.) Vertical Wall	32	Small Car	8	Hood
			Pickup	15	Hood / Fender
	Texas Tyle T411 Bridge Rail	32	Pickup	24	Hood / Fender
Steel Tubular Rails	Illinois Side-Mounted Bridge Rail	32	Small Car	0	None
			Pickup	13	Hood / Fender
	Steel Bridge Rail with Tube Rail System for Transverse Decks	36	Pickup	21	Hood / Fender
	Texas Type T6 Bridge Rail	27.75	Pickup	30	Hood / Fender
	California Type 115 Bridge Rail	30	Pickup	30	Hood / Fender
Steel Tubular Rails on Curbs	Illinois 2399 Bridge Rail	32	Small Car	6	Hood
			Pickup	11	Fender
	NETC Bridge Rail, Curb Mounted	34	Small Car	3	Hood
			Pickup	12	Hood / Fender
Concrete / Steel Combination Bridge Rails	Minnesota Combination Bridge Rail	35	Small Car	0	None
			Pickup	24	Hood
	BR27C Bridge Railing on Deck	42	Small Car	0	None
			Pickup	10	Hood
Timber Bridge Rails	GC-8000 Bridge Rail for Longitudinal Decks	33	Pickup	24	Hood / Fender
	Wood Bridge Rail with Curb System for Transverse Decks	33	Pickup	21	Hood / Fender

### 3.6.2 Zone of Intrusion Study

In October 2010, MwRSF published a research report titled *Zone of Intrusion Study* [25]. This report detailed the results of nonlinear finite element testing using LS

DYNA simulations to investigate the ZOI for an NCHRP-350 2000P pickup truck [26]. This pickup truck simulation impacted a 40-in. (1,016-mm) tall, F-shape parapet at TL-2 and TL-3 testing conditions. The ZOI was determined to be 5 in. (127 mm). It was observed that with a barrier height of 40 in. (1,016 mm), the vehicle protrusion over the barrier was limited to the front corner of the hood and a small section of the fender.

Under NCHRP Report No. 350 TL-2 test no. 2-11 conditions [26], 45 mph (72.4 kph) and at a 25 degree angle, the ZOI for the pickup truck was predicted to be between 1.8 in. (46 mm) and 2.5 in. (64 mm). The authors attribute the variation in this ZOI value to the mesh quality of the simulation model and the overall system geometry.

### **3.6.3 Zone of Intrusion for Permanent 9.1-Degree Single-Slope Concrete Barriers**

In March 2014, MwRSF published a research report that detailed efforts involving simulation results from a Wisconsin Department of Transportation (WisDOT) single-slope concrete barrier. ZOI values were calculated for a pickup truck at three different single-slope parapet heights. The ZOI for 36, 42, and 56-in (914, 1,067, and 1,422-mm) tall barriers were 12.2 in. (310 mm), 6.4 in. (163 mm) and 0 in. (0 mm), respectively. Additionally, during this simulation effort, the left fender always protruded the farthest behind the barrier, which was followed by the corner of the engine hood [27].

### **3.6.4 Signs on Concrete Median Barriers**

The Texas A&M Transportation Institute (TTI) completed a study in April 2013 to determine the safety of mounting signs on the top of concrete median barriers [28]. This report detailed study efforts, including a literature review, simulation effort, and four full-scale crash tests.



The four full-scale crash tests completed by TTI occurred with a 2270P pickup truck under MASH TL-3 guidelines. During this testing series, a 2.5-in. (64-mm) outside diameter schedule 80 pipe was used to mount to the sign and the parapet, and different connection methods were tested between each individual test. During all of the crash tests, the vehicle extended over the front face of the barrier and contacted the sign and sign support assembly, but no snagging occurred. The authors determined that the addition of the sign assembly did not decrease the safety of the concrete parapet [28].

### **3.7 Lincoln Nebraska Fence Examples**

A survey of two different fences used in close proximity to the travelled way was completed in Lincoln, Nebraska. The first design consisted of an aesthetic vertical debris fence mounted on top of a concrete parapet. The second system was very similar to the protective fence used by Iowa, as is shown in Figure 11.

#### **3.7.1 Aesthetic Debris Fence**

The first fence example that was analyzed in Lincoln, Nebraska is located near the corner of North Antelope Parkway and Salt Creek Roadway. This design consists of a fence and baseplate mounted on the top of a vertical concrete bridge rail. This rail measures 42 in. (1067 mm) tall, and the debris fence is mounted in the middle of the rail, 8 in. (203 mm) behind its front face.

The aesthetic fence design is composed of wire mesh panels containing cyclic wave designs on both the top of the mesh structure and on panels that are bolted to the mesh. Rectangular vertical posts, 5 in. x 4 in. x 3/8 in. (127 mm x 102 mm x 10 mm), measuring 8 ft-7 1/2 in. (2.6 m) were placed 8 ft (2.4 m) on center. These posts were connected to panels containing two horizontal stiffeners, one at the bottom and one 4 ft

(1.2 m) above the parapet and another aesthetic stiffener at the top containing a sinusoidally-varying design. These panels also contained vertical posts at the beginning and end of each panel section. All vertical posts and longitudinal stiffeners located in the mesh structure were fabricated with rectangular steel tube measuring 2 in. x 2 in. x ¼ in. (51 mm x 51 mm x 6 mm). The wire mesh panels were connected to the vertical posts with a total of six ¼-in. (6-mm) self-tapping screws. A baseplate measuring 8 in. x 8 in. x ½ in. (203 mm x 203 mm x 13 mm) , was used to secure the vertical posts to the concrete bridge rail and was held in place with four 6-in. (152-mm) long by 3/8-in. (10-mm) diameter anchor bolts. CAD details of both the fence and parapet design are shown in Figures 45 through 47.

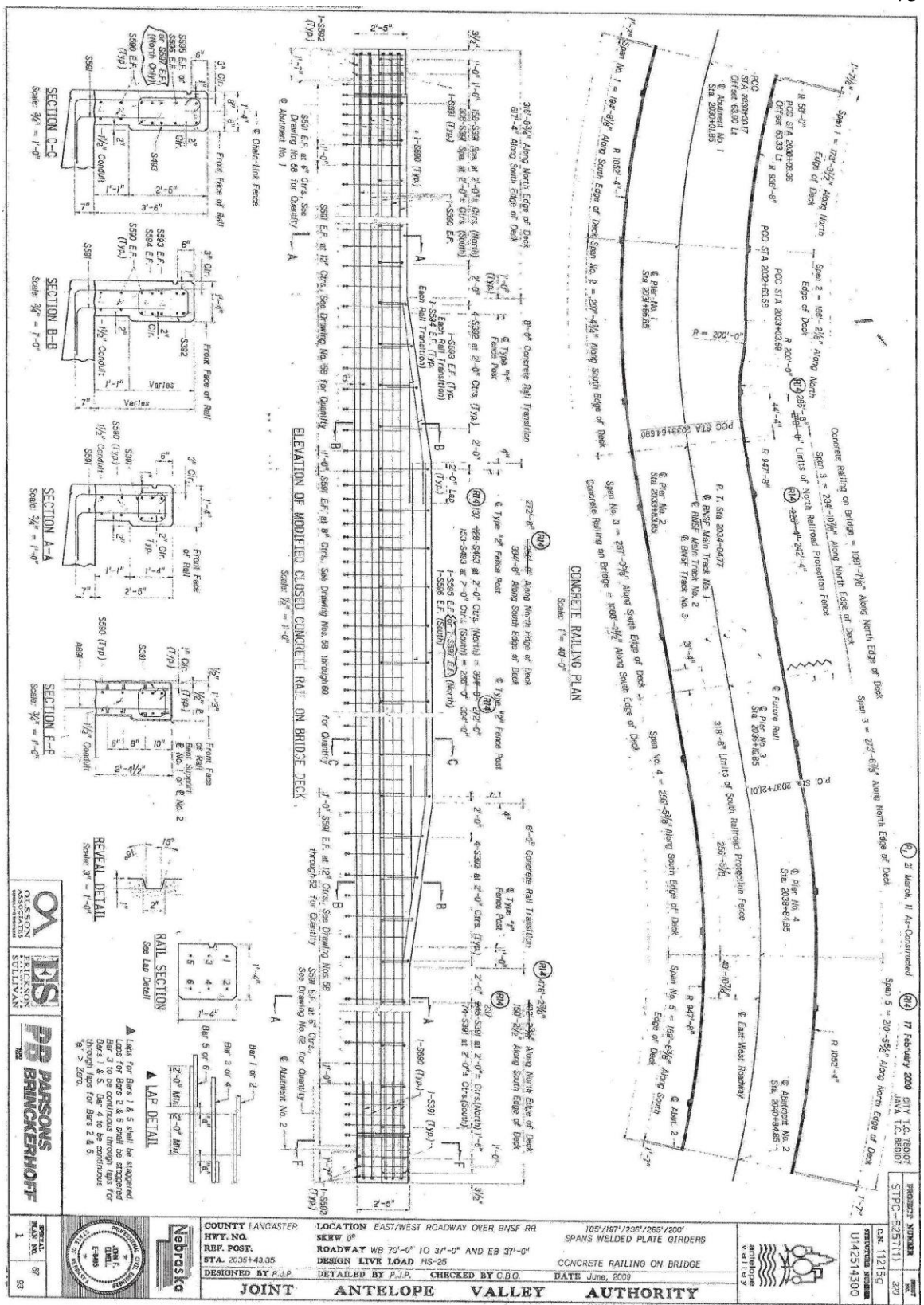


Figure 45. Aesthetic Debris Fence Bridge Rail Details

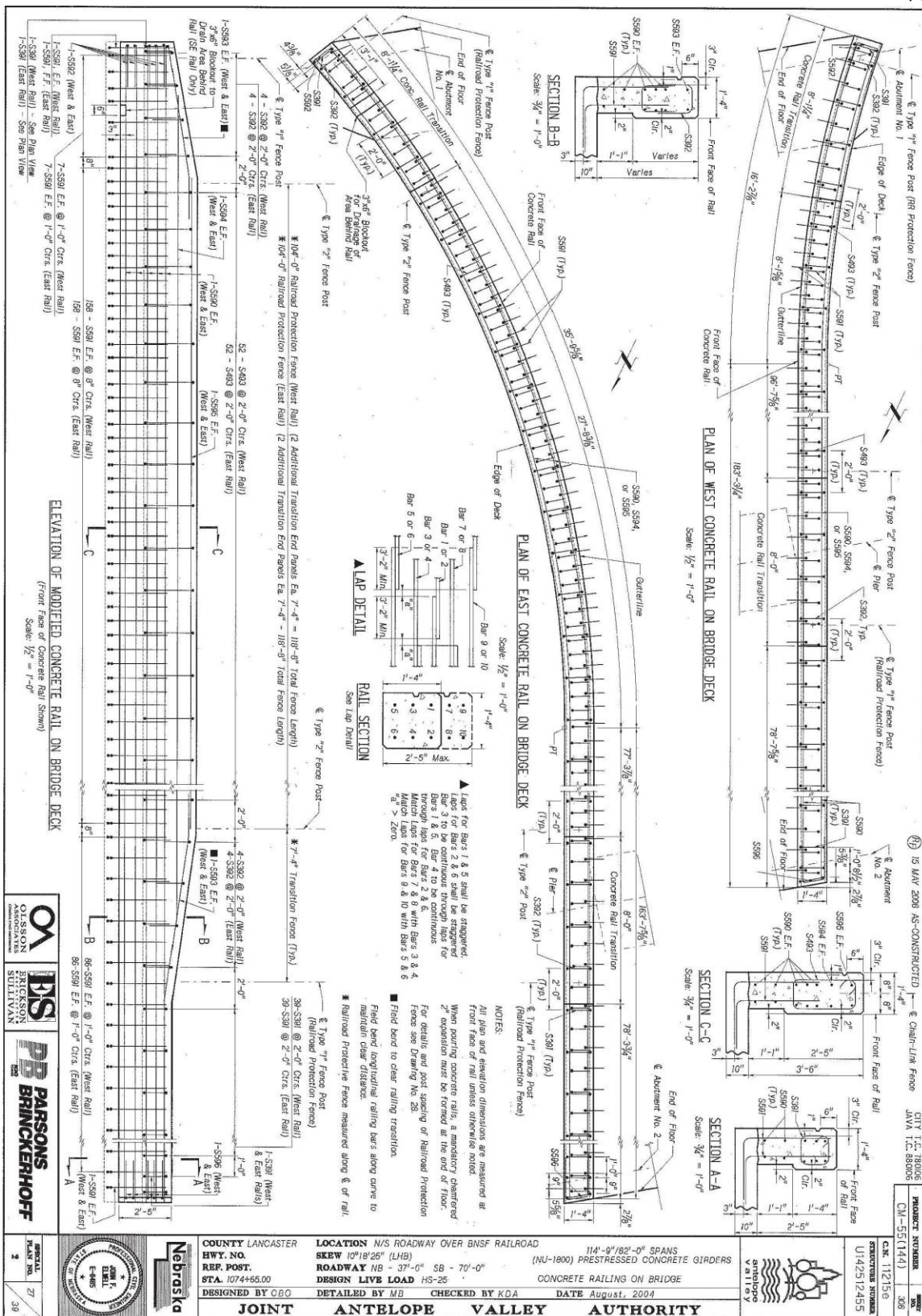


Figure 46. Aesthetic Debris Fence Bridge Parapet and Placement Details



This aesthetic debris fence design was located close to the design headquarters of MwRSF. This design was examined, because some panels within the fence structure were missing, as shown in Figures 48 through 50. Under closer inspection, it was discovered that the self-drilling screws used to secure the fence panels to the vertical posts were breaking off and ratchet straps were being used to secure the panels to the posts, as shown in Figures 50 and 51. This design shows the importance of correctly securing the fence and highlights the need for stronger connections to guarantee that the fence components do not fall onto the roadway or railway tracks.



Figure 48. Aesthetic Debris Fence Overview



Figure 49. Aesthetic Design Missing Panels

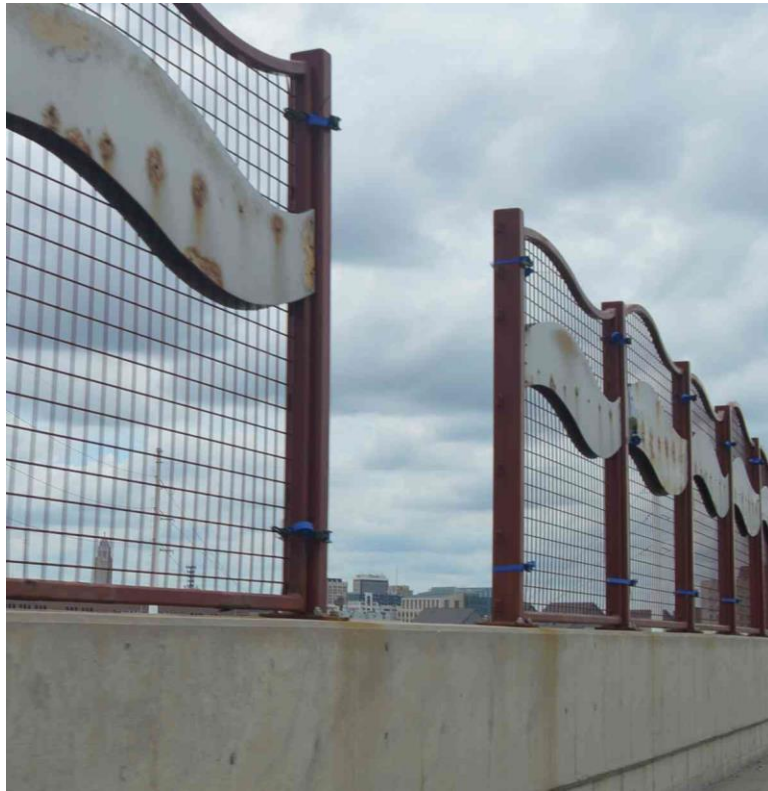


Figure 50. Aesthetic Design Missing Panel



Figure 51. Aesthetic Design Broken Screws

### 3.7.2 Combination Rail and Pedestrian Fence

Another design used in Lincoln, Nebraska, and located on the 27<sup>th</sup> Street and Salt Creek Roadway overpass, is very similar to the Iowa combination pedestrian rail and debris fence shown in Figure 11. This design, as shown in Figure 52, is representative of the common, curved, fence designs used by states for pedestrian and debris containment. There are three longitudinal stiffeners used within the design, one is placed at the bottom of the fence and the other two are within the curved upper section of the structure. There is also a hand rail that runs longitudinally along the length of the system. Iowa DOT does not wish to use this system in conjunction with any sort of pedestrian walkway so an additional handrail would not be needed.



Figure 52. Lincoln Pedestrian Fence



### 3.8 Design Standards

#### 3.8.1 Iowa Chain-Link Fence Standards

Iowa DOT currently specifies criteria for the installation and maintenance of chain-link fence near the roadway. These guidelines were analyzed to determine design requirements for a debris fence mounted on top of a concrete parapet [29].

The structural elements used for both the vertical posts and horizontal stiffeners must meet one of the following requirements:

1. AASHTO M 181 Grade 1 guidelines or ASTM F1083 Schedule 40 and
2. AASHTO M 181 Grade 2 or ASTM F1043 Group IC

The chain-link fabric used in the debris fence design, unless otherwise noted in contract documents, must include:

1. 9-gauge coated wire with a breaking strength of 1,290 pounds;
2. Height of fabric of 72 inches;
3. Selvage knuckled at both the top and bottom; and
4. Mesh size  $2 \pm \frac{1}{8}$  inches.

Additionally, the chain-link fabric must conform to one of the following options:

1. Zinc coated fabric meeting requirements of ASTM A 392, Class 2 or AASHTO M 181 Type 1, Class D;
2. Aluminum coated fabric meeting requirements of AASHTO M181, Type II; and
3. PVC coated fabric requirements of ASTM F668, Class 2b or AASHTO M181, Type IV, Class B Fused.

Any tension wires used within a parapet-mounted debris fence design in Iowa shall either meet requirements of AASHTO M 181 or one of the following:

1. ASTM A 824 or A 817, Type II, Class 3;
2. ASTM A 824 or A 817, Type 1; and
3. ASTM F 1664, PVC (Vinyl) Coated, Class 2b.

Brace and tie wires must meet requirements of ASTM F 626 and be either zinc or aluminum coated. They must also meet these additional requirements:

1. Where specified, round metallic-coated tie wires, clips and hog rings shall be polymer coated to match the color of the chain-link fabric as selected from ASTM 934 and
2. The coating process and metallic-coated core wire materials shall be in accordance with ASTM F 668.

The fittings used to secure the chain link to the structural members must comply with the following:

1. Attach braces to posts using fittings which will hold both the post and the post and brace rigidly;
2. Use diagonal truss rods of  $\frac{3}{8}$ -in. diameter, round steel rods with appropriate commercial means for tightening;
3. Furnish a locknut or other device to hold the tightening device in place;
4. Furnish a suitable sleeve or coupling device, recommended by the manufacturer, to connect sections of top rail and to provide for expansion and contraction;

5. Use stretcher bars no less than  $\frac{3}{8}$  in. diameter, or equivalent cross sectional area, with suitable clamps for attaching fabric to corner, end, or gate posts; and
6. All fittings must conform to AASHTO M 181 or ASTM F 626.

Anchor bolts used to secure the debris fence to the parapet must comply with the following requirements:

1. Use full-length galvanized bolts;
2. Comply with ASTM F 1554, Grade 105, S4 (-20°F);
3. Threads are to comply with ANSH/ASME B1.1 for UNC thread series, Class 2A tolerance;
4. The end of each anchor bolt intended to project from the concrete is to be color coded to identify the grade; and
5. Do not bend or weld anchor bolts.

Any nuts that are used within the debris fence design must conform to the following specifications:

1. Comply with ASTM A 563, Grade DH or ASTM A 194, Grade 2H;
2. Use heavy hex;
3. Use ANSI/ASME B1.1 for UNC thread series, Class 2B tolerance; and
4. Nuts may be over-tapped according to the allowance requirements of ASTM A563.

Any washers used in the system must comply with ASTM F 436 Type 1 requirements. The debris fence design may include the need to weld some of the structural members, and Iowa Department of Transportation states that these welds must

comply with ANSI/AWS D1.1 Structural Welding Code procedures and requirements.

The Iowa standards require that items along the roadway be able to withstand three-second wind gusts up to 90 mph (144.8 kmh).

### **3.8.2 Union Pacific and BNSF Standards**

Rail companies, such as Union Pacific and BNSF, require certain guidelines when parapet-mounted fencing is used above railway overpasses in Iowa. They require that on sidewalk or trail facilities that the top of the fence should be curved to discourage climbing over the fence. The standards also note that when BSNF and Union Pacific ask for parapet-mounted fences, the Iowa DOT generally proposes that the fence be omitted in lieu of a 44-in. (1,118 -mm) tall concrete barrier [29].

## **4 DESIGN AND ANALYSIS – DEBRIS FENCE**

### **4.1 Overview**

This chapter focuses primarily on the vertical posts in the debris fence. The Iowa DOT debris fence was to include the design of six main components:

- Bridge rail / parapet
- Vertical posts
- Post-to-rail attachments
- Horizontal fence stiffeners (frame)
- Chain link mesh
- Chain link attachments to posts and horizontal stiffeners

Due to limitations on time, this thesis was focused on the selection of the parapet and vertical posts. Additional recommendations were provided for the other members, but the sizing, selection, and design of those components were delegated for future analysis.

### **4.2 Debris Fence Design Objectives**

State DOT standards were summarized, and an internal ranking system was applied based on debris fence safety, constructability, and cost. The use of standardized components was also prioritized. Based on this review, the preferred configurations were the Florida DOT design, which utilized vertical round posts and two saddle brackets to the back side of the parapet, and the Texas DOT design, which utilized a single saddle bracket and a lower through bolt which passed through the post into the back side of the parapet.

Iowa DOT was shown the results of the literature review and state DOT standards. The following attributes of the debris fence were prioritized based on that meeting:

- A single, standard parapet shape would be selected for the debris fence installation. Adaptations to other bridge rail or parapet shapes would be considered at a future time.
- Posts were to be placed on the back side of the parapet to reduce engagement within the impacting vehicle's ZOI.
- Two saddle clamps were recommended, which would fasten the post to the back side of the parapet.
- No structurally-stiff horizontal stiffeners would be placed within passenger vehicle ZOI.
- Post-to-rail attachments (specifically, bolted attachments) should not experience damage, result in concrete cracking, or require replacement during a design impact scenario.

Post sizing and spacing for the debris fence were determined based on a structural analysis. Using the maximum flexural and shear capacity of the selected post size, the clamp spacing was selected to allow the posts to yield backward during an impact scenario. Based on additional discussion, the Iowa DOT stated that they would prefer to limit the amount of horizontal members in the design. This justification was based on their concern that the connection points between the horizontal members could fail during an impact and spear into an impacting vehicle. Because these horizontal members add to the overall aesthetics of the fence, the Iowa DOT stated that they wished to retain one

member at the top of the fence. To make up for the lack of horizontal stiffness, the Iowa DOT stated their preference to use longitudinal tension wires. These wires offer an added benefit of limiting large pieces of the debris fence from falling off the parapet during an impact event. When the debris fence experiences a vehicular impact, it is very important to limit the damage of the anchor rods, which will guarantee that they do not have to be replaced. Thus, the capacity of the vertical posts must be limited to allow them to fail far before the anchor connections. The design and analysis are explained in further detail in the following sections.

### **4.3 Parapet Selection**

Recently, MwRSF crash tested an optimized bridge railing under MASH TL-4 conditions for the Midwest Pooled Fund Program. The final report of this research has not been completed, but this test has been deemed successful under the MASH TL-4 criteria. The Iowa DOT has specified that this barrier will be their new standard configuration under TL-4 impact conditions, and they have requested that the selected debris fence prototype be used in conjunction with this TL-4 optimized bridge railing.

The railing, as shown in Figures 53 and 54, consists of a single-slope, half-section, reinforced concrete parapet and stands 36-in. (914-mm) tall after placement of a 3-in. (76-mm) overlay. The base of the barrier measures 10 in. (254 mm) in width and tapers up to a minimum of 8 in. (203 mm) at the top of the structure. The railing consists of multiple longitudinal and vertical pieces of rebar with the top two longitudinal bars being 4 in. (102 mm) and 5¼ in. (133 mm) below the top of the railing. A design variation incorporating head ejection criteria is compared to the crash-tested design in Figure 55, which has the second piece of longitudinal rebar 6.62 in. (168 mm) below the

top of the barrier. Thus, any connections to the backside of the bridge railing should be at a minimum of  $7\frac{3}{4}$  in. (197 mm) below the top of the railing to prevent any chance of the rebar being struck when holes are drilled into the parapet for the placement of anchors.



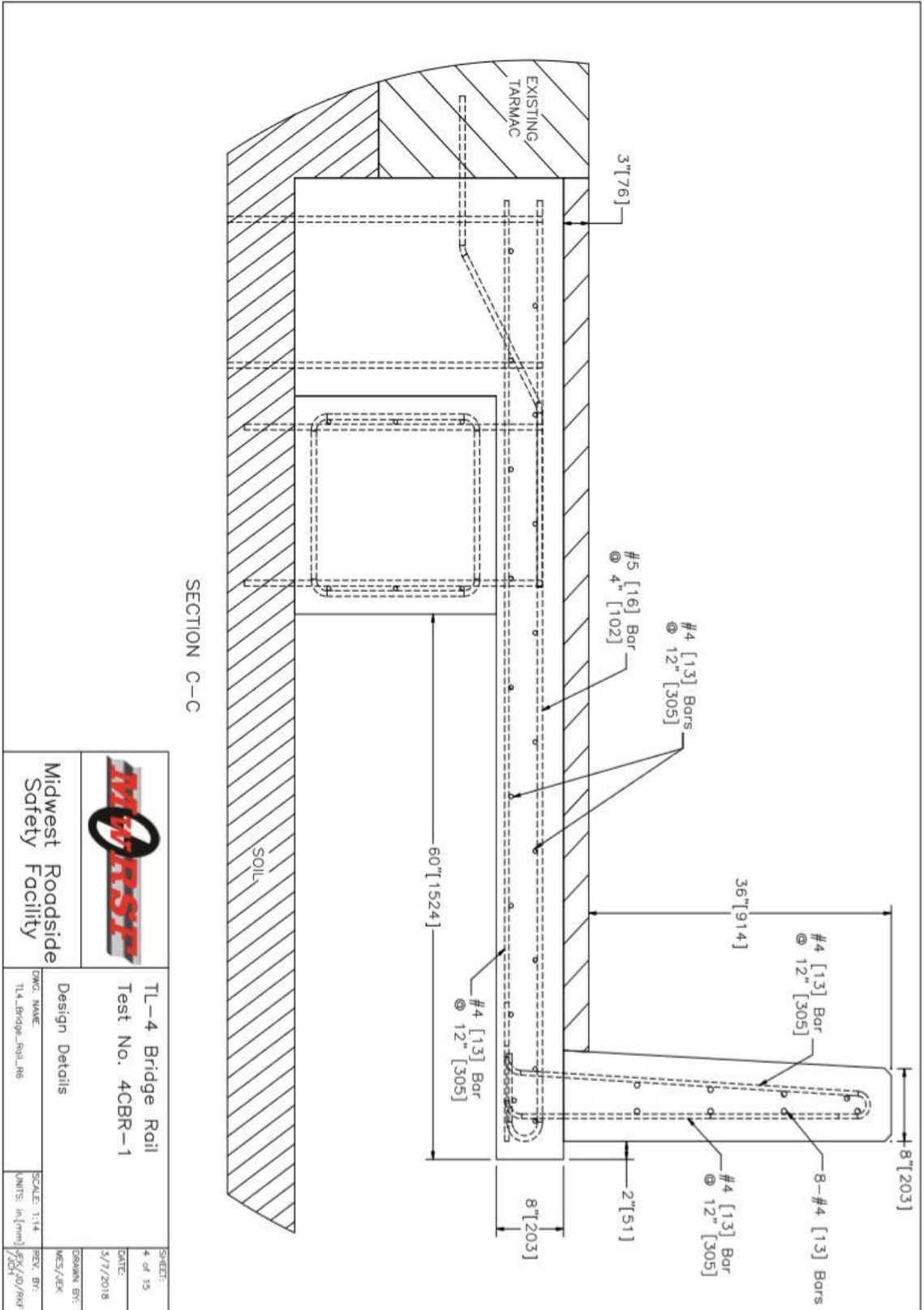


Figure 53. TL-4 Bridge Rail

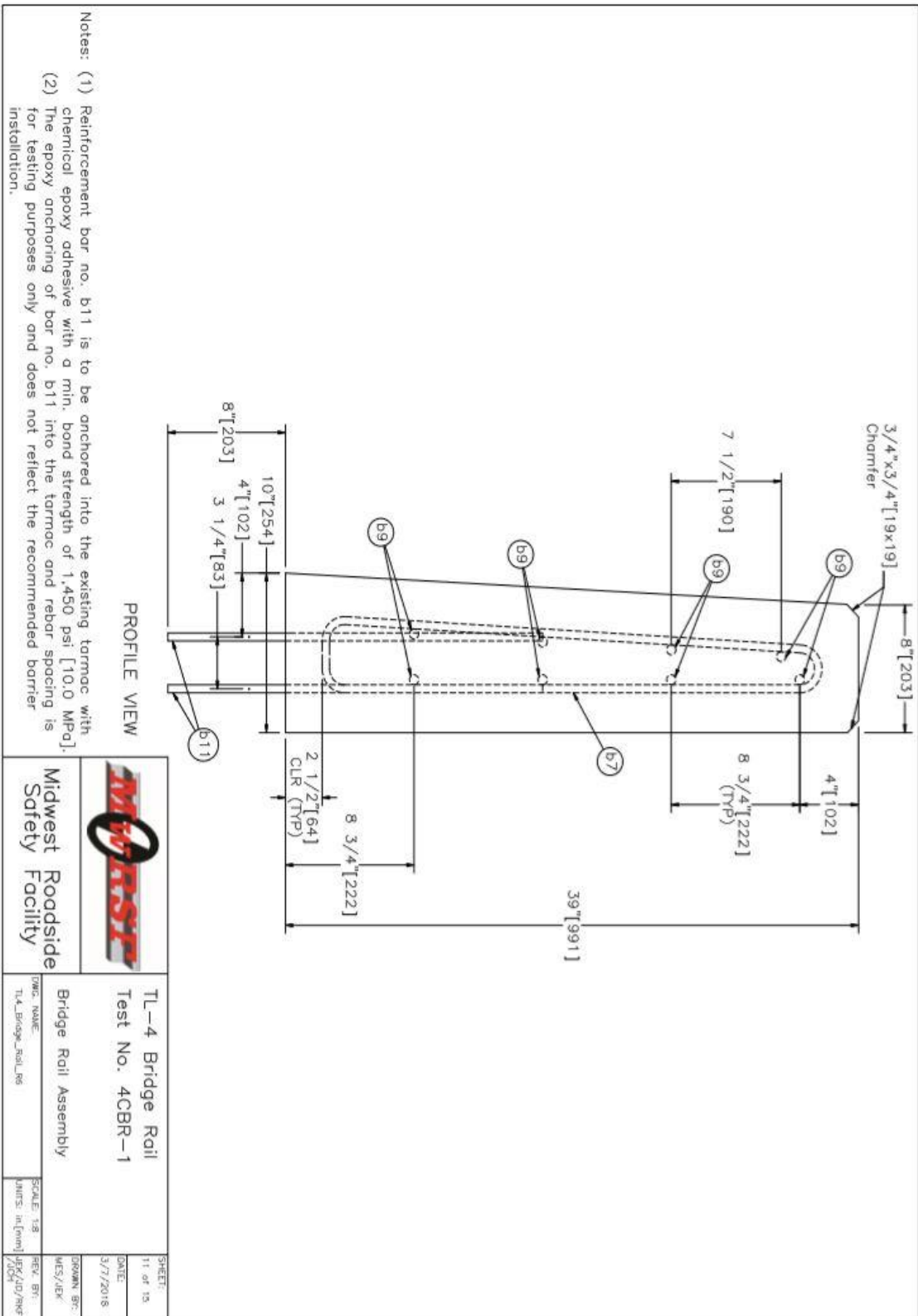


Figure 54. TL-4 Bridge Rail Rebar Placement

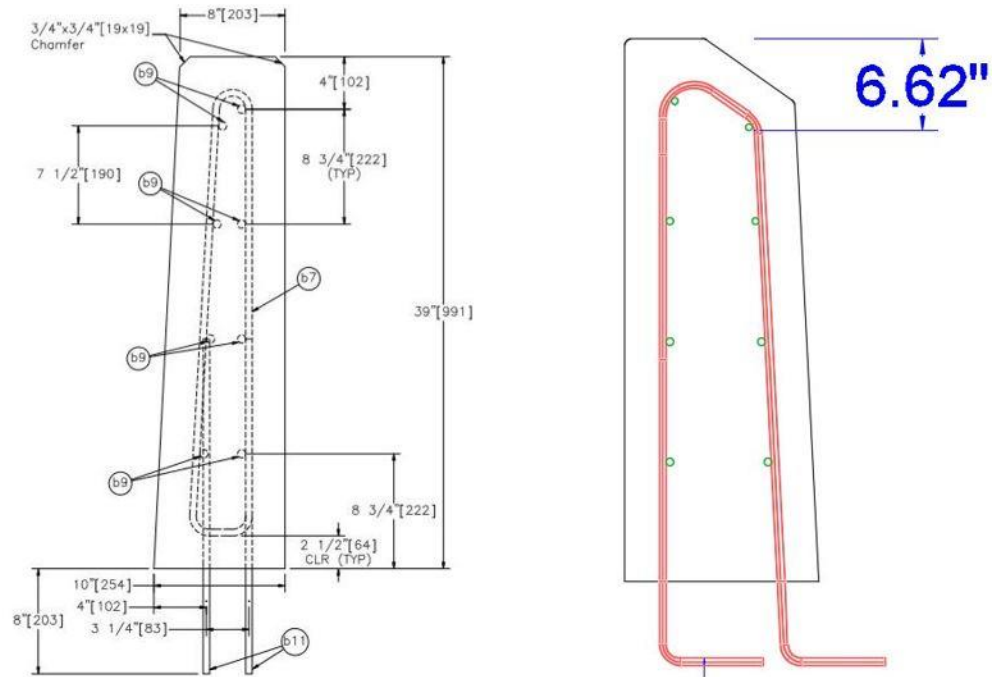


Figure 55. Comparison of TL-4 Barriers

#### 4.4 Loading Conditions

The components in this debris fence can potentially be subjected to a total of five different loading conditions as shown:

1. A lateral load during a vehicular impact;
2. A longitudinal load during a vehicular impact;
3. A wind load on the front of the fence;
4. A wind load on the back of the fence and;
5. A dead load from the weight of the fence material, which will always be present.

During any of these loading conditions, it is paramount that the anchor connections in the back of the parapet are maintained and are not subjected to forces that could cause them to fail. This decision is based on the difficulty and expense with drilling

the holes and replacing the anchors. Thus, it is preferred that the vertical posts and saddle brackets fail before the anchorage connections. The following sections will mathematically detail each of the loading conditions.

#### **4.4.1 Lateral Impact Loading**

A lateral vehicular impact into the debris fence will place a load onto the vertical posts and chain-link, which will then be transferred through the posts and into the saddle clamps and anchor connections as a tensile load. In this loading scenario, the largest tensile load will be transferred into the top brackets and anchor connections. The tensile load within the lower bracket will be negligible. Thus, the contribution of the lower bracket was not involved with this mathematical derivation to represent a worst case scenario. A diagram showing the lateral loading is shown in Figure 56, a definition of the variables is shown in Table 5, and the full mathematical derivation is given in Appendix A.

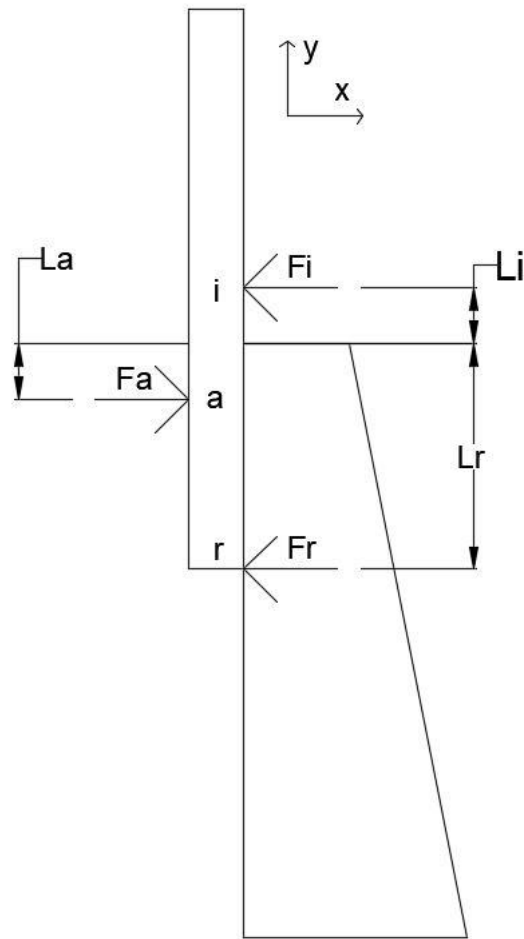


Figure 56. Lateral Impact Loading Configuration

Table 5. Lateral Impact Loading Variables

Variable	Definition
$F_i$	Impact Force
$F_a$	Tensile Force at Top Clamp
$F_r$	Reaction Force at Bottom of Post
$L_i$	Distance Between Impact and Top of Parapet
$L_a$	Distance Between Top Clamp and Top of Parapet
$L_r$	Distance Between Bottom of Post and Top of Parapet

A static force balance and moment sum at points i, a, and r of the lateral impact

yields the following equations:

$$\sum F_x = 0 = -F_i + F_a - F_r \quad (1)$$

$$\sum M_i = 0 = F_a(L_i + L_a) - F_r(L_r + L_i) \quad (2)$$

$$\sum M_a = 0 = F_i(L_i + L_a) - F_r(L_r - L_a) \quad (3)$$

$$\sum M_r = 0 = F_i(L_i + L_r) - F_a(L_r - L_a) \quad (4)$$

$$F_i = \frac{F_r(L_r - L_a)}{(L_i + L_a)} \quad (5)$$

$$F_a = \frac{F_r(L_i + L_r)}{(L_i + L_a)} \quad (6)$$

$$F_r = \frac{F_a(L_i + L_a)}{(L_i + L_r)} \quad (7)$$

Next, the shear and moment diagrams can be obtained and are shown in Figure

57.

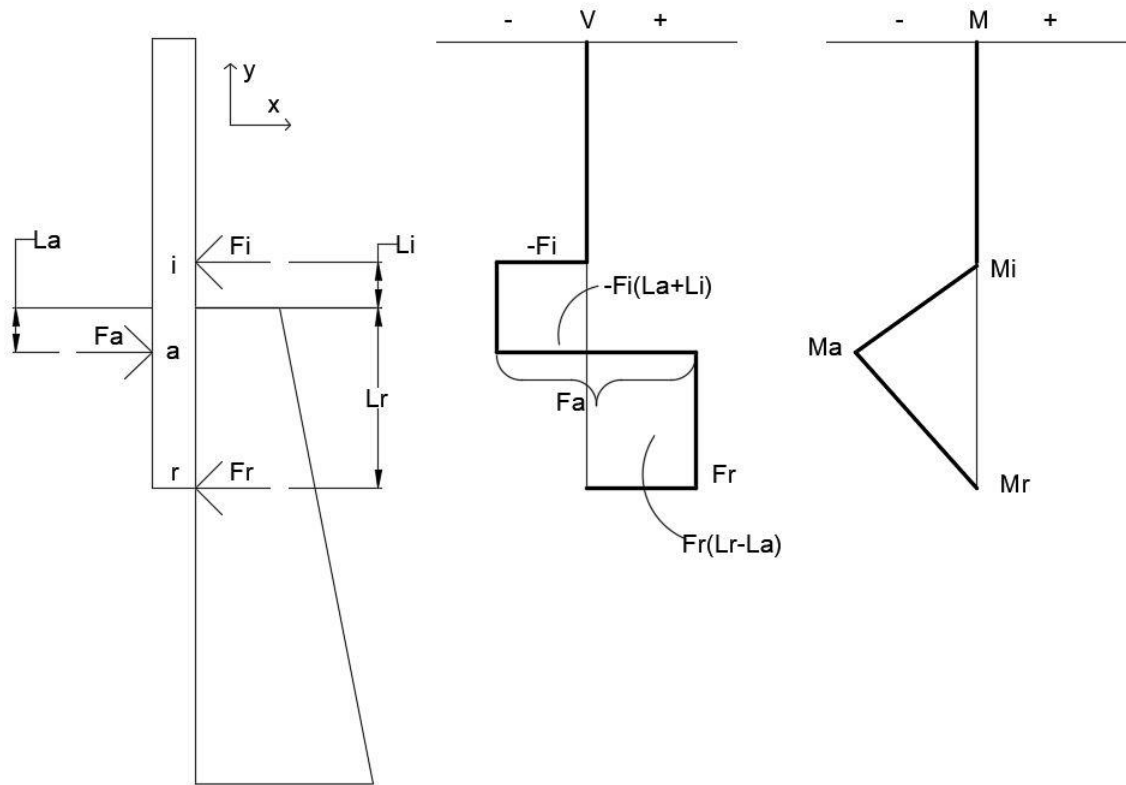


Figure 57. Shear and Moment Diagrams for Lateral Impact

The shear diagram shows that the maximum force occurs at the top clamp during a lateral impact. The moment diagram shows that the maximum moment during a lateral impact occurs at the top clamp, which can be stated mathematically with the following equations:

$$M_a = F_i(L_a + L_i) \quad (8)$$

$$M_a = F_r(L_r - L_a) \quad (9)$$

#### 4.4.2 Longitudinal Impact Loading

A longitudinal vehicular impact into the debris fence will place a load onto the vertical posts and chain-link, which will then be transferred through the posts and into the

saddle clamps and anchor connections as a shear load. A diagram showing the longitudinal loading is shown in Figure 58, a definition of the variables is shown in Table 6, and the full mathematical derivation is given in Appendix B.

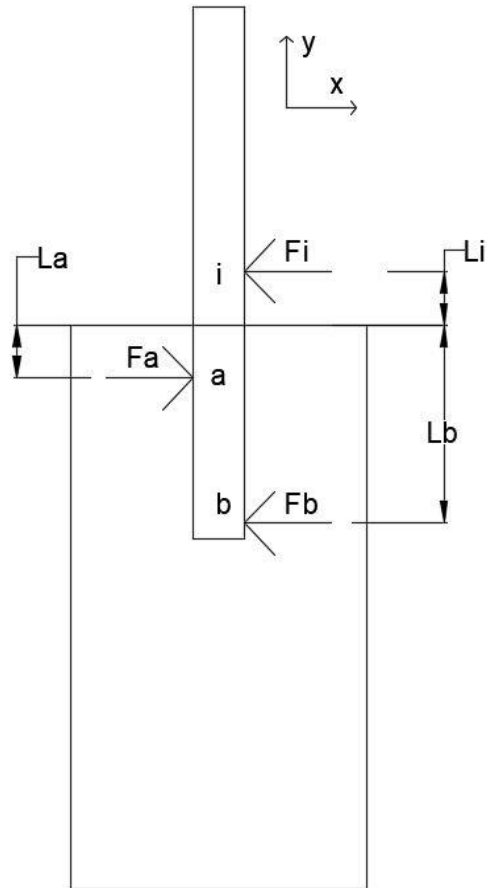


Figure 58 Longitudinal Impact Loading Configuration

Table 6. Longitudinal Impact Loading Variables

Variable	Definition
$F_i$	Impact Force
$F_a$	Shear Force at Top Clamp
$F_b$	Shear Force at Bottom Clamp
$L_i$	Distance Between Impact and Top of Parapet
$L_a$	Distance Between Top Clamp and Top of Parapet
$L_b$	Distance Between Bottom Clamp and Top of Parapet



A static force balance and moment sum at points i, a, and b of the longitudinal impact yields the following equations:

$$\sum F_x = 0 = -F_i + F_a - F_b \quad (10)$$

$$\sum M_i = 0 = F_a(L_i + L_a) - F_b(L_b + L_i) \quad (11)$$

$$\sum M_a = 0 = F_i(L_i + L_a) - F_b(L_b - L_a) \quad (12)$$

$$\sum M_b = 0 = F_i(L_i + L_b) - F_a(L_b - L_a) \quad (13)$$

Through substitution and solving these equations, the forces at i, a, and b can be determined:

$$F_i = \frac{F_b(L_b - L_a)}{(L_i + L_a)} \quad (14)$$

$$F_a = \frac{F_b(L_i + L_b)}{(L_i + L_a)} \quad (15)$$

$$F_b = \frac{F_a(L_i + L_a)}{(L_i + L_b)} \quad (16)$$

Next, the shear and moment diagrams can be obtained and are shown in Figure

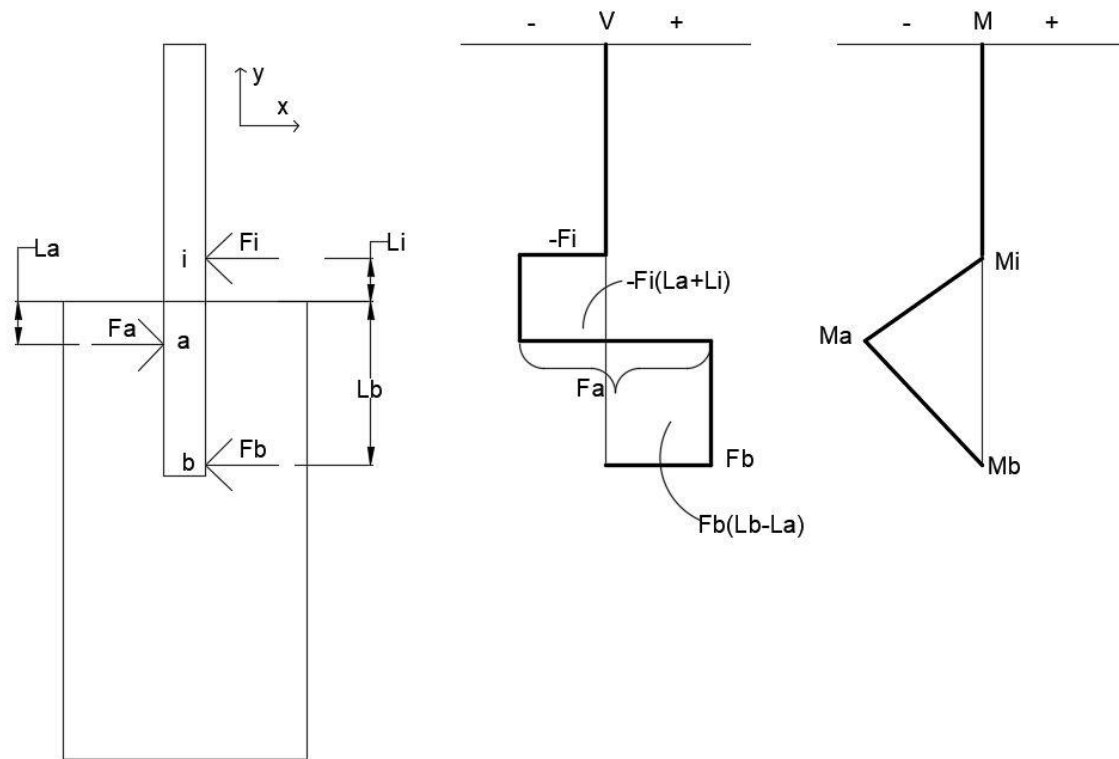


Figure 59. Shear and Moment Diagrams for Longitudinal Impact

The shear diagram shows that the maximum force occurs at the top clamp during a lateral impact. The moment diagram shows that the maximum moment during a longitudinal impact occurs at the top clamp. This can be stated mathematically with the following equations:

$$M_a = F_i(L_a + L_i) \quad (17)$$

$$M_a = F_b(L_b - L_a) \quad (18)$$

#### 4.4.3 Front Wind Loading

Lateral wind blowing onto the front side of the fence structure will place a load onto the vertical posts and chain-link mesh, which will then be transferred through the posts and into the saddle clamps and anchor connections as a tensile load. In this loading scenario, the largest tensile load will be transferred into the top brackets and anchor

connections. Thus, the lower bracket did not represent a worst-case design scenario. A diagram showing the front wind loading scenario and its corresponding shear and moment diagrams are shown in Figure 60, a definition of the variables is shown in Table 7, and the full mathematical derivation is given in Appendix C.

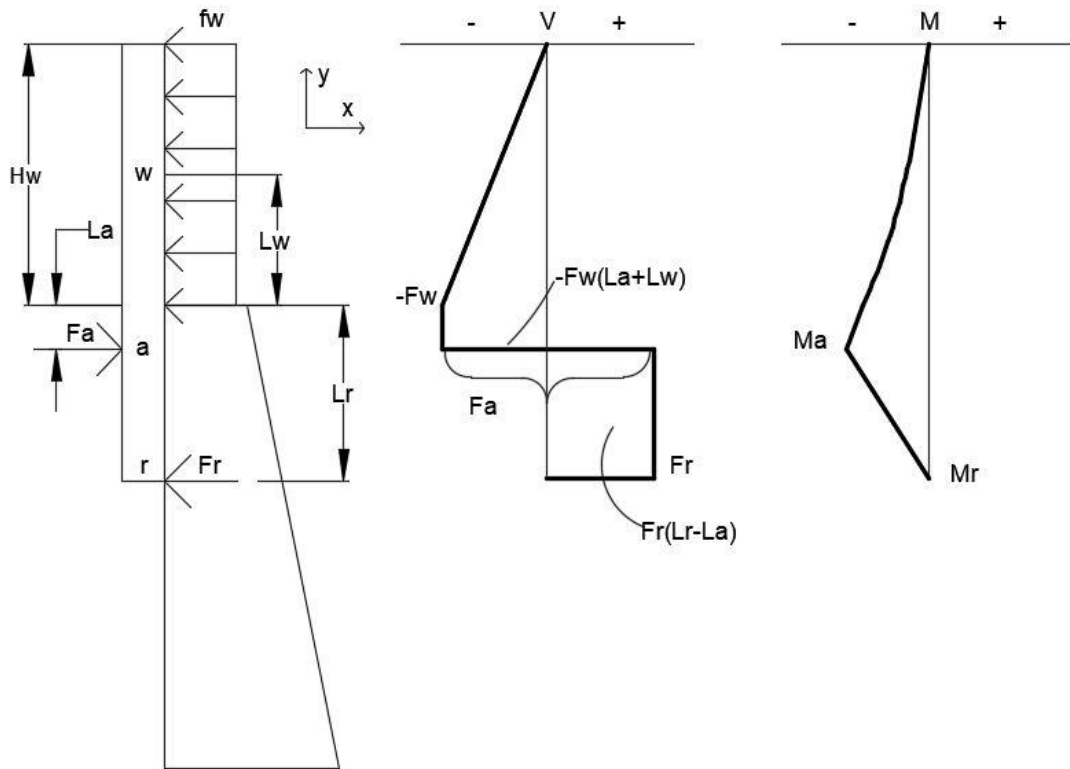


Figure 60. Front Wind Loading Configuration

Table 7. Front Wind Loading Variables

Variable	Definition
$f_w$	Wind Load Per Unit Length
$F_w$	Total Effective Wind Load
$F_a$	Tensile Force at Top Clamp
$F_r$	Reaction Force at Bottom of Parapet
$H_w$	Chain-Link Height
$L_w$	Distance Between Center of Wind Load and Top of Parapet
$L_a$	Distance Between Top Clamp and Top of Parapet
$L_r$	Distance Between Bottom of Post and Top of Parapet

To simplify this situation, the total effective wind load can be transferred to a point load at its centroid. A diagram showing this scenario and its corresponding shear and moment diagrams are shown in Figure 61. Note that this simplified loading condition is similar to the later and longitudinal impact loading scenarios.

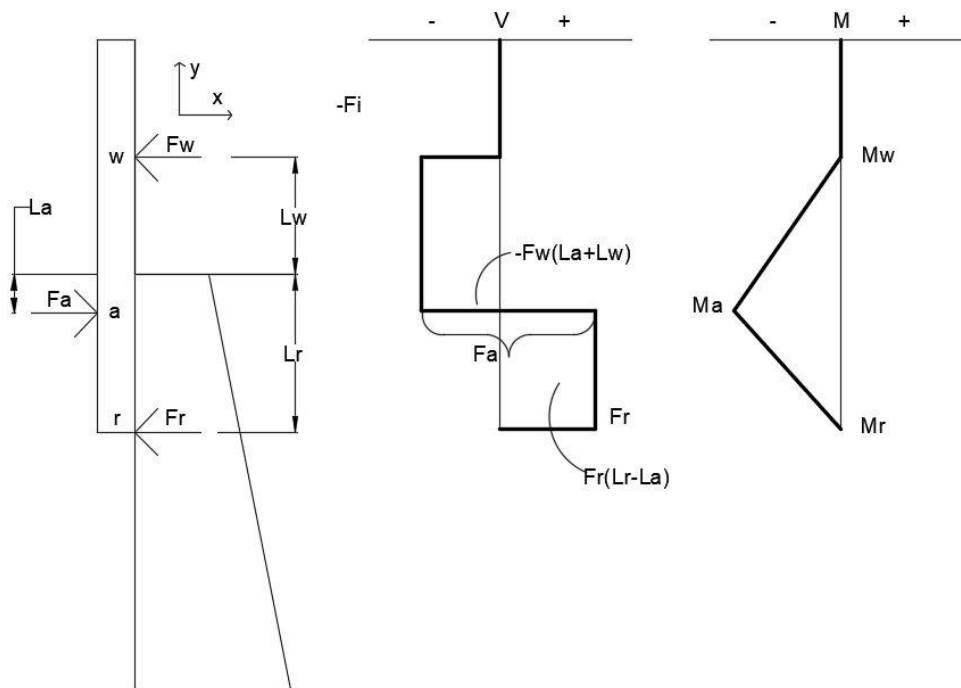


Figure 61. Simplified Loading Configuration

Note, that the forces and moments obtained through the simplified model are equivalent to the actual configuration and only differ in the look of the shear and moment diagram. A static force balance and moment sum at points w, a, and r, of the front wind loading simplified scenario yields the following equations:

$$\sum F_x = 0 = -F_w + F_a - F_r \quad (19)$$

$$\sum M_w = 0 = F_a(L_w + L_a) - F_r(L_r + L_w) \quad (20)$$

$$\sum M_a = 0 = F_w(L_w + L_a) - F_r(L_r - L_a) \quad (21)$$

$$\sum M_r = 0 = F_w(L_w + L_r) - F_a(L_r - L_a) \quad (22)$$

Through substitution and solving these equations the forces at a, and r can be determined:

$$F_a = \frac{F_w(L_r + L_w)}{(L_r - L_a)} \quad (23)$$

$$F_r = \frac{F_w(L_w + L_a)}{(L_r - L_a)} \quad (24)$$

The shear diagram shows that the maximum force occurs at the top clamp during a front wind loading scenario. The moment diagram shows that the maximum moment during a front wind loading scenario occurs at the top clamp. This can be stated mathematically with the following equations:

$$M_a = F_w(L_a + L_w) \quad (25)$$

$$M_a = F_r(L_r - L_a) \quad (26)$$

#### 4.4.4 Back Wind loading

Lateral wind blowing onto the back side of the fence structure will place a load onto the vertical posts and chain-link mesh, which will then be transferred through the posts and into the saddle clamps and anchor connections as a tensile load. In this loading scenario, the largest tensile load will be transferred into the bottom clamp and anchor connections. In this derivation the tensile force at the top clamp and anchor connections were neglected. A diagram showing the back wind loading is shown in Figure 62, a definition of the variables is shown in Table 8, and the full mathematical derivation is given in Appendix D.

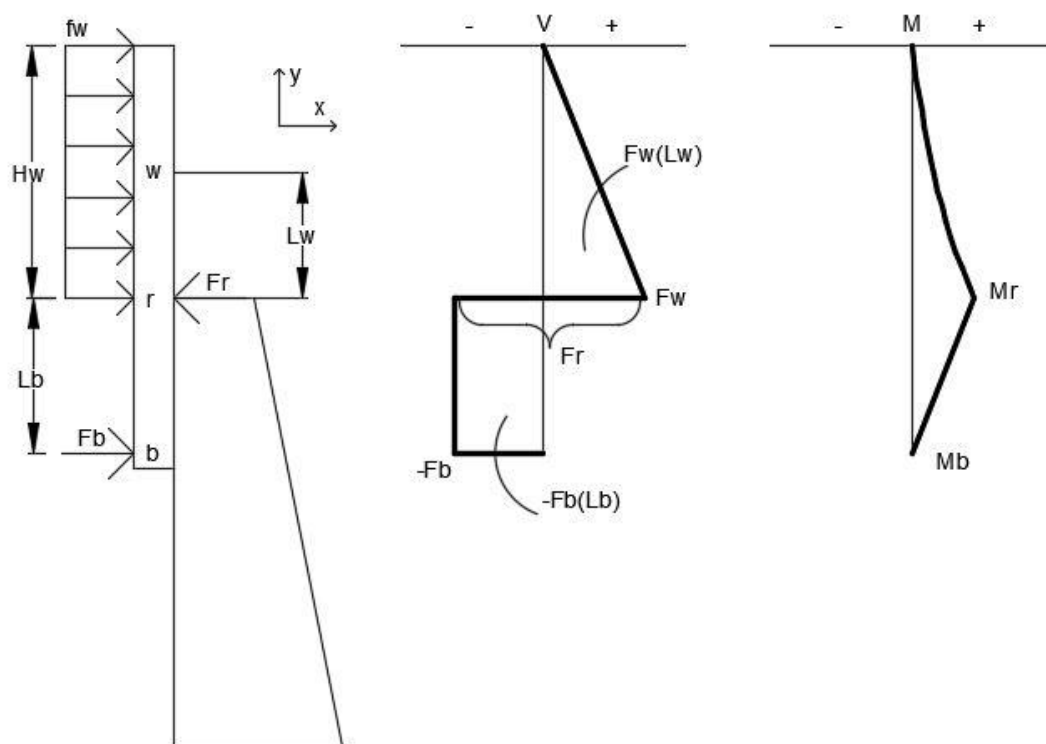


Figure 62 Back Wind Loading Configuration

Table 8. Back Wind Loading Variables

Variable	Definition
$f_w$	Wind Load Per Unit Length
$F_w$	Total Effective Wind Load
$F_b$	Tensile Force at Bottom Clamp
$F_r$	Reaction Force at Top of Parapet
$H_w$	Chain-Link Height
$L_w$	Distance Between Center of Wind Load and Top of Parapet
$L_b$	Distance Between Bottom Clamp and Top of Parapet

To simplify this situation the total effective wind load can be transferred to a point load at its centroid. A diagram showing this scenario and its corresponding shear and moment diagrams are shown in Figure 63.

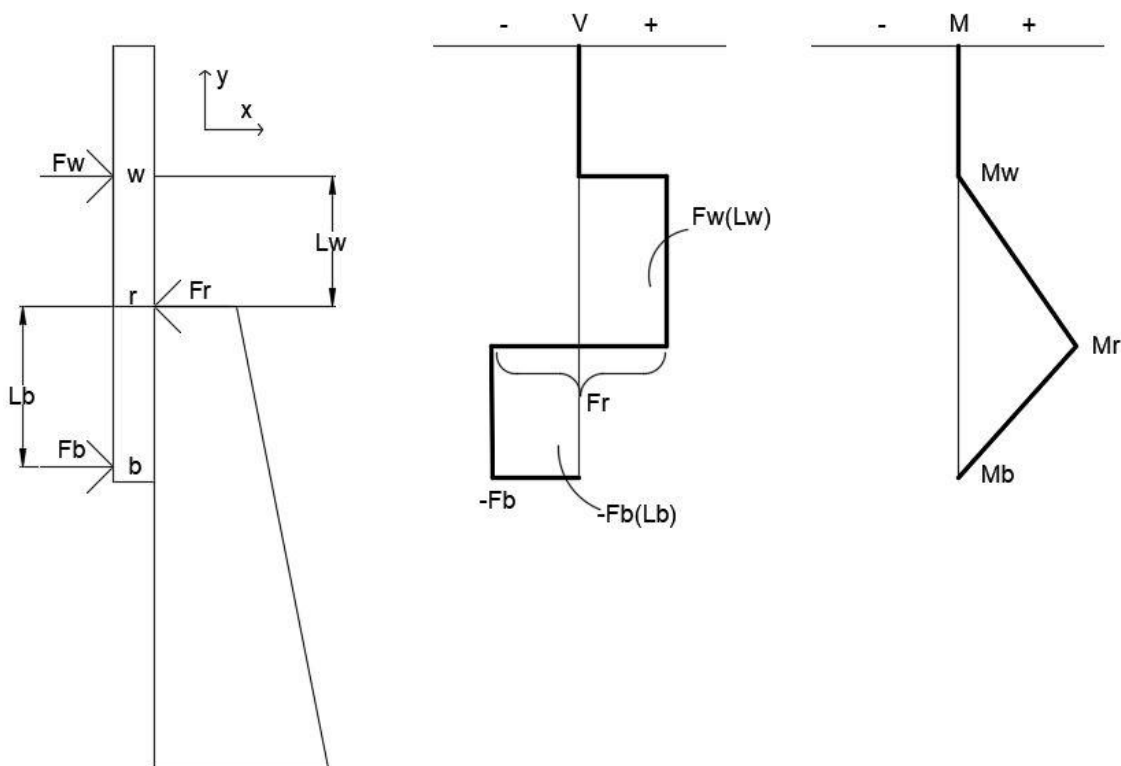


Figure 63. Simplified Back Wind Loading

Note, that the forces and moments obtained through the simplified model are equivalent to the actual configuration and only differ in the look of the shear and moment diagram. A static force balance and moment sum at points w, r, and b of the back wind scenario yields the following equations:

$$\sum F_x = 0 = F_w + F_b - F_r \quad (27)$$

$$\sum M_w = 0 = -F_r L_w + F_b (L_b + L_w) \quad (28)$$

$$\sum M_r = 0 = -F_w L_w + F_b L_b \quad (29)$$

$$\sum M_b = 0 = -F_w (L_w + L_b) + F_r L_b \quad (30)$$

Through substitution and solving these equations the forces at r, and b can be determined:

$$F_r = \frac{F_w (L_w + L_b)}{L_b} \quad (31)$$

$$F_b = \frac{F_w L_w}{L_b} \quad (32)$$

The shear diagram shows that the maximum force occurs at the top of the parapet during a back wind loading scenario. The moment diagram shows that the maximum moment during a back wind loading scenario occurs at the top of the parapet. This can be stated mathematically with the following equations:

$$M_r = F_w L_w \quad (33)$$

$$M_r = F_b L_b \quad (34)$$



#### 4.4.5 Dead Load

The weight of the fence components will result in a vertical dead load, which is equivalent to the sum of all components within one section of the fence. A diagram showing the dead load configuration is shown in Figure 64, a definition of the variables is shown in Table 9, and the full mathematical derivation is given in Appendix E.

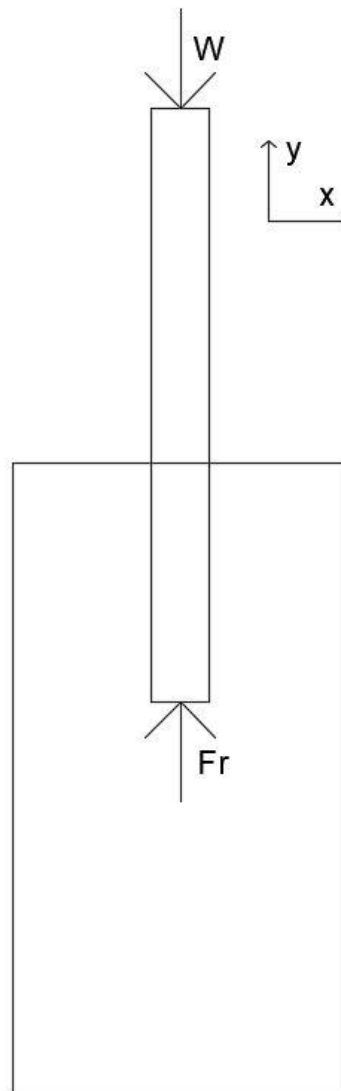


Figure 64. Dead Load Configuration

Table 9. Variable Definitions

Variable	Definition
W	Weight of Dead Load
Fr	Reaction Force due to Dead Load

$$\sum F_y = 0 = -W + F_r \quad (35)$$

$$W = F_r \quad (36)$$

Additionally, it is recommended that a load factor of 1.2 be used to determine the applied dead load for the design [30].

$$W = 1.2 * F_r \quad (37)$$

#### 4.5 Post Selection Based on Wind Load

The Chain Link Fence Manufacturers Institute published information regarding the selection of line posts and line post spacing in wind and snow prone areas [31]. The guidelines are detailed in the *Chain Link Fence Wind Load Guide for the Selection of Line Post and Line Post Spacing* and were derived from ASCE 7-10 standards and guidelines [32]. This informational guide can be used to select the correct post spacing for chain-link fence structures based off of anticipated wind gusts and icing effects, vertical post diameter, chain-link mesh size and diameter, and fence height. Additionally, these guidelines were formulated under the following assumptions:

1. Wind is acting in a direction normal to the face of the fence fabric and applied on the fabric side of the line post.

2. Line posts are considered to be embedded into the ground surface in accordance with the minimum size and depth established according to the 2009 International Building Code and ASTM F567.
3. All posts are Schedule 40 Pipe and considered to be embedded in air-entrained concrete with a minimum 2,500 psi compressive strength to a depth consistent with local soil types and conditions.

It was assumed that the structural capacity of the clamping mechanisms to the backside of the parapet would offer the same strength as the concrete foundation. Under these assumptions, the following equation was formulated to determine the maximum recommended spacing of vertical posts in a chain-link fence structure.

$$S' = hC_1C_2C_3 \quad (38)$$

Where:

- $S'$  = Post Spacing (ft)
- $h$  = Coefficient Based on Fence Height and Post Diameter
- $C_1$  = Coefficient Based on Mesh and Fabric Size
- $C_2$  = Coefficient Based on Wind Exposure
- $C_3$  = Coefficient Based on Ice Exposure

Note that the Chain Link Fence Manufactures Institute recommends a post spacing equal to  $S'$  or 10 ft (3.0 m).

#### **4.5.1 Iowa Wind Spacing and Sizing Requirements**

Current Iowa DOT requirements dictate the following:

1. Any item placed along the roadway must be able to withstand wind gusts up to 90 mph (149 kph).
2. Standards say that the wire height of the structure must be at least 6 ft (1.8 m) tall.
3. The mesh gap size must be at least 2 in. (51 mm) and should be composed of #9 gauge wire.

#### 4.5.2 Selection of Parameters and Pipe Sizing

Using these values in conjunction with the *Chain Link Fence Wind Load Guide for the Selection of Line Post and Line Post Spacing*, the coefficient values were determined and are shown below:

1. A  $C_1$  value of 7.26 was based off of a 2-in. (51-mm) gap size and #9 gauge wire;
2. A  $C_2$  value of 0.55 was obtained for a wind coefficient value, because this design will potentially be used in any type of environment; and
3. A  $C_3$  value of 0.45 was obtained, because it is very likely that the areas in Iowa where this fence will be used are likely to experience heavy ice storms.

The last coefficient, 'h', is a function of the fence height post diameter, post material, and wind speed. Iowa DOT specifies that the fence should be a minimum of 6 ft (1.8m) tall and be designed to withstand 90 mph (145 kph) winds, but the lowest wind value given in the guidelines is 105 mph (169 kph). Following the Iowa DOT guidelines given in Section 3.8.1 and selecting schedule 40 ASTM F1043 Regular Grade 30 ksi (207 MPa) yields the h values shown in Table 10.

Table 10. 'h' Values

Outside Diameter (in.)	h
1.875	1.2
2.375	2.3
2.875	4.4
3.5	7.3
4	10.2

Based on the selection parameters, the post spacing is given by the following equation:

$$S' = h(7.26)(0.55)(0.45) \quad (39)$$

Using this information and differing post diameter, multiple post spacings were determined and are shown in Table 11. Note that all of the coefficients were selected to represent the worst-case environmental conditions [31].

Table 11. Calculated Vertical Post Spacing

<b>Outside Diameter (in.)</b>	<b>Post Spacing (ft)</b>
1.875	2.16
2.375	4.13
2.875	7.91
3.5	13.12
4	18.33

The guidelines recommend that the maximum spacing should be 10 ft (3 m), and the data in Table 11 shows that this value is reached between a vertical post's outside diameter of  $2\frac{7}{8}$  in. (73 mm) and  $3\frac{1}{2}$  in. (89 mm). Linear interpolation from this table indicates that the post size will be optimized with an outside diameter of 3 in. (76 mm) and a post spacing of 10 ft (3 m). However, a 3-in. (76-mm) outside diameter, schedule 40 pipe is not a standard size. Alternative options, which satisfy the wind loading requirements, which include commonly-produced post sizes, such as  $3\frac{1}{2}$  in. (89 mm) posts spaced at 10 ft (3m) or  $2\frac{7}{8}$  in. (73 mm) posts spaced at 8 ft (2.4 m).

When the proposed debris fence experiences a significant impact event, it is preferred that the vertical posts plastically deform or fracture to reduce vehicle snag concerns. Thus, the flexural and shear capacities of the post should be minimized to the lowest acceptable value after satisfying the design criteria. Therefore,  $2\frac{7}{8}$ -in. (73-mm) outside diameter schedule 40 pipes spaced at 8 ft (2.4 m) centers were selected for the post size and spacing, respectively.

## 4.6 Minimum Design for Wind Loading

The ASCE published information regarding the typical wind loads that buildings and other structures experience based off of expected maximum wind velocities and geographical placement of the structure. These guidelines are detailed in ASCE 7-10 *Minimum Design Loads for Buildings and Other Structures* [32] and were followed to determine maximum wind loading on a fence using a 2-in. (51-mm) mesh spacing and 6 through 11 gauge wire. The equation for calculating the maximum expected wind loads is shown below. Note, ASCE 7-10 introduced wind speed maps that are to be used with a load factor equal to 1.0 for Load and Resistance Factor Design (LRFD).

$$F = q_z A C_D \quad (40)$$

Where: F = Maximum Wind load, (N)  
 $q_z$  = Maximum Dynamic Pressure, (Pa)  
 A = Projected Area, (m<sup>2</sup>)  
 $C_D$  = Drag Coefficient

### 4.6.1 Dynamic Pressure

The first step was to determine the maximum overall dynamic pressure imparted to the fence structure. The equation for this pressure calculation is shown below and is given in Section 27.3.2 of the ASCE guidelines. Using this equation and a maximum expected wind speed of 115 mph (185 kph), which is shown in the guidelines, and results in a conservative design force compared to a 90 mph (145 kph) wind speed given by the Iowa DOT. The maximum dynamic pressure experienced by the debris fence structure was calculated to be 0.22 psi (1,501 Pa).

$$q_z = 0.613 K_z K_{zT} K_D V^2 \quad (41)$$

Where:  $q_z$  = Maximum Dynamic Pressure, (Pa)  
 $K_z$  = Velocity Pressure Exposure Coefficient, 1.09

$K_{ZT}$  = Topographic Factor, 1

$K_D$  = Wind Directionality Factor, 0.85

$V$  = Maximum Expected Wind Velocity, (m/s), 51.4 m/s

#### 4.6.2 Projected Area

Next, the surface area exposed to the pressure can be determined. Current Iowa guidelines state that the chain-link fence should be at least 6 ft (1.8 m) tall, have a 2-in. (51-mm) mesh gap size, and the calculations given by the Chain Link Fence Manufacturers depict a maximum post spacing of 8 ft (2.4 m). The exposed areas subjected to the wind over each 2-in. (51-mm) gap mesh size for a 6 ft x 8 ft (1.8 m x 2.4 m) section of the fence for 6 through 11 gauge wires are shown in Table 12. The mathematical details for this calculation are given in Appendix F.

Table 12. Chain-Link Area Exposed to Wind

Wire Gauge	Chain Link Area Exposed to Wind	
	2 in. Mesh (ft <sup>2</sup> )	2 in. Mesh (m <sup>2</sup> )
6 gauge	14.39	1.34
7 gauge	12.92	1.20
8 gauge	11.59	1.08
9 gauge	10.39	0.97
10 gauge	9.31	0.86
11 gauge	8.33	0.77

#### 4.6.3 Drag Coefficient

The drag coefficient seen in Equation (40) is a function of fluid density, viscosity, speed, as well as object geometry. These values along with experimentally-determined results can be used to determine the drag coefficient.

The Reynolds Number is used to estimate the drag coefficient and can be calculated using Equation (42). The density and dynamic viscosity of air at 80 F (26.7 C) were used, and the characteristic length scale was the diameter of the chain-link mesh.

These calculated Reynolds Numbers can then be used in conjunction with the graph shown in Figure 65 to determine the drag coefficient. It is difficult to obtain accurate drag coefficients when using a logarithmic plot, but tabulated values are not readily accessible. Table 13 shows the calculated Reynolds numbers and drag coefficients for 6 through 11 gauge chain-link fabric.

$$R_e = \frac{\rho V L}{\mu} \quad (42)$$

Where:  $R_e$  = Reynolds Number  
 $\rho$  = Fluid Density (kg/m<sup>3</sup>)  
 $V$  = Fluid Velocity (m/s)  
 $L$  = Characteristic Length Scale (m)  
 $\mu$  = Dynamic Viscosity (Pa-s)

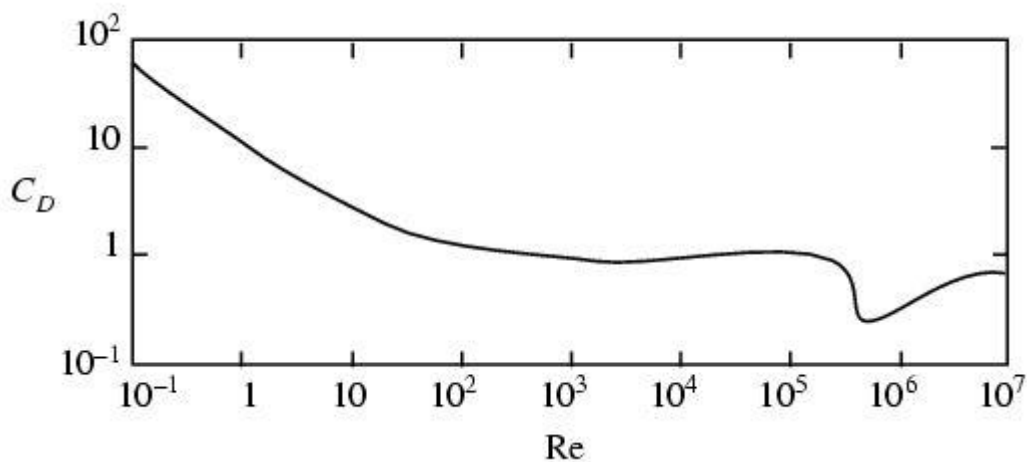


Figure 65. Drag Coefficient vs Reynolds Number for Cylinders [33]



Table 13. Calculated Reynolds Numbers and Drag Coefficients

Wire Gauge	Wind Loads	
	2 in. Mesh (lbf)	2 in. Mesh (N)
6 gauge	271	1,204
7 gauge	284	1,261
8 gauge	291	1,293
9 gauge	293	1,304
10 gauge	292	1,298
11 gauge	287	1,278

#### 4.6.4 Maximum Wind Loading

After the dynamic pressure change, projected area, and drag coefficients were determined, the maximum wind loading was calculated using Equation (40). These results are shown in Table 14. Generally, it would be expected that the drag forces would increase as the projected area increased. Thus, the larger gauge wire should experience larger drag forces, but the results displayed below do not agree with this assumption. All of the calculated Reynolds Numbers fall between 290,000 and 540,000, and these values are actually located in a transition zone that experiences a rapid decrease in the measured drag coefficient. This reduction in the drag coefficient leads to very similar drag values as the diameter of the wire is increased from 11 to 6 gauge.

Table 14. Maximum Expected Wind Loads

Wire Gauge	Wind Loads	
	2 in. Mesh (lbf)	2 in. Mesh (N)
6 gauge	271	1,204
7 gauge	284	1,261
8 gauge	291	1,293
9 gauge	293	1,304
10 gauge	292	1,298
11 gauge	287	1,278

Following the Iowa DOT guidelines, 9-gauge wire was used in the design of this debris fence system. This results in a maximum force of 293 lbf (1,304 N). This maximum force was used to confirm the structural integrity of the fence design subjected to wind loading.

#### 4.7 Design of Members for Flexure

Chapter F of the *AISC Steel Construction Manual* [34] was consulted to determine the maximum allowable flexural capacity to design vertical posts that will yield during an impact. Sections F1, General Provisions, and F8, Round HSS, are of particular interest in the design of a parapet-mounted debris containment fence. Iowa currently uses circular pipes in the protection fence shown in Figure 11. To limit the cost and use of nonstandard members, round pipe was selected for the proposed debris fence.

To determine the nominal plastic flexural strength, Equation (43) was utilized.

$$\phi_b M_n = \phi_b F_y Z \quad (\text{AISC F8} - 1) \quad (43)$$

Where:

- $\phi_b M_n$  = Design Flexural Strength (kip-in.)
- $F_y$  = Specified Minimum Yield Stress (ksi)
- $Z$  = Plastic section modulus (in.<sup>3</sup>)
- $\phi_b = 0.9$ , Resistance Factor for Flexure

Section F7 of the *AISC Steel Construction Manual* lists the steps to determine the plastic nominal flexural strength of a steel member. Following the Iowa DOT guidelines, shown in Section 3.8.1, ASTM F1083 regular grade schedule 40 piping, containing a specified yield stress of 30 ksi (207 MPa), was selected as the vertical posts used in the debris fence [35]. Plastic section modulus values were obtained from Part 1 of the Steel Manual. Next, Equation (43) was used to calculate the nominal plastic flexural strength

for schedule 40 pipes containing outside pipe diameters ranging from 1.66 in. (42 mm) to 3½ in. (89 mm). These values are shown below in Table 15.

Table 15. Nominal Plastic Flexural Strength

Size NPS	Pipe OD (in.)	Plastic Section Modulus (in. <sup>3</sup> )	Nominal Plastic Flexural Strength (kip-in.)
1.25	1.66	0.305	8.24
1.5	1.9	0.421	11.37
2	2.375	0.713	19.25
2.5	2.875	1.37	36.99
3	3.5	2.19	59.13

To minimize bending strength and maximize efficiency of the design by, a 2½-in. (64-mm) schedule 40 NPS pipe with a nominal flexural strength of 36.99 kip-in (4.18 kN-m) was recommended.

#### 4.8 Design of Members for Shear

Chapter G of the *AISC Steel Construction Manual* [34] was consulted to determine the maximum shear capacity of the vertical posts. As with the plastic bending stress, the vertical posts were assumed to be circular pipe sections, and the shear strength of the posts was calculated to determine if impact loads were likely to cause posts to shear off. To determine the shear capacity, Equation (44) can be utilized.

$$\phi_v V_n = \frac{\phi_b F_y A_g}{2} \quad (\text{AISC G5} - 1) \quad (44)$$

Where:  $V_n$  = Design Shear Strength (kips)  
 $F_y$  = Specified Minimum Yield Stress (ksi)  
 $A_g$  = Gross Cross-Sectional Area (in.<sup>2</sup>)  
 $\phi_v$  = 0.9, Resistance Factor for Shear

Using the post sizing guidelines obtained from the wind spacing and sizing requirements, a gross cross-sectional area value of 1.59 in<sup>2</sup>, as shown in Part I of the Steel

Manual, and ASTM F1083 regular grade schedule 40 piping with a specified minimum yield stress of 30 ksi (345 MPa), the design shear strength of the 2½-in. (64-mm) NPS pipe was calculated as 21.47 kips (95.5kN).

#### **4.9 Verification of Design for Wind Loading**

In order to determine that the flexure and shear values experienced by the pipe during maximum wind loading scenarios are below the calculated flexural and shear capacity of the pipe, the following assumptions were made:

1. The maximum wind load is 293 lbf (1,304 N), as shown in Section 4.6.4;
2. The top clamp will be located 8 in. (203 mm) below the top of the parapet;
3. The bottom clamp will be located 14 in. (356 mm) below the top of the parapet and;
4. The chain-link mesh height will be 6 ft (1.8 m), as shown in Section 3.8.1, and the wind load will act as a point load 36 in. (914 mm) above the parapet.

##### **4.9.1 Front Wind Loading**

Using the simplified model of the front wind loading scenario shown in Figure 66 and Equations (45) through (47), the flexural and shear capacity of the pipe can be compared against obtained values due to wind loading. These results are shown in Table 16.

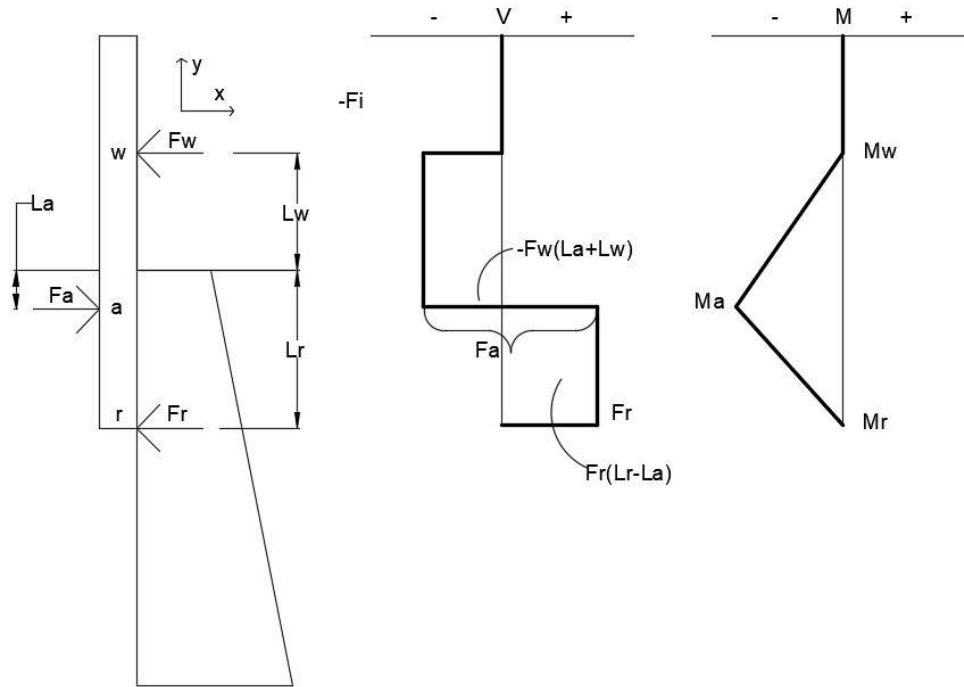


Figure 66. Front Wind Loading Simplified Configuration

$$F_a = \frac{F_w(L_r + L_w)}{(L_r - L_a)} \tag{45}$$

$$F_r = \frac{F_w(L_w + L_a)}{(L_r - L_a)} \tag{46}$$

$$M_a = F_w(L_a + L_w) \tag{47}$$

Table 16. Front Wind Loading Results

Fw (kips)	Fa (kips)	Fr (kips)	Ma (kip-in.)
0.293	2.44	2.15	12.89

The maximum flexural value of 12.89 kip-in. (1.46 kN-m), in a front wind loading scenario, occurs at the top bracket and is lower than the maximum flexural capacity of the pipe, given in Section 4.7 as 36.99 kip-in (4.18 kN-m).

The maximum shear value of 2.44 kips (10.9 kN), in a front wind loading scenario occurs at the top bracket and is lower than the maximum shear capacity of the pipe, given in Section 4.8 as 21.47 kips (95.5kN).

Thus, it is expected that the fence will not yield during frontal wind loading scenarios.

#### 4.9.2 Back Wind Loading

Using the simplified model of the back wind loading scenario shown in Figure 67 and Equations (48) through (50) the flexural and shear capacity of the pipe can be compared against obtained values due to wind loading. These results are shown in Table 17.

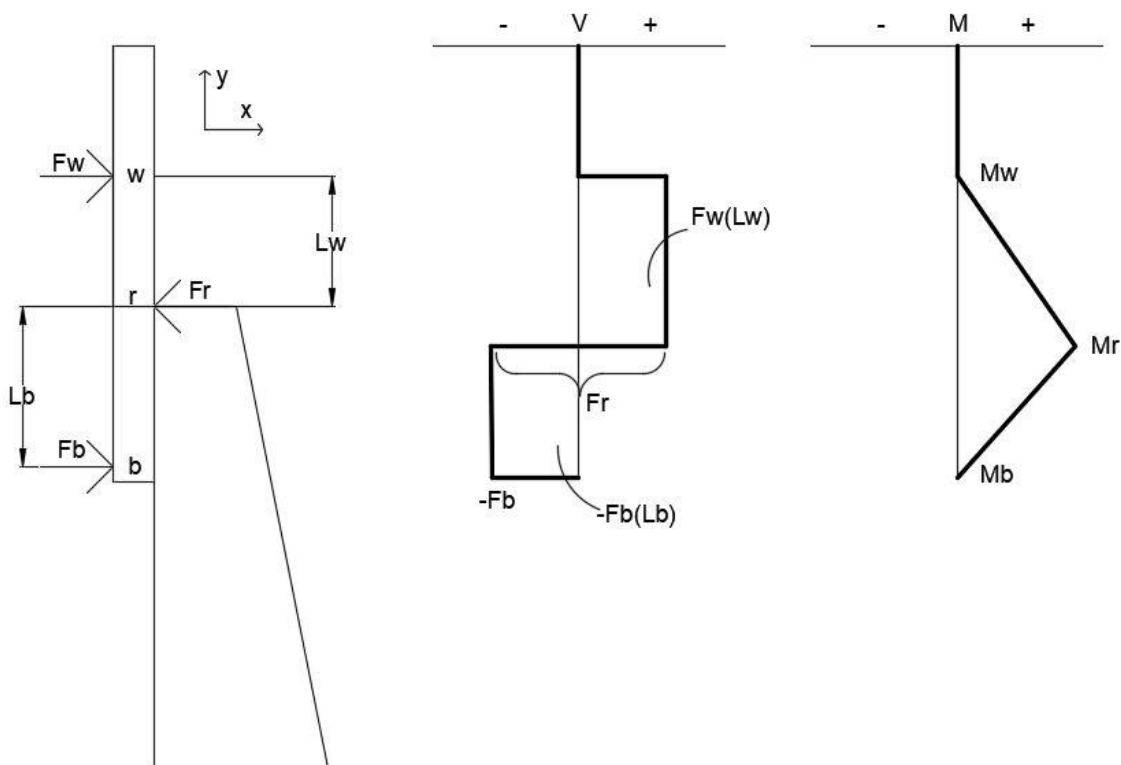


Figure 67. Back Wind Loading Simplified Configuration

$$F_r = \frac{F_w(L_w + L_b)}{L_b} \quad (48)$$

$$F_b = \frac{F_w L_w}{L_b} \quad (49)$$

$$M_r = F_w L_w \quad (50)$$

Table 17. Back Wind Loading Results

Fw (kips)	Fr (kips)	Fb (kips)	Mr (kip-in.)
0.293	1.05	0.753	10.55

The maximum flexural value of 10.55 kip-in. (1.19 kN-m), in a back wind loading scenario, occurs at the top of the parapet and is lower than the maximum flexural capacity of the pipe, given in Section 4.7 as 36.99 kip-in (4.18 kN-m).

The maximum shear value of 1.05 kips (10.9 kN), in a back wind loading scenario, occurs at the top of the parapet and is lower than the maximum shear capacity of the pipe, given in Section 4.8 as 21.47 kips (95.5kN).

Thus, it is expected that the fence will not yield during back wind loading scenarios.

#### 4.10 Estimation of Impact Force to Yield Posts

As stated previously it is preferred that the posts within this debris fence yield backwards during an impact to limit the potential snag between the fence and impacting vehicle. Note that the impact force will be the same for both the lateral and longitudinal loading scenarios. Thus, only the lateral impact scenario was analyzed, this loading configuration is shown in Figure 68. The force at point i, a, and r can be estimated using Equations (51) through (53) and the following assumptions:

1. The maximum moment in the system will be located at the top clamp and is equal to the flexural capacity of the pipe;
2. The top clamp will be located 8 in. (203 mm) below the top of the parapet;
3. The bottom clamp will be located 14 in. below the top of the parapet and;
4. The impact will occur 3 in. (76 mm) above the top of the parapet.

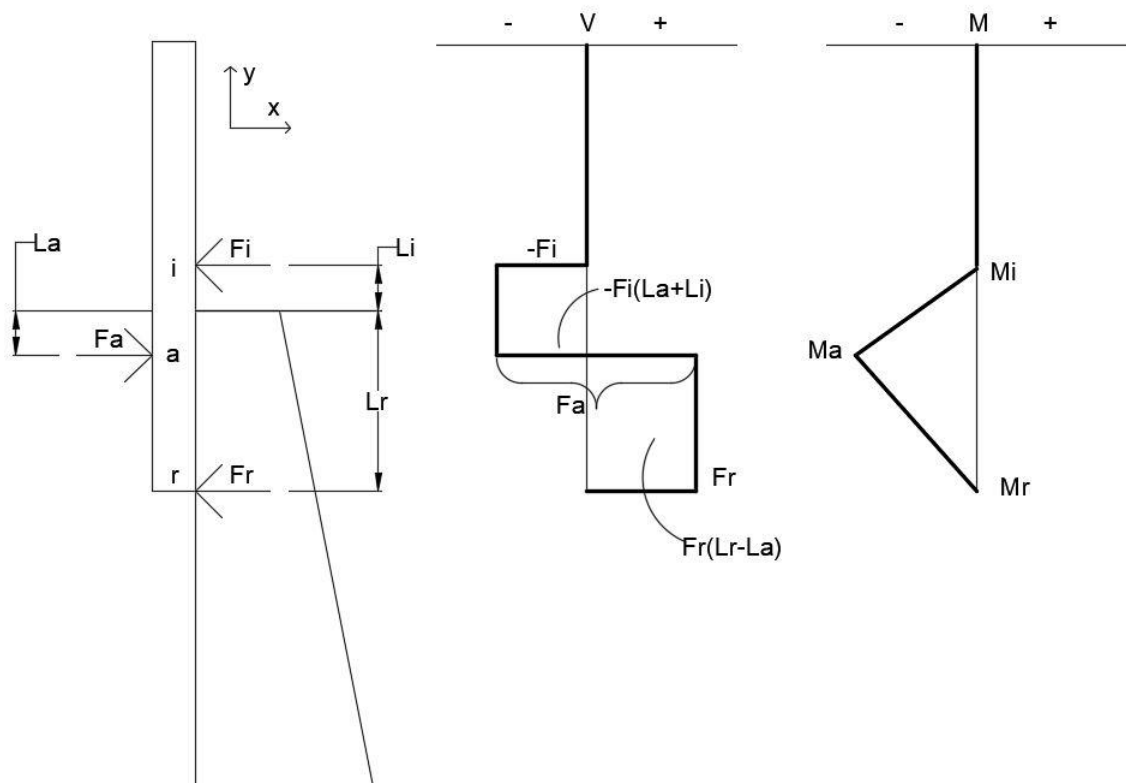


Figure 68. Lateral Impact Loading Configuration

$$M_a = F_i(L_a + L_i) \quad (51)$$

$$F_r = \frac{F_i(L_i + L_a)}{(L_r - L_a)} \quad (52)$$

$$F_a = \frac{F_r(L_i + L_r)}{(L_i + L_a)} \quad (53)$$



Table 18. Resulting Forces

<b>Fi (kips)</b>	<b>Fa (kips)</b>	<b>Fr (kips)</b>
3.36	9.53	6.17

An impact force of 3.36 kips (15.0 kN) is needed to yield the post backwards during an impact, as shown in Table 18.

## **5 ADDITIONAL PRELIMINARY DEBRIS FENCE COMPONENT DESIGNS**

### **5.1 Overview**

The following information are current best estimates for components that will be revisited and revised in future studies. These design and selections are potential options that may be selected at a future date.

### **5.2 Longitudinal Stiffeners**

As shown in the literature review of this report, states commonly use small diameter pipes or tension wires as longitudinal members in their parapet mounted debris fences. These members help to maintain the chain-link in high wind situations and can be connected using wire ties to lessen sagging of the chain-link between vertical posts. MwRSF researchers believed that using tension wires may result in less vehicle damage during an impact. The critical failure points of these tubes within the ZOI are at connection points between the tubes, where rail ends could disengage and spear an impacting vehicle. Therefore, tension wires are preferred for stiffening the lower portion of the fence.

The fence design currently used by Florida, as shown in Figures 6 through 8, only uses tension wires which most likely are used to eliminate vehicle snag on longitudinal posts and mesh within the ZOI. However, using tension wires without a fence frame could reduce the aesthetics of the system. High wind loading environments may cause the fence to sway, and tolerances in the fence construction may cause the top of the fence to wander or appear irregular, which decreases the overall aesthetic quality. A frame on the top of the fence may fix or hide fence irregularities and provide a “clean” appearance for the system, without compromising safety. Therefore, Iowa DOT decided to pursue a

fence design incorporating a top structural member to frame the fence, and two intermediate tension wires, similar to the Texas design, as shown in Figure 27.

The use of tension wires offers an added benefit of limiting fence debris from falling onto the tracks below during an impact event. It is imperative that large pieces of the structure do not break off and fall onto the track during a vehicular impact. Another method for limiting this debris may be to use the idea presented in Section 3.3. To retain any debris on the bridge after an impact, an additional wire could be installed in the upper frame.

The upper frame can be designed in multiple ways, but it is very important that installers have access to the tension wire in case it needs replaced. A potential option is shown below in Figures 69 and 70. This design consists of two main components. The first is a circular section of pipe with a piece of angle iron welded to the top. This pipe would be placed directly into the vertical posts after their installation and will be secured with one bolt. The second piece is the longitudinal member, which would be placed on top of the angle iron and secured with two bolts. This longitudinal member would allow both the top of the chain link fence and a tension cable to be placed within. These would then be secured along the member with bolts.

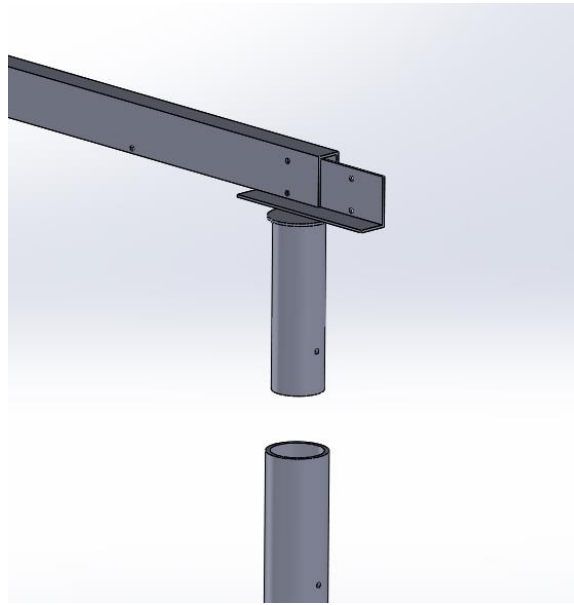


Figure 69. Potential Top Rail Isometric Back View

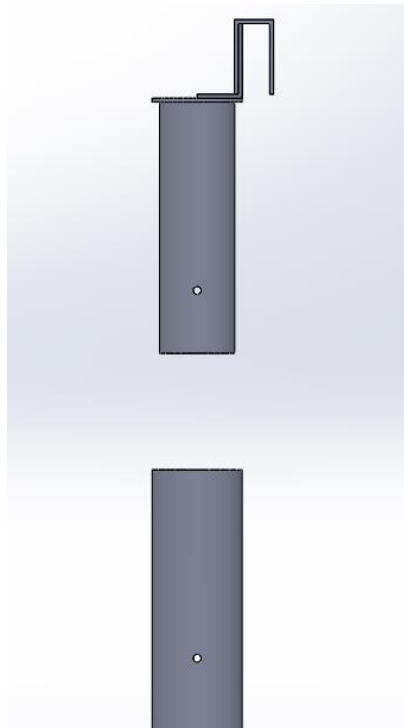


Figure 70. Potential Top Rail Side View

Note, this is not the proposed design to be used within the parapet fence but one potential option.

### 5.3 Clamp Spacing and Design

To limit vertical sagging of the fence a bolt can be placed horizontally through the saddle clamp and will need to be able to withstand anticipated dead loads. This is similar to what Florida currently uses, as shown in Figure 8. One such potential design is shown in Figure 71.

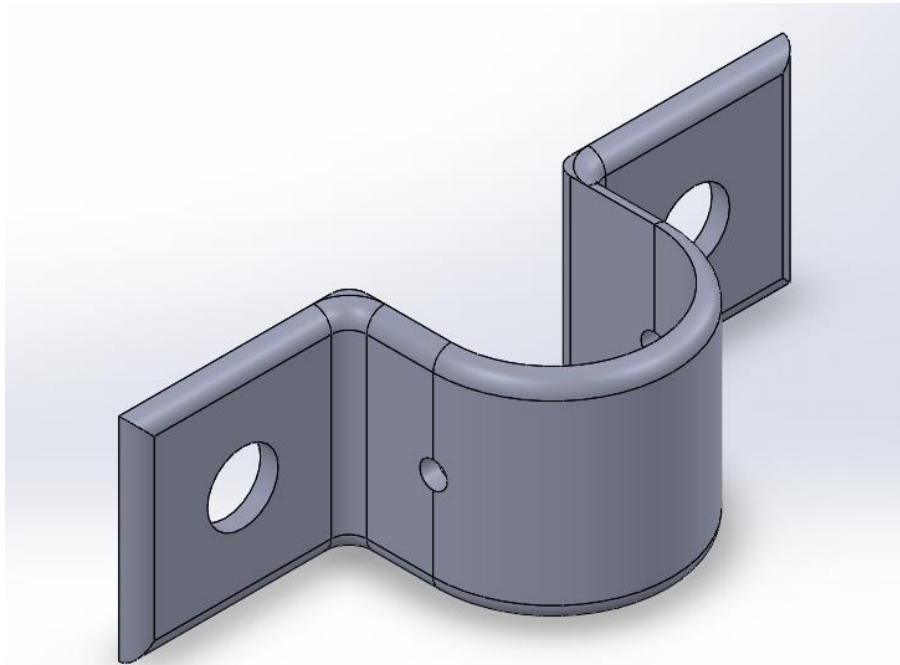


Figure 71. Potential Saddle Clamp Design

Note, this is not the proposed design to be used within the parapet fence but one potential option.

## **Part I**

### **6 SUMMARY CONCLUSIONS AND RECOMMENDATIONS**

Part I of this thesis detailed the results of a literature review and the initial design and analysis of vertical posts used with a debris fence system. Five different loading scenarios were investigated. Using these loading scenarios, and Iowa DOT criteria post sizing and spacing requirements were determined to be able to withstand expected wind loads.

The literature review, conducted for the Iowa DOT, resulted in obtaining state debris fence designs, previous real word crashes, crash tests related to debris fences, ZOI information, debris fence examples in Lincoln, Nebraska, and Iowa DOT design standards.

Due to safety and constructability concerns the Iowa DOT asked that the proposed design include vertical posts mounted to the back of the bridge rail. This allows additional offset from the barrier and reduces the chance that an impacting vehicle will come into contact with the debris fence. Saddle clamps were chosen as the method of attachment to the back of the parapet because they are commonly used by state DOTs and because of a successful crash test, under AASHTO PL-2 conditions, of a similar system by TTI.

Five different loading scenarios were investigated in this analysis and are as follows:

1. A lateral load during a vehicular impact;
2. A longitudinal load during a vehicular impact;
3. A wind load on the front of the fence;

4. A wind load on the back of the fence and;
5. A dead load from the weight of the fence material, which will always be present.

Post sizing, spacing, and material requirements were selected to allow the vertical posts and fence structure to be maintained during high wind loading events but yield out of the way during vehicular impacts to decrease the likelihood of snagging between the structure and impacting vehicle.

Typically, states use horizontal tubes within their debris fence designs to allow longitudinal stiffness of the system and to limit the amount of sway during high wind events, but there is a chance that impacting vehicles could cause these longitudinal members to break apart at connection points and spear the vehicle. In an effort to prevent this sort of vehicle and system interaction the Iowa DOT requested that tension cables be used within the design and the horizontal frame be limited to the top of the system. It is expected that under MASH TL-3 conditions there will be little to no interaction between the vehicle and the top of the debris fence.

It is recommended that additional work be complete in order to determine the correct design of the horizontal rail, saddle clamps, and anchorage connections that will be used in the design.

## **PART II**

### **7 INTRODUCTION – POST SOIL INTERACTION FORCES**

#### **7.1 Background**

This Part II effort details the results and analysis of bogie tests. These tests were conducted using steel tubes with varying cross-section geometries, embedment depths, and two different soil types. These tests were conducted to evaluate the effectiveness of the modified Midwest Guardrail System (MGS) in both strong and weak soils. Therefore, both types of soil were utilized in the bogie testing program. The strong soil met AASHTO standard soil designation M147 Grade B requirements. The weak soil met AASHTO standard soil designation A3. Post-soil interaction forces and energy-dissipation characteristics were compared for all tests. From these comparisons, the 96-in. embedment depth was found to provide adequate impact properties in both strong and weak soils.

This section of this thesis will summarize the results and analysis of a total of seventeen dynamic bogie tests of a square, thin-walled tube impacted in both weak and strong soils. During this testing series, post width and post embedment depth were evaluated to determine the importance of these variables on the overall post-soil interaction forces. A total of 23 tests were originally planned. However after the post yielding occurred the actual test matrix was modified. Post yielding, instead of post displacement within the soil, was observed for both strong and weak soil tests.

#### **7.2 Research Objectives**

The first objective was to determine how changes in post width, post embedment depth, and soil type effect overall post-soil interaction forces. The second objective was



to display this data in a meaningful and impactful way that would be beneficial in both analytical and computational studies.

### **7.3 Scope**

Nineteen bogie tests were conducted on different post geometries with various embedment depths in both weak and strong soil types. During two of these tests, the posts yielded; thus, only the data from seventeen of the tests was analyzed in detail. The target impact speed for all tests was 25 mph (40.2 kph). The posts were impacted 25 in. (635 mm) above the ground line perpendicular to the front face of the post, which created a classical “head-on” or full frontal impact with strong-axis bending. The bogie testing matrix is shown in Figure 72. Material specifications, mill certifications, and certificates of conformity for the posts are shown in Appendix G.

Two different types of soil were utilized in the tests. The first soil, a compacted sand that met AASHTO standard soil designation A-3, was utilized for test nos. P3G-1 through P3G-6, P3G-13 through P3G-15, and P3G-22, through P3G-23. Sand was utilized in the tests to represent the least desirable soil conditions that could be encountered in the installation of an upgraded Midwest Guardrail System (MGS). The second type of soil utilized in the remaining tests was a compacted, coarse, crushed limestone material that met AASHTO standard soil designation M147 Grade B, which is consistent with the strong soil required for compliance testing according to MASH 2016 [1]. Soil specifications are shown in Appendix G.

Table 19. Test Matrix

est No.	Post Type	Bogie Approximate Weight lb	Bogie Target Speed mph	Post Embedment Depth in.	Post Height Visible Above- Ground line in.	Soil Type
P3G-1	8"x6"x3/16"	1,876	25	48	36	Weak
P3G-2	8"x6"x3/16"	1,876	25	48	36	Weak
P3G-3	8"x6"x3/16"	1,876	25	72	36	Weak
P3G-4	8"x8"x3/16"	1,876	25	72	36	Weak
P3G-5	8"x6"x3/16"	1,876	25	96	36	Weak
P3G-6	8"x8"x3/16"	1,876	25	96	36	Weak
P3G-7	8"x6"x3/16"	1,876	25	48	36	Strong
P3G-8	8"x8"x3/16"	1,876	25	48	36	Strong
P3G-9	8"x6"x3/16"	5,212	25	72	36	Strong
P3G-10*		1,876	25	72	36	Strong
P3G-11*		1,876	25	96	36	Strong
P3G-12*		1,876	25	96	36	Strong
P3G-13	8"x4"x3/16"	1,876	25	78	32	Weak
P3G-14	8"x4"x3/16"	1,876	25	90	32	Weak
P3G-15	8"x4"x3/16"	1,876	25	102	32	Strong
P3G-16	8"x4"x3/16"	1,876	25	40	32	Strong
P3G-17	8"x8"x3/8"	5,212	25	48	36	Strong
P3G-18	8"x6"x3/8"	5,212	25	72	36	Strong
P3G-19	8"x8"x3/8"	5,005	25	72	36	Strong
P3G-20	8"x6"x3/8"	5,005	25	96	36	Strong
P3G-21*		5,005	25	96	36	Strong
P3G-22	8"x4"x3/8"	1,876	25	90	32	Weak
P3G-23	8"x4"x3/8"	1,876	30	102	32	Weak

\* designates test was not run

Test No.	Bogie	Bogie Weight (lb)	Bogie Speed (mph)	Post Embed Depth in. [mm]	Post Height in. [mm] (Y)	Post (Z)	Soil Type	Additional Notes
P3G-1	3	1876	25	48 [1219]	36 [914]	a1	Weak	
P3G-2	3	1876	25	48 [1219]	36 [914]	a2	Weak	
P3G-3	3	1876	25	72 [1829]	36 [914]	a3	Weak	
P3G-4	3	1876	25	72 [1829]	36 [914]	a4	Weak	
P3G-5	3	1876	25	96 [2438]	36 [914]	a5	Weak	
P3G-6	3	1876	25	96 [2438]	36 [914]	a6	Weak	
P3G-7	3	1876	25	48 [1219]	36 [914]	a1	Strong	
P3G-8	3	1876	25	48 [1219]	36 [914]	a2	Strong	
P3G-9	2	5212	25	72 [1829]	36 [914]	a3	Strong	
P3G-10	3	1876	25	72 [1829]	36 [914]	a4	Strong	Not conducted due to post yielding in test no. P3G-9
P3G-11	3	1876	25	96 [2438]	36 [914]	a5	Strong	Not conducted due to post yielding in test no. P3G-9
P3G-12	3	1876	25	96 [2438]	36 [914]	a6	Strong	Not conducted due to post yielding in test no. P3G-9
P3G-13	3	1876	25	78 [1981]	32 [813]	a7	Weak	
P3G-14	3	1876	25	90 [2286]	32 [813]	a8	Weak	
P3G-15	3	1876	25	102 [2591]	32 [813]	a9	Weak	
P3G-16	3	1876	25	40 [1016]	32 [813]	a10	Strong	
P3G-17	2	5212	25	48 [1219]	36 [914]	b1	Strong	
P3G-18	2	5212	25	72 [1829]	36 [914]	b2	Strong	
P3G-19	2	5005	25	72 [1829]	36 [914]	b3	Strong	Same bogie (no. 2) as previous tests but switched impact heads for remainder of tests due to damage from post
P3G-20	2	5005	30	96 [2438]	36 [914]	b4	Strong	
P3G-21	3	1876	25	96 [2438]	36 [914]	b5	Strong	Not conducted due to post yielding in test no. P3G-20
P3G-22	3	1876	25	90 [2286]	32 [813]	b6	Weak	
P3G-23	3	1876	30	102 [2591]	32 [813]	b7	Weak	

	NSRI Phase III Bogie Tests 1-29		SHEET: 1 of 10
	Test Matrix		DATE: 6/29/2016
DWG. NAME: Phase_III_Bogie_Tests_1-29_R3	SCALE: 1:40 UNITS: in. [mm]	DRAWN BY: DJM	REV. BY: CSSS

Figure 72. Test Matrix, Test Nos. P3G-1 through P3G-23

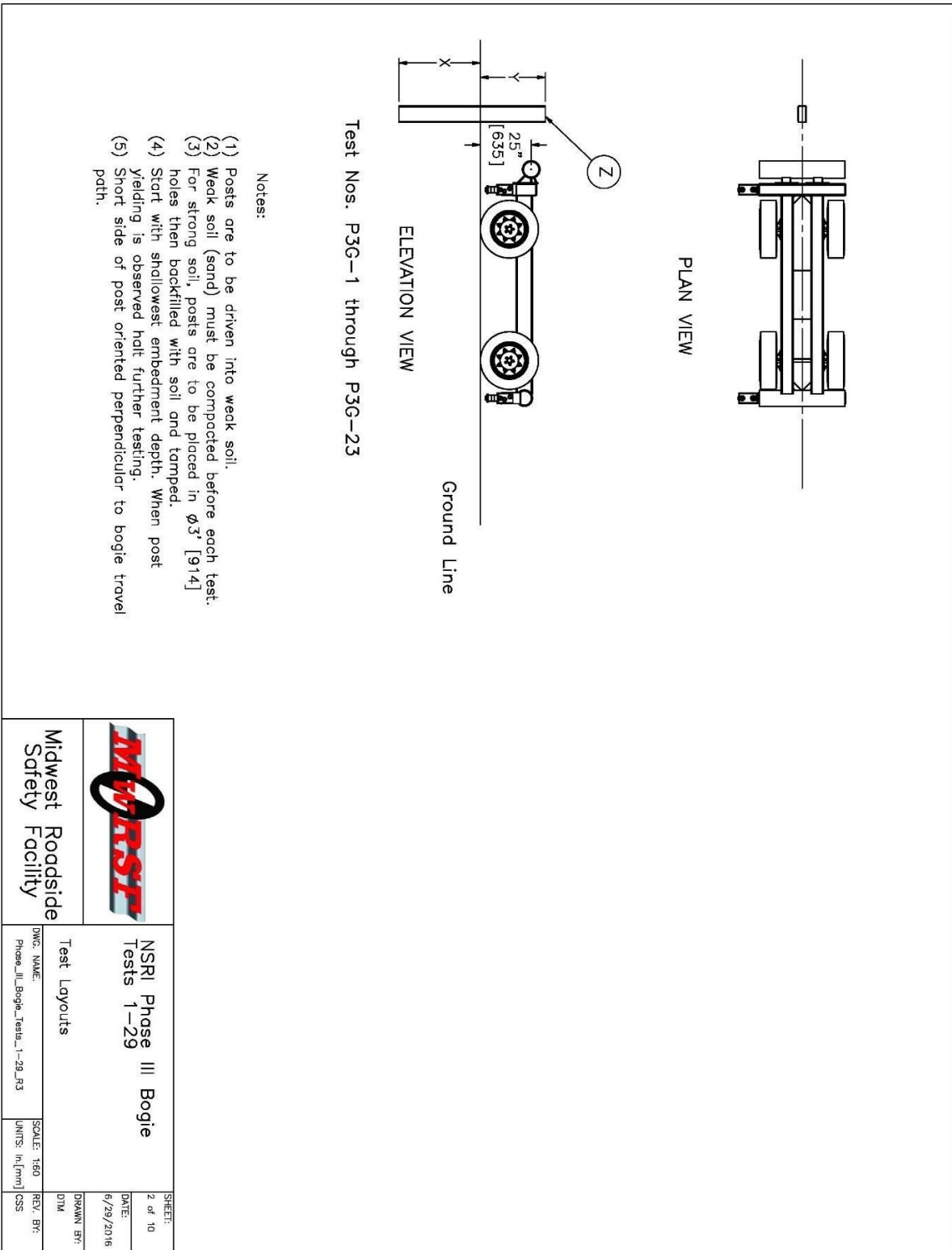
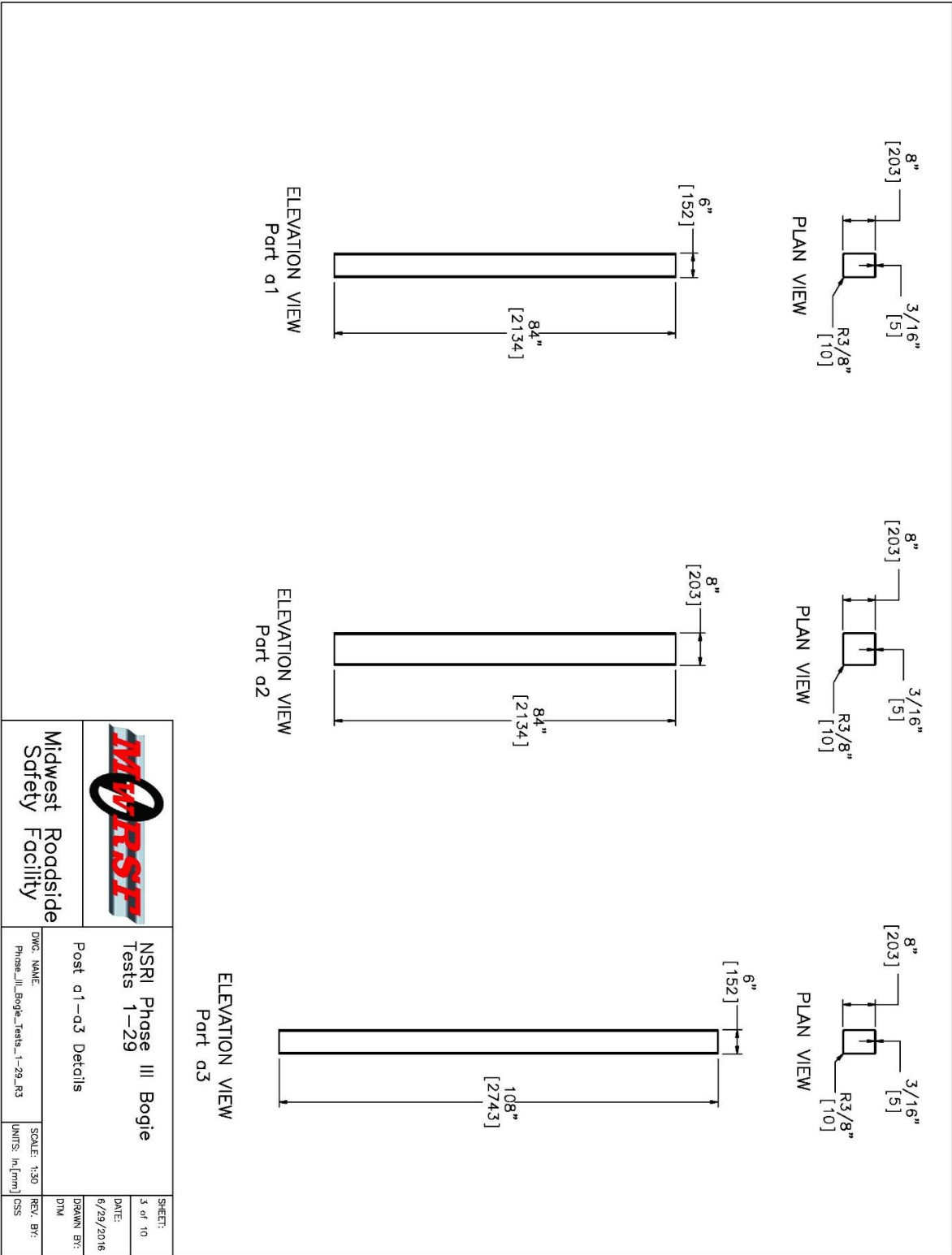


Figure 73. Test and Bogie Layout




		NSRI Phase III Bogie Tests 1-29		SHEET: 3 of 10
		Post a1-a3 Details		DATE: 6/29/2016
Midwest Roadside Safety Facility		DWG. NAME: Phase_III_Bogie_tests_1-29_R3	SCALE: 1:30 UNITS: in [mm]	DRAWN BY: DTM
				REV. BY: CSS

Figure 74. Post a1-a3 Details, Test Nos. P3G-1 through P3G-23

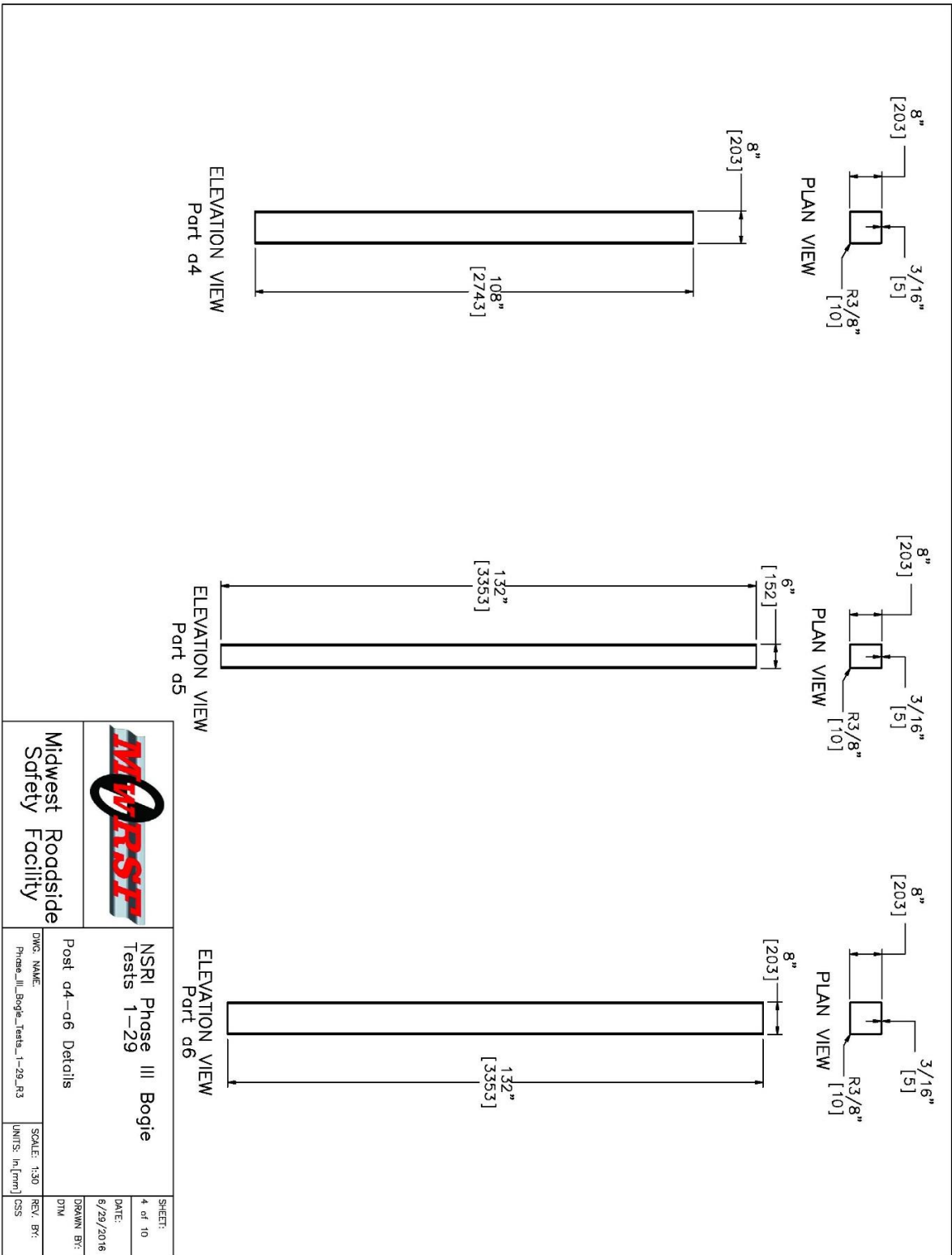


Figure 75. Post a4-a6 Details, Test Nos. P3G-1 through P3G-23

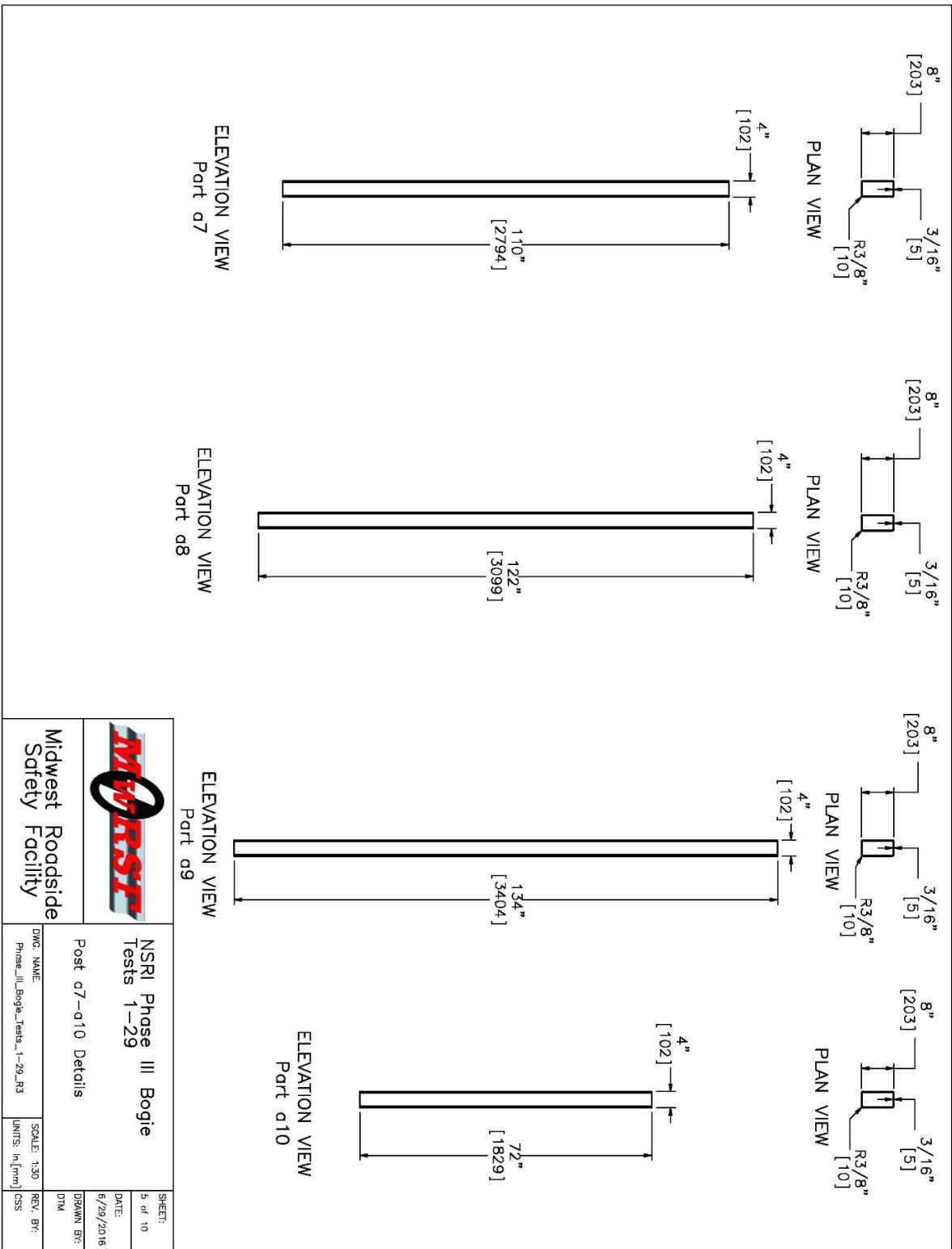


Figure 76. Post a7-a10 Details, Test Nos. P3G-1 through P3G-23

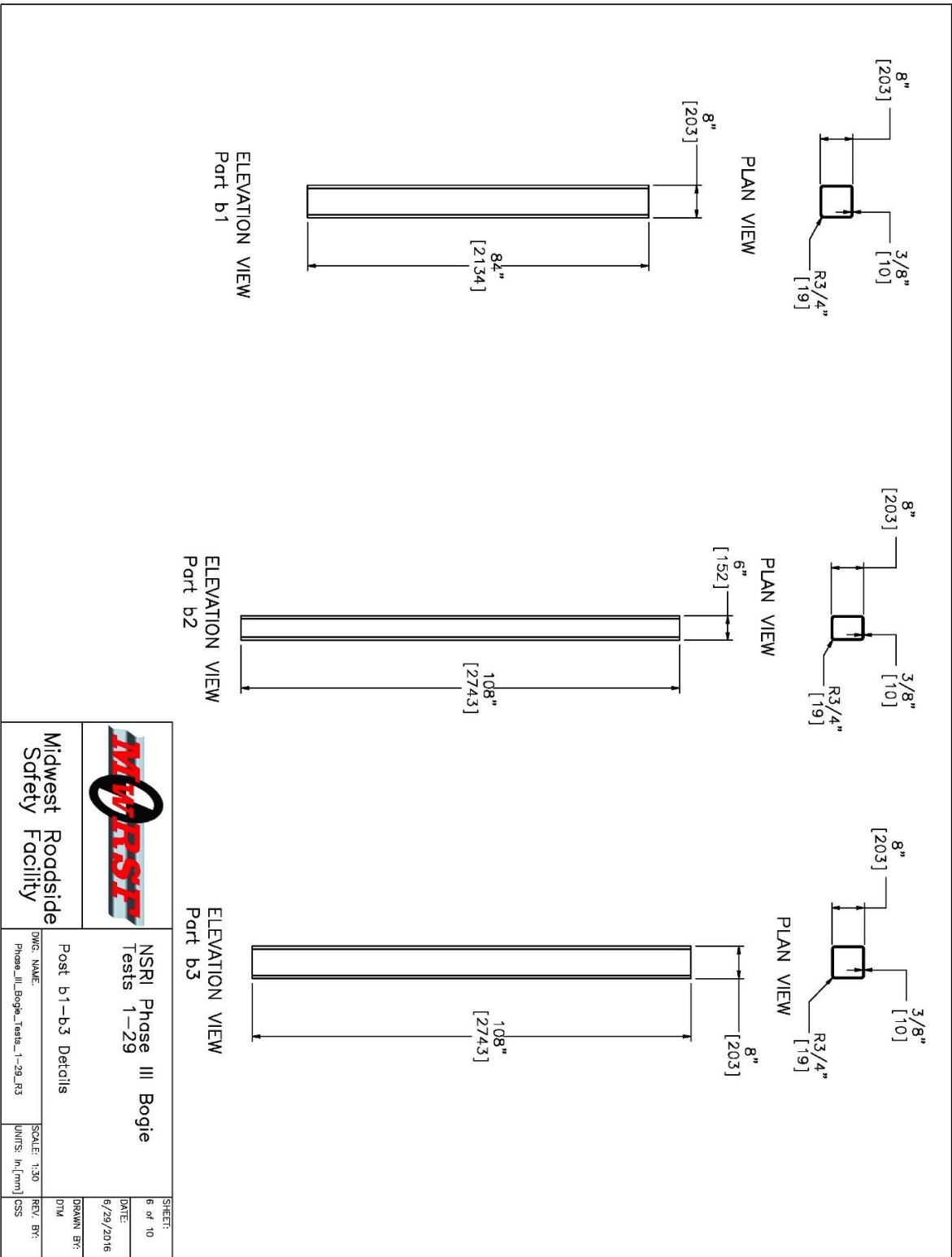


Figure 77. Post b1-b3 Details, Test Nos. P3G-1 through P3G-23



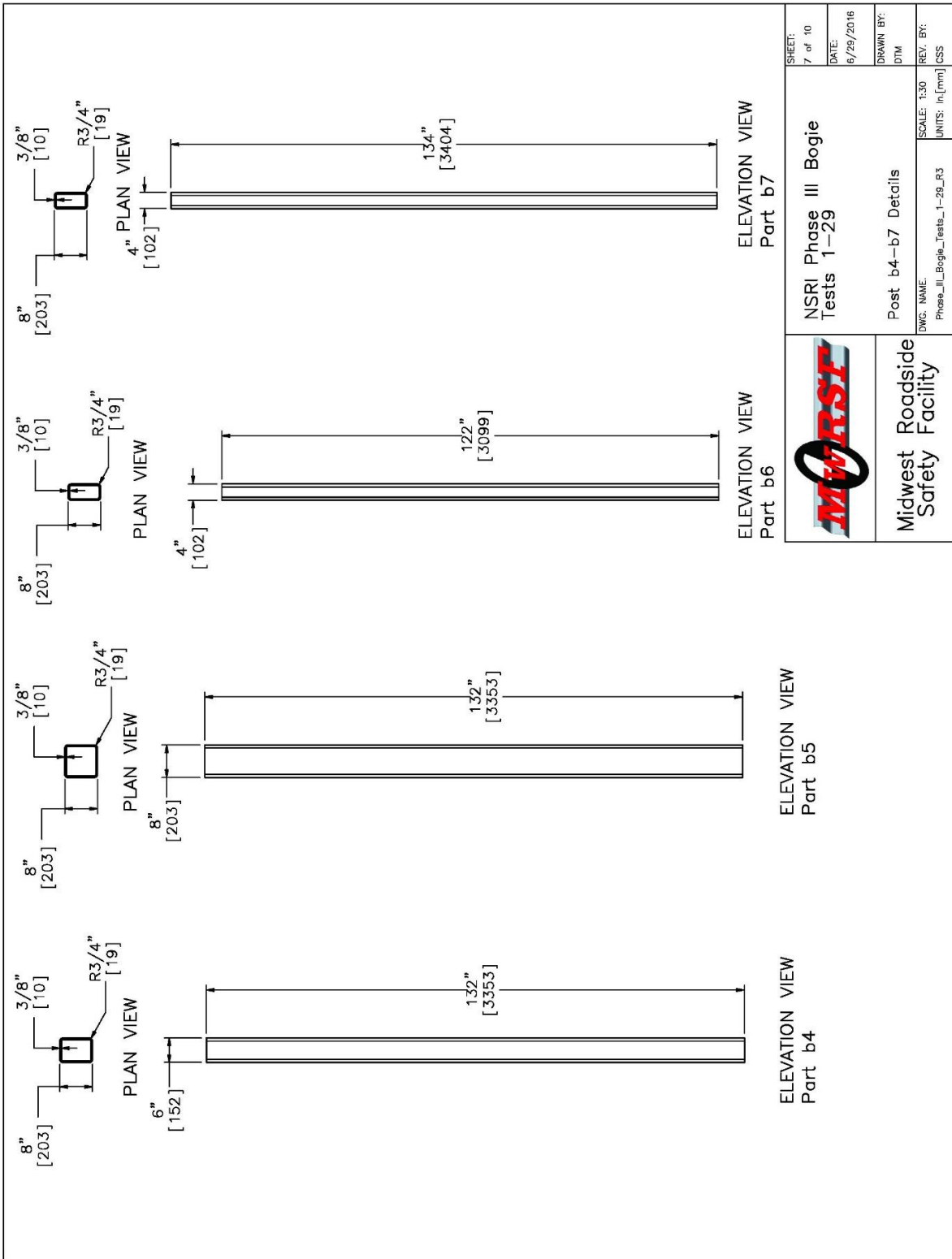


Figure 78. Post b4-b7 Details, Test Nos. P3G-1 through P3G-23

	NSRI Phase III Bogie Tests 1-29	SHEET: 7 of 10 DATE: 6/29/2016 DRAWN BY: DTM REV. BY: CSS
	Post b4-b7 Details	SCALE: 1:30 UNITS: In, [mm]

## 7.4 Equipment and Instrumentation

During the dynamic bogie tests, several types of equipment and instrumentation were utilized to collect and record data, including a bogie vehicle, accelerometers, a retroreflective speed trap, high-speed and standard-speed digital video, and still cameras.

### 7.4.1 Bogie Vehicles

Two rigid-frame bogies were used to impact the posts. A variable-height, detachable impact head was used in all tests. The bogie head was constructed of 8-in. (203-mm) diameter, ½-in. (13-mm) thick standard steel pipe, with ¾-in. (19-mm) neoprene belting wrapped around the pipe to prevent local damage to the post during the impact event. The impact head was bolted to the bogie vehicle, creating a rigid frame with an impact height of 25 in. (635 mm). Bogie no. 3, which was used with the impact head in test nos. P3G-1 through P3G-8 and P3G-13 through P3G-16, is shown in Figure 79. Bogie no. 2, which was used with the impact head in test nos. P3G-9 and P3G-17 through P3G-23, is shown in Figure 80. For the first three tests utilizing bogie no. 2, test nos. P3G-9, P3G-17, and P3G-18, the test weight of the bogie with the accelerometers and mountable impact head was 5,212 lb (2364 kg). The weight of the bogie no. 3 with the addition of the mountable impact head and accelerometers was 1,876 lb (851 kg). During test no. P3G-18, bogie no. 2 sustained damage to the impact head. Thus, for test nos. P3G-21 through P3G-23, a different impact head was substituted, and the weight of the bogie, accelerometers, and new impact head was 5,005 lb (2,270 kg).



Figure 79. Rigid-Frame Bogie No. 3 and Guidance Track



Figure 80. Rigid-Frame Bogie No. 2 and Guidance Track

#### 7.4.2 Test Vehicle

A pickup truck with a reverse-cable, tow system was used to propel the bogie to the respective target impact speed for each test. When the bogie approached the end of the guidance system, it was released from the tow cable, allowing it to be free rolling

when it impacted the post. A remote-controlled braking system was installed on the bogie, thus allowing it to be brought safely to rest after the test.

### **7.4.3 Accelerometers**

Two accelerometer systems were mounted on the bogie vehicle near its center of gravity (c.g.) to measure the acceleration in the longitudinal, lateral, and vertical directions. However, only the longitudinal acceleration data was processed and reported herein.

The two systems, the SLICE-1 and SLICE-2 units, were modular data acquisition systems manufactured by Diversified Technical Systems (DTS) of Seal Beach, California. The acceleration sensors were mounted inside the bodies of custom-built SLICE 6DX event data recorders and recorded data at 10,000 Hz to the onboard microprocessor. Each SLICE 6DX was configured with 7 GB of non-volatile flash memory, a range of  $\pm 500$  g's, a sample rate of 10,000 Hz, and a 1,650 Hz (CFC 1000) anti-aliasing filter. The "SLICEWare" computer software program and a customized Microsoft Excel worksheet were used to analyze and plot the accelerometer data.

### **7.4.4 Retroreflective Optic Speed Trap**

The retroreflective optic speed trap was used to determine the speed of the bogie vehicle before impact. Three retroreflective targets, spaced at approximately 18-in. intervals, were applied to the side of the vehicle. When the emitted beam of light was reflected by the targets and returned to the Emitter/Receiver, a signal was sent to the data acquisition computer, recording at 10,000 Hz, as well as the external LED box activating the LED flashes. The speed was then calculated using the spacing between the retroreflective targets and the time between the signals. LED lights and high-speed digital

video analysis are only used as a backup in the event that vehicle speeds cannot be determined from the electronic data.

#### **7.4.5 Digital Photography**

One AOS high-speed digital video camera and two GoPro digital video cameras were used to document all tests. The AOS high-speed camera had a frame rate of 500 frames per second and both GoPro video cameras had a frame rate of 240 frames per second. The cameras were placed laterally from the post, with a view perpendicular to the bogie's direction of travel. A Nikon D5300 digital still camera was also used to document pre- and post-test conditions for all tests.

#### **7.5 End of Test Determination**

When the impact head initially contacts the test article, the force exerted by the surrogate test vehicle is approximately parallel to the bogie's direction of travel. However, as the post rotates, the surrogate test vehicle's orientation changes with respect to the impact face of the post. This introduces two sources of error: (1) the contact force between the impact head and the post has a vertical component and (2) the impact head slides upward along the test article. Therefore, only the initial portion of the accelerometer trace should be used since variations in the data become significant as the system rotates and the surrogate test vehicle overrides the system. Additionally, guidelines were established to define the end of test time using the high-speed video of the impact. The first occurrence of the surrogate vehicle overriding/losing contact with the test article was used to determine the end of the test.

## 7.6 Data Processing

The electronic accelerometer data obtained in dynamic testing was filtered using the SAE Class 60 Butterworth filter conforming to the SAE J211/1 specifications [37]. The pertinent acceleration signal was extracted from the bulk of the data signals. The processed acceleration data was then multiplied by the mass of the bogie to get the impact force using Newton's Second Law. Next, the acceleration trace was integrated to find the change in velocity versus time. Initial velocity of the bogie, calculated from the pressure tape switch data, was then used to determine the bogie velocity, and the calculated velocity trace was integrated to find the bogie's displacement. This displacement is also the displacement of the post. Combining the previous results, a force vs. deflection curve was plotted for each test. Finally, integration of the force vs. deflection curve provided the energy vs. deflection curve for each test.

## **8 EFFECT OF PARAMETER VARIATION ON POST-SOIL FORCES**

### **8.1 Introduction and Motivation**

Researchers compiled the results of the bogie testing and conducted a parametric study to determine what trends, if any, could be identified based on the dynamic component testing. Some of the parameters which were investigated included post width, post embedment depth, and soil strength.

Univariate analysis was conducted based on similarities from test execution. For example, during the post width comparison, data from tests with posts containing different widths were compared at the same embedment depth and soil strength. Results were plotted graphically and trends were identified, although additional research is necessary to confirm the trend at extrapolated conditions.

### **8.2 Post Width**

During this testing series, an attempt was made to quantify the effect that post width has on the post-soil interaction forces by comparing the results of dynamic post tests with different widths installed in similar soils and embedment depths. Posts with widths of 6 in (152 mm) and 8 in. (203 mm) were tested at an embedment depths of 48 in. (1219 mm) and 72 in. (1829 mm) in strong and weak soils. These two post widths were additionally tested at a 96-in (2,438 mm) embedment in weak soil. All tests that experienced a post yield were neglected from this analysis in order to isolate the post-soil response.

#### **8.2.1 48-in. Embedment in Weak Soil**

Tests P3G-1 (HSS 6-in. x 8-in. x 84-in. x 3/16-in.) and P3G-2 (HSS 8-in. x 8-in. x 84-in. x 3/16-in.) were conducted at an embedment depth of 48 in. (1,219 mm) in weak

soil. Graphs of force vs. displacement and energy vs. displacement can be seen in Figures 81 and 82. The average force values for both widths at 5, 10, 15, and 20 in. (127, 254, 381, and 508 mm) of displacement are shown numerically in Table 20.

Table 20. P3G-1 and P3G-2 Average Force Comparison— 48-in. Embedment in Weak Soil

	@ 5 in.	@ 10 in.	@ 15 in.	@ 20 in.
<b>P3G-1 Average Force (kip)</b> 6 in. x 8 in. x 84 in. long by 3/16 in. thick tube	12.80	7.96	6.43	5.66
<b>P3G-2 Average Force (kip)</b> 8 in. x 8 in. x 84 in. long by 3/16 in. thick tube	13.62	8.72	6.89	6.05
<b>Percent Difference</b>	6.4%	9.6%	7.3%	6.8%



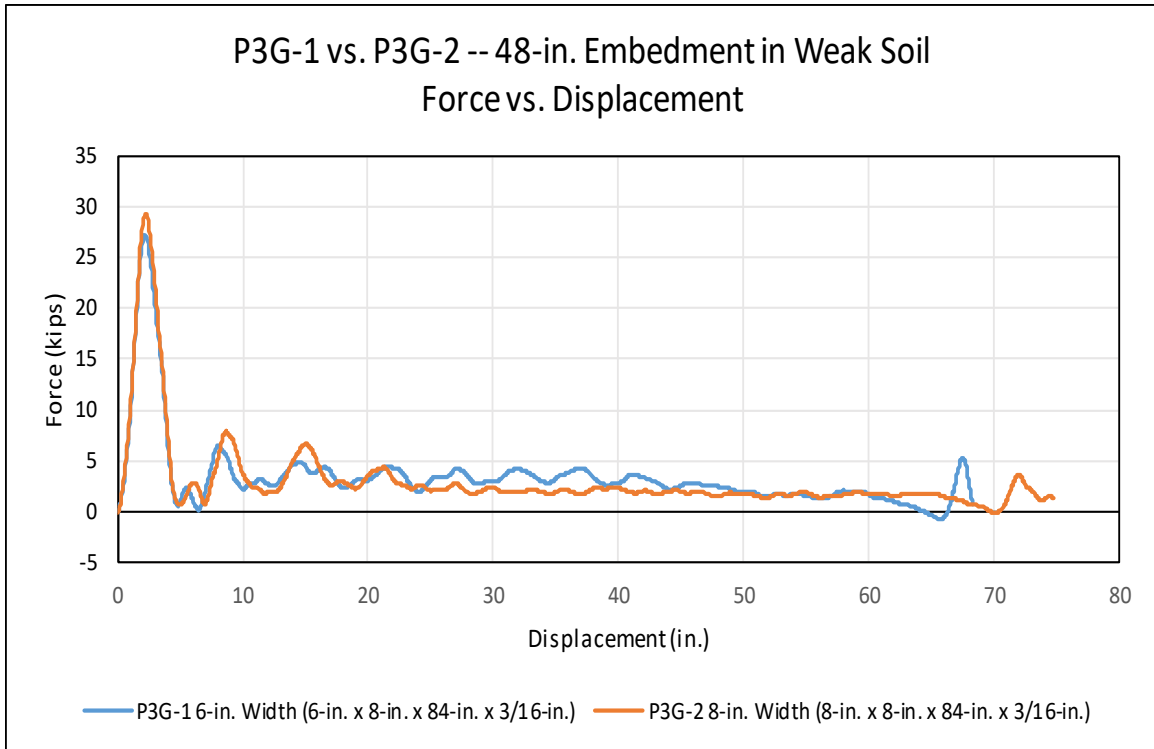


Figure 81. Force vs. Displacement for P3G-1 and P3G-2

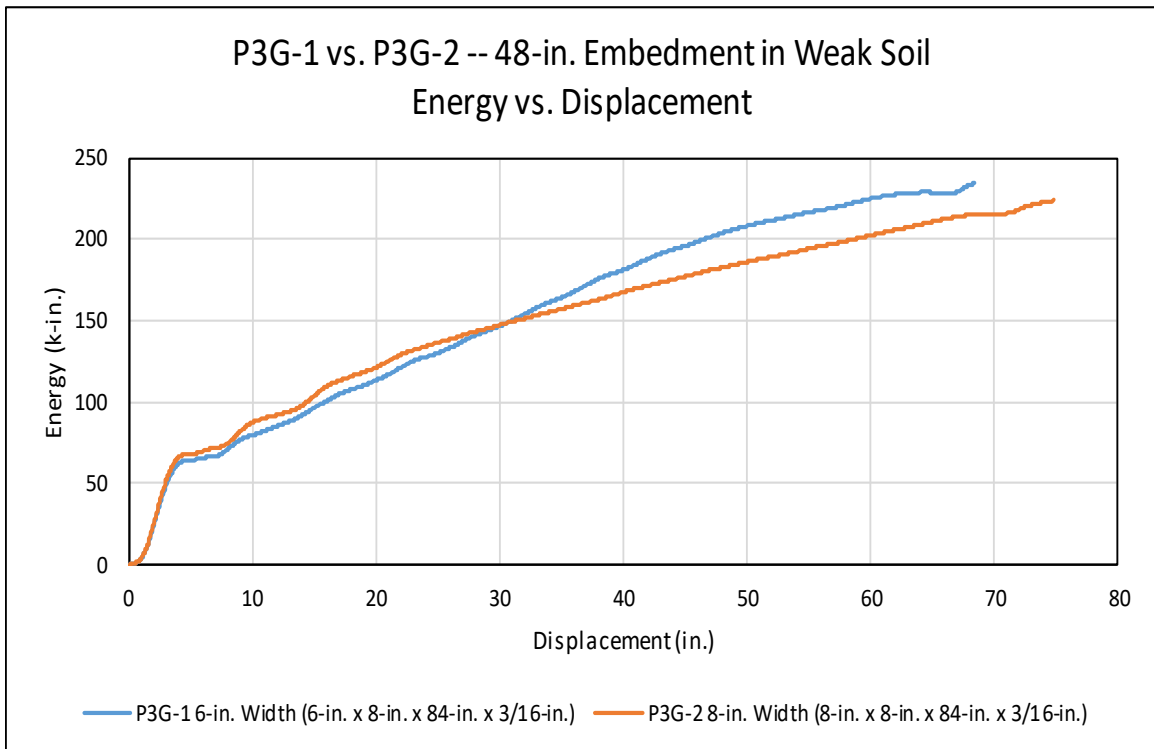


Figure 82. Energy vs. Displacement for P3G-1 and P3G-2

### 8.2.2 72-in. Embedment in Weak Soil

Tests P3G-3 (HSS 6-in. x 8-in. x 108-in. x 3/16-in.) and P3G-4 (HSS 8-in. x 8-in. x 108-in. x 3/16-in.) were conducted at an embedment depth of 72 in. (1,829 mm) in weak soil. Graphs of force vs. displacement and energy vs. displacement can be seen in Figures 83 and 84. Average force values for both widths at 5, 10, 15, and 20 in. (127, 254, 381, and 508 mm) of displacement are shown numerically in Table 21.

Table 21. P3G-3 and P3G-4 Average Force Comparison – 72-in. Embedment in Weak Soil

	@ 5 in.	@ 10 in.	@ 15 in.	@ 20 in.
<b>P3G-3 Average Force (kip)</b> 6 in. x 8 in. x 108 in. long by 3/16 in. thick tube	17.92	11.59	10.09	9.66
<b>P3G-4 Average Force (kip)</b> 8 in. x 8 in. x 108 in. long by 3/16 in. thick tube	20.45	13.90	12.57	11.99
<b>Percent Difference</b>	14.1%	19.9%	24.6%	24.1%

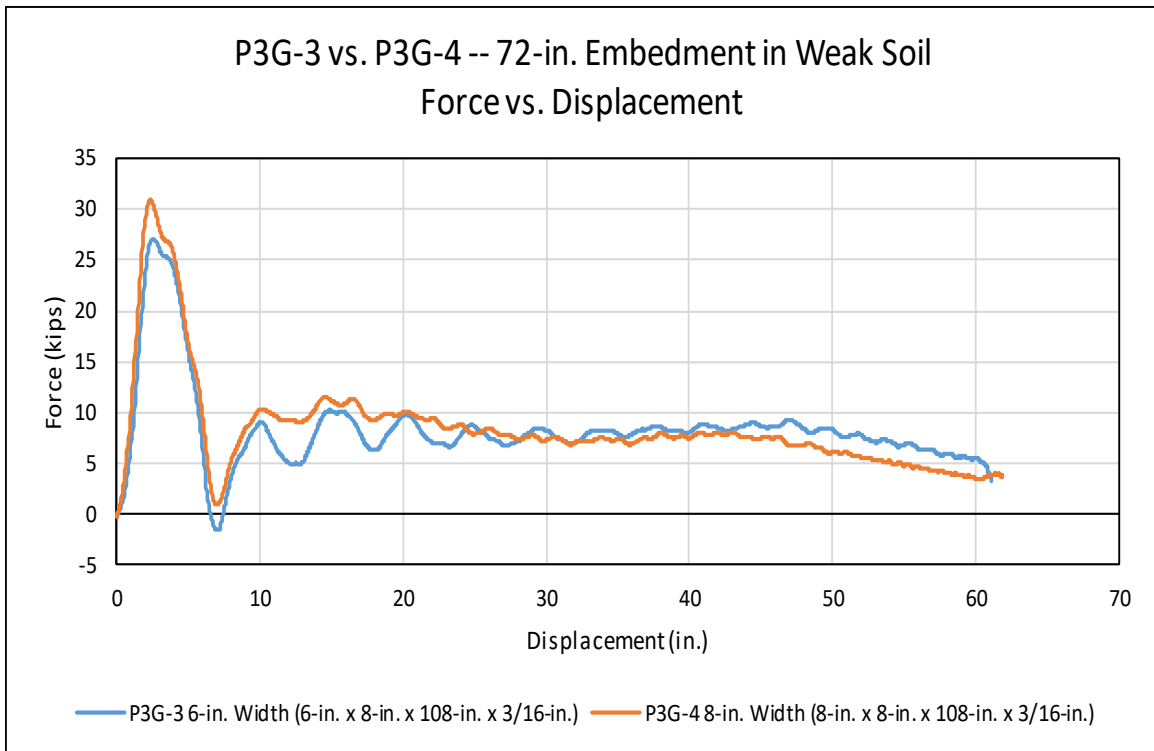


Figure 83. Force vs. Displacement for P3G-3 and P3G-4

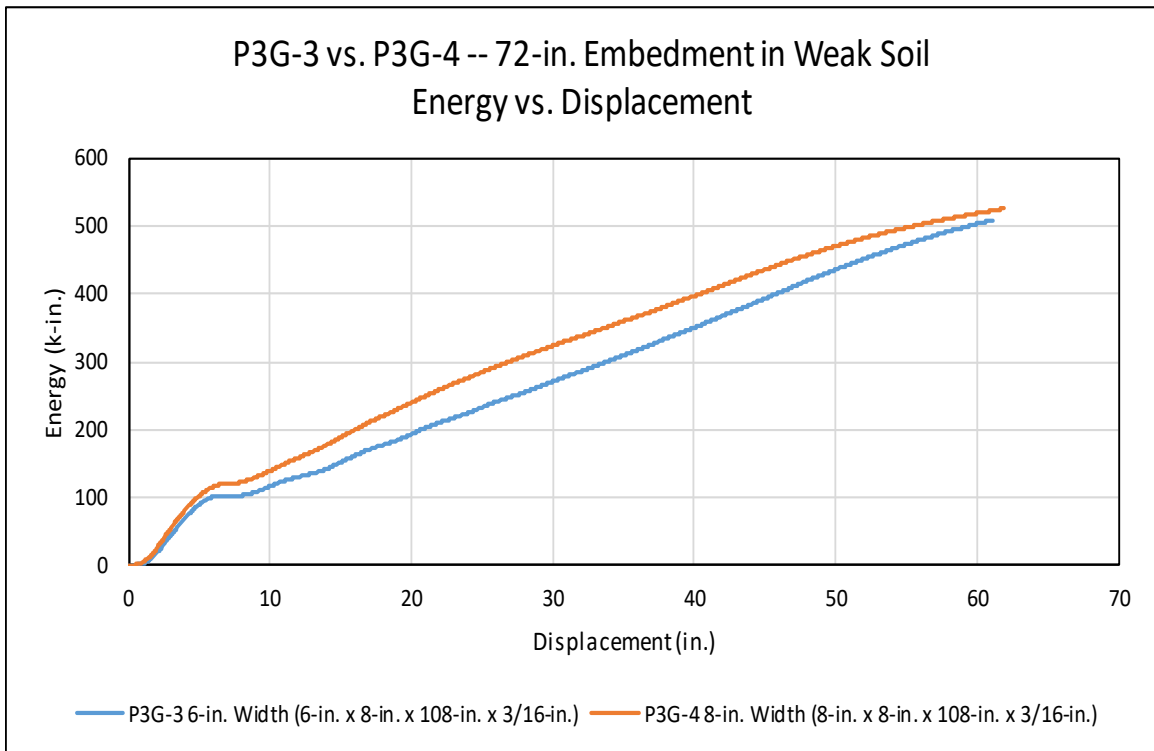


Figure 84. Energy vs. Displacement for P3G-3 and P3G-4

### 8.2.3 96-in. Embedment in Weak Soil

Tests P3G-5 (6-in. x 8-in. x 132-in. x 3/16-in.) and P3G-6 (8-in. x 8-in. x 132-in. x 3/16-in.) were conducted at an embedment depth of 96 in. (2,438 mm) in weak soil.

Graphs of force vs displacement and energy vs. displacement can be seen in Figures 85 and 86. Average force values for both widths at 5, 10, 15, and 20 in. (127, 254, 381, and 508 mm) of displacement are shown numerically in Table 22.

Table 22. P3G-5 and P3G-6 Average Force Comparison – 96-in. Embedment in Weak Soil

	@ 5 in.	@ 10 in.	@ 15 in.	@ 20 in.
<b>P3G-5 Average Force (kip)</b> 6 in. x 8 in. x 132 in. long by 3/16 in. thick tube	20.04	18.68	17.74	17.38
<b>P3G-6 Average Force (kip)</b> 6 in. x 8 in. x 132 in. long by 3/16 in. thick tube	20.13	19.54	18.94	18.76
<b>Percent Difference</b>	0.4%	4.6%	6.7%	8.0%

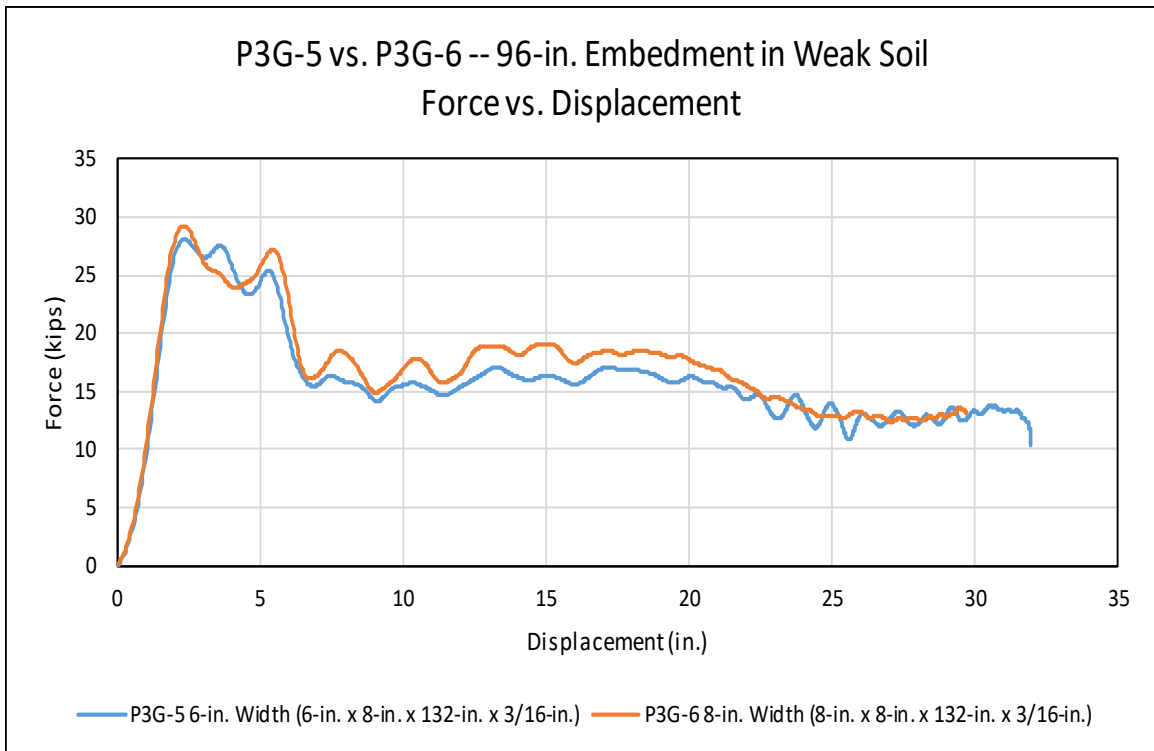


Figure 85. Force vs. Displacement for P3G-5 and P3G-6

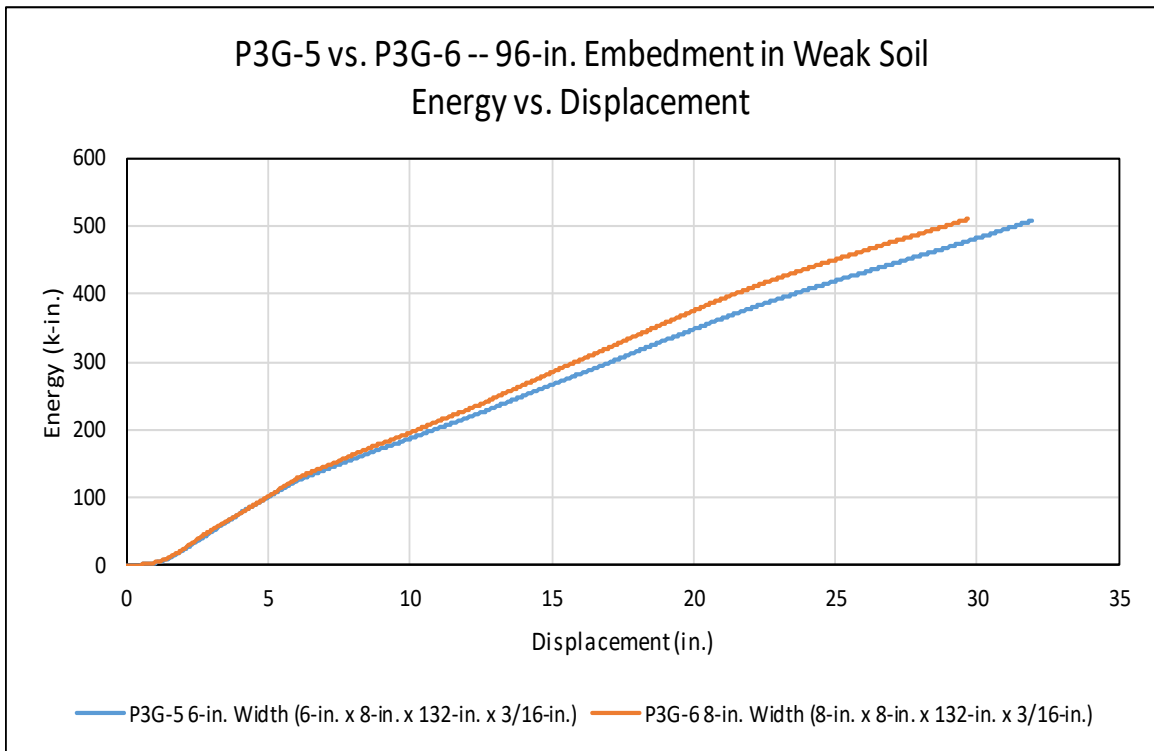


Figure 86. Energy vs. Displacement for P3G-5 and P3G-6

### 8.2.4 48-in. Embedment in Strong Soil

Tests P3G-7 (HSS 6-in. x 8-in. x 84-in. x 3/16-in.) and the average between P3G-8 (HSS 8-in. x 8-in. x 84-in. x 3/16-in.) and P3G-17 (HSS 8-in. x 8-in. x 84-in. x 3/8-in.) were conducted at an embedment depth of 48 in. (1,219 mm) in strong soil. P3G-8 and P3G-17 were averaged together because the only difference between the two tests was the post thickness and both tests behaved similarly to each other except for a small inertial spike at the beginning of the test. Graphs of force vs. displacement and energy vs. displacement can be seen in Figures 87 and 88. Average force values for both widths at 5, 10, 15, and 20 in. (127, 254, 381, and 508 mm) of displacement are shown numerically in Table 23.

Table 23. P3G-7 and the average of P3G-8 and P3G-17 Average Force Comparison – 48-in. Embedment in Strong Soil

	@ 5 in.	@ 10 in.	@ 15 in.	@ 20 in.
<b>P3G-7 Average Force (kip)</b> 6 in. x 8 in. x 84 in. long by 3/16 in. thick tube	15.03	14.75	14.13	13.14
<b>P3G-8 &amp; P3G-17 Composite Average Force (kip)</b> 8 in. x 8 in. x 84 in. long by 3/16 in. and 3/8 in. thick tube	22.06	21.68	20.27	18.72
<b>Percent Difference</b>	46.7%	47.0%	43.5%	42.4%

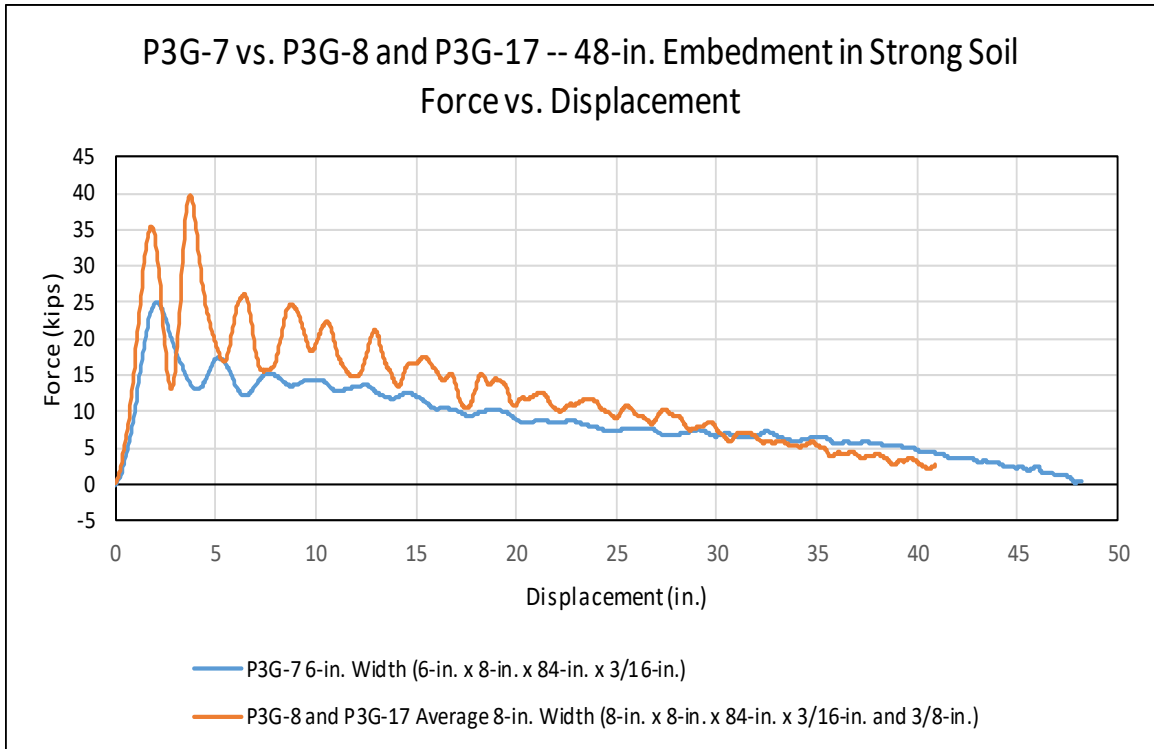


Figure 87. Force vs. Displacement for P3G-7 and the average of P3G-8 and P3G-17

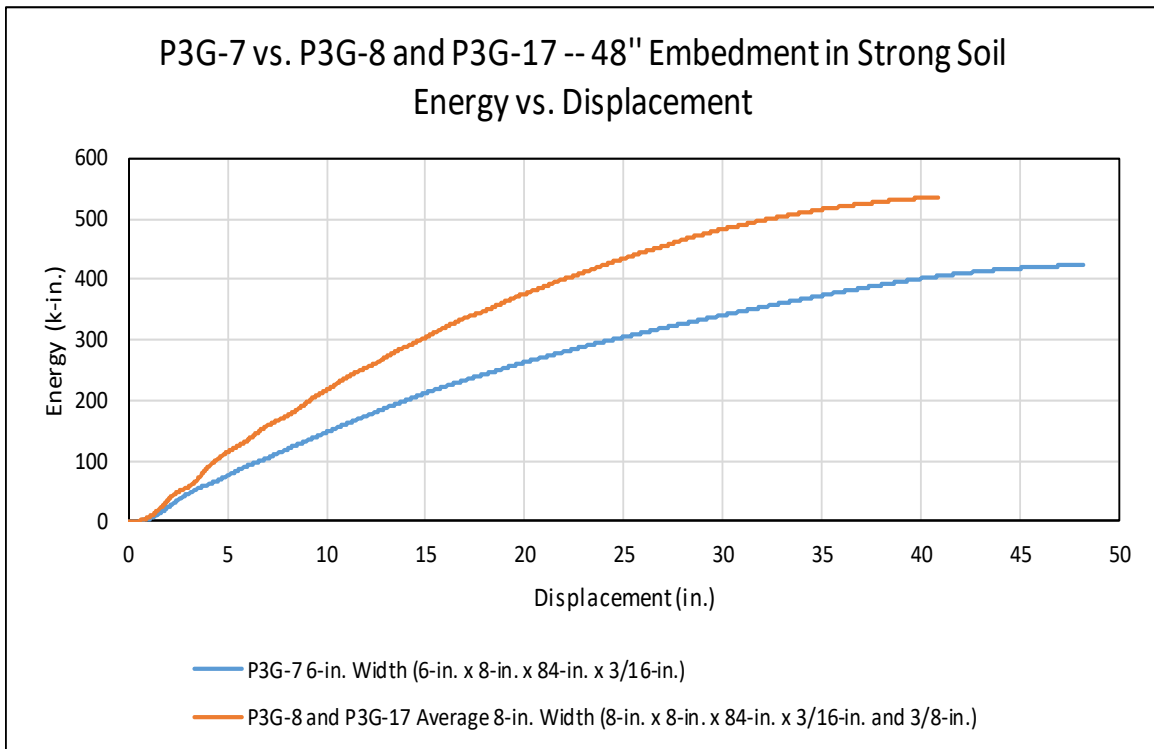


Figure 88. Energy vs. Displacement for P3G-7 and the average of P3G-8 and P3G-17

### 8.2.5 72-in. Embedment in Strong Soil

P3G-18 (HSS 6-in. x 8-in. x 108-in. x 3/8-in.) and P3G-19 (HSS 8-in. x 8-in. x 108-in. x 3/8-in.) were conducted at an embedment depth of 72 in. (1,829 mm) in strong soil. Graphs of force vs. displacement and energy vs. displacement can be seen in Figures 89 and 90. Average force values for both widths at 5, 10, 15, and 20 in. (127, 254, 381, and 508 mm) of displacement are shown numerically in Table 24.

Table 24. P3G-18 and P3G-19 Average Force Comparison – 72-in. Embedment in Strong Soil

	@ 5 in.	@ 10 in.	@ 15 in.	@ 20 in.
<b>P3G-18 Average Force (kip)</b> 6 in. x 8 in. x 108 in. long by 3/8 in. thick tube	29.89	26.75	28.38	28.85
<b>P3G-19 Average Force (kip)</b> 8 in. x 8 in. x 108 in. long by 3/8 in. thick tube	33.20	30.29	31.73	32.05
<b>Percent Difference</b>	11.1%	13.3%	11.8%	11.1%



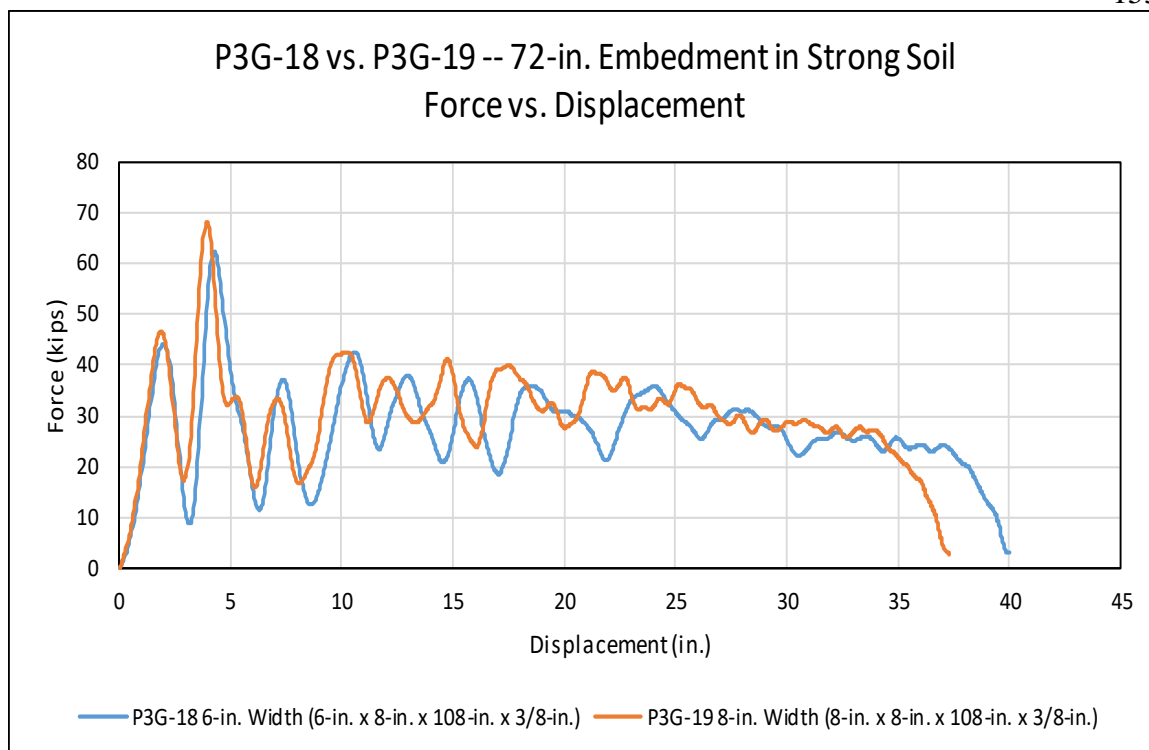


Figure 89. Force vs. Displacement for P3G-18 and P3G-19

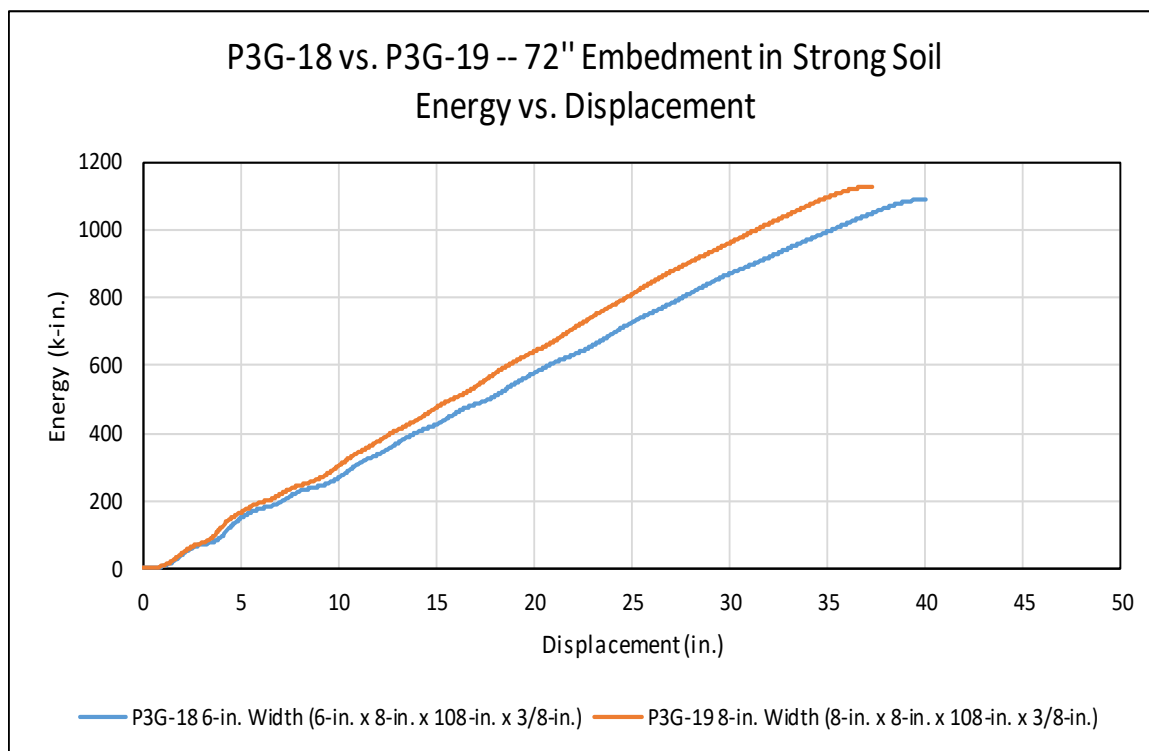


Figure 90. Energy vs. Displacement for P3G-18 and P3G-19

### 8.2.6 Post Width Discussion

If the average force at 15 in. (381 mm) of displacement for all of the tests in weak soil are compared, it can be seen that the 8-in. wide posts at embedment depths of 48 and 96 in. (1,219 and 2,438 mm) experienced forces 7.2 and 6.7 percent greater than a post with a 6 in. (152 mm) width. These values are very similar, but the increase in post-soil forces were more dramatic at an embedment depth of 72 in. (1,829 mm). At this intermediate depth, the 8-in. (203-mm) post width experienced an average force 24.6 percent higher than seen with a 6-in. (152-mm) post width at 15 in. (381 mm) of deflection. Since these results do not provide a consistent trend, a clear determination as to how post width at different embedment depths effects the overall post-soil interaction in weak soil was not possible. Even though it was not possible to glean clear and consistent results from this data series, it does suggest that post width at lower and higher embedment depths has little effect on the post-soil interaction forces. Further, post embedment depth was a strong indicator of these forces. At intermediate depths, it appears that post width plays a meaningful role in the force data. In this testing series, only posts with 6-in. (152-mm) and 8-in (203-mm) widths were tested, which limited the ability to further define the variation in post-soil interaction forces as the post width varied in weak soil.

The tests completed in strong soil showed inconsistent results when comparing their average force values at 15 in. (381 mm) of displacement. At an embedment depth of 48 in. (1,245 mm), the 8 in. (203 mm) wide posts experienced an average force 43.5 percent larger than the corresponding test with a width of 6 in. (152 mm). At a 72-in. (1,829-mm) embedment, the 8-in. (203-mm) wide posts experienced an average force

11.8 percent larger than the corresponding tests with a 6-in. (152-mm) width. The tests completed in strong soil demonstrated larger increases in post-soil forces with an increase in post width as compared to the tests completed in weak soil. With only two data points, it was difficult to determine any specific finding with regards to the effect of post width on the overall post-soil interaction forces. However, the results suggest that as embedment depth increases, the effect of post width on the post-soil forces decreases.

The results obtained for the comparison of 6-in and 8-in. (152-mm and 203-mm) wide posts found that the post-soil interaction forces tend to increase as the post width increases. Nearly all of the tests completed in both weak and strong soils follow this overall trend, but when the tests are compared against each other no conclusion can be made to establish an exact mathematical relationship. Force increase values between a 6-in. and 8-in. (152-mm and 203-mm) width are shown below in Table 25. In order to better define the effect of post width on the post soil interaction forces, additional post testing is needed. This expanded testing should include additional post widths, such as 4 and 10 in. (102 and 254 mm), additional embedment depths, such as 30 and 90 in. (762 and 2,286 mm), and multiple tests should be conducted at each width, embedment depth and soil type.

Table 25. Force Increase from 6-in. to 8-in. Width

Testing Configuration	Force Increase from 6-in. to 8-in. Width	Force Increase at 15-in. of Displacement
48-in. Embedment in Weak Soil	1.06 - 1.10	1.07
72-in. Embedment in Weak Soil	1.14 - 1.25	1.25
96-in. Embedment in Weak Soil	1.00 - 1.08	1.07
48-in. Embedment in Strong Soil	1.42 - 1.47	1.43
72-in. Embedment in Strong Soil	1.11 - 1.13	1.12

### 8.3 Embedment Depth

During this testing series, an attempt was made to quantify the effect of post embedment depth on post-soil interaction forces by comparing the results of dynamic posttests with different embedment depths installed with similar post widths and soil types. Posts embedded at 78, 90, and 102 in. (1,981, 2,286 and 2,591 mm) were tested with a post width of 4 in. (102 mm) in weak soil. Embedment depths of 48 and 72 in. (1,219 and 1,829 mm) were tested with post widths of 6 and 8 in (152 and 203 mm) in weak and strong soil. These two post widths were additionally tests at a 96-in. (2,438 mm) embedment depth in weak soil. It has been previously reported that the post-soil interaction forces due to the soil pressure increase with the square of the ratio of post embedment depths, as shown mathematically below and found in MASH [1].

$$F_2 = F_1 \left( \frac{E_{D2}}{E_{D1}} \right)^2 \quad (54)$$

#### 8.3.1 4-in. Width in Weak Soil

Test P3G-13 (HSS 4 in. x 8 in. x 110 in. x 3/16 in.) (102 mm x 203 mm x 2,794 mm x 5 mm), P3G-14 (HSS 4 in. x 8 in. x 122 in. x 3/16 in.) (102 mm x 203 mm x 3,099 mm x 5 mm), P3G-22 (HSS 4 in. x 8 in. x 122 in. x 3/8 in.) (102 mm x 203 mm x 3,099 mm x 10 mm) and P3G-15 (HSS 4 in. x 8 in. x 134 in. x 3/16 in.) (102 mm x 203 mm x 3,404 mm x 5 mm) had posts with widths of 4 in. (102 mm) and were tested in weak soil. Initially, it was hypothesized that test P3G-22 could be averaged with test P3G-14, because the only difference between these two tests was the post thickness. However, P3G-22 and P3G-14 were analyzed separately, because post-soil interactions were not

similar. Force vs. displacement and energy vs. displacement is provided in Figures 91 and 92.

Average force for embedment depths of 78, 90, and 102 in. (1,981, 2,286, and 2,591 mm) at 5, 10, 15, and 20 in. (127, 254, 381, and 508 mm) of displacement are shown numerically in Tables 26 through 28. A table comparing all test results for a 4-in. (102-mm) post width in weak soil is shown in Table 29.

Equation (54) suggests that the forces seen in a post at a 90-in. (2,286-mm) embedment should be around 33 percent higher than the forces seen in a post at a 78-in. (1,981-mm) embedment. This finding was not confirmed with test results, as shown in Table 26, with a post thickness of 3/16 in. (5 mm), it can be seen that Equation (54) correlates less with the experimental data at 20 in. (508 mm) of displacement but at 10 in. (254 mm) the experimental data agrees with the analytical relationship. When the data shown in Table 26 are averaged across all 20 in. (508 mm) of displacement a 1.5 percent error between the theoretical and experimental data is obtained.

In test P3G-22 (HSS 4-in. x 8-in. x 122-in. x 3/8-in.), the post thickness was doubled to 3/8 in. (10 mm). As mentioned previously, it was originally assumed that the overall dynamic response should not differ much after the thickness was doubled, except for a small inertial spike at the beginning. However, the data did not match these expectations. Table 26 shows that throughout the test the post-soil force equation vastly overestimates the post-soil interaction forces. This suggests that Equation (54) is not valid when the post thickness is changed.

Table 26. Test Nos. P3G-13, P3G-14, P3G-22, and P3G-15 Average Force Values - 4-in.

Width in Weak Soil

	@ 5"	@ 10"	@ 15"	@20"
<b>P3G-13 Average Force (kip), 78-in. Embedment</b> HSS 4-in. x 8-in. x 110-in. x 3/16-in.	9.10	8.39	7.37	6.97
<b>P3G-14 Average Force (kip), 90-in. Embedment</b> HSS 4-in. x 8-in. x 122-in. x 3/16-in.	11.62	11.18	10.21	10.00
<b>P3G-22 Average Force (kip), 90-in. Embedment</b> HSS 4-in. x 8-in. x 122-in. x 3/8-in.	19.55	14.99	13.74	13.58
<b>P3G-15 Average Force (kip), 102-in. Embedment</b> HSS 4-in. x 8-in. x 134-in. x 3/16-in.	11.15	12.64	12.81	12.85

Table 27 compares tests P3G-13 (HSS 4-in. x 8-in. x 110-in. x 3/16-in.) and P3G-15 (HSS 4-in. x 8-in. x 134-in. x 3/16-in.), which were tested at embedment depths of 72 in. and 102 in. (1,828 and 2,591 mm). Equation (54) suggests that the forces seen in a post at a 102-in. (2,591-mm) embedment depth should be approximately 71 percent higher than those experienced by a post embedded at 72 in. (1,829 mm). Averaging the results in Table 27 across all 20 in. (508 mm) results in a 9.1 percent error between the experimental and theoretical data.

Table 27. Test nos. P3G-13 and P3G-15 Force Values- 4-in. Width in Weak Soil

	@ 5"	@ 10"	@ 15"	@20"
<b>P3G-13 Average Force (kip), 78-in. Embedment</b> HSS 4-in. x 8-in. x 110-in. x 3/16-in.	9.10	8.39	7.37	6.97
<b>P3G-15 Average Force (kip), 102-in. Embedment</b> HSS 4-in. x 8-in. x 134-in. x 3/16-in.	11.15	12.64	12.81	12.85

Tests P3G-14 (HSS 4-in x 8-in. x 122-in. x 3/16-in.) and P3G-15 (HSS 4-in. x 8-in. x 134-in. x 3/16-in.) were tested at embedment depths of 90 and 102 in. (2,286 and

2,591 mm). Equation (54) suggests that a post embedded at 102 in. (2,591 mm) should experience forces which are approximately 28 percent higher than the force experienced by a post embedded at 90 in. (2,286). Results are summarized in Table 21. In general, estimates approached the experimental value but

Table 28 Equation (54) did not represent the test data very well.

In test P3G-22 (HSS 4-in. x 8-in. x 122-in. x 3/8-in.) the post thickness was doubled to 3/8 in. (10 mm). It was assumed that the overall dynamic response would not differ except for a small inertial spike at the beginning of the test, but the data shown in Table 28 indicates that the thicker post sustained a higher average force throughout the impact.

Table 28. Test nos. P3G-14 and P3G-15 Average Force Values – 4-in. Width in Weak Soil

	@ 5"	@ 10"	@ 15"	@20"
<b>P3G-14 Average Force (kip), 90-in. Embedment</b> HSS 4-in. x 8-in. x 122-in. x 3/16-in.	11.62	11.18	10.21	10.00
<b>P3G-15 Average Force (kip), 102-in. Embedment</b> HSS 4-in. x 8-in. x 134-in. x 3/16-in.	11.15	12.64	12.81	12.85

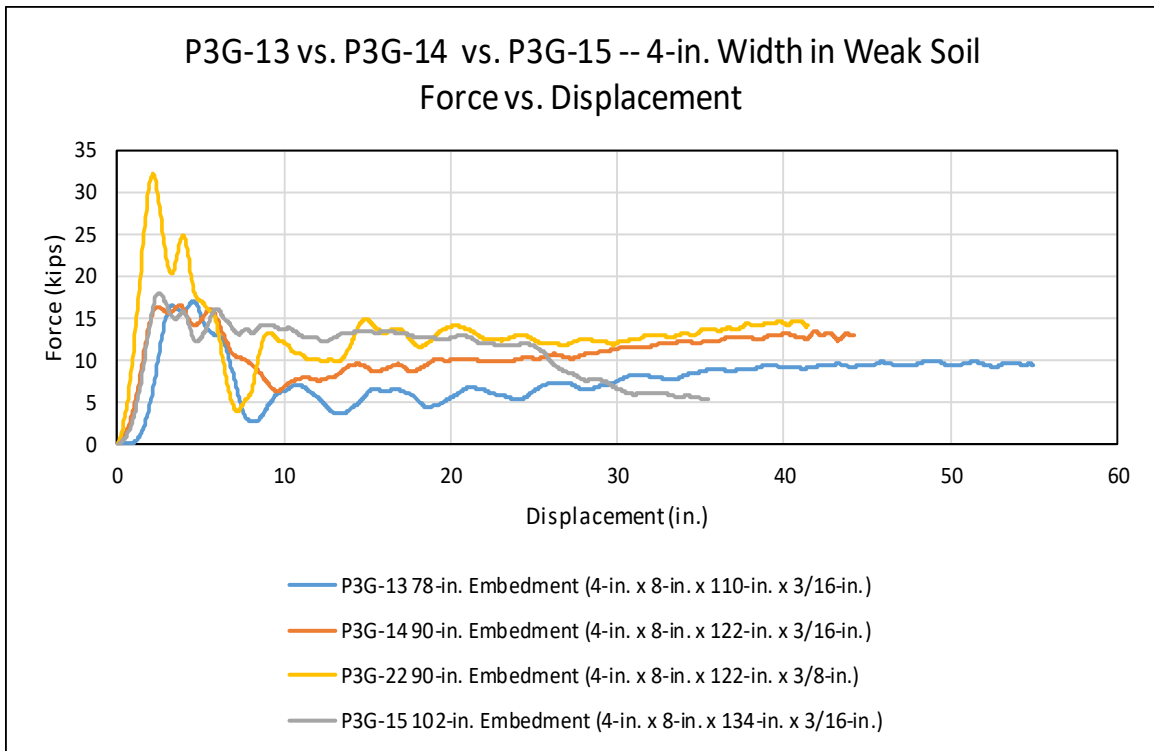


Figure 91. Force vs. Displacement for P3G-13, P3G-14, P3G-22 and P3G-15

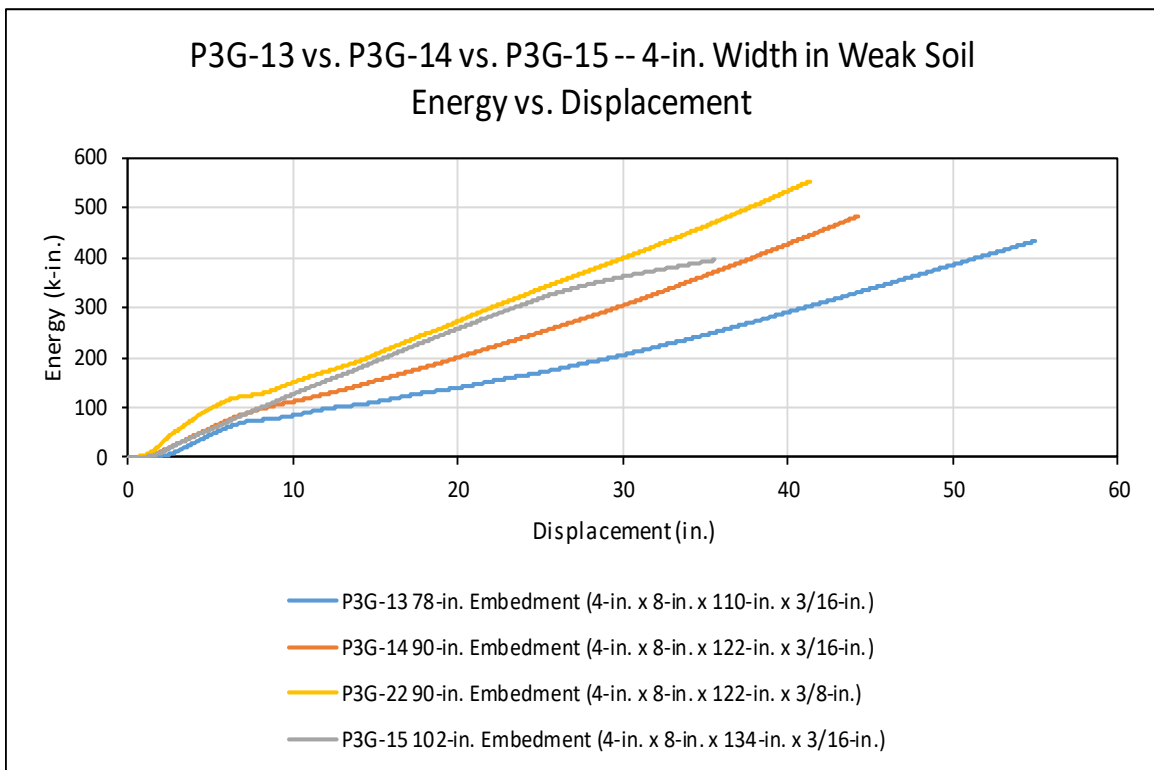


Figure 92. Energy vs. Displacement for P3G-13, P3G-14, P3G-22, and P3G-15



Table 29 below shows the expected and actual increase seen in the post-soil interaction forces as the embedment depth of the posts increases from 90 to 102 in. (2,286 and 2,591 mm). The data obtained from P3G-22 (HSS 4-in. x 8-in. x 122-in. x 3/8-in.) was not included in this summary table because of the large discrepancies seen between the expected and actual force increases when comparing this test to the other tests. This discrepancy suggests that the change in post thickness at these embedment depths and at a post width of 4 in. (102 mm) impacts the validity of Equation (54), but more testing is needed to confirm these results.

Table 29. Expected vs. Actual Force Increase – 4-in. Width in Weak Soil

4-in Width In Weak Soil		
Embedment Change (in.)	Expected Force Increase	Actual Force Increase
78: 90	1.33	1.28 -1.43
78 : 102	1.71	1.23 - 1.84
90 : 102	1.28	.96 - 1.29

### 8.3.2 6-in. Width in Weak Soil

Tests P3G-1 (HSS 6-in. x 8-in. x 84-in. x 3/16-in.), P3G-3 (HSS 6-in. x 8-in. x 108-in. x 3/16-in.) and P3G-5 (HSS 6-in. x 8-in. x 132-in. x 3/16-in.) had posts with widths of 6 in. (152 mm) and were tested in weak soil. Force vs. displacement and energy vs. displacement can be seen in Figures 93 and 94. Average post-soil forces for embedment depths of 48, 72, and 96 in. (1,219, 1,829, 2,438 mm) at 5, 10, 15, and 20 in. (127, 254, 381, and 508 mm) of displacement are shown in Tables 30 through 32, and a comparison of all tests conducted with a 6-in. (152-mm) post width in weak soil are shown in Table 33.

Equation (54) suggests that the forces seen in a post at an embedment depth of 72 in. (1,829 mm) should be around 125 percent higher than the values seen in a post at an embedment depth of 48 in. (1,219 mm). Based on average force computations, researchers determined that the equation overestimated the post-soil resistance force, as shown in Table 30.

Table 30. Test nos. P3G-1 and P3G-3 Average Force Values- 6-in. Width in Weak Soil

	@ 5"	@ 10"	@ 15"	@20"
<b>P3G-1 Average Force (kip), 48-in. Embedment</b> HSS 4-in. x 8-in. x 110-in. x 3/16-in.	12.80	7.96	6.43	5.66
<b>P3G-3 Average Force (kip), 72-in. Embedment</b> HSS 4-in. x 8-in. x 122-in. x 3/16-in.	17.92	11.59	10.09	9.66

Test nos. P3G-1 (HSS 6-in. x 8-in. x 84-in. x 3/16-in.) and P3G-5 (HSS 6-in. x 8-in. x 108-in. x 3/16-in.) were embedded to depths of 48 in. and 96 in. (1,219 mm and

2,438 mm) respectively. Equation (54) suggests that the soil resistance forces in a post with a 96-in. (2,438 mm) embedment depth should be 300 percent larger than the forces experienced by a post with a 48-in. (1,219 mm) embedment. The average force values shown in the table range from approximately a 56 to 207 percent increase, which is significantly less than what is expected.

Table 31. Test nos. P3G-1 and P3G-5 Average Force Values- 6-in. Width in Weak Soil

	@ 5"	@ 10"	@ 15"	@ 20"
<b>P3G-1 Average Force (kip), 48-in. Embedment</b> HSS 4-in. x 8-in. x 110-in. x 3/16-in.	12.80	7.96	6.43	5.66
<b>P3G-5 Average Force (kip), 90-in. Embedment</b> HSS 4-in. x 8-in. x 122-in. x 3/8-in.	20.04	18.68	17.74	17.38

Tests P3G-3 (HSS 6-in. x 8-in. x 108-in. x 3/16-in.) and P3G-5 (HSS 6-in. x 8-in. x 132-in. x 3/16-in.) were completed with embedment depths of 72 in. and 96 in. (1,829 mm and 2,438 mm), respectively. Equation (54) states that the post-soil interaction forces seen in a post at a depth of 96 in. (2,438 mm) should be approximately 77 percent higher than the corresponding forces seen in a post embedded at 72 in. (1,829 mm). As shown in Table 32 the data indicates that at 15 and 20 in. (381 and 508 mm) of deflection the analytical model correlated well with the experimental data, but at smaller deflections the correlation was not apparent.

Table 32. Test nos. P3G-3 and P3G-5 Average Force Values- 6-in. Width in Weak Soil

	@ 5"	@ 10"	@ 15"	@20"
<b>P3G-3 Average Force (kip), 72-in. Embedment</b> HSS 4-in. x 8-in. x 122-in. x 3/16-in.	17.92	11.59	10.09	9.66
<b>P3G-5 Average Force (kip), 90-in. Embedment</b> HSS 4-in. x 8-in. x 122-in. x 3/8-in.	20.04	18.68	17.74	17.38

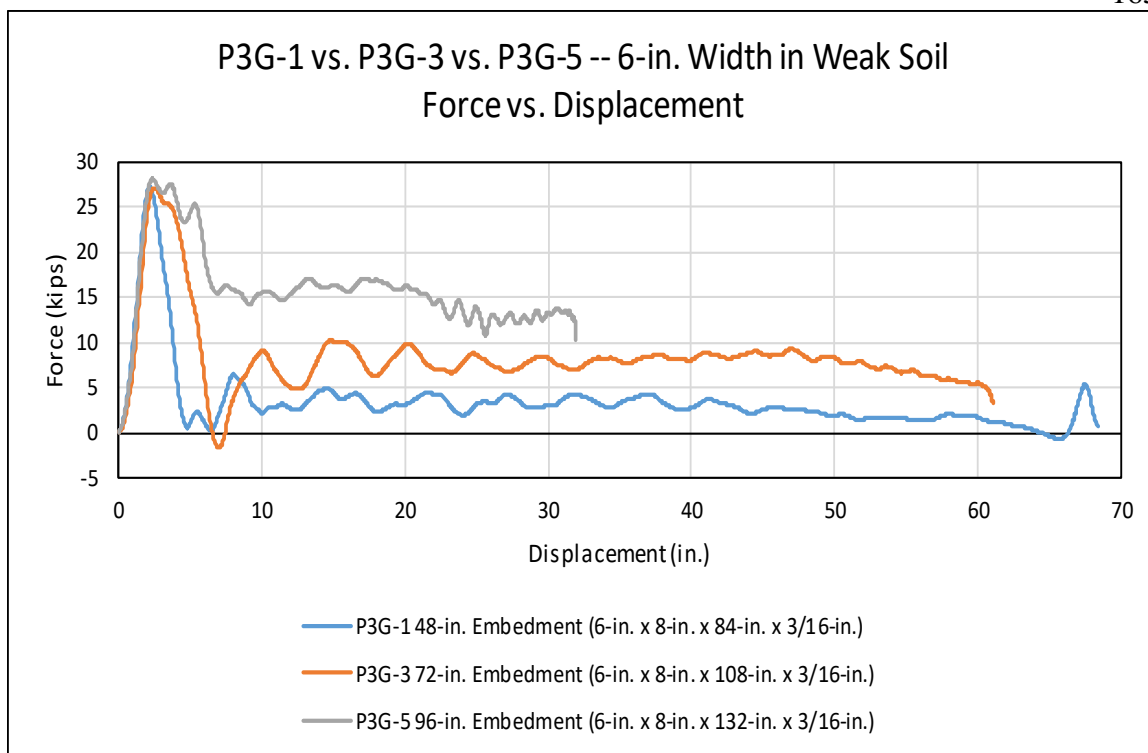


Figure 93. Force vs. Displacement for P3G-1, P3G-3 and P3G-5

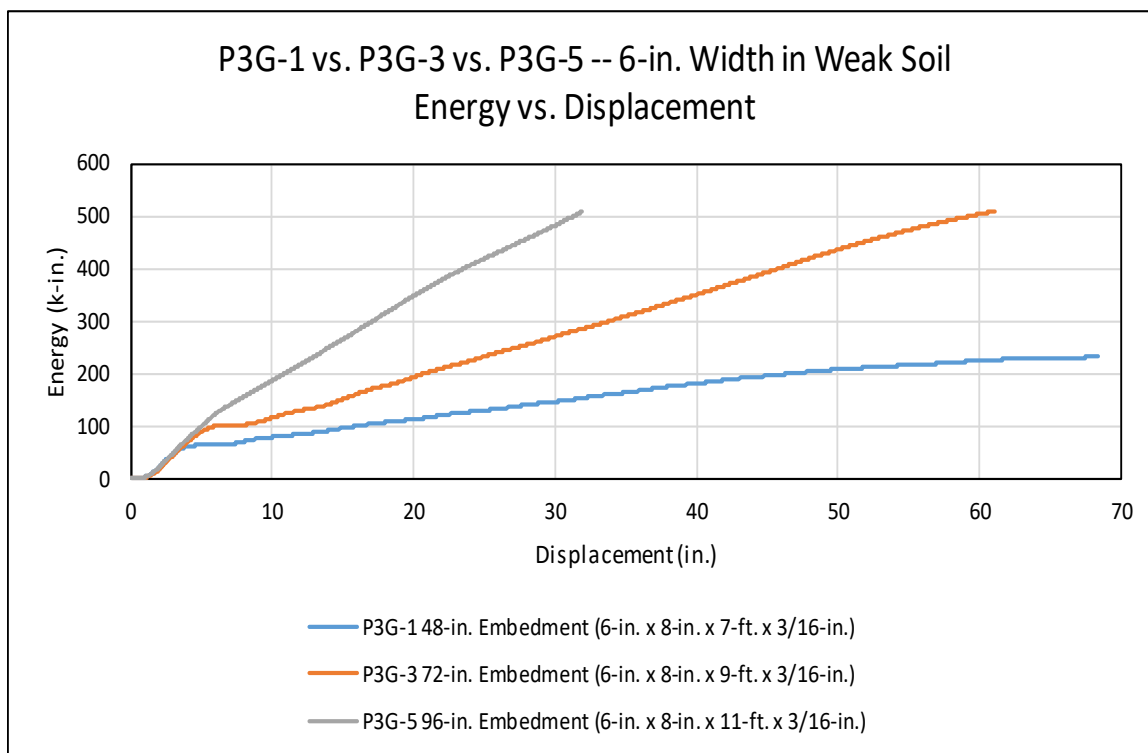


Figure 94. Energy vs. Displacement for P3G-1, P3G-3, and P3G-5

Table 33. Expected vs. Actual Force Increase – 6-in. Width in Weak Soil

6-in. Width in Weak Soil		
Embedment Change	Expected Force Increase	Actual Force Increase
48 : 72	2.25	1.40 - 1.71
48 : 96	4.00	1.57 - 3.07
72 : 96	1.78	1.12 - 1.8

### 8.3.3 8-in. Width in Weak Soil

Tests P3G-2 (HSS 8-in. x 8-in. x 84-in. x 3/16-in.), P3G-4 (HSS 8-in. x 8-in. x 108-in. x 3/16-in.) and P3G-6 (HSS 8-in. x 8-in. x 132-in. x 3/16-in.) had posts with widths of 8 in. (203 mm) and were tested in weak soil. Force vs. displacement and energy vs. displacement can be seen in Figures 95 and 96. Average post-soil forces for embedment depths of 48, 72, and 96 in. (1,219, 1,829, and 2,438 mm) at 5, 10, 15, and 20 in. (127, 254, 381, and 508 mm) of displacement are shown numerically in Tables 34 through 36, and a table comparing all tests conducted with an 8-in. (203-mm) width in weak soil is shown in Table 37.

Equation (54) suggests that the forces experienced in a post at an embedment depth of 72 in. (1,829 mm) should be around 125 percent higher than the force experienced in a post at an embedment depth of 48 in. (1,219 mm). However, as the displacement increases from 5 to 20 in. (127 to 508 mm), the difference in the forces experienced increased from approximately 50 to 98 percent as shown in Table 34. Again, Equation (54) overestimated the effect of embedment depths on forces.

Table 34. Test nos. P3G-2 and P3G-4 Average Force Values – 8-in. Width in Weak Soil

	@ 5"	@ 10"	@ 15"	@20"
<b>P3G-2 Average Force (kip), 48 in. Embedment</b> HSS 8-in. x 8-in. x 84-in. x 3/16-in.	13.62	8.72	6.89	6.05
<b>P3G-4 Average Force (kip), 72-in. Embedment</b> HSS 8-in. x 8-in. x 108-in. x 3/16-in.	20.45	13.90	12.57	11.99

Table 35 compares tests P3G-2 (HSS 8-in. x 8-in. x 84-in. x 3/16-in.) and P3G-6 (HSS 8-in. x 8-in. x 132-in. x 3/16-in.) which were completed with embedment depths of 48 in. and 96 in. (1,219 to 2,438-mm). Equation (54) suggests that the forces seen in a post at a 96-in. (2,438-mm) embedment should be 300 percent larger than the forces seen in a post at a 48-in. (1,219-mm) embedment. The equation-driven embedment depth amplification over predicted soil forces, which was consistent with other test results.

Table 35. Test nos. P3G-2 and P3G-6 Average Force Values – 8-in. Width in Weak Soil

	@ 5"	@ 10"	@ 15"	@20"
<b>P3G-2 Average Force (kip), 48 in. Embedment</b> HSS 8-in. x 8-in. x 84-in. x 3/16-in.	13.62	8.72	6.89	6.05
<b>P3G-6 Average Force (kip), 90-in. Embedment</b> HSS 8-in. x 8-in. x 132-in. x 3/16-in.	20.13	19.54	18.94	18.76

Tests P3G-4 (HSS 8-in. x 8-in. x 108-in. x 3/16-in.) and P3G-6 (HSS 8-in. x 8-in. x 132-in. x 3/16-in.) were completed at 72 and 96-in. (1,829 and 2,438-mm) embedment depths. Using Equation (54) the estimated soil resistive forces for a post with an embedment depth of 96 in. (2,438 mm) should be approximately 78 percent higher than the corresponding soil resistive forces for a post with an embedment depth of 72 in.

(1,829 mm). Once again, physical test data indicated lower post-soil resistive force than the equation estimated.

Table 36. Test nos. P3G-4 and P3G-6 Average Force Values – 8-in. Width in Weak Soil

	@ 5"	@ 10"	@ 15"	@ 20"
<b>P3G-4 Average Force (kip), 72-in. Embedment</b> HSS 8-in. x 8-in. x 108-in. x 3/16-in.	20.45	13.90	12.57	11.99
<b>P3G-6 Average Force (kip), 90-in. Embedment</b> HSS 8-in. x 8-in. x 132-in. x 3/16-in.	20.13	19.54	18.94	18.76



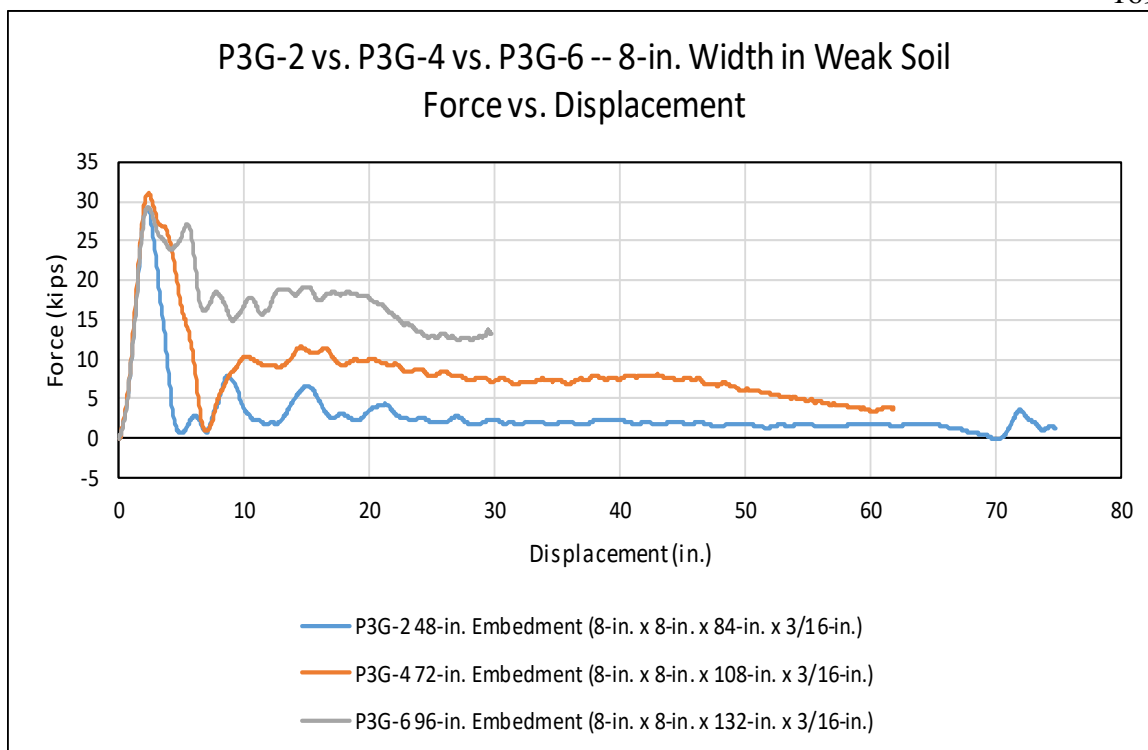


Figure 95. Force vs. Displacement for P3G-2, P3G-4 and P3G-6

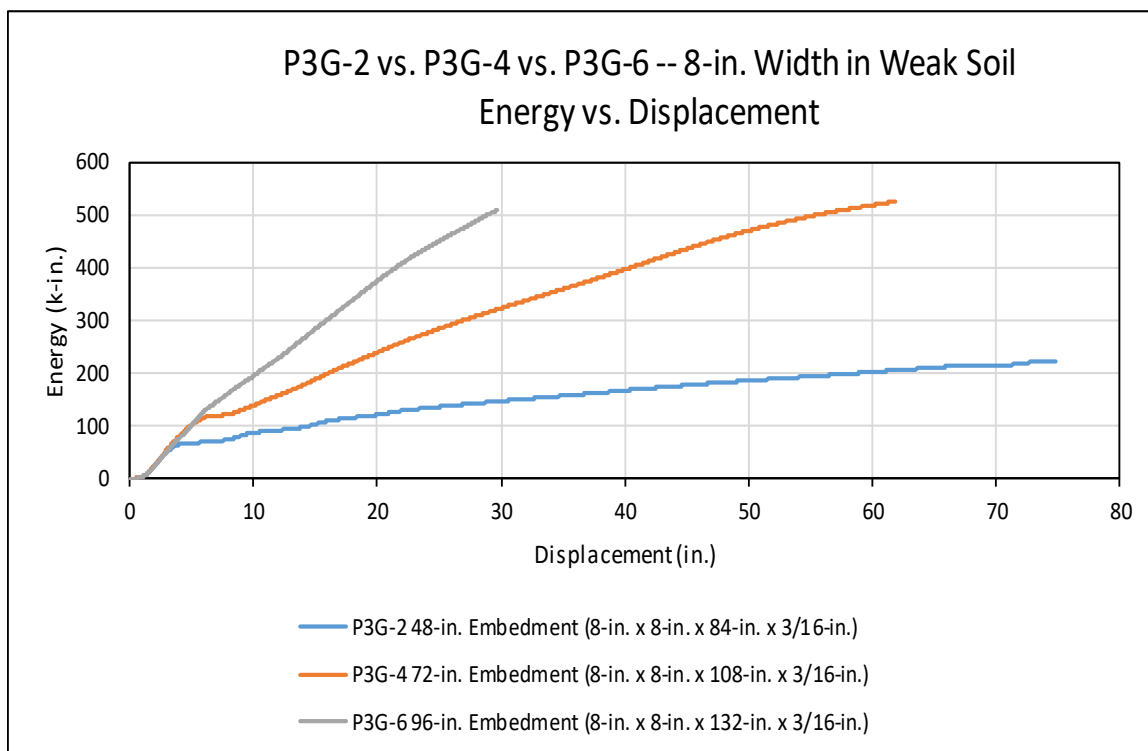


Figure 96. Energy vs. Displacement for P3G-2, P3G-4 and P3G-6

Table 37. Expected vs. Actual Force Increase – 8-in. Width in Weak Soil

8-in. Width in Weak Soil		
Embedment Change	Expected Force Increase	Actual Force Increase
48 : 72	2.25	1.5 - 1.98
48 : 96	4.00	1.48 - 3.10
72 : 96	1.78	.98 - 1.57

### 8.3.4 6-in. Width in Strong Soil

Tests P3G-7 (HSS 6-in. x 8-in. x 84-in. x 3/16-in.), P3G-18 (HSS 6-in. x 8-in. x 108-in. x 3/8-in.) had posts with widths of 6 in. (152 mm) and were tested in strong soil. Force vs. displacement and energy vs. displacement can be seen in Figures 97 and 98. Average post-soil forces for embedment depths of 48 and 72 in. (1,219 and 1,829 mm) at 5, 10, 15, and 20 in. (127, 254, 381, 508 mm) of displacement are shown in Table 38, and a table comparing all tests conducted with a 6-in. (152-mm) width in strong soil is shown in Table 39.

Using Equation (54), the soil resistive forces for a post at an embedment depth of 72 in. (1,829 mm) should be approximately 125 percent larger than the post-soil forces associated with an embedment depth of 48 in. (1,219 mm). Table 36 shows that at large soil displacements, the difference in the average force values was approximately 120 percent. Thus, experimental data correlates well with the analytical model at large deflections of 15 in. or more.

Table 38. Test nos. P3G-7 and P3G-18 Average Force Values – 6'' Width in Strong Soil

	@ 5"	@ 10"	@ 15"	@20"
<b>P3G-7 Average Force (kip), 48 in. Embedment</b> HSS 6-in. x 8-in. x 84-in. x 3/16-in.	15.03	14.75	14.13	13.14
<b>P3G-18 Average Force (kip), 72-in. Embedment</b> HSS 6-in. x 8-in. x 108-in. x 3/8-in.	29.89	26.75	28.38	28.85

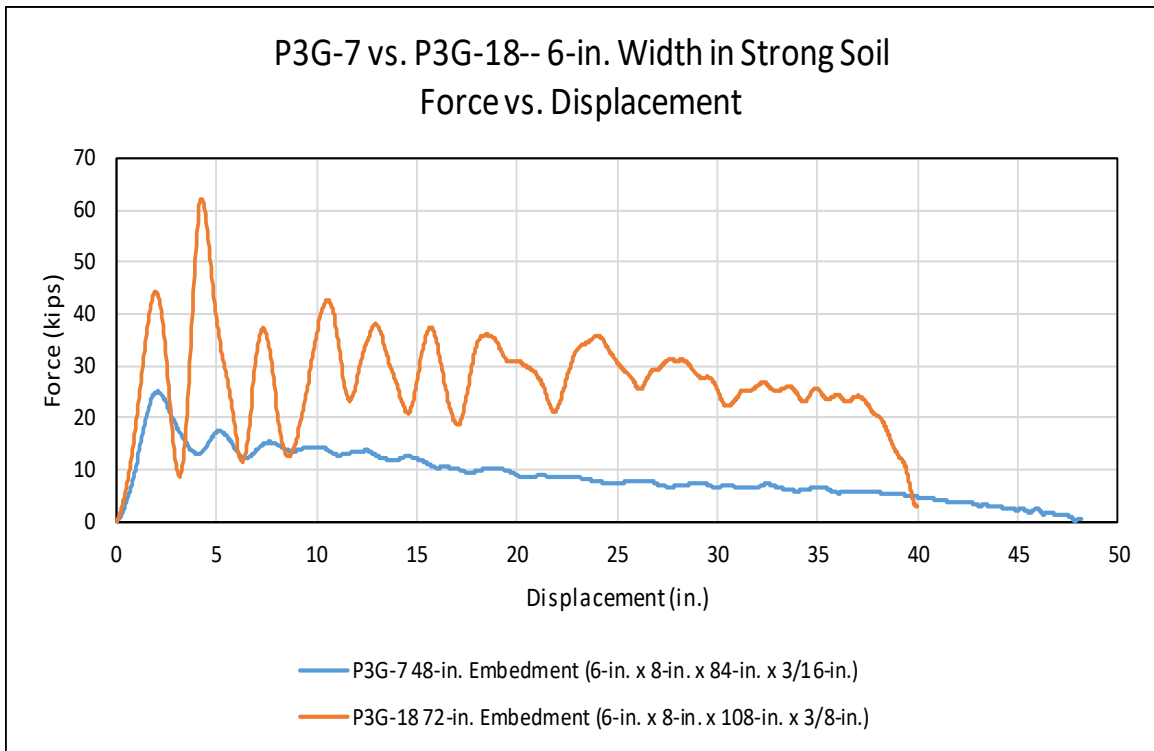


Figure 97. Force vs. Displacement for P3G-7 and P3G-18

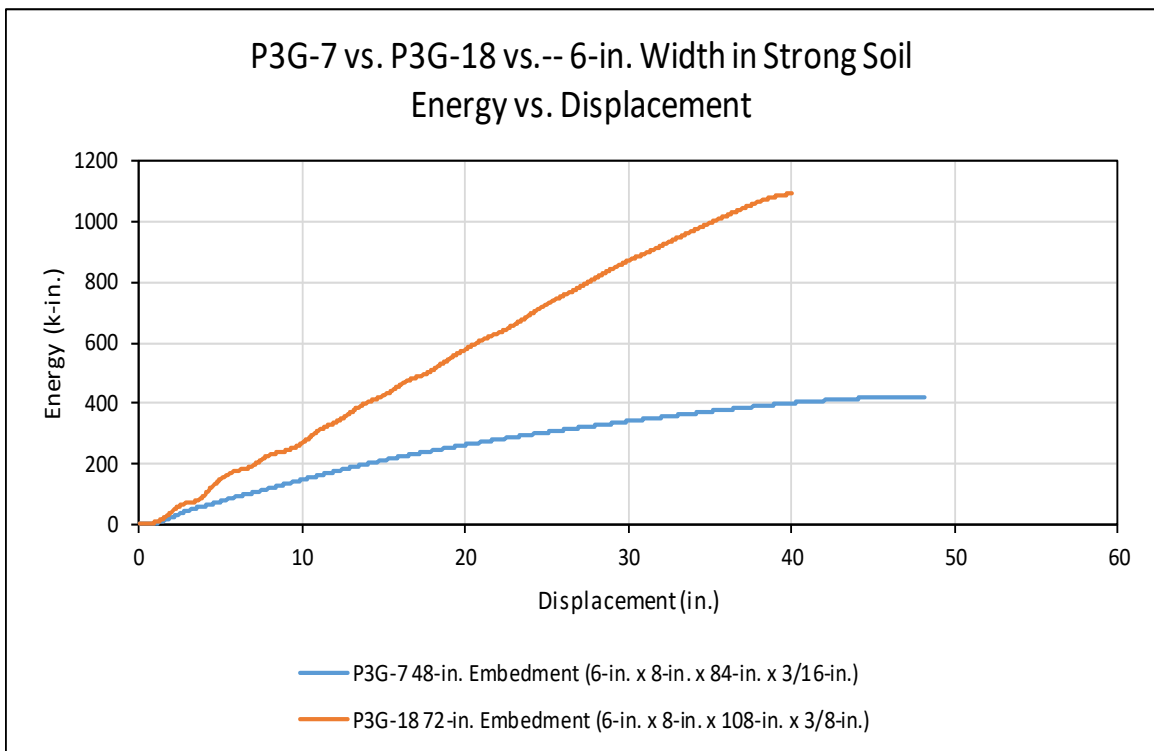


Figure 98. Energy vs. Displacement for P3G-7 and P3G-18

Table 39. Expected vs. Actual Force Increase – 6-in. Width in Strong Soil

6-in. Width in Strong Soil		
Embedment Change	Expected Force Increase	Actual Force Increase
48 : 72	2.25	1.99 - 2.2

### 8.3.5 8-in. Width in a Strong Soil

Test nos. P3G-8 and P3G-17 (HSS 8-in. x 8-in. x 84-in. x 3/16-in. and 3/8-in.), which hold embedment depths of 48 in, were averaged together and plotted with test no P3G-19 (HSS 8-in. x 8-in. x 108-in. x 3/8-in.), which had an embedment depth of 72 in. Force vs. displacement and energy vs. displacement can be seen in Figures 99 and 100. Average post-soil forces for embedment depths of 48 and 72 in. (1,219 1,829 mm) at 5, 10, 15, and 20 in. (127, 254, 381, 508 mm) of displacement are shown in Table 40.

Equation (54) suggests that the forces seen in a post at an embedment depth of 72 in. (1,829 mm) should be approximately 125 percent higher than the values seen in a post at an embedment depth of 48 in. (1,219 mm). Test results indicated that the equation overestimated post-soil forces at all bogie displacements.

Table 40. The average of Test nos. P3G-8 and P3G-17 and Test no. P3G-19 Average Force Values – 8-in. Width in Strong Soil

	@ 5"	@ 10"	@ 15"	@ 20"
<b>P3G-8 and P3G-17 Average Force (kip), 48 in. Embedment</b> HSS 8-in. x 8-in. x 84-in. x 3/16-in. and 3/8 in.	22.06	21.68	20.27	18.72
<b>P3G-19 Average Force (kip), 72-in. Embedment</b> HSS 8-in. x 8-in. x 108-in. x 3/8-in.	33.20	30.29	31.73	32.05

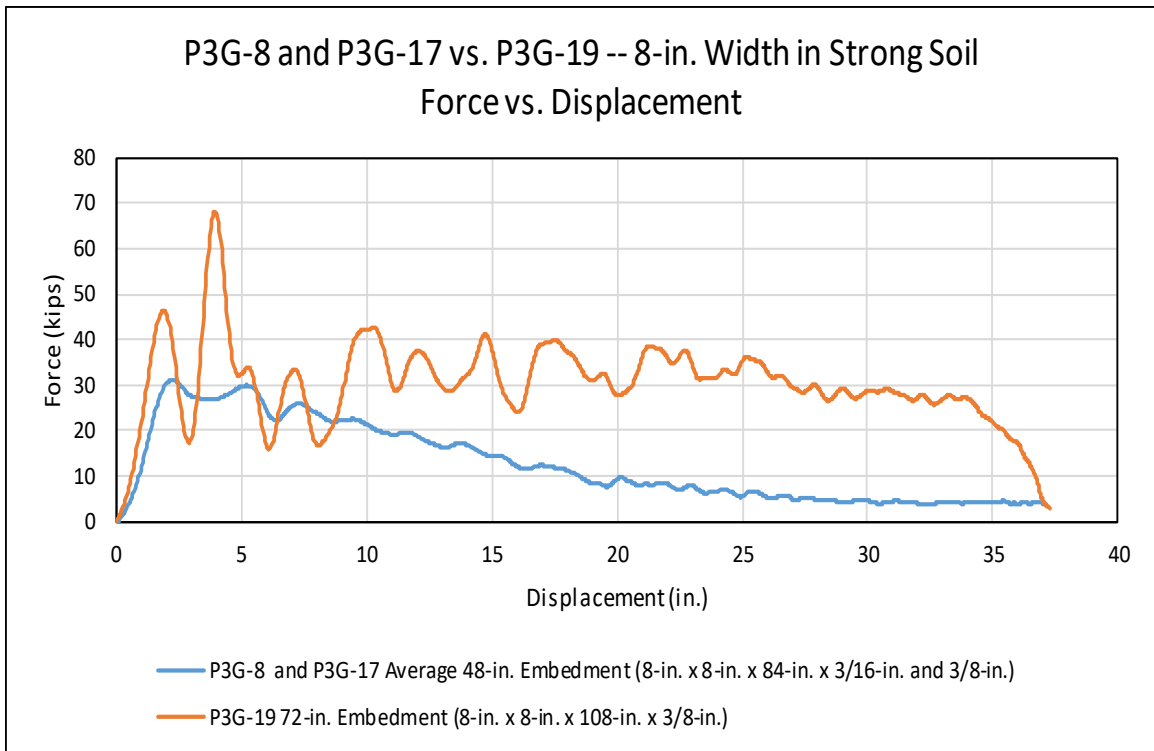


Figure 99. Force vs. Displacement for the average of P3G-8 and P3G-17

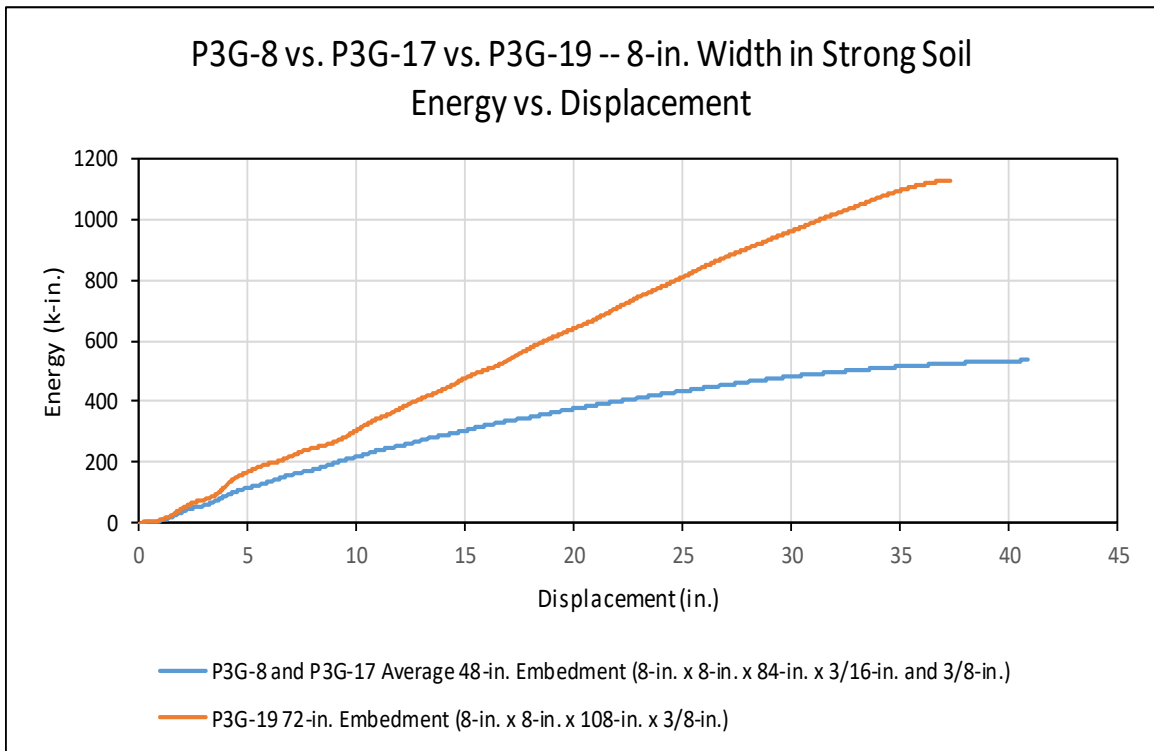


Figure 100. Energy vs. Displacement for the Average of P3G-8 and P3G- and P3G-19

Table 41. Expected vs. Actual Force Increase – 8-in. Width in Strong Soil

8-in. Width in Strong Soil		
Embedment Change	Expected Force Increase	Actual Force Increase
72 : 48	2.25	1.4 - 1.71

### 8.3.6 Embedment Depth Discussion

Historically, the post-soil force estimation shown in Equation (54) has been used to estimate the stiffening effect of increasing embedment depth. Although higher embedment depths were associated with increased post-soil forces, the increase was not consistent with predictions. For example, the experimental data for posts with 6 in. (152 mm) widths tested in strong soil showed that the equation overestimates the forces at 15 in. (381 mm) of deflection by approximately 25 percent, while the equation overestimates the post-soil forces for an 8-in. (203-mm) wide post by approximately 70 percent at 15 in. (381 mm) of deflection. No constant coefficient was determined to relate all post-soil results based on width or embedment depth.

The average post-soil forces at 15 in. (381 mm) of deflection were plotted and are shown in Figure 101. A summary table test results is shown in Table 42. Test data shows that as the difference in embedment depths increases, the assumed parabolic relationship is not as effective, but for small changes in embedment the result is more reasonable.

If more tests at different embedment depths and widths were completed a graph such as the one shown below could potentially be used to estimate, through linear interpolation, the post-soil interaction forces for different embedment depths. Additional dynamic post testing at different widths and embedment depths needs to be completed before this type of tool can accurately predict the forces seen in posts at different embedment depths.

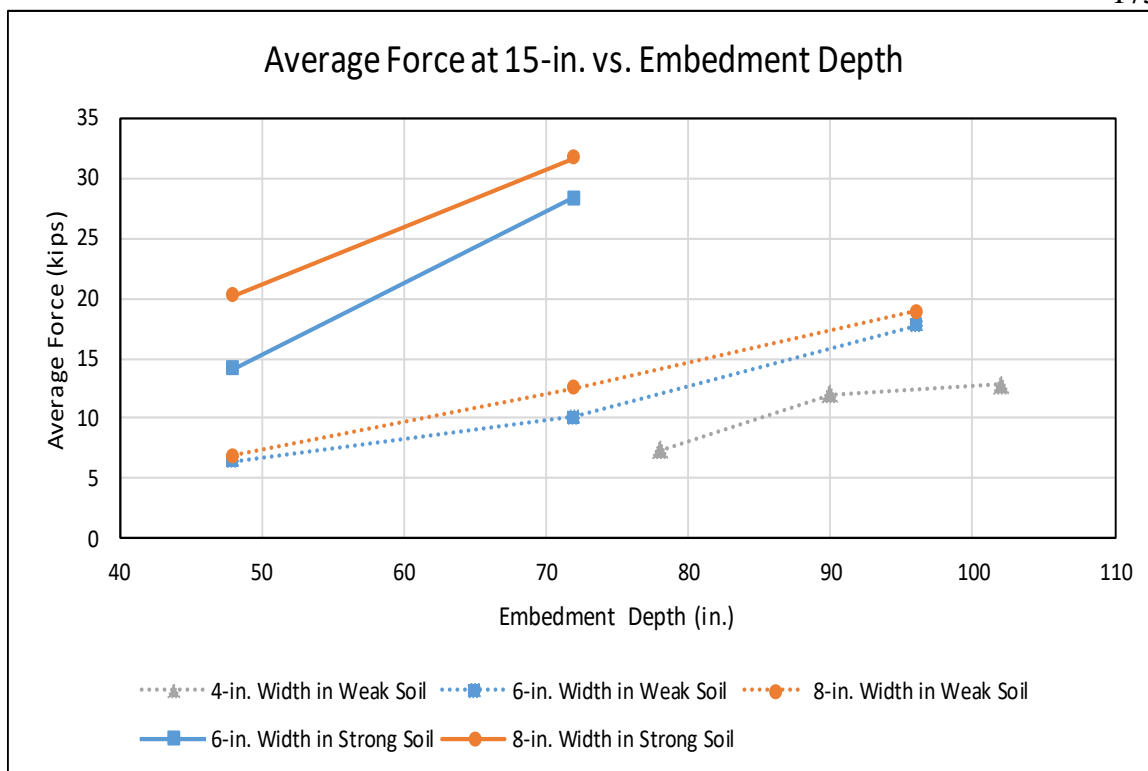


Figure 101. Average Forces at 15 in. of Deflection vs. Embedment Depth

Table 42. Expected vs Actual Force Increase

Embedment Change (in.)	Expected Force Increase	Actual Increase				
		4-in. Weak Soil	6-in. Weak Soil	8-in. Weak Soil	6-in. Strong Soil	8-in. Strong Soil
78 : 90	1.33	1.28 - 1.43	-	-	-	-
78 : 102	1.71	1.23 - 1.84	-	-	-	-
90 : 102	1.28	.96 - 1.29	-	-	-	-
48 : 72	2.25	-	1.40 - 1.71	1.5 - 1.98	1.99 - 2.2	1.4 - 1.71
48 : 96	4.00	-	1.57 - 3.07	1.48 - 3.10	-	-
72 : 96	1.78	-	1.12 - 1.8	.98 - 1.57	-	-

## 8.4 Soil Type

During this testing series an attempt to quantify the effect of soil strength on post-soil interaction forces was completed by comparing results for tests of posts with similar widths and embedment depths installed in different soils.

Testing was completed on posts with both 6 and 8-in. (152 and 203-mm) widths in embedment depths of 48 and 72 in. (1,219 and 1,829 mm) in both weak and strong soil.

### 8.4.1 6-in. Width in a 48-in Embedment

Tests P3G-1 (HSS 6-in. x 8-in. x 84-in. x 3/16-in.) and P3G-7 (HSS 6-in. x 8-in. x 84-in. x 3/16-in.) contained posts with 6-in. (152-mm) widths and were tested in a 48-in. (1,219-mm) embedment depth in both weak and strong soils. Force vs. displacement and energy vs. displacement can be seen in Figures 102 and 103. Average post-soil forces at 5, 10, 15, and 20 in. (127, 254, 381, and 508 mm) of displacement are shown numerically in Table 43.

The data in this table shows that the percent difference of the average forces between the posts installed in weak versus strong soil increased from approximately 17 to 132 percent as the displacement increased from 5 to 20 in. (127 to 508 mm) of deflection.



Table 43. Test nos. P3G-1 and P3G-7 Average Force Values – 6-in. Width in a 48-in.

## Embedment

	@ 5"	@ 10"	@ 15"	@ 20"
<b>P3G-1 Average Force (kip), 48 in. Embedment</b> HSS 6-in. x 8-in. x 84-in. x 3/16-in., Weak Soil	12.80	7.96	6.43	5.66
<b>P3G-7 Average Force (kip), 48-in. Embedment</b> HSS 6-in. x 8-in. x 84-in. x 3/16-in., Strong Soil	15.03	14.75	14.13	13.14
<b>Average Force Ratio</b>	1.17	1.85	2.20	2.32

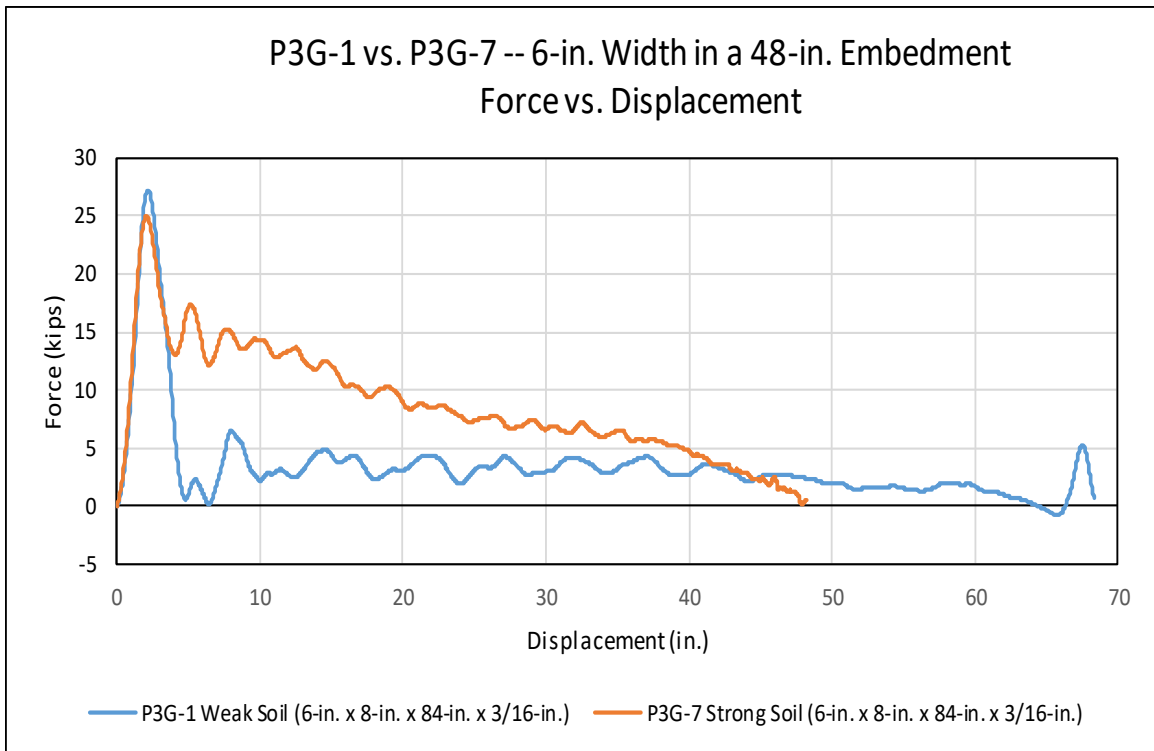


Figure 102. Force vs. Displacement for P3G-1 and P3G-7

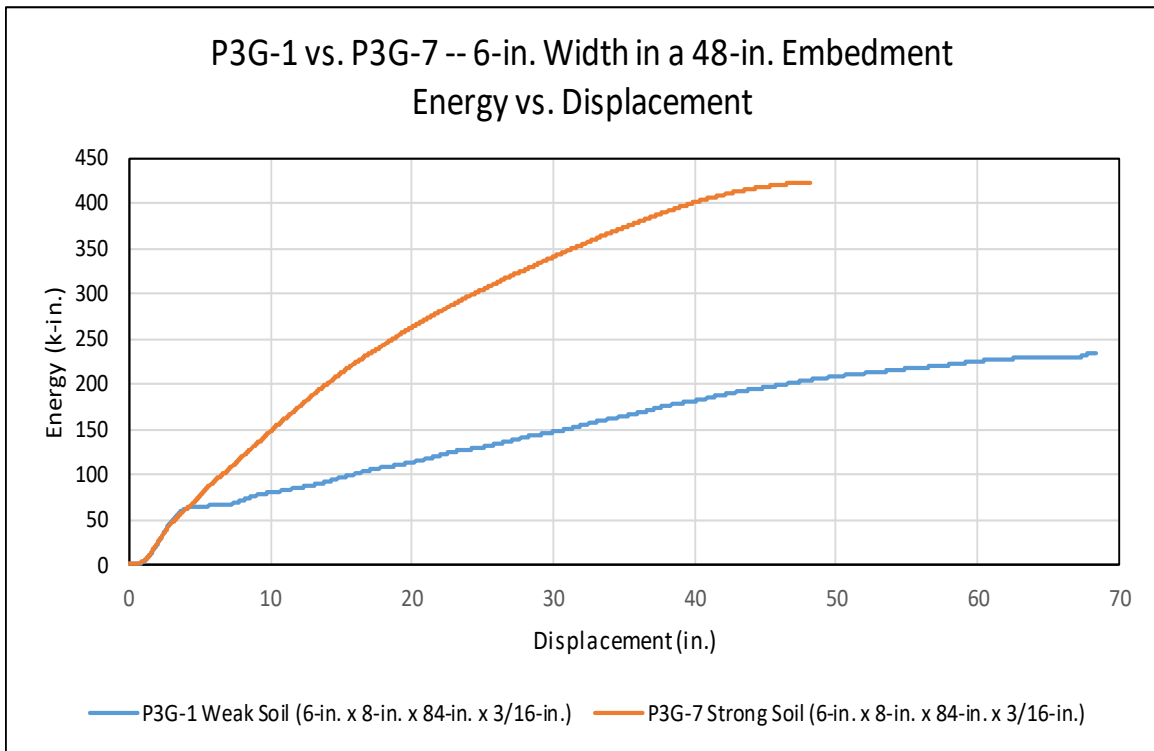


Figure 103. Energy vs. Displacement for P3G-1 and P3G-7

### 8.4.1 6-in. Width in a 72-in. Embedment

Tests P3G-3 (HSS 6-in. x 8-in. x 9-ft. x 3/16-in.) and P3G-18 (HSS 6-in. x 8-in. x 9-ft. x 3/8-in.) contained posts with 6-in. (152-mm) widths and were tested in a 72-in. (1,829-mm) embedment depth in both weak and strong soils. Force vs. displacement and energy vs. displacement can be seen in Figures 104 and 105. Average post-soil forces at 5, 10, 15, and 20 in. (127, 254, 381, and 508 mm) of displacement are shown numerically in Table 44.

The data in this table shows that the percent difference of the average forces between the posts installed in weak versus strong soil increased from approximately 66 to 199 percent as the displacement increased from 5 to 20 in. (127 to 508 mm) of deflection.

Table 44. Test nos. P3G-3 and P3G-18 Average Force Values – 6-in. Width in a 72-in. Embedment

	@ 5"	@ 10"	@ 15"	@ 20"
<b>P3G-3 Average Force (kip), 72 in. Embedment</b> HSS 6-in. x 8-in. x 108-in. x 3/16-in., Weak Soil	17.92	11.59	10.09	9.66
<b>P3G-18 Average Force (kip), 72-in. Embedment</b> HSS 6-in. x 8-in. x 108-in. x 3/16-in., Strong Soil	29.89	26.75	28.38	28.85
<b>Average Force Ratio</b>	1.67	3.98	2.81	2.99

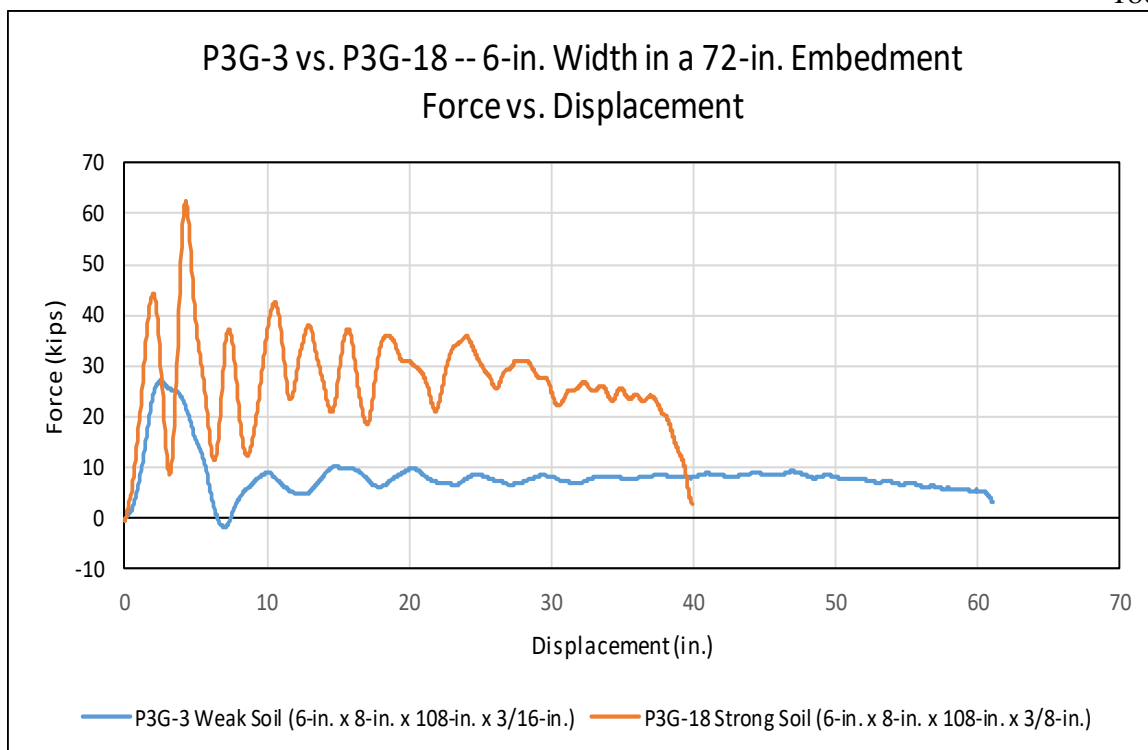


Figure 104. Force vs. Displacement for P3G-3 and P3G-18

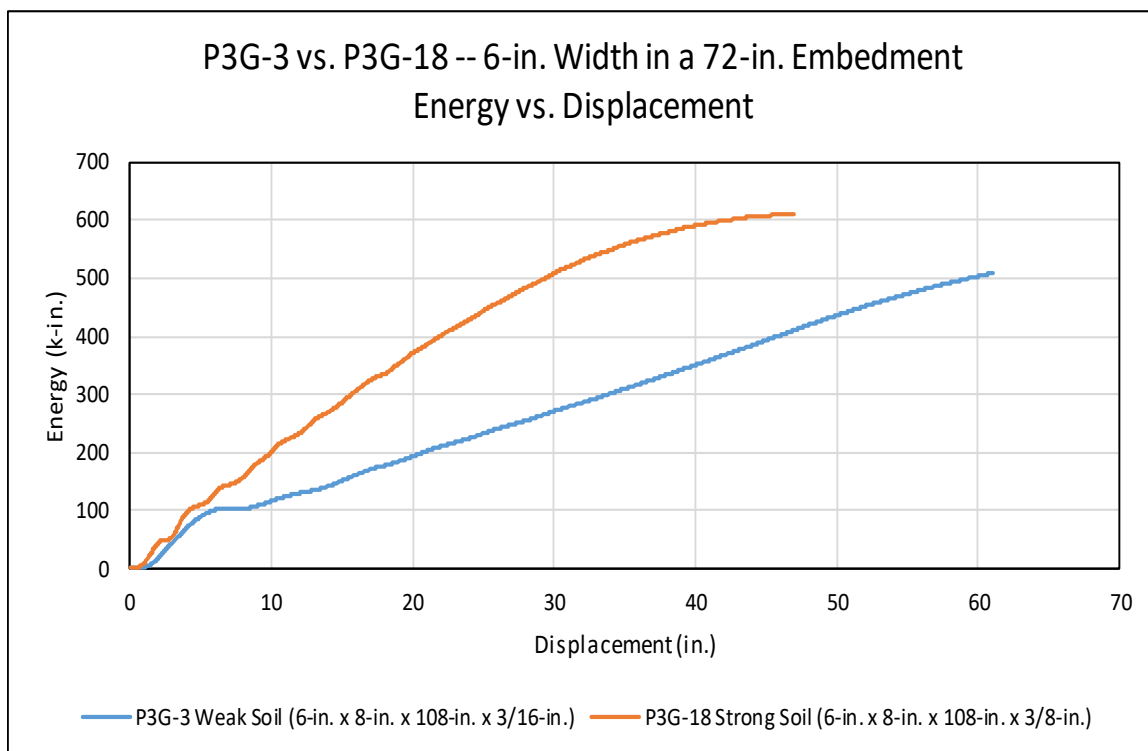


Figure 105. Energy vs. Displacement for P3G-3 and P3G-18

### 8.4.2 8-in. Width in a 48-in. Embedment

Tests P3G-2 (HSS 8-in. x 8-in. x 84-in. x 3/16-in.) and the average of P3G-8 and P3G-17 (HSS 8-in. x 8-in. x 84-in. x 3/16-in. and 3/8-in.) utilized posts with 8-in. (203-mm) widths and were tested with 48-in. (1,219-mm) embedment depths in both weak and strong soil, respectively. Force vs. displacement and energy vs. displacement can be seen in Figures 106 and 107. Average post-soil forces at 5, 10, 15, and 20 in. (127, 254, 381, and 508 mm) of displacement are shown numerically in Table 45.

The data in this table shows that the percent difference of the average forces between the posts installed in weak versus strong soil increased from approximately 62 to 210 percent as the displacement increased from 5 to 20 in. (127 to 508 mm) of deflection.

Table 45. Test nos. P3G-2 and the average of P3G-8 and P3G-17 Average Force Values – 8-in. Width in a 48-in. Embedment

	@ 5"	@ 10"	@ 15"	@ 20"
<b>P3G-2 Average Force (kip), Weak Soil</b> HSS 8-in. x 8-in. x 84-in. x 3/16-in.	13.62	8.72	6.89	6.05
<b>P3G-8 &amp; P3G-17 Average Force (kip), Strong Soil</b> HSS 8-in. x 8-in. x 84-in. x 3/16-in. and 3/8-in.	22.06	21.68	20.27	18.72
<b>Average Force Ratio</b>	1.62	2.49	2.94	3.09

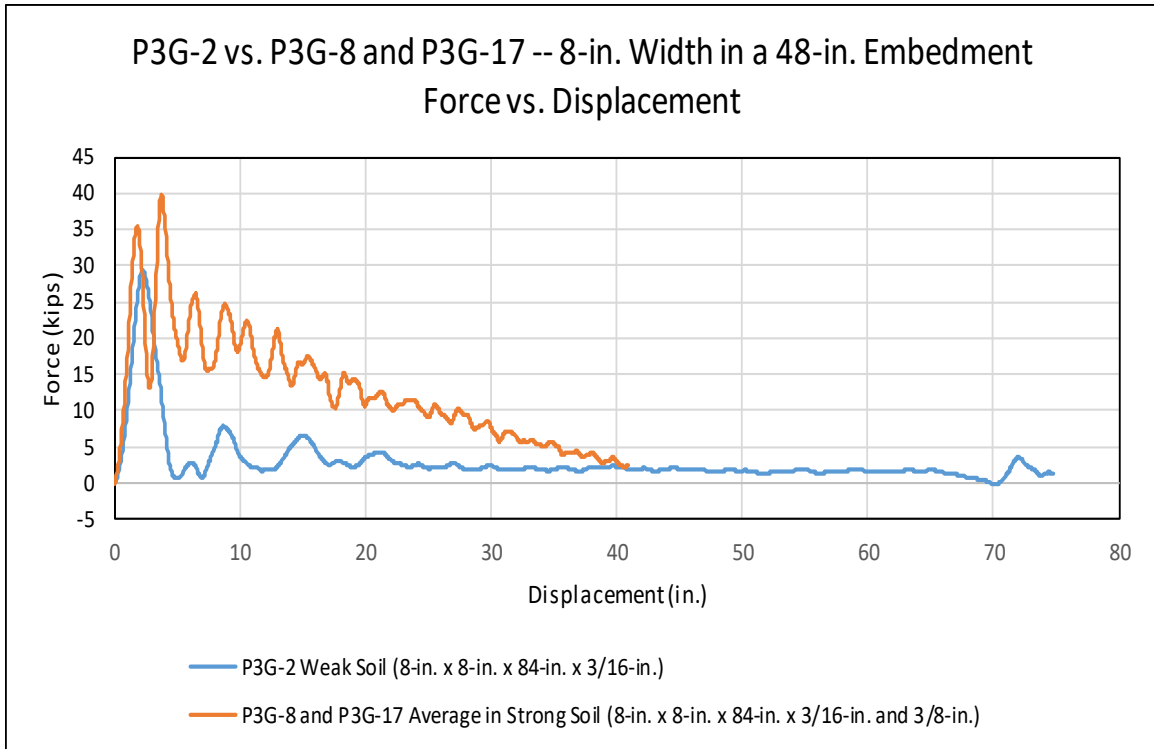


Figure 106. Force vs. Displacement for P3G-2 and the average of P3G-8 and P3G-17

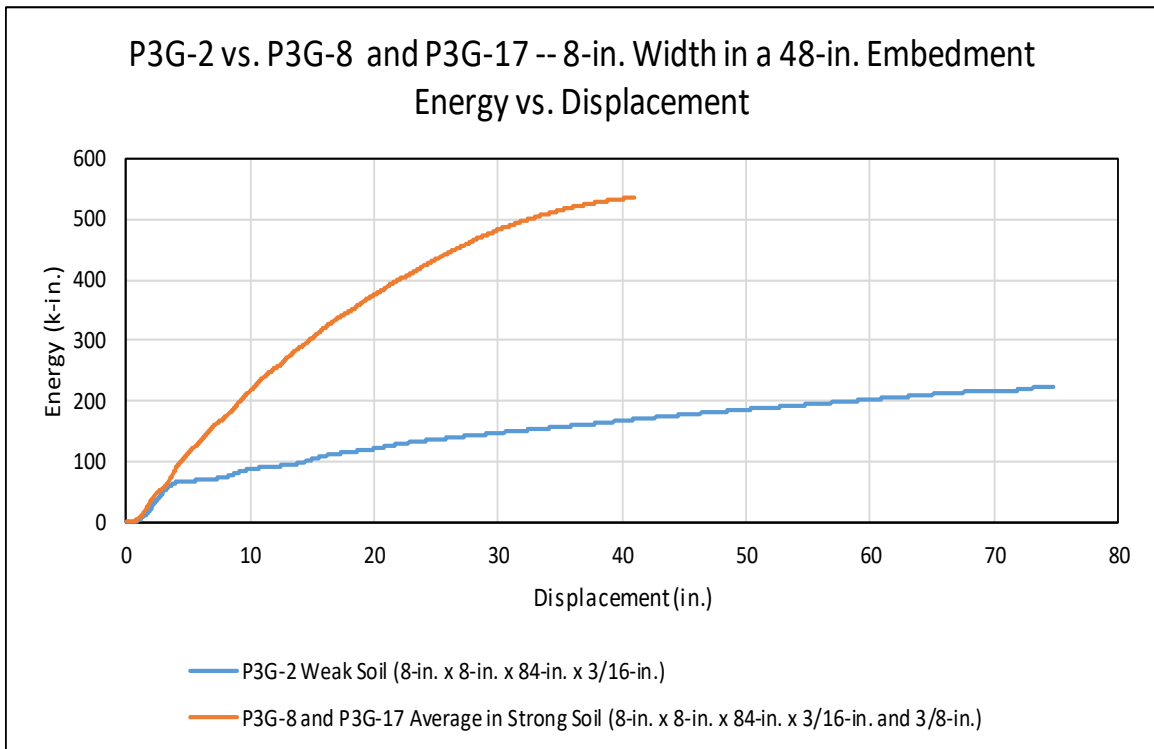


Figure 107. Energy vs. Displacement for P3G-2 and the average of P3G-8 and P3G-17

### 8.4.3 8-in. Width in a 72-in. Embedment

Tests P3G-4 (HSS 8-in. x 8-in. x 108-in. x 3/16-in.) and P3G-19 (HSS 8-in. x 8-in. x 108-in. x 3/8-in.) utilized 8-in. (203-mm) wide posts and were tested with 72-in. (1,829-mm) embedment depths in both weak and strong soils, respectively. Graphs of force vs. displacement and energy vs. displacement can be seen in Figures 108 and 109. Average force values at 5, 10, 15, and 20 in. (127, 254, 381, and 508 mm) of displacement are shown numerically in Table 46.

The data in this table shows that the percent difference of the average forces between the posts installed in weak versus strong soil increased from approximately 62 to 167 percent as the displacement increased from 5 to 20 in. (127 to 508 mm) of deflection.

Table 46. Test nos. P3G-4 and P3G-19 Average Force Values – 8-in. Width in a 48-in. Embedment

	@ 5"	@ 10"	@ 15"	@ 20"
<b>P3G-4 Average Force (kip), 72 in. Embedment</b> HSS 6-in. x 8-in. x 84-in. x 3/16-in., Weak Soil	20.45	13.90	12.57	11.99
<b>P3G-19 Average Force (kip), 72-in. Embedment</b> HSS 6-in. x 8-in. x 84-in. x 3/16-in., Strong Soil	33.20	30.29	31.73	32.05
<b>Average Force Ratio</b>	1.62	2.18	2.52	2.67

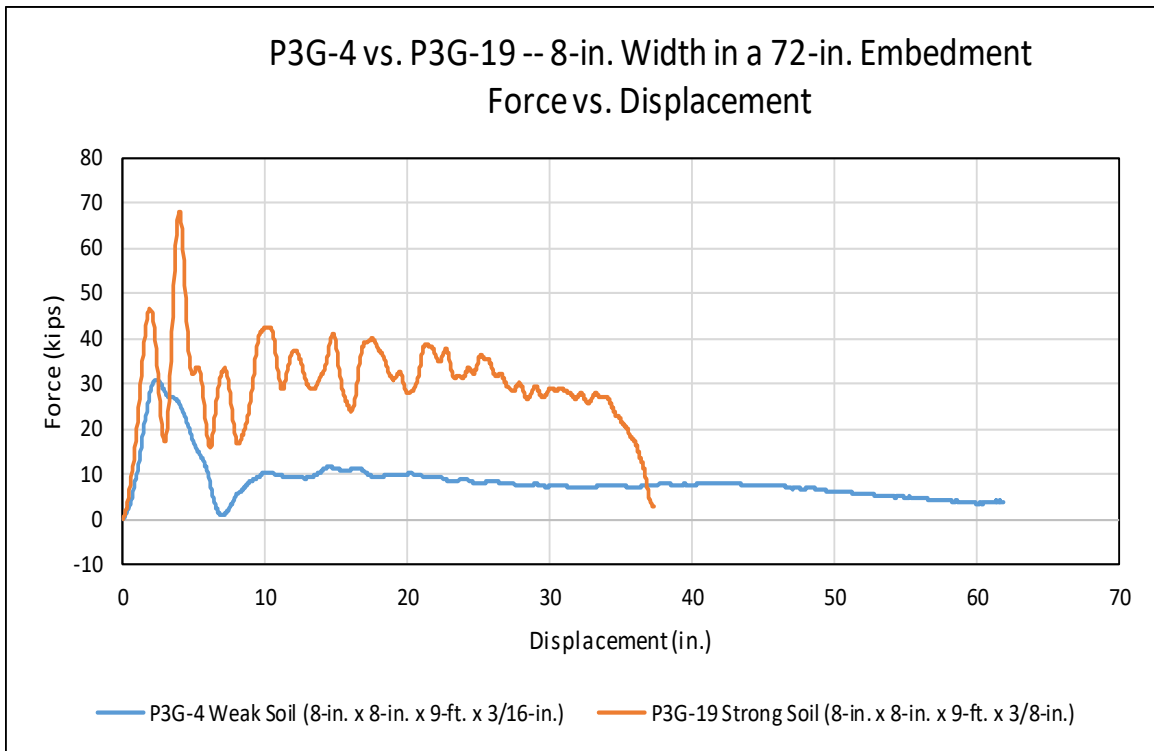


Figure 108. Force vs. Displacement for P3G-2 and the average of P3G-8 and P3G-17

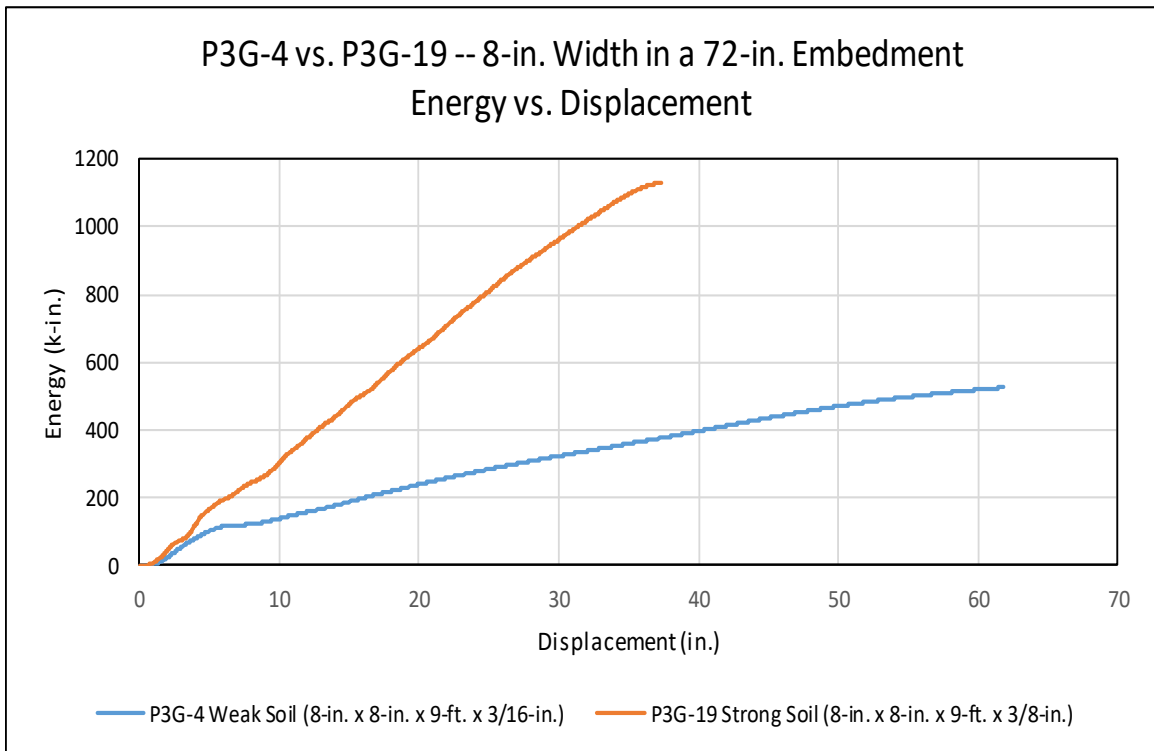


Figure 109. Energy vs. Displacement for P3G-2 and the average of P3G-8 and P3G-17



#### 8.4.4 Soil Discussion

The tests comparing weak and strong soils routinely shows that as the post deflection increases from 5 in. to 20 in. (127 mm to 508 mm), the average post-soil interaction forces for the tests completed in strong soil experiences forces 1.17 to 3.09 times the forces seen for the tests completed in weak soil, as shown in Table 47.

Unfortunately, no obvious relationship could be determined regarding the effect of post width and embedment depth. For example, as the embedment depth increased from 48 to 72 in. (1,219 to 1,829 mm) with a 6-in. (152 mm) width post the average forces increased. The 8-in. wide posts, however had a different trend. More testing is recommended to discover the overlying principles of the post-soil interaction forces when the soil type is changed from weak to strong.

Table 47. Force Increase from Weak to Strong Soil

Testing Configuration	Force Increase from Weak to Strong Soil	Force Increase at 15-in. of Displacement
6-in. Width in a 48-in. Embedment	1.17 - 2.32	2.2
6-in. Width in a 72-in. Embedment	1.67 - 2.99	2.81
8-in. Width in a 48-in. Embedment	1.62 - 3.09	2.94
8-in. Width in a 72-in. Embedment	1.62 - 2.67	2.53

## **8.5 Dimensionless Number Study**

### **8.5.1 Purpose and Motivation**

Dimensionless numbers or groups are quantities that do not contain any physical dimensions and therefore may be used in any dimensionally consistent system.

Frequently, non-dimensional relationships are explored to minimize the size of a test matrix. Dimensionless groups can be used to solve for important relationships.

Dimensionless groups were created to investigate how post width, post thickness, and embedment depth were related. Instead of having to test all of these parameters individually it may be possible to just modify the dimensionless groups and perform a limited number of additional tests. This would save time and money by limiting the total number of experiments that need to be conducted.

In this research study, multiple tests were completed with different post widths, embedment depths, thicknesses, and two types of soil, a smaller strong-soil matrix of the test results were unavailable due to post yielding. As a result, strong soil relationships were sparse and not explored in detail.

### **8.5.2 Buckingham Pi Theorem**

The Buckingham Pi theorem is one of the most common methods used to obtain dimensionless or “pi” groups and can be completed with minimal mathematical training. First, the important variables of the system need to be examined and understood. It was determined that during the post impacts detailed in this thesis that the most important variables governing the force at 15 in. (318 mm) of deflection were the bogie velocity, post embedment depth, post mass, post width, and post thickness. A more rigorous

mathematical definition of this relationship can be seen below, and the variable definitions are shown in Table 48.

$$F = f(V_B, E_D, m_P, W_P, t_P)$$

Table 48. Pi Variables

$\pi_1$	1 <sup>st</sup> . Pi Group
$\pi_2$	2 <sup>nd</sup> . Pi Group
$\pi_3$	3 <sup>rd</sup> . Pi Group
F	Measured Force at 15 in. of Deflection
$W_P$	Post Width
$t_P$	Post Thickness
$V_B$	Bogie Velocity
$E_D$	Post Embedment Depth
$m_P$	Post Mass
L	Length
T	Time
M	Mass

After the variables are discovered and listed the dimensions of each variable needs to be stated, which for this situation can be seen below. Note that there are a total of 6 different variables containing a total of three different dimensions, which are mass, length and time.

$$F: \{MLT^{-2}\}; V_B: \{LT^{-1}\}; E_D: \{L\}; m_P: \{M\}; W_P: \{L\}; t_P: \{L\}$$

Next, after the number of variables and the number of dimensions is known the number of pi groups can be calculated with the equation seen below.

$$\text{No. of Pi Groups} = \text{No. of Variables} - \text{No. of dimensions}$$

$$\text{No. of Pi Groups} = 6 - 3 = 3$$

The equation above shows that a total of 3 Pi groups are needed to describe this experimental situation. After the number of Pi groups are determined the number of repeating variables also needs to be found. This process is shown mathematically below.

$$\text{No. of Repeating Variables} = \# \text{ of Variables} - \# \text{ of Pi Groups}$$

$$\text{No. of Repeating Variables} = 6 - 3 = 3$$

There is no concrete way to determine which variables should be repeating while using the Buckingham Pi Theorem but after many iterations it was determined that the bogie velocity, post width, and post mass would yield three correct Pi groups. The derivation of these Pi groups is shown in the next section.

### 8.5.3 Derivation of Dimensionless Groups

Using the Buckingham Pi Theorem described above, three dimensionless groups were obtained and are shown below. As mentioned previously, the bogie velocity, post embedment and post mass were chosen as the three repeating variables in this situation. Dimensional relationships were modified until a unitless Pi group was obtained, as shown below. The variable and dimension definitions used in the derivation of these Pi groups are shown in Table 48.

$$\pi_1 = V_B^a W_P^b m_P^c F$$

$$\{LT^{-1}\}^a \{L\}^b \{M\}^c \{MLT^{-2}\} = \{MTL\}^0$$

$$\{M\}^{(c+1)} \{T\}^{(-a-2)} \{L\}^{(a+b+1)} = \{MTL\}^0$$

$$M: c + 1 = 0; c = -1$$

$$T: -a - 2 = 0; a = -2$$

$$L: a + b + 1 = -2 + b + 1 = 0; b = 1$$

$$\pi_1 = \frac{FW_P}{V_B^2 m_P}$$

$$\pi_2 = V_B^a W_P^b m_P^c E_D$$

$$\{LT^{-1}\}^a\{L\}^b\{M\}^c\{L\} = \{MTL\}^0$$

$$\{M\}^{(c)}\{T\}^{(-a)}\{L\}^{(a+b+1)} = \{MTL\}^0$$

$$M: c = 0$$

$$T: -a = 0$$

$$L: a + b + 1 = 0 + b + 1 = 0; b = -1$$

$$\pi_2^{-1} = \frac{E_D}{W_P}$$

$$\pi_2 = \frac{W_P}{E_D}$$

$$\pi_3 = V_B^a W_P^b m_P^c t_P$$

$$\{LT^{-1}\}^a\{L\}^b\{M\}^c\{L\} = \{MTL\}^0$$

$$\{M\}^{(c)}\{T\}^{(-a)}\{L\}^{(a+b+1)} = \{MTL\}^0$$

$$M: c = 0$$

$$T: -a = 0$$

$$L: a + b + 1 = 0 + b + 1 = 0; b = -1$$

$$\pi_3^{-1} = \frac{t_P}{W_P}$$

$$\pi_3 = \frac{W_P}{t_P}$$

Summarized:

$$\pi_1 = \frac{FW_P}{V_B^2 m_P}$$

$$\pi_2 = \frac{W_P}{E_D}$$

$$\pi_3 = \frac{W_p}{t_p}$$

#### 8.5.4 Dimensionless Graph

Using the Buckingham Pi Theorem explained above, three dimensionless groups were co-plotted and results are shown in Figure 110. This graph shows for small  $\pi_2$  values, the relationship between  $\pi_1$  and  $\pi_2$  is linear. As  $\pi_2$  increases the relationship between  $\pi_1$  and  $\pi_2$  becomes parabolic or exponential. However, data is still limited, and although results are promising no definitive relationship was recommended.

Results were also plotted based on the  $\pi_3$  values. The two curves at the lower  $\pi_3$  values, seen on the left in Figure 110, have nearly the same slope; this could mean that under a certain  $\pi_2$  threshold value the dependency on the  $\pi_2$  value is very weak. If this is true, a single curve relationship can represent this data, this suggests that the thickness of the post, on the post-soil interaction forces, is not an important parameter until the ratio of width to embedment depth is large.

For example, an engineer or designer could solve for the average post-soil force at 15 in. (381 mm) of deflection with a known width, thickness, embedment depth, and mass based on a prescribed velocity. This could be completed by first solving for  $\pi_2$  and  $\pi_3$ .  $\pi_2$  will tell you the position on the x-axis and Pi 3 will tell you which of the curves you should be using. Then these two groups can be used to solve for the  $\pi_1$  group which can be used to back calculate the average force at 15 in. of deflection. As mentioned previously without more data, it is hard to use this type of graph as each

individual curve follows a particular Pi 3 value, and correct interpolation between these curves is very difficult, if not impossible.

With the addition of more data to this diagram, either through experiments or computations, this method of force prediction could potentially, with accuracy, assist engineers when they are designing structures that require rectangular posts. Additionally, higher accuracy will be obtained with the addition of a soil bulk modulus or shear modulus, and the soil density, but the test data using strong soil was limited. Thus, these parameters were not taken into account with this this study.

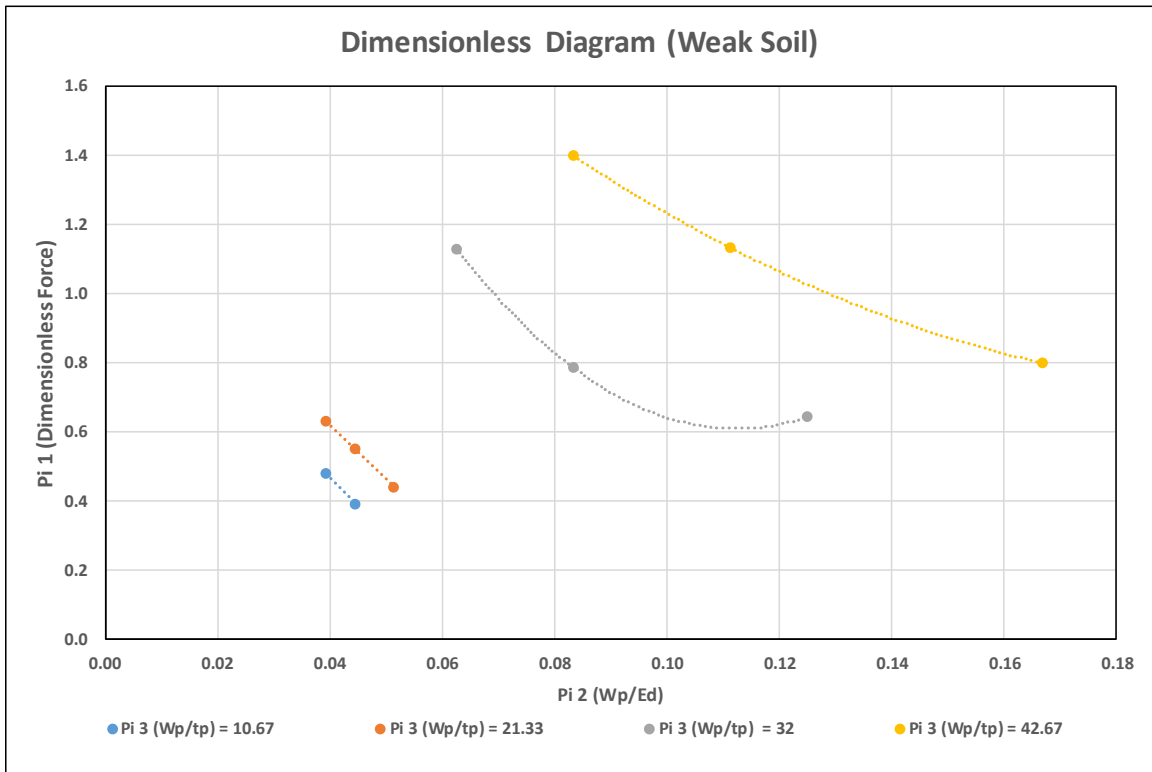


Figure 110. Dimensionless Diagram (Weak Soil)

Table 49. Dimensionless Groups Values

<b>Pi 3 (Wp/tp) = 10.67</b>	
<b>PI 1 (F)</b>	<b>Pi 2 (Wp/Ed)</b>
0.392	0.044
0.479	0.039

<b>Pi 3 (Wp/tp) = 21.33</b>	
<b>PI 1 (F)</b>	<b>Pi 2 (Wp/Ed)</b>
0.441	0.051
0.551	0.044
0.630	0.039

<b>Pi 3 (Wp/tp) = 32</b>	
<b>PI 1 (F)</b>	<b>Pi 2 (Wp/Ed)</b>
0.643	0.125
0.785	0.083
1.130	0.063

<b>Pi 3 (Wp/tp) = 42.67</b>	
<b>PI 1 (F)</b>	<b>Pi 2 (Wp/Ed)</b>
0.800	0.167
1.135	0.111
1.399	0.083



## 9 SUMMARY, CONCLUSIONS, AND RECOMMENDATIONS

Determining the effect of parameter variations on the overall post-soil interaction forces during an impact scenario is no trivial task. In an effort to quantify the relationship between parameter variations and the overall post-soil interaction forces a testing regime was initiated and completed by incrementally changing post width, post embedment depth and soil type during bogie testing of thin walled rectangular posts. Comparisons were made between posts containing 6 and 8-in. (152 and 203-mm) widths, strong and weak soil, and post embedment depths of 48, 72, 90, 96 and 102 in. (1,219, 1,829, 2,286, and 2,591 mm).

Testing of the posts containing 6 and 8 in. (152 and 203 mm) widths showed that the post-soil interaction forces increased as the width was increased. This relationship was shown in both weak and strong soils and at embedment depths of 48, 72, and 96 in. (1,219, 1,829, 2,438 mm). For example, the tests completed in weak soil show that at a 48 and 96-in. (1,219 and 2,438-mm) embedment the force seen in the larger width was 1.07 times larger than the force seen in the smaller width, at 15 in. (381 mm) of deflection, but the force seen in the larger width at a 72-in. (1,829-mm) embedment was 1.25 times larger than the force seen in the smaller width, at 15 in. (381 mm) of deflection.

An attempt to determine dimensionless groups for weak soil post testing results showed excellent promise, but data was too sparse to determine definite relationships. The three dimensionless groups are shown below.

$$\pi_1 = \frac{FW_P}{V_B^2 m_P}$$

$$\pi_2 = \frac{W_P}{E_D}$$

$$\pi_3 = \frac{W_P}{t_P}$$

Data from testing a 4 in. (102 mm) post in weak soil at embedment depths of 78, 90, and 102 in. (1,981, 2,286, and 2,591 mm) in weak soil and the data from testing 6 and 8 in. (152 and 203 mm) width posts in 48, 72, and 96 in. (1,219, 1,829, and 2,438 mm) in weak and strong soil showed that as the embedment depth was increased the post-soil interaction forces also increased, but the increase was lower than what was suggested by Equation (54), shown below. The tests completed with the 4 in. (102 mm) post width had average post-soil interaction forces at 15 in. (381 mm) of deflection very similar to the prediction using Equation (54), but the tests completed with post widths of 6 and 8 in. (152 and 203 mm) diverged significantly from the equation predictions.

$$F_2 = F_1 \left( \frac{E_{D2}}{D_{D1}} \right)^2$$

Results obtained from comparing tests completed in weak soil to those completed in strong soil show that during all of the tests the post-soil interaction forces seen in strong soil was always larger than what was seen in weak soil. Due to the minimal amount of data available for this comparison there were no other meaningful results garnered from this data set.

The amount of differentiation required to correctly research post-soil interaction forces in an impact scenario is quite overwhelming and is a function of multiple parameters including: impact velocity, embedment depth, post mass, post width, post thickness, soil density, and soil shear or bulk modulus. Using some of these variables in

conjunction with the Buckingham Pi theorem yielded 3 dimensionless groups relating these variables to the post-soil interaction forces seen at 15 in. (381 mm) of deflection.

As mentioned above more testing with different widths and embedment depths is recommended to further analyze this situation.

**10 REFERENCES**

1. *Manual for Assessing Safety Hardware (MASH), Second Edition*, American Association of State Highway and Transportation Officials (AASHTO), Washington, D.C., 2016.
2. *Standard Plans*, California State Transportation Agency (Caltrans), California, 2015.
3. *Standard Construction Drawings*, Delaware Department of Transportation (DelDOT), Delaware, Dec. 30, 2014.
4. *Standard Plans for Bridge Construction*, Florida Department of Transportation (FDOT), Florida, Nov. 11, 2017.
5. *Standard Drawings*, Idaho Transportation Department (ITD), Idaho, October. 2017.
6. *Standard Plans*, Indiana Department of Transportation (INDOT), Indiana, September. 4, 2012.
7. *Bridge Deck Rail Bridge Standards*, Iowa Department of Transportation (IowaDot), Iowa, August. 29, 2016.
8. *Standard Drawings*, Kansas Department of Transportation (KDOT), Kansas, May 2, 2015.
9. *Book of Standards – For Highway & Incidental Structures*, Maryland Department of Transportation (MDOT), Maryland, September. 24, 2013.
10. *Standard Plates*, Minnesota Department of Transportation (MnDOT), Minnesota, August. 28, 2017.
11. *Bridge Office Policies and Procedures*, Nebraska Department of Roads Bridge Divison, Nebraska, 2016.
12. *Bridge Construction Details*, New Jersey Department of Transportation (NJDOT), New Jersey, July 19, 2017.
13. *Standard Sheets – English – USC*, New York Department of Transportation (NYSDOT), New York, July 14, 2016.
14. *Standard Details*, Oregon Department of Transportation (ODOT), Oregon, 2018.
15. *CAD Standards*, Texas Department of Transportation (TxDOT), Texas, March, 2018.
16. *Bridge Manual Standard Drawings*, Wisconsin Department of Transportation, Wisconsin, July 7, 2017.

17. Buth, E., and Menges, W., *Crash Testing and Evaluation of Retrofit Bridge Railings and Transition*, Texas Transportation Institute, Texas A&M University, College Station, Texas, 1995.
18. *Guide Specifications for Bridge Railings*, American Association of State Highway and Transportation Officials (AASHTO), Washington, D.C., 1989
19. Polivka, K.A., Faller, R.K., Keller, E.A., Sicking, D.L., Rohde, J.R., and Holloway, J.C., *Design and Evaluation of the TL-4 Minnesota Combination Traffic/Bicycle Bridge Rail*, Final Report to the Midwest States' Regional Pooled Fund Program, Transportation Research Report No. TRP-03-74-98, Project No. SPR-3(17), Midwest Roadside Safety Facility, University of Nebraska-Lincoln, Lincoln, Nebraska, November 1998.
20. Caldwell, C. *Investigation of the Crashworthiness of Barrier Mounted Hardware: Barrier Mounted Sign and Signpost*, Final Report to the Roadside Safety Research Group of the California Department of Transportation. Caltrans, Sacramento, California, June 2011.
21. Miller, S., *Fencing Saves Driver from Plunging off Valley View Bridge*, Cleveland Channel 19 News, Cleveland Ohio, April 5, 2018. <<http://www.cleveland19.com/story/37892707/fencing-saves-driver-from-plunging-off-valley-view-bridge>> Last accessed July 13, 2018
22. NASS CASE Viewer CASE ID: 828018044, April, 2014. <https://crashviewer.nhtsa.dot.gov/nass-cds/CaseForm.aspx?xsl=main.xsl&CaseID=828018044>> Last accessed July 16, 2018.
23. NASS CASE Viewer CASE ID: 727019493, September, 2015. <https://crashviewer.nhtsa.dot.gov/nass-cds/CaseForm.aspx?xsl=main.xsl&CaseID=727019493>> Last accessed July 16, 2018.
24. Keller E.A., Sicking, D.L., Faller, R.K., Polivka, K.A., and Rohde, J.R., *Guidelines for Attachments to Bridge Rails and Median Barriers*, Final Report to the Midwest States' Regional Pooled Fund Program, Transportation Research Report No. TRP-03-98-03, Project No. SPR-3(17), Midwest Roadside Safety Facility, University of Nebraska-Lincoln, Lincoln, Nebraska, February 26, 2003.
25. Reid, J.D., and Sicking, D.L., *Zone of Intrusion Study*, Final Report to the Midwest States' Regional Pooled Fund Program, Transportation Research Report No. TRP-03-242-10, Midwest Roadside Safety Facility, University of Nebraska-Lincoln, Lincoln, Nebraska, October 15, 2010.
26. Ross, H.E., Sicking, D.L., Zimmer, R.A., and Michie, J.D., *Recommended Procedures for the Safety Performance Evaluation of Highway Features*, National Cooperative Highway Research Program (NCHRP) Report No. 350, Transportation Research Board, Washington, D.C., 1993.

27. Stolle, C.J., Reid, J.D., and Faller, R.K., *Zone of Intrusion for Permanent 9.1-Degree Single-Slope Concrete barriers*, Final Report to the Wisconsin Department of Transportation, Transportation Research Report No. TRP-03-292-13, Midwest Roadside Safety Facility, University of Nebraska-Lincoln, Lincoln, Nebraska, March 14, 2014.
28. Abu-Odeh, A., Williams, W., Ferdous, R., Spencer, M., Bligh, R., and Menges, W., *Signs on Concrete Median Barriers*, Texas Transportation Institute, University of Texas A&M, College Station, Texas, April, 2013.
29. *IOWA DOT GS-15006 – General Supplemental Specifications for Highway and Bridge Construction.*, Iowa DOT, April 17, 2018. <[https://iowadot.gov/specifications/new\\_docs/GS-15004.pdf](https://iowadot.gov/specifications/new_docs/GS-15004.pdf)> Last accessed July 25, 2018.
30. *LRFD Load Combinations*, BG Structural Engineering, <[http://www.bgstructuralengineering.com/BGASCE7\\_10/BGASCE7002/BGASCE700202.htm](http://www.bgstructuralengineering.com/BGASCE7_10/BGASCE7002/BGASCE700202.htm)> Last accessed December 1, 2018.
31. *Chain Link Fence Wind Load Guide for the Selection of Line Post and Line Post Spacing*, Chain Link Manufactures Institute, June, 2016.
32. *Minimum Design Loads for Buildings and Other Structures*. 2010. American Society of Civil Engineers.
33. *Cylinder Drag – from Eric Weisstein*, Wolfram Research <<http://scienceworld.wolfram.com/physics/CylinderDrag.html>> Last accessed November 29, 2018.
34. *Steel Construction Manual*, American Institute of Steel Design (AISC), Fifteenth Edition, First Printing, 2017.
35. *Full-weight Hot-dip Galvanized ASTM F1083 Schedule 40 Pipe*, Wheatland Tube, <<https://www.wheatland.com/wp-content/uploads/2017/12/F1083-Schedule-40-Specifications.pdf>> Last accessed November 30, 2018
36. *Chain Link Galvanized Fence*, Your Fence Store, <<http://www.yourfencestore.com/cl/clgal.htm>> Last accessed December 1, 2018.
37. Society of Automotive Engineers (SAE), *Instrumentation for Impact Test – Part I – Electronic Instrumentation*, SAE J211/1 MAR95, New York City, NY, July, 2007.

**11 APPENDICES**

**Appendix A. Lateral Impact**



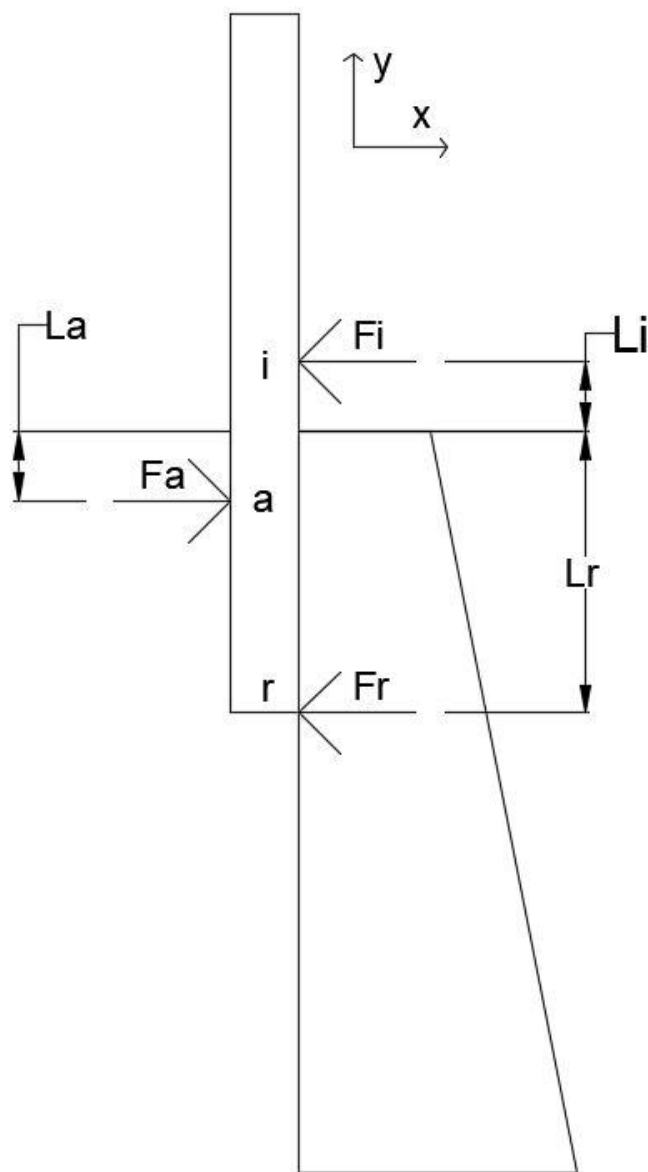


Figure A-1. Lateral Impact Loading Configuration

Table A-1. Variable Definitions

Variable	Definition
$F_i$	Impact Force
$F_a$	Tensile Force at Top Clamp
$F_r$	Reaction Force at Bottom of Post
$L_i$	Distance Between Impact and Top of Parapet
$L_a$	Distance Between Top Clamp and Top of Parapet
$L_r$	Distance Between Bottom of Post and Top of Parapet

$$\sum F_x = 0 = -F_i + F_a - F_r$$

$$F_i = F_a - F_r \text{ (Eqn. 1)}$$

$$\sum M_i = 0 = F_a(L_i + L_a) - F_r(L_r + L_i)$$

$$F_a = \frac{F_r(L_r + L_i)}{(L_i + L_a)} \text{ (Eqn. 2)}$$

Sub Eqn. 2 into Eqn. 1

$$F_i = \frac{F_r(L_r + L_i)}{(L_i + L_a)} - F_r$$

$$F_i = F_r \left[ \left( \frac{L_r + L_i}{L_i + L_a} \right) - 1 \right]$$

$$F_i = F_r \left[ \frac{(L_r + L_i) - (L_i + L_a)}{(L_i + L_a)} \right]$$

$$F_i = \frac{F_r(L_r - L_a)}{(L_i + L_a)} \text{ (Eqn. 3)}$$

$$\sum M_a = 0 = F_i(L_i + L_a) - F_r(L_r - L_a)$$

$$F_i = \frac{F_r(L_r - L_a)}{(L_i + L_a)} \text{ (Eqn. 4)}$$

Eqn. 3 is equal to Eqn. 4 ✓

$$\sum M_r = 0 = F_i(L_i + L_r) - F_a(L_r - L_a)$$

$$F_i = \frac{F_a(L_r - L_a)}{(L_i + L_r)} \text{ (Eqn. 5)}$$

Sub Eqn. 5 into Eqn. 1

$$\frac{F_a(L_r - L_a)}{(L_i + L_r)} = F_a - F_r$$

$$F_r = F_a - F_a \left[ \frac{(L_r - L_a)}{(L_i + L_r)} \right]$$

$$F_r = F_a \left[ 1 - \frac{(L_r - L_a)}{(L_i + L_r)} \right]$$

$$F_r = F_a \left[ \frac{(L_i + L_r) - (L_r - L_a)}{(L_i + L_r)} \right]$$

$$F_r = \frac{F_a(L_i + L_a)}{(L_i + L_r)}$$

$$F_a = \frac{F_r(L_i + L_r)}{(L_i + L_a)} \quad (\text{Eqn. 6})$$

Eqn. 2 is equal to Eqn. 6 ✓

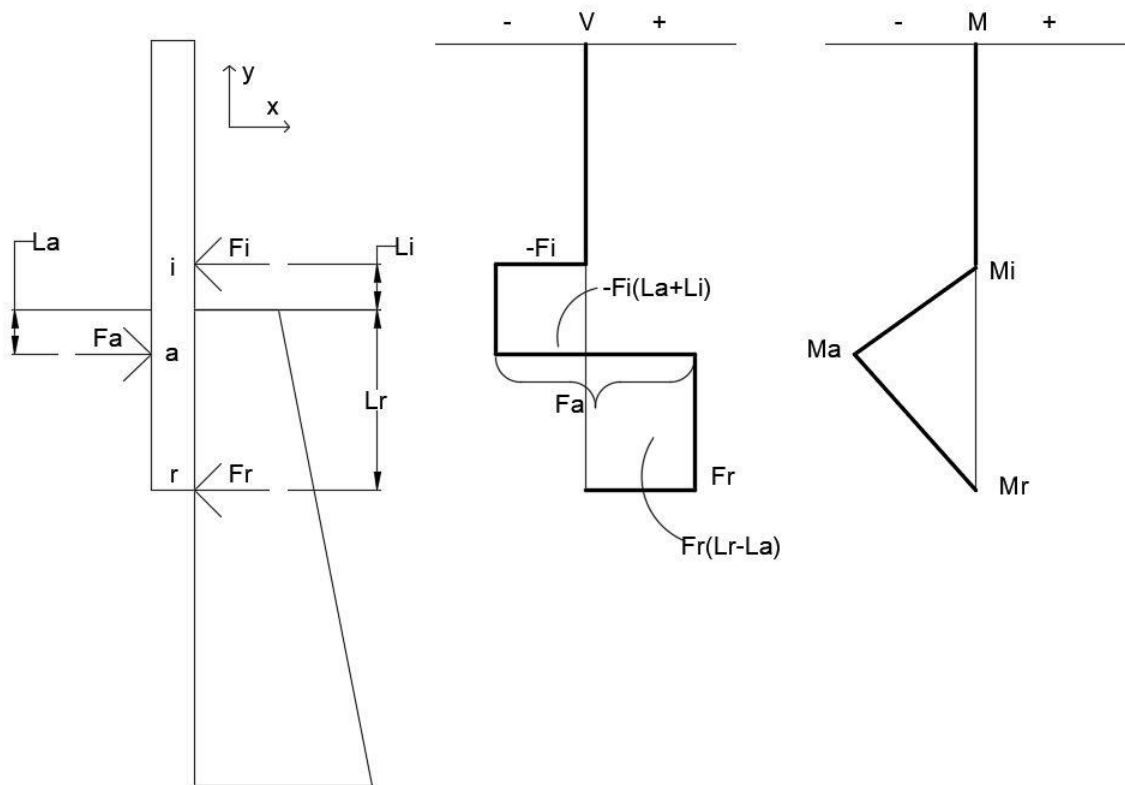


Figure A-2. Lateral Impact Shear and Moment Diagrams

$$0 = -F_i(L_a + L_i) + F_r(L_r - L_a)$$

$$F_i(L_a + L_i) = F_r(L_r - L_a)$$

$$F_i = \frac{F_r(L_r - L_a)}{(L_i + L_a)} \quad (\text{Eqn. 7})$$

Eqn. 7 is equal to Eqn. 4 ✓

$$M_a = F_i(L_a + L_i)$$

$$M_a = F_r(L_r - L_a)$$

$F_a$  = The Maximum Tension Force Imparted into Upper Anchors

$M_a$  = The Maximum Bending Moment

Appendix B. **Longitudinal Impact**

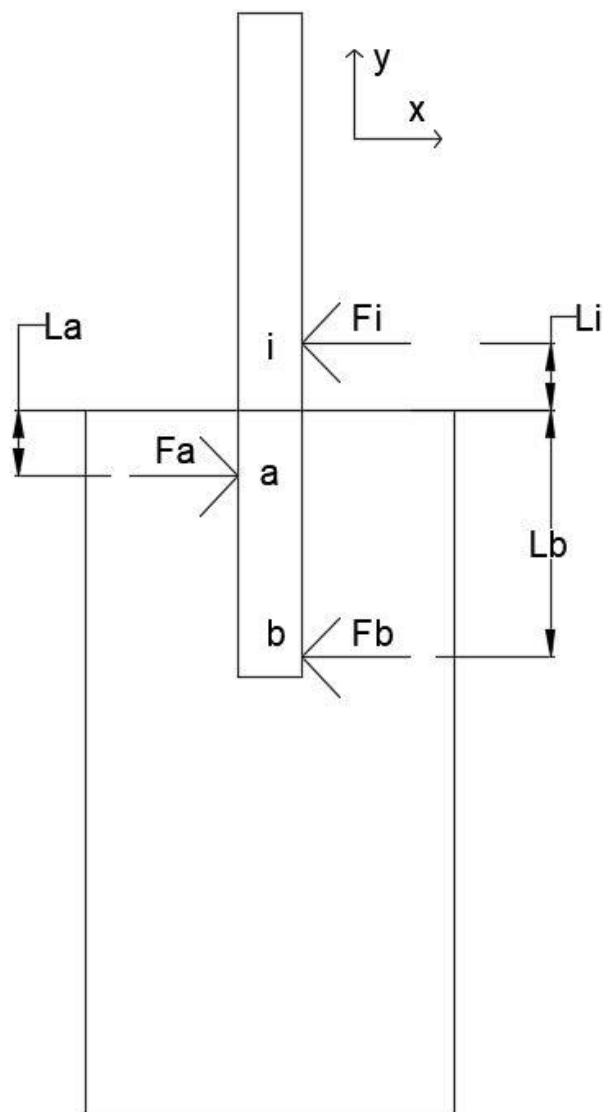


Figure B-1. Longitudinal Impact Loading Configuration

Table B-1. Variable Definitions

Variable	Definition
$F_i$	Impact Force
$F_a$	Shear Force at Top Clamp
$F_b$	Shear Force at Bottom Clamp
$L_i$	Distance Between Impact and Top of Parapet
$L_a$	Distance Between Top Clamp and Top of Parapet
$L_b$	Distance Between Bottom Clamp and Top of Parapet

$$\sum F_x = 0 = -F_i + F_a - F_b$$

$$F_i = F_a - F_b \text{ (Eqn. 1)}$$

$$\sum M_i = 0 = F_a(L_i + L_a) - F_b(L_b + L_i)$$

$$F_a = \frac{F_b(L_b + L_i)}{(L_i + L_a)} \text{ (Eqn. 2)}$$

Sub Eqn. 2 into Eqn. 1

$$F_i = \frac{F_b(L_b + L_i)}{(L_i + L_a)} - F_b$$

$$F_i = F_b \left[ \left( \frac{L_b + L_i}{L_i + L_a} \right) - 1 \right]$$

$$F_i = F_b \left[ \frac{(L_b + L_i) - (L_i + L_a)}{(L_i + L_a)} \right]$$

$$F_i = \frac{F_b(L_b - L_a)}{(L_i + L_a)} \text{ (Eqn. 3)}$$

$$\sum M_a = 0 = F_i(L_i + L_a) - F_b(L_b - L_a)$$

$$F_i = \frac{F_b(L_b - L_a)}{(L_i + L_a)} \text{ (Eqn. 4)}$$

Eqn. 3 is equal to Eqn. 4 ✓

$$\sum M_b = 0 = F_i(L_i + L_b) - F_a(L_b - L_a)$$

$$F_i = \frac{F_a(L_b - L_a)}{(L_i + L_b)} \text{ (Eqn. 5)}$$

Sub Eqn. 5 into Eqn. 1

$$\frac{F_a(L_b - L_a)}{(L_i + L_b)} = F_a - F_b$$

$$F_b = F_a - F_a \left[ \frac{(L_b - L_a)}{(L_i + L_b)} \right]$$

$$F_b = F_a \left[ 1 - \frac{(L_b - L_a)}{(L_i + L_b)} \right]$$

$$F_b = F_a \left[ \frac{(L_i + L_b) - (L_b - L_a)}{(L_i + L_b)} \right]$$

$$F_b = \frac{F_a(L_i + L_a)}{(L_i + L_b)}$$

$$F_a = \frac{F_b(L_i + L_b)}{(L_i + L_a)} \quad (\text{Eqn. 6})$$

Eqn. 2 is equal to Eqn. 6 ✓



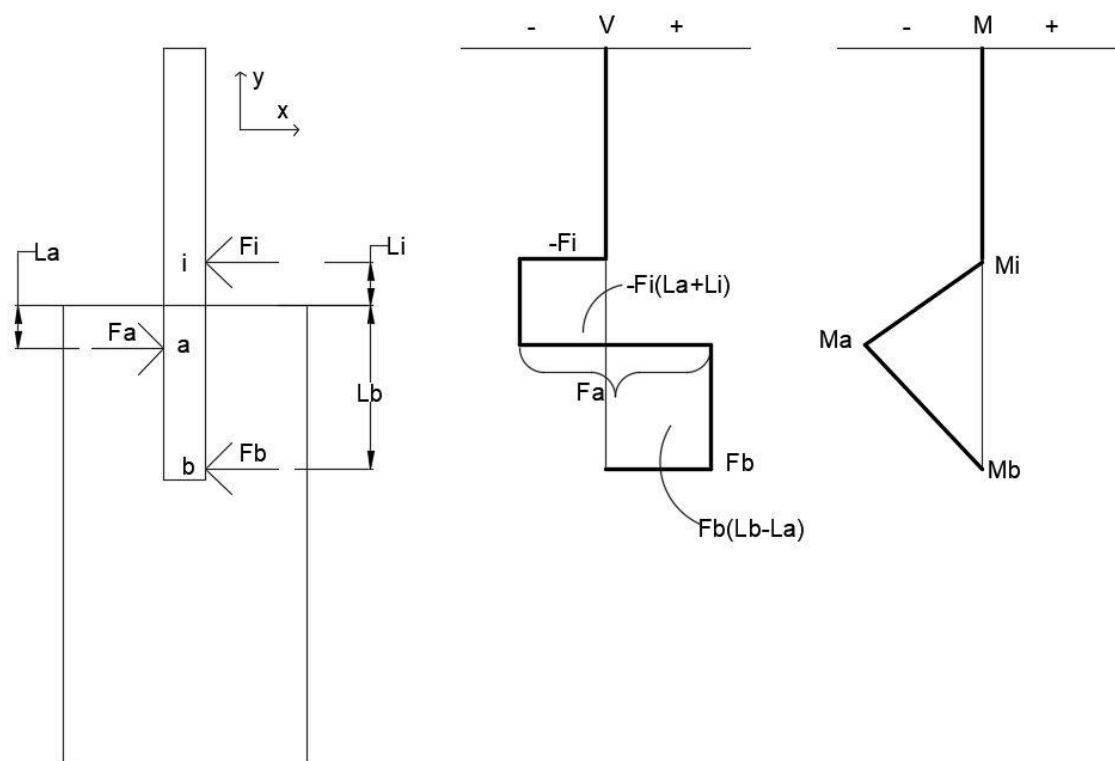


Figure B-2. Longitudinal Impact Shear and Moment Diagrams

$$0 = -F_i(L_a + L_i) + F_b(L_b - L_a)$$

$$F_i(L_a + L_i) = F_b(L_b - L_a)$$

$$F_i = \frac{F_b(L_b - L_a)}{(L_i + L_a)} \quad (\text{Eqn. 7})$$

Eqn. 7 is equal to Eqn. 4 ✓

$$M_a = F_i(L_a + L_i)$$

$$M_a = F_b(L_b - L_a)$$

$F_a$  = The Maximum Shear Force Imparted into Upper Anchors

$M_a$  = The Maximum Bending Moment

$F_b$  = The Maximum Shear Force Imparted into Lower Anchors

**Appendix C. Front Wind Loading**

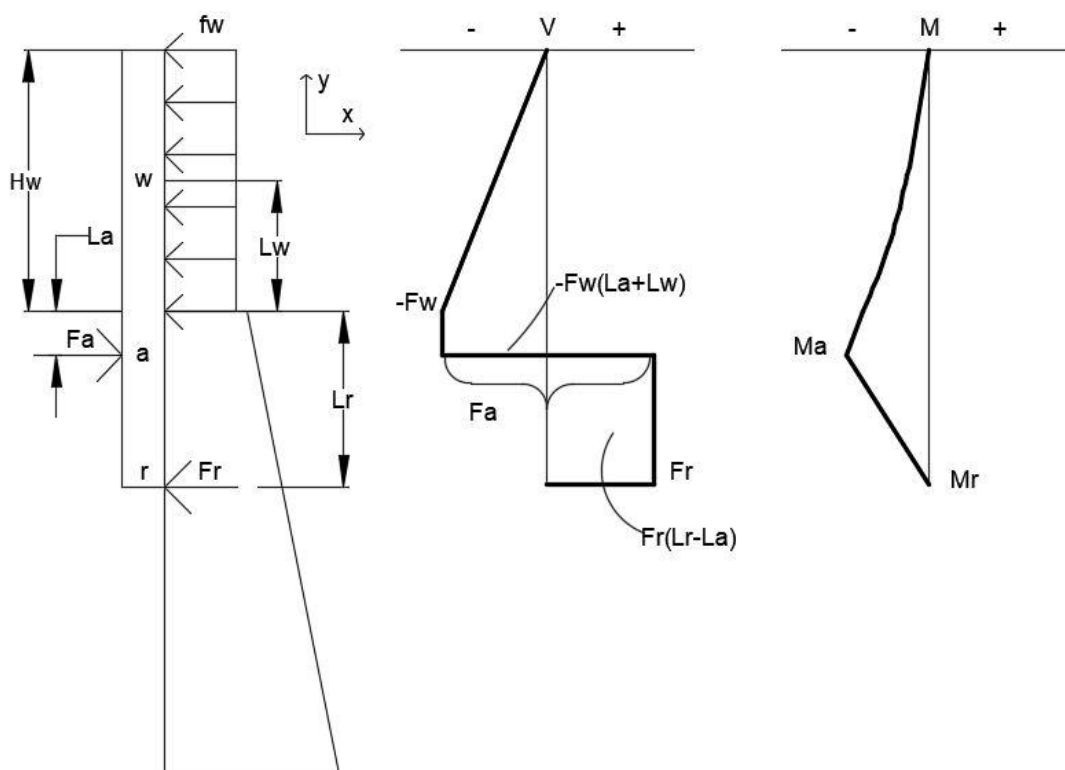


Figure C-1. Front Wind Loading

Table C-1. Variable Definitions

Variable	Definition
$fw$	Wind Load Per Unit Length
$Fw$	Total Effective Wind Load
$Fa$	Tensile Force at Top Clamp
$Fr$	Reaction Force at Bottom of Parapet
$Hw$	Chain-Link Height
$Lw$	Distance Between Center of Wind Load and Top of Parapet
$La$	Distance Between Top Clamp and Top of Parapet
$Lr$	Distance Between Bottom of Post and Top of Parapet

First, the total effective wind load on the structure must be determined:

$$\int_0^{H_w} f_w dy = F_w \quad (55)$$

Next, the centroid of the wind load can be determined:

$$\bar{y} = \frac{\sum y_i A_i}{\sum A_i} \quad (56)$$

$$\bar{y} = \frac{L_w * f_w * 1}{f_w * 1} = L_w \quad (57)$$

Now, a simplified model of the system that represents the wind load as a point load can be created and is shown below.

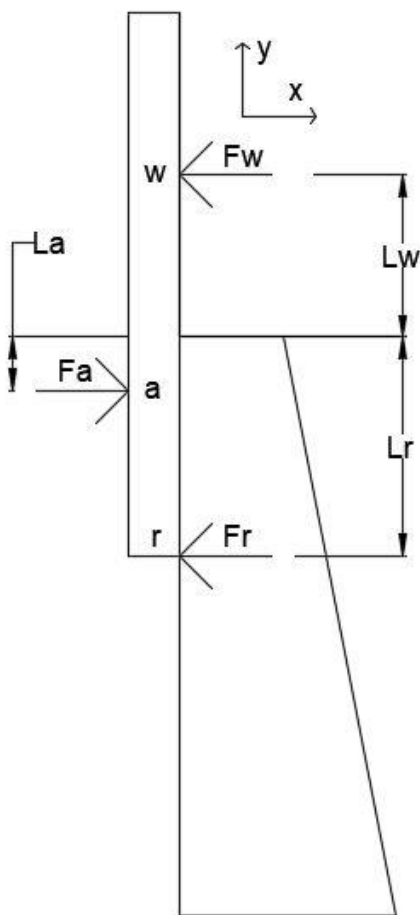


Figure C-2. Front Wind Loading – Simplified Model

$$\sum F_x = 0 = -F_w + F_a - F_r$$

$$F_w = F_a - F_r \quad (\text{Eqn. 1})$$

$$\sum M_w = 0 = F_a(L_w + L_a) - F_r(L_r + L_w)$$

$$F_a = \frac{F_r(L_r + L_w)}{(L_w + L_a)} \quad (\text{Eqn. 2})$$

Sub Eqn. 2 into Eqn. 1

$$F_w = \frac{F_r(L_r + L_w)}{(L_w + L_a)} - F_r$$

$$F_w = F_r \left[ \left( \frac{L_r + L_w}{L_w + L_a} \right) - 1 \right]$$

$$F_w = F_r \left[ \frac{(L_r + L_w) - (L_w + L_a)}{(L_w + L_a)} \right]$$

$$F_w = \frac{F_r(L_r - L_a)}{(L_w + L_a)} \quad (\text{Eqn. 3})$$

$$\sum M_a = 0 = F_w(L_w + L_a) - F_r(L_r - L_a)$$

$$F_w = \frac{F_r(L_r - L_a)}{(L_w + L_a)} \quad (\text{Eqn. 4})$$

Eqn. 3 is equal to Eqn. 4 ✓

$$\sum M_r = 0 = F_w(L_w + L_r) - F_a(L_r - L_a)$$

$$F_w = \frac{F_a(L_r - L_a)}{(L_w + L_r)} \quad (\text{Eqn. 5})$$

Sub Eqn. 5 into Eqn. 1

$$\frac{F_a(L_r - L_a)}{(L_w + L_r)} = F_a - F_r$$

$$F_r = F_a - F_a \left[ \frac{(L_r - L_a)}{(L_w + L_r)} \right]$$

$$F_r = F_a \left[ 1 - \frac{(L_r - L_a)}{(L_w + L_r)} \right]$$

$$F_r = F_a \left[ \frac{(L_w + L_r) - (L_r - L_a)}{(L_w + L_r)} \right]$$

$$F_r = \frac{F_a(L_w + L_a)}{(L_w + L_r)}$$

$$F_a = \frac{F_r(L_w + L_r)}{(L_w + L_a)} \quad (\text{Eqn. 6})$$

Eqn. 2 is equal to Eqn. 6 ✓

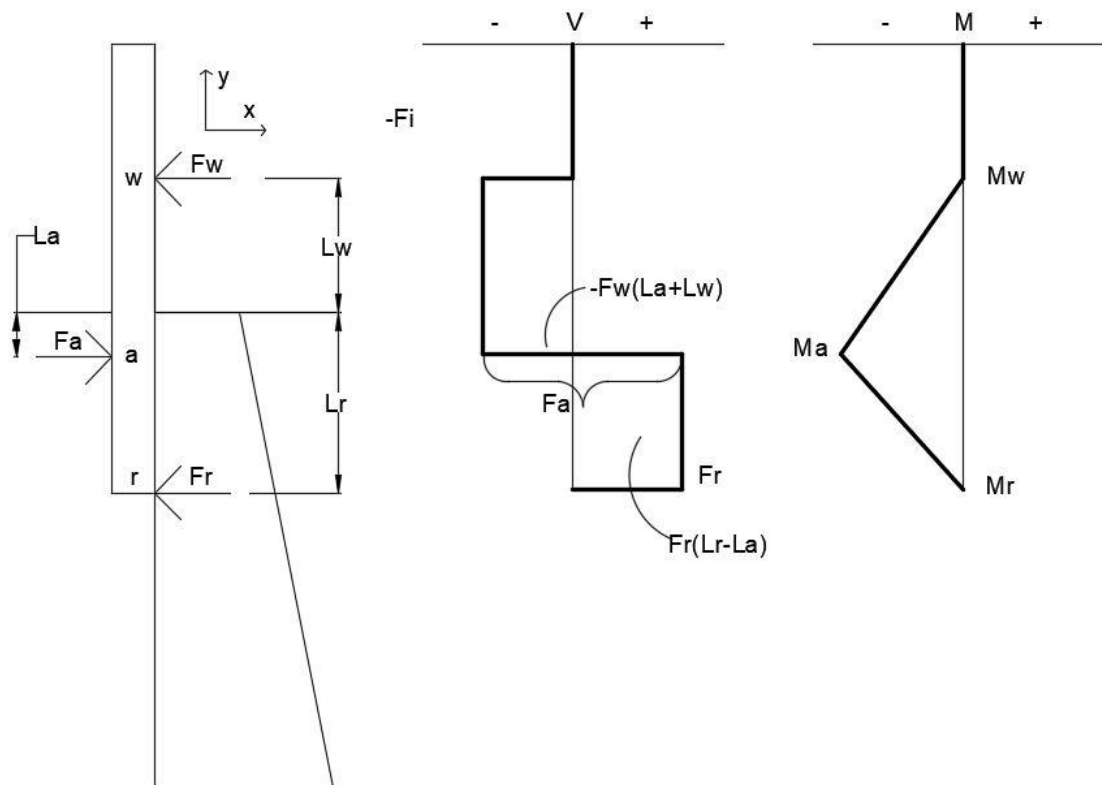


Figure C-3. Simplified Front Wind Loading Shear and Moment Diagrams

$$0 = -F_w(L_a + L_w) + F_r(L_r - L_a)$$

$$F_w(L_a + L_w) = F_r(L_r - L_a)$$

$$F_w = \frac{F_r(L_r - L_a)}{(L_w + L_a)} \quad (\text{Eqn. 7})$$

Eqn. 7 is equal to Eqn. 4 ✓

$$M_a = F_i(L_a + L_i)$$

$$M_a = F_r(L_r - L_a)$$

$F_a$  = The Maximum Tension Force Imparted into Upper Anchors from Wind

$M_a$  = The Maximum Bending Moment from Wind

Appendix D. **Back Wind Loading**



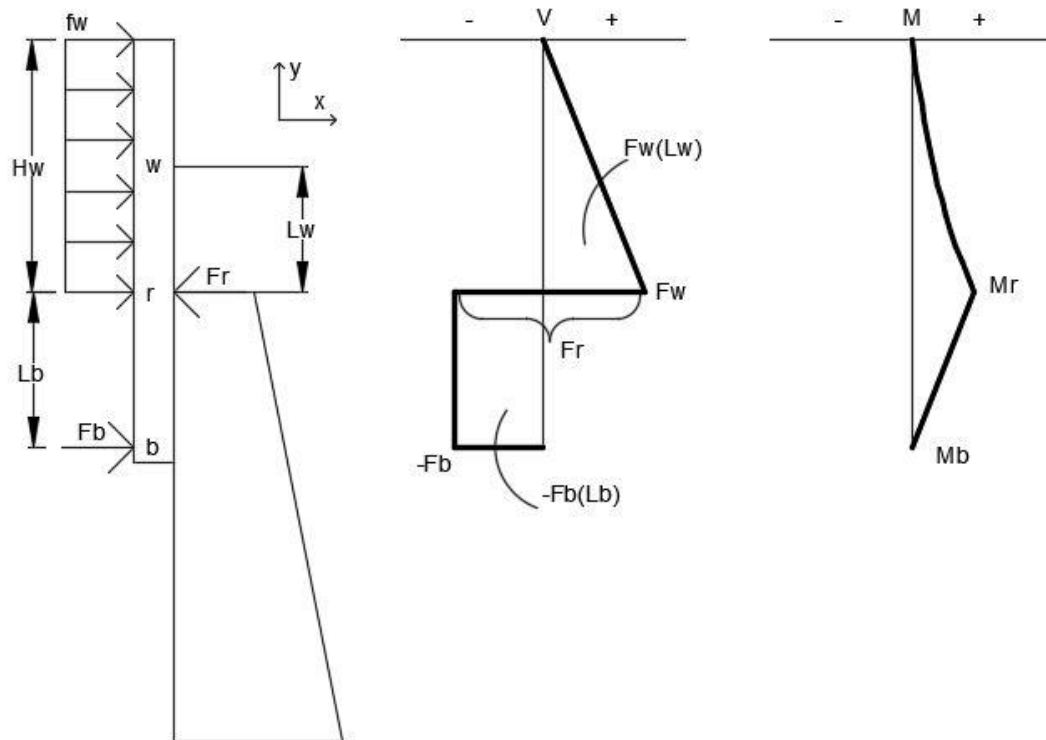


Figure D-1. Back Wind Loading

Table D-1. Variable Definitions

Variable	Definition
$f_w$	Wind Load Per Unit Length
$F_w$	Total Effective Wind Load
$F_b$	Tensile Force at Bottom Clamp
$F_r$	Reaction Force at Top of Parapet
$H_w$	Chain-Link Height
$L_w$	Distance Between Center of Wind Load and Top of Parapet
$L_b$	Distance Between Bottom Clamp and Top of Parapet

In this derivation the tensile force at the top clamp was neglected and only the tensile force at the bottom clamp was considered to represent the worst case scenario.

First, the total effective wind load on the structure must be determined:

$$\int_0^{H_w} f_w dy = F_w \quad (58)$$

Next, the centroid of the wind load can be determined:

$$\bar{y} = \frac{\sum y_i A_i}{\sum A_i} \quad (59)$$

$$\bar{y} = \frac{L_w * f_w * 1}{f_w * 1} = L_w \quad (60)$$

Now, a simplified model of the system that represents the wind load as a point load can be created and is shown below.

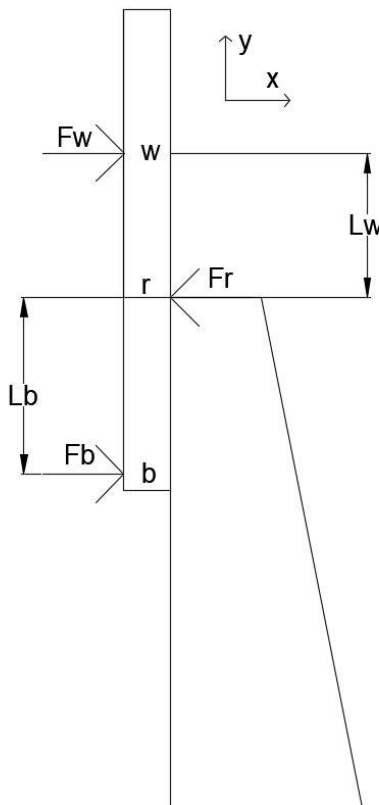


Figure D-2. Back Wind Loading – Simplified Model

$$\sum F_x = 0 = F_w + F_b - F_r$$

$$F_w = F_r - F_b \quad (\text{Eqn. 1})$$

$$\sum M_w = 0 = -F_r L_w + F_b (L_b + L_w)$$

$$F_b = \frac{F_r L_w}{(L_b + L_w)} \quad (\text{Eqn. 2})$$

Sub Eqn. 2 into Eqn. 1

$$F_w = F_r - \frac{F_r L_w}{(L_w + L_b)}$$

$$F_w = F_r \left[ 1 - \frac{L_w}{(L_b + L_w)} \right]$$

$$F_w = F_r \left[ \frac{(L_w + L_b) - L_w}{(L_b + L_w)} \right]$$

$$F_w = \frac{F_r L_b}{(L_w + L_b)} \quad (\text{Eqn. 3})$$

$$\sum M_r = 0 = -F_w L_w + F_b L_b$$

$$F_w = \frac{F_b L_b}{L_w} \quad (\text{Eqn. 4})$$

Sub Eqn. 4 into Eqn. 1

$$\frac{F_b L_b}{L_w} = F_r - F_b$$

$$F_r = \frac{F_b L_b}{L_w} + F_b$$

$$F_r = F_b \left( \frac{L_b}{L_w} + 1 \right)$$

$$F_r = F_b \left( \frac{L_b + L_w}{L_w} \right)$$

$$F_b = F_r \left( \frac{L_w}{L_b + L_w} \right) \quad (\text{Eqn. 5})$$

*Eqn. 5 is equal to Eqn. 2 ✓*

$$\sum M_b = 0 = -F_w(L_w + L_b) + F_r L_b$$

$$F_w = \frac{F_r L_b}{(L_w + L_b)}$$

*Eqn. 6 is equal to Eqn. 3 ✓*

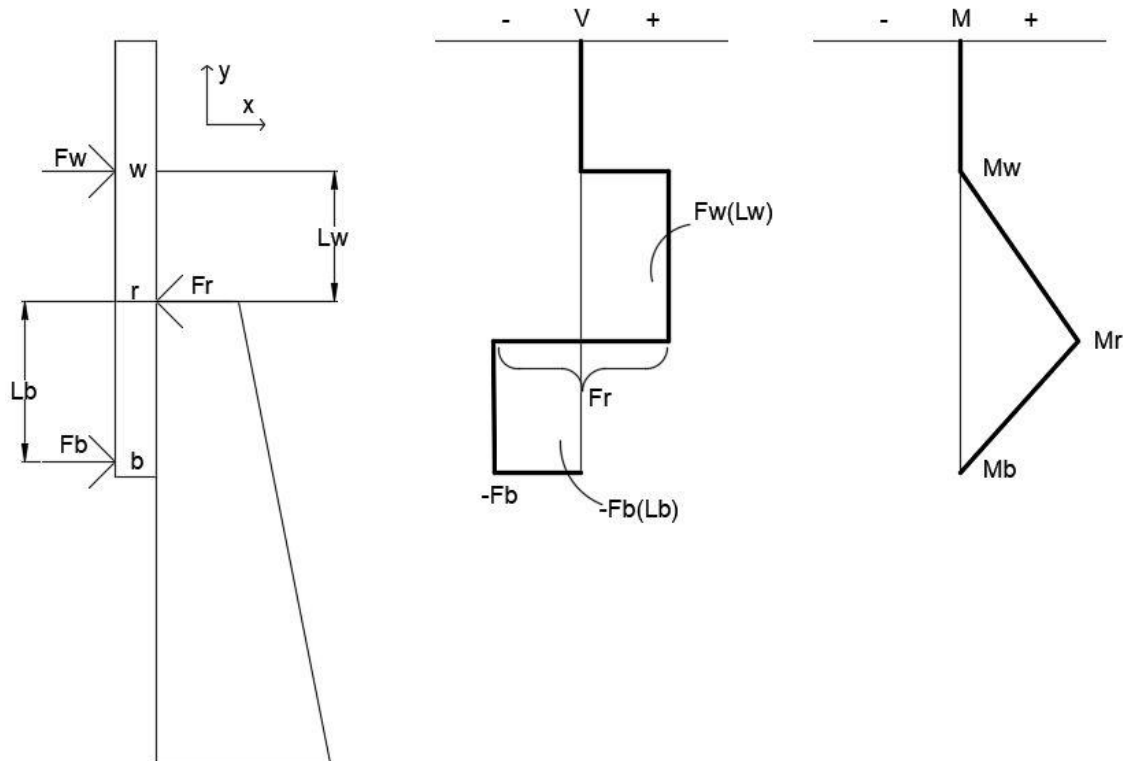


Figure D-3. Simplified Back Wind Loading Shear and Moment Diagrams

$$0 = F_w(L_w) - F_b(L_b)$$

$$F_w = \frac{F_b L_b}{L_w}$$

*Eqn. 7 is equal to Eqn. 4*

$$M_r = F_w L_w$$

$$M_r = F_b L_b$$

Appendix E. **Dead Load**

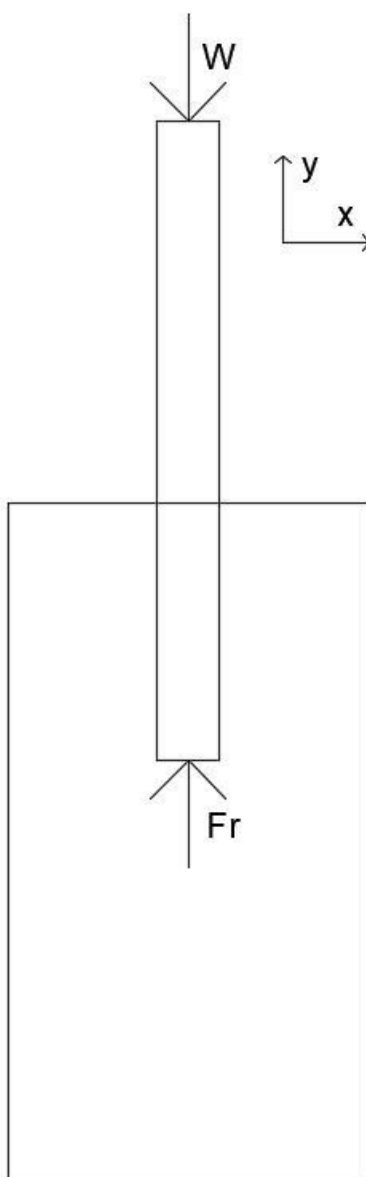


Figure E-1. Dead Load Configuration

Table E-1. Variable Definitions

<b>Variable</b>	<b>Definition</b>
W	Weight of Dead Load
Fr	Reaction Force due to Dead Load

$$\sum F_y = 0 = -W + F_r$$

$$W = F_r$$

*F<sub>r</sub> = Shear Force Imparted into Horizontal Bolts*



Appendix F. **Chain Link Area Determination**

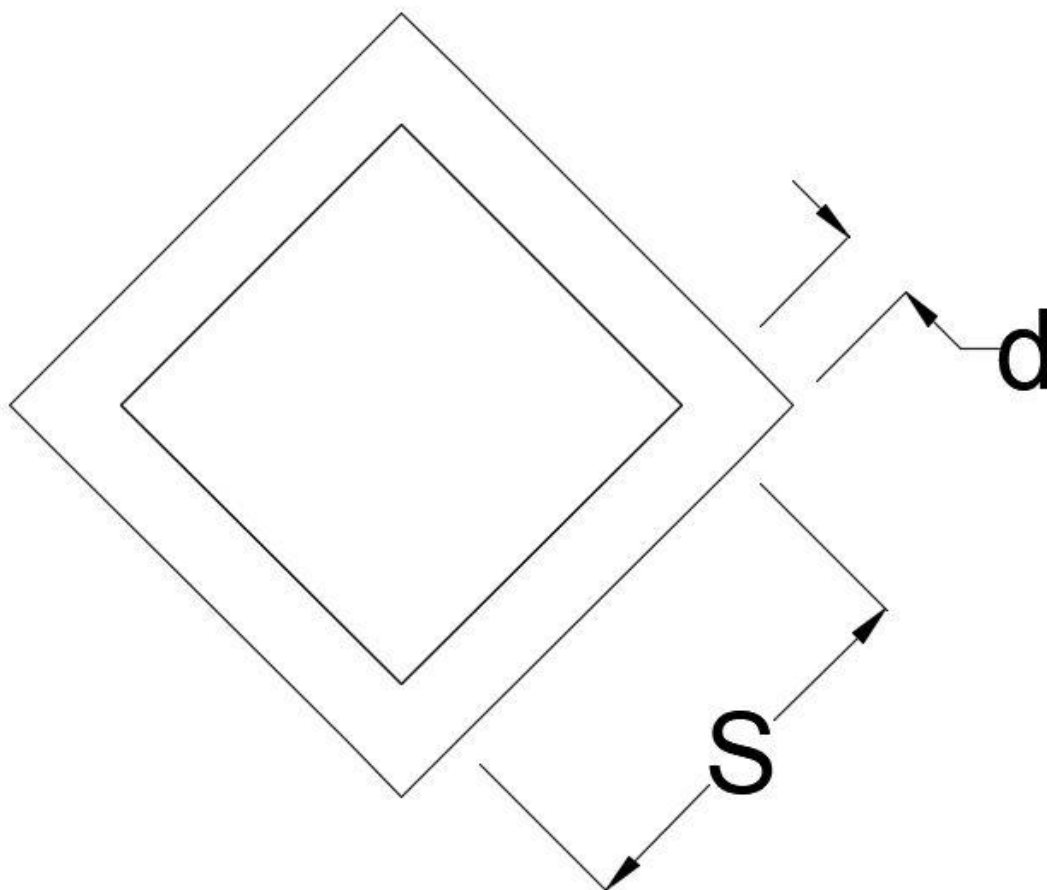


Figure F-1. Chain-Link Representation

Table F-1. Variable Definitions

Variable	Definition
$d$	Diamater of Chain-Link
$S$	Chain-Link Mesh Size
$A_l$	Total Area in One Link
$A_m$	Surface Area in One Link
$P$	Percent of Area Exposed to Wind in One Link
$A_f$	Area of Fence Section
$A_p$	Total Chain Link Area per Fence Section
$H$	Fence Height
$L$	Fence Section Length

$$A_l = (S + d)^2$$

$$A_m = 4d(S + d)$$

$$P = \frac{A_m}{A_l}$$

$$A_f = HL$$

$$A_p = PHL$$

Appendix G. **Material Specifications**

Table G-1. Bill of Materials, Test Nos. P3G-1 Through P3G-16

Item No.	QTY.	Description	Material Spec	Reference
a1	1	HSS 8"x6"x3/16"x84" Long Tube	ASTM A500 Grade B Galv.	H#A76506
a2	1	HSS 8"x8"x3/16"x84" Long Tube	ASTM A500 Grade B Galv.	H#0181456
a3	1	HSS 8"x6"x3/16"x108" Long Tube	ASTM A500 Grade B Galv.	H#A76506
a4	1	HSS 8"x8"x3/16"x108" Long Tube	ASTM A500 Grade B Galv.	H#0181456
a5	1	HSS 8"x6"x3/16"x132" Long Tube	ASTM A500 Grade B Galv.	H#A76506
a6	1	HSS 8"x8"x3/16"x132" Long Tube	ASTM A500 Grade B Galv.	H#0181456
a7	1	HSS 8"x4"x3/16"x110" Long Tube	ASTM A500 Grade B Galv.	H#659620
a8	1	HSS 8"x4"x3/16"x122" Long Tube	ASTM A500 Grade B Galv.	H#659620
a9	1	HSS 8"x4"x3/16"x134" Long Tube	ASTM A500 Grade B Galv.	H#659620
a10	1	HSS 8"x4"x3/16"x72" Long Tube	ASTM A500 Grade B Galv.	H#659620
d1	-	AASHTO A-3 Sand	No. 40 Sieve-51% min. pass No. 200 Sieve-10% max pass Plasticity Index-NP Fine Sand	SMT R#16-436/16-495
d2	-	Standard Strong Soil	AASHTO M147 Grade B	

Table G-2. Bill of Materials, Test Nos. P3G-17 Through P3G-23

Item No.	QTY.	Description	Material Spec	Reference
b1	1	HSS 8"x8"x3/8"x84" Long Tube	ASTM A500 Grade B	R#16-645 H#824011
b2	1	HSS 8"x6"x3/8"x108" Long Tube	ASTM A500 Grade B	R#16-645 H#Y25146
b3	1	HSS 8"x8"x3/8"x108" Long Tube	ASTM A500 Grade B	R#16-645 H#824011
b4	1	HSS 8"x6"x3/8"x132" Long Tube	ASTM A500 Grade B	R#16-645 H#Y25146
b5	1	HSS 8"x8"x3/8"x132" Long Tube	ASTM A500 Grade B	R#16-645 H#824011
b6	1	HSS 8"x4"x3/8"x122" Long Tube	ASTM A500 Grade B	R#16-645 H#W23427

b7	1	HSS 8"x4"x3/8"x134" Long Tube	ASTM A500 Grade B	R#16-645 H#W23427
d1	-	AASHTO A-3 Sand	No. 40 Sieve-51% min. pass No. 200 Sieve- 10% max. pass Plasticity Index-NP Fine Sand	R#16-436/ R#16-495
d2	-	Standard Strong Soil	AASHTO M147 Grade B	Sieve Report provided

NORFOLK IRON & METAL CO.  
03/25/2016  
M.T.R. Cover Sheet

NORFOLK IRON NORFOLK  
3001 N VICTORY RD  
NORFOLK, NE 68702

METALWORKS INC  
301 P STREET BLDG B  
LINCOLN, NE 68508

Sales Order 01113397  
Customer PO: 15906

Certifications For The Material You Ordered Are Listed Below  
Thank You For Your Business

Heat	Item	Item Description	Width	Length
0181456	23441	TUBE 8x 8x 3/16 A500B	.0000	240.0000
A76506	01203	TUBE 8x 6x 3/16 A500B	.0000	240.0000
659620	01185	TUBE 8x 4x 3/16 A500B	.0000	240.0000

NSRI PHASE III STEEL TUBES  
R#16-497 March 2016 SMT

\*\*\* End Of Page \*\*\*

Figure G-1. 8-in. Square x  $\frac{3}{16}$ -in. Steel Tubes, Test Nos. P3G-1 Through P3G-16



**BULL MOOSE  
TUBE**

BULL MOOSE TUBE ELKHART FACILITY  
CERTIFICATION OF TESTS  
EN 10204:2004 TYPE 3.1 CERT

09/08/15  
Page 1 of 1

1819 Clarkson Rd.  
Chesterfield, Missouri 63017

BILL TO Norfolk Iron & Metal Company  
P.O. Box 1129  
Norfolk NE 68701

SHIP TO Norfolk Iron & Metal (KS)  
1701 East South Avenue  
Emporia KS 668019788

B/L Number 359323 Ship Via J244\_J173T

8" X 6" X 0.187 HR X 40'		Order #	503891															
152.4 X 203.2 mm		Purchase Order #	04009961															
ASTM A500-13 GRADE B & C		Item #	101384 3844															
		Customer Item #	01206															
Raw Material is of Domestic Origin - Melted and Manufactured in the USA																		
Heat # = A76506 P NG																		
C	MN	P	S	AL	SI	CB	CU	CR	NI	V	MO	B	TI	N	CE	YLD psi	TSN psi	ELN %
.060	.450	.009	.002	.031	.030	.014	.090	.060	.040	.002	.020	0.000	.001	.006	.165	56830	64380	33
10" X 6" X 0.250 HR X 40'		Order #	503891															
152.4 X 254.0 mm		Purchase Order #	04009961															
ASTM A500-13 GRADE B & C		Item #	101412 3848															
		Customer Item #	01240															
Raw Material is of Domestic Origin - Melted and Manufactured in the USA																		
Heat # = C74870 P NG																		
C	MN	P	S	AL	SI	CB	CU	CR	NI	V	MO	B	TI	N	CE	YLD psi	TSN psi	ELN %
.190	.650	.009	.002	.026	.030	0.000	.080	.060	.040	.001	0.000	0.000	0.000	0.000	.324	62435	75410	32
5" SQ X 0.250 HR X 40'		Order #	503891															
127.0 mm		Purchase Order #	04009961															
ASTM A500-13 GRADE B & C		Item #	100262 3200															
		Customer Item #	01091															
Raw Material is of Domestic Origin - Melted and Manufactured in the USA																		
Heat # = S63002 P NG																		
C	MN	P	S	AL	SI	CB	CU	CR	NI	V	MO	B	TI	N	CE	YLD psi	TSN psi	ELN %
.070	.710	.012	.011	.054	.012	.038	.010	.040	0.000	0.000	.001	0.000	0.000	0.003	.199	67210	75620	31
6" SQ X 0.250 HR X 40'		Order #	503891															
152.4 mm		Purchase Order #	04009961															
ASTM A500-13 GRADE B & C		Item #	100272 3840															
		Customer Item #	01218															
Raw Material is of Domestic Origin - Melted and Manufactured in the USA																		
Heat # = T1904 P NG																		
C	MN	P	S	AL	SI	CB	CU	CR	NI	V	MO	B	TI	N	CE	YLD psi	TSN psi	ELN %
.050	.620	.009	.011	.037	.012	.025	.140	.060	.060	.002	.020	0.000	.001	.006	.185	62300	71330	34

Quality Manager: *Robert Habesl*

THIS WELDED STEEL TUBING IS MANUFACTURED IN THE UNITED STATES OF AMERICA AND HAS BEEN PRODUCED IN ACCORDANCE WITH THE STATED SPECIFICATION. LADLE CHEMISTRIES ARE REPORTED FROM DOCUMENTS PROVIDED BY THE SUPPLYING STEEL MILL. ANY PHYSICAL AND MECHANICAL TESTING RESULTS SHOWN ON THIS CERTIFICATION ARE CORRECT AS CONTAINED IN THE RECORDS OF THE COMPANY.

Figure G-2. 8-in. x 6-in. x 3/16-in. Steel Tube, Test Nos. P3G-1 Through P3G-23





**BULL MOOSE  
TUBE**

1819 Clarkson Rd.  
Chesterfield, Missouri 63017

BULL MOOSE TUBE ELKHART FACILITY  
CERTIFICATION OF TESTS  
EN 10204:2004 TYPE 3.1 CERT

12/18/15  
Page 1 of 2

**BILL TO** Norfolk Iron & Metal Company  
P.O. Box 1129  
Norfolk NE 68701

**SHIP TO** Norfolk Iron & Metal Company (NE)  
3001 Victory Rd.  
Norfolk NE 68701-0000

B/L Number 368106 Ship Via M5015\_RN217T

8" X 6" X 0.187 HR X 48'  
152.4 X 203.2 mm  
ASTM A500-13 GRADE B & C

Ladle Analysis and Physicals  
Structural-Dual Certified

Order # 512722  
Purchase Order # 01019048  
Item # 101385 3844

Customer Item #

Raw Material is of Domestic Origin - Melted and Manufactured in the USA

Heat # = A76506

P NG

C	MN	P	S	AL	SI	CB	CU	CR	NI	V	MO	B	TI	N	CE	YLD psi	TSN psi	ELN %
.060	.450	.009	.002	.031	.030	.014	.090	.060	.040	.002	.020	0.000	.001	.006	.165	56830	64380	33

3" X 2" X 0.250 HR X 20'  
50.8 X 76.2 mm  
ASTM A500-13 GRADE B & C

Ladle Analysis and Physicals  
Structural-Dual Certified

Order # 512704  
Purchase Order # 01019048  
Item # 102011 1284

Customer Item # 00969

Raw Material is of Domestic Origin - Melted and Manufactured in the USA

Heat # = T03337

P NG

C	MN	P	S	AL	SI	CB	CU	CR	NI	V	MO	B	TI	N	CE	YLD psi	TSN psi	ELN %
.090	.650	.013	.008	.039	.013	.001	.010	.040	.010	.097	.007	0.000	.001	.006	.231	54270	71330	32

12" SQ X 0.250 HR X 48'  
304.8 mm  
ASTM A500-13 GRADE B & C

Ladle Analysis and Physicals  
Structural-Dual Certified

Order # 512731  
Purchase Order # 01019048  
Item # 108321 7680

Customer Item #

Raw Material is of Domestic Origin - Melted and Manufactured in the USA

Heat # = T3019

P NG

C	MN	P	S	AL	SI	CB	CU	CR	NI	V	MO	B	TI	N	CE	YLD psi	TSN psi	ELN %
.060	.640	.011	.002	.029	.023	.027	.140	.070	.070	.003	.020	0.000	.001	.007	.203	66540	73860	32

12" SQ X 0.250 HR X 48'  
304.8 mm  
ASTM A500-13 GRADE B & C

Ladle Analysis and Physicals  
Structural-Dual Certified

Order # 512731  
Purchase Order # 01019048  
Item # 108321 7680

Customer Item #

Raw Material is of Domestic Origin - Melted and Manufactured in the USA

Heat # = T3159

P NG

C	MN	P	S	AL	SI	CB	CU	CR	NI	V	MO	B	TI	N	CE	YLD psi	TSN psi	ELN %
.060	.630	.010	.010	.034	.024	.022	.140	.070	.120	.002	.020	0.000	.001	.007	.205	63110	71760	33

Quality Manager: *Slydant*

THIS WELDED STEEL TUBING IS MANUFACTURED IN THE UNITED STATES OF AMERICA AND HAS BEEN PRODUCED IN ACCORDANCE WITH THE STATED SPECIFICATION. LADLE CHEMISTRIES ARE REPORTED FROM DOCUMENTS PROVIDED BY THE SUPPLYING STEEL MILL. ANY PHYSICAL AND MECHANICAL TESTING RESULTS SHOWN ON THIS CERTIFICATION ARE CORRECT AS CONTAINED IN THE RECORDS OF THE COMPANY.

Figure G-3. 8-in. x 6-in. x 3/16-in. Tubes, Test Nos. P3G-1 through P3G-23



**MATERIAL TEST REPORT**  
**ORIGINAL**

M/C No. MC0000036894  
Date 03/09/2016

BL No. SH0000042509  
Destination NORFOLK IRON&METAL - NORFOLK NE  
Supplier NORFOLK IRON&METAL - BILL TO

**MARUICHI LEAVITT PIPE & TUBE, LLC**  
1717 W. 115th St.  
Chicago, IL 60643  
TEL: (773) 239-7700 FAX: (773) 239-1023

Customer PO No. / Customer Item No.	SPEC	SIZE	No of PCS	Heat No	Chemical Composition(Ladle Analysis)													Tensile Test			Hydrostatic Test		Bending Test	Remarks
					C (%)	Si (%)	Mn (%)	P (%)	S (%)	Cr (%)	Ni (%)	Co (%)	Mo (%)	V (%)	Yield Strength (PSI)	Tensile Strength (PSI)	Elongation (%)	Pressure (PSI)	Failure Result					
1	ASTM A500/A500M-13 GRADE B ERW TUBING	5IN x 5IN x 0.375IN x 48FT HRB	6,442	821S04140	18	1	76	12	5	16	10	20	4	1	67,730	76,314	30				SA0000098862 A500 Grade B/C			
2	ASTM A500/A500M-13 GRADE B ERW TUBING	5IN x 5IN x 0.375IN x 48FT HRB	6,442	822S35110	20	1	82	11	7	20	10	30	4	2	59,134	76,720	31				SA0000098862 A500 Grade B/C			
3	ASTM A500/A500M-13 GRADE B ERW TUBING	6IN x 6IN x 0.313IN x 40FT HRB	5,602	0179212	18	1	80	8	10	70	20	40	10	0	55,621	69,405	33				SA0000098862 A500 Grade B/C			
4	ASTM A500/A500M-13 GRADE B ERW TUBING	8IN x 4IN x 0.188IN x 20FT HRB	13,952	659620	16	2	80	7	6	20	20	20	20	8	56,480	65,449	31				SA0000098862 A500 Grade B/C			
5	ASTM A500/A500M-13 GRADE B ERW TUBING	8IN x 4IN x 0.250IN x 20FT HRB	6,848	A46782	20	3	75	12	2	10	10	30	4	1	64,517	80,974	29				SA0000098862 A500 Grade B/C			
6	ASTM A500/A500M-13 GRADE B ERW TUBING	8IN x 4IN x 0.250IN x 24FT HRB	8,216	B38101	20	3	78	10	2	20	10	30	4	1	61,666	72,396	26				SA0000098862 A500 Grade B/C			

**Made and Melted in The U.S.A.**  
This material has not come in direct contact with mercury during the manufacturing or testing processes. No Weld Repair.  
Remarks:

We hereby certify that the material described herein conforms fully to the said specification.

Maruichi Leavitt Pipe & Tube, LLC  
F-824-101 - Rev. 0

Figure G-4. 8-in. x 4-in. x 3/16-in. Steel Tubes, Test Nos. P3G-1 through P3G-16



**MATERIAL TEST REPORT**  
**ORIGINAL**

M/C No. MC000003107Z  
Date 05/21/2015

BL No. SH0000035763  
Destination NORFOLK IRON&METAL - EMPORIAKS  
Supplier NORFOLK IRON&METAL - BILLTO

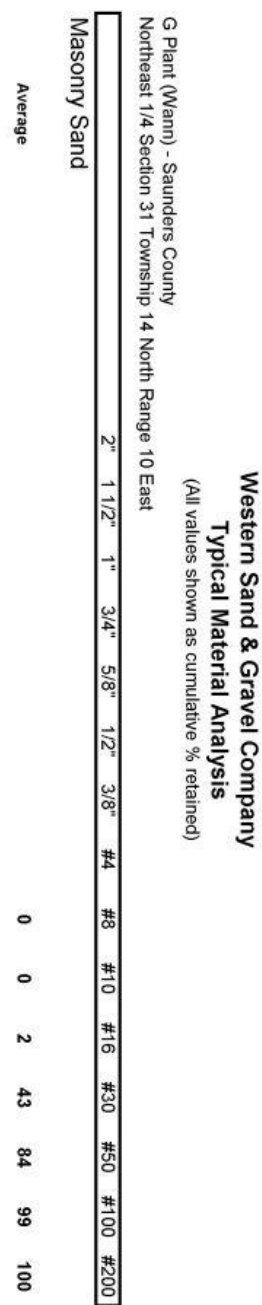
**MARUICHI LEAVITT PIPE & TUBE, LLC**  
1717 W. 115th St.  
Chicago, IL 60643  
TEL: (773) 239-7700 FAX: (773) 239-1023

Customer PO No. / Customer Item No	SPEC	No of PCS	Heat No	Chemical Composition(Ladle Analysis)											Tensile Test			Hydrostatic Test		Bending Test	Remarks
				C (%)	Si (%)	Mn (%)	P (%)	S (%)	Cu (%)	Ni (%)	Cr (%)	Mo (%)	V (%)	Yield Strength (PSI)	Tensile Strength (PSI)	Elongation (%)	Pressure (PSI)	Flattening Test			
7 ASTM A500/A500M-13 GRADE B ERW TUBING 8IN x 8IN x 0.189IN x 40FT HRB 04009389 / 20954		6	0181456	17	3	66	9	7	50	10	40	10	0	63,158	75,612	27			SA0000085433 A500 Grade B/C		
8 ASTM A500/A500M-13 GRADE B ERW TUBING 8IN x 4IN x 0.375IN x 40FT HRB 04009389 / 01201		6	0112162	19	1	79	12	6	40	10	30	10	0	57,865	67,381	31			SA0000085433 A500 Grade B/C		
9 ASTM A500/A500M-13 GRADE B ERW TUBING 6IN x 6IN x 0.500IN x 20FT HRB 04009389 / 04866		4	0112161	19	1	83	10	6	30	10	30	10	0	54,649	63,149	34			SA0000085433 A500 Grade B/C		
10 ASTM A500/A500M-13 GRADE B ERW TUBING 6IN x 6IN x 0.375IN x 40FT HRB 04009389 / 04865		6	0112163	18	1	81	10	7	30	20	30	10	0	57,248	67,519	35			SA0000085433 A500 Grade B/C		

**Made and Melted in The U.S.A**  
This material has not come in direct contact with mercury during the manufacturing or testing processes. No Weld Repair.  
Remarks:

We hereby certify that the material described herein conforms fully to the said specification.  
  
Maruichi Leavitt Pipe & Tube, LLC  
F-824-101 - Rev. 0

Figure G-5. 8-in. Square x 3/16-in. Tubes, Test Nos. P3G-1 through P3G-16



NSRI TRAFFIC CALMING AND PHASE III  
 A3 SAND GRADATION REPORT  
 MARCH 2016 SMT R#16-436/16-495

Figure G-6. Sand, Test Nos. P3G-1 through P3G-23



**REIMERS KAUFMAN CONCRETE PRODUCTS CO.**  
 6200 Cornhusker Highway, Lincoln, NE 68529  
 402-434-1855 Fax: 402-434-1877  
 www.ReimersKaufman.com

**Delivery Ticket**

**Bill To:**  
 91121 UNL LANDSCAPING DEPARTMENT  
 ATTN ACCOUNTING DEPT  
 1340 N 17TH ST  
 LINCOLN NE 68508-126

**Ship To:**  
 2005 WINDMILL ROADSIDE SAFETY FAC  
 4630 N/W 36TH ST

**Ship From:**  
 REIMERS KAUFMAN CONCRETE PROD  
 6200 CORNHUSKER HWY  
 LINCOLN NE 68507

**Driver:** KEN H.  
**Truck#:**  
**Ordered By:**

Order Number: SP 1675783 522310 Delivery Date: 03/21/16 Customer PO Number:

**Delivery Directions:**  
 PULL  
 DO NOT MAIL TO CUSTOMER, SEND TO SITE

**Waiver:** Received material below in accordance with order. Purchaser or agent waives all claims for personal or property damage caused by seller's truck when delivery is made beyond the street curb line.

Line	Item Description	PCS	Picked	Quantity	Back Order	Units	Unit Price	Discount	Extension
1	FINE MASONRY SAND BULK WARNING: Handling and use of this product for any purpose without wearing an approved and properly maintained Abrasive Blasting Hood or similar respiratory device may result in serious injury and/or death. Do not use any of this product for dry sand blasting without first confirming that proper precautionary devices are available and being used, including but not limited to an approved blasting hood and respiratory device and precautions to prevent dust from coming into contact with eyes and skin. Blasting may break down natural silica in this product and create freshly fractured respirable crystalline silica, which is extremely hazardous and which may cause silicosis. A blasting program may also generate fatal lung disease. DUMP TRUCK DELIVERY CHARGE DUMP TRUCK	FMS		28,500.00		LB	.00575		163.88
2						EA	65.00		65.00

Received by \_\_\_\_\_

Print Name/Company \_\_\_\_\_

Tax Code: RKNTE Nebraska Tax Exempt  
 Shipment Weight: 28,500.00  
 Shipment Cubic:

Sub Total	228.88
Sales Tax	228.88
Total Amount	457.76
Down Payment	228.88
Balance Due	228.88

**Returns:** No returns w/o invoice. No returns on unusable material, seconds, architectural, decorative, all special order materials, and fractional units. All returnable materials subject to 50% restocking charge. No returns accepted after 30 days from date of purchase.  
**Terms:** All invoices must be paid within 30 days of invoice. Past due accounts will be charged an interest rate of 1.5% per month which is 18% per year.

Document: \_\_\_\_\_ Print Date: 03/21/16 Print Time: 11:47 Page: 1 of 1

Figure G-7. Sand, Test Nos. P3G-1 through P3G-23

Atlas ABC Corp (Atlas Tube Chicago)  
 1855 East 122nd Street  
 Chicago, Illinois, USA  
 60633  
 Tel: 773-646-4500  
 Fax: 773-646-6128



Ref.B/L: 80705090  
 Date: 02.24.2016  
 Customer: 179

**MATERIAL TEST REPORT**

**Sold to**

Steel & Pipe Supply Compan  
 PO Box 1688  
 MANHATTAN KS 66505  
 USA

**Shipped to**

Steel & Pipe Supply Compan  
 401 New Century Parkway  
 NEW CENTURY KS 66031  
 USA

Material: 8.0x4.0x375x20'0"0(2x5). Material No: 800403752000 Made in: USA  
 Melted in: USA  
 Sales order: 1070149 Purchase Order: 4500259967 Cust Material #: 6680040037520  

Heat No	C	Mn	P	S	Si	Al	Cu	Cb	Mo	Ni	Cr	V	Ti	B	N
W23427	0.180	0.800	0.008	0.007	0.015	0.053	0.010	0.005	0.003	0.010	0.030	0.001	0.001	0.000	0.005

Bundle No	PCs	Yield	Tensile	Eln.2in	Certification	CE: 0.32
M800615987	10	065817 Psi	078912 Psi	33 %	ASTM A500-13 GRADE B&C	

Material Note:  
 Sales Or.Note:

Material: 8.0x4.0x375x20'0"0(2x5). Material No: 800403752000 Made in: USA  
 Melted in: USA  
 Sales order: 1070149 Purchase Order: 4500259967 Cust Material #: 6680040037520  

Heat No	C	Mn	P	S	Si	Al	Cu	Cb	Mo	Ni	Cr	V	Ti	B	N
W23427	0.180	0.800	0.008	0.007	0.015	0.053	0.010	0.005	0.003	0.010	0.030	0.001	0.001	0.000	0.005

Bundle No	PCs	Yield	Tensile	Eln.2in	Certification	CE: 0.32
M800615988	10	065817 Psi	078912 Psi	33 %	ASTM A500-13 GRADE B&C	

Material Note:  
 Sales Or.Note:

Material: 10.0x2.0x250x40'0"0(2x4). Material No: 1000202504000 Made in: USA  
 Melted in: USA  
 Sales order: 1069603 Purchase Order: 4500259905 Cust Material #: 66100020025040  

Heat No	C	Mn	P	S	Si	Al	Cu	Cb	Mo	Ni	Cr	V	Ti	B	N
266012	0.200	0.650	0.008	0.005	0.020	0.030	0.099	0.001	0.020	0.040	0.050	0.003	0.002	0.000	0.007

Bundle No	PCs	Yield	Tensile	Eln.2in	Certification	CE: 0.34
M800615918	8	051769 Psi	067325 Psi	34 %	ASTM A500-13 GRADE B&C	

Material Note:  
 Sales Or.Note:

*Jason Richard*  
 Authorized by Quality Assurance:  
 The results reported on this report represent the actual attributes of the material furnished and indicate full compliance with all applicable specification and contract requirements.  
 Computed per the AWS D1.1 method.



Figure G-8. 8-in. x 4-in. x 3/8-in. Tube, Test Nos P3G-17 through P3G-23

Atlas ABC Co. p (Atlas Tube Chicago)  
 1855 East 172nd Street  
 Chicago, Illinois, USA  
 60633  
 Tel: 773 646 4500  
 Fax: 773 646 6128



Ref.B/L: 80706896  
 Date: 03.09.2016  
 Customer: 179

**MATERIAL TEST REPORT**

**Sold to**

Steel & Pipe Supply Compan  
 PO Box 1888  
 MANHATTAN KS 66505  
 USA

**Shipped to**

Steel & Pipe Supply Compan  
 1020 West Fort Gibson  
 CATOOSA OK 74015  
 USA

Material: 8.0x6.0x375x40"0"0(2x3) Material No: 800603754000 Made in: USA  
 Melted in: USA  
 Sales order: 1075626 Purchase Order: C450005637 Cust Material #: 6680060037540

Heat No	C	Mn	P	S	Si	Al	Cu	Cb	Mo	Ni	Cr	V	Ti	B	N
Y25146	0.180	0.790	0.006	0.005	0.013	0.058	0.020	0.004	0.005	0.010	0.030	0.001	0.001	0.000	0.006
Bundle No	PCs	Yield	Tensile	Eln.2in	Certification					CE: 0.32					
M800608387	6	064868 Psi	076207 Psi	33 %	ASTM A500-13 GRADE B&C										

Material Note:  
 Sales Or.Note:

Material: 8.0x6.0x500x20"0"0(2x3) Material No: 800605002000 Made in: USA  
 Melted in: USA  
 Sales order: 1075627 Purchase Order: C450005637 Cust Material #: 6680060050020

Heat No	C	Mn	P	S	Si	Al	Cu	Cb	Mo	Ni	Cr	V	Ti	B	N
A46596	0.190	0.770	0.008	0.001	0.030	0.038	0.010	0.001	0.004	0.010	0.020	0.000	0.002	0.000	0.006
Bundle No	PCs	Yield	Tensile	Eln.2in	Certification					CE: 0.33					
M800616895	6	059021 Psi	068700 Psi	32 %	ASTM A500-13 GRADE B&C										

Material Note:  
 Sales Or.Note:

Material: 12.0x4.0x375x40"0"0(2x3) Material No: 1200403754000 Made in: USA  
 Melted in: USA  
 Sales order: 1075624 Purchase Order: C450005637 Cust Material #: 66120040037540

Heat No	C	Mn	P	S	Si	Al	Cu	Cb	Mo	Ni	Cr	V	Ti	B	N
T05056	0.190	0.760	0.008	0.006	0.016	0.051	0.020	0.005	0.006	0.010	0.030	0.001	0.001	0.000	0.005
Bundle No	PCs	Yield	Tensile	Eln.2in	Certification					CE: 0.33					
M900825038	6	062688 Psi	077941 Psi	33 %	ASTM A500-13 GRADE B&C										

Material Note:  
 Sales Or.Note:

*James Richard*  
 Authorized by Quality Assurance:  
 The results reported on this report represent the actual attributes of the material furnished and indicate full compliance with all applicable specification and contract requirements.  
 Computed using the AWS D.1.1 method.



Figure G-9. 8-in. x 6-in. x 3/8-in. Tube, Test Nos. P3G-17 through P3G-23

Atlas Tube Canada ULC  
 200 Clark St.  
 Harrow, Ontario, Canada  
 NOR 1G0  
 Tel: 519-738-3541  
 Fax: 519-738-3537



Ref.B/L: 80700594  
 Date: 01.27.2016  
 Customer: 179

**MATERIAL TEST REPORT**

**Sold to**

Steel & Pipe Supply Compan  
 PO Box 1688  
 MANHATTAN KS 66505  
 USA

**Shipped to**

Steel & Pipe Supply Compan  
 401 New Century Parkway  
 NEW CENTURY KS 66031  
 USA

Material: 8.0x8.0x375x40'0"0(3x2). Material No: 800803754000 Made in: Canada  
 Melted in: Canada  
 Sales order: 1064256 Purchase Order: C455002220 Cust Material #: 6580037540

Heat No	C	Mn	P	S	Si	Al	Cu	Cb	Mo	Ni	Cr	V	Ti	B	N
824011	0.200	0.800	0.011	0.007	0.012	0.040	0.038	0.005	0.002	0.011	0.035	0.002	0.002	0.000	0.004
Bundle No	PCs	Yield	Tensile	Eln.2in	Certification				CE: 0.35						
M201099577	6	063136 Psi	074151 Psi	35.1 %	ASTM A500-13 GRADE B&C										

Material Note:  
 Sales Or.Note:

Material: 12.0x12.0x500x40'0"0(2x1). Material No: 1201205004000 Made in: Canada  
 Melted in: Canada  
 Sales order: 1064256 Purchase Order: C455002220 Cust Material #: 65120050040

Heat No	C	Mn	P	S	Si	Al	Cu	Cb	Mo	Ni	Cr	V	Ti	B	N
824111	0.200	0.800	0.013	0.010	0.019	0.038	0.036	0.006	0.003	0.014	0.036	0.002	0.002	0.000	0.004
Bundle No	PCs	Yield	Tensile	Eln.2in	Certification				CE: 0.35						
M201100604	2	057867 Psi	067582 Psi	40.3 %	ASTM A500-13 GRADE B&C										

Material Note:  
 Sales Or.Note:

Material: 2.0x2.0x250x20'0"0(10x5).-D Material No: 0200202502000-D Made in: USA  
 Melted in: Canada  
 Sales order: 1063861 Purchase Order: C455002217 Cust Material #: 6520025020

Heat No	C	Mn	P	S	Si	Al	Cu	Cb	Mo	Ni	Cr	V	Ti	B	N
823638	0.170	0.800	0.013	0.009	0.015	0.059	0.057	0.002	0.003	0.015	0.038	0.002	0.002	0.000	0.000
Bundle No	PCs	Yield	Tensile	Eln.2in	Certification				CE: 0.32						
M300889373	50	073391 Psi	086298 Psi	24.7 %	ASTM A500-13 GRADE B&C										

Material Note:  
 Sales Or.Note:

*Jason Richard*  
 Jason Richard

Authorized by Quality Assurance:  
 The results reported on this report represent the actual attributes of the material furnished and indicate full compliance with all applicable specification and contract requirements.  
 CE calculated using the AWS D1.1 method.



Figure G-10. 8-in. x 8-in. x 3/8-in. Tube, Test Nos. P3G-17 through P3G-23



## Appendix H. **Bogie Test Results**

The results of the recorded data from each accelerometer for every dynamic bogie test are provided in the summary sheets found in this appendix. Summary sheets include acceleration, velocity, and deflection vs. time plots as well as force vs. deflection and energy vs. deflection plots.

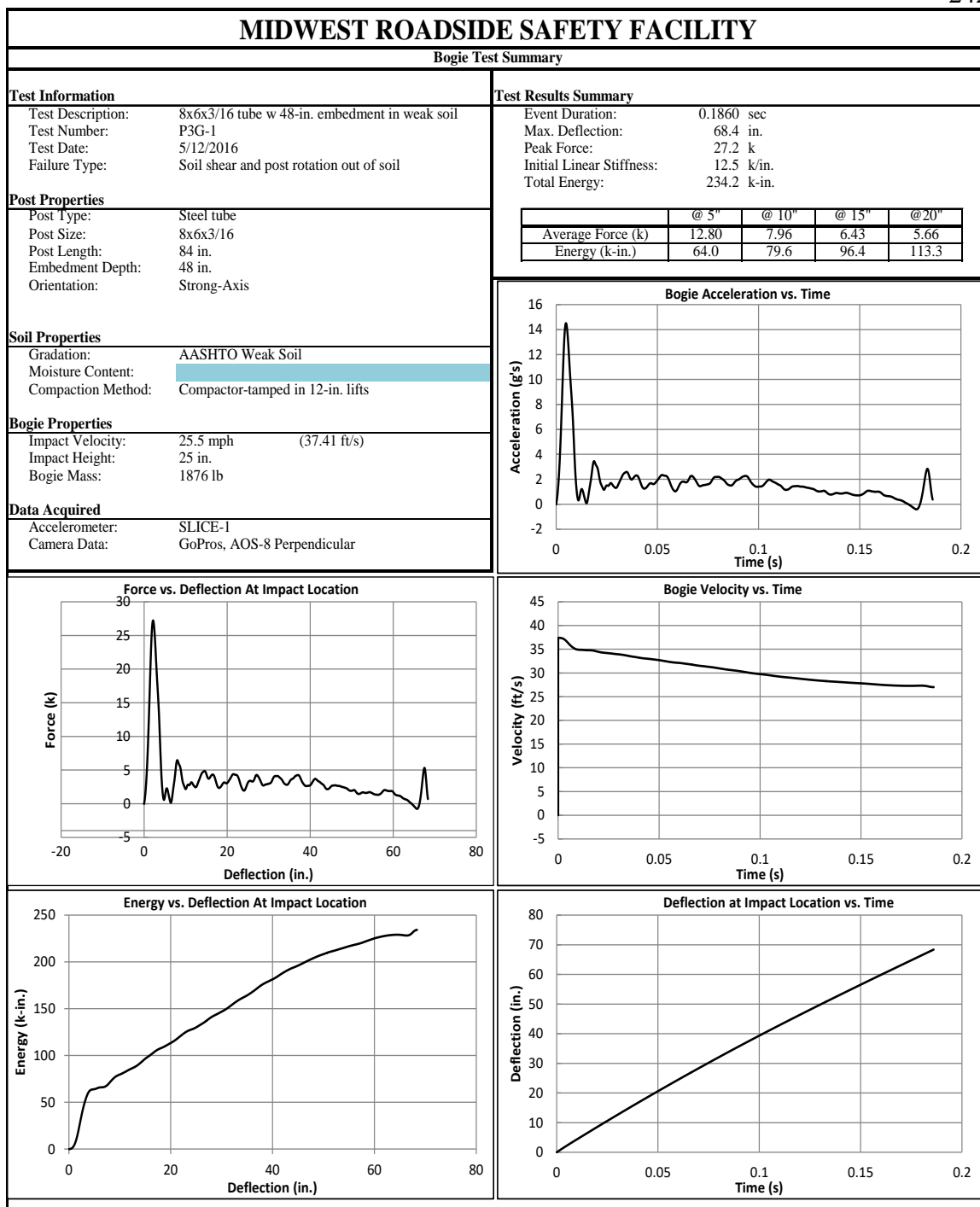


Figure H-1. Test No. P3G-1 Results (SLICE-1)

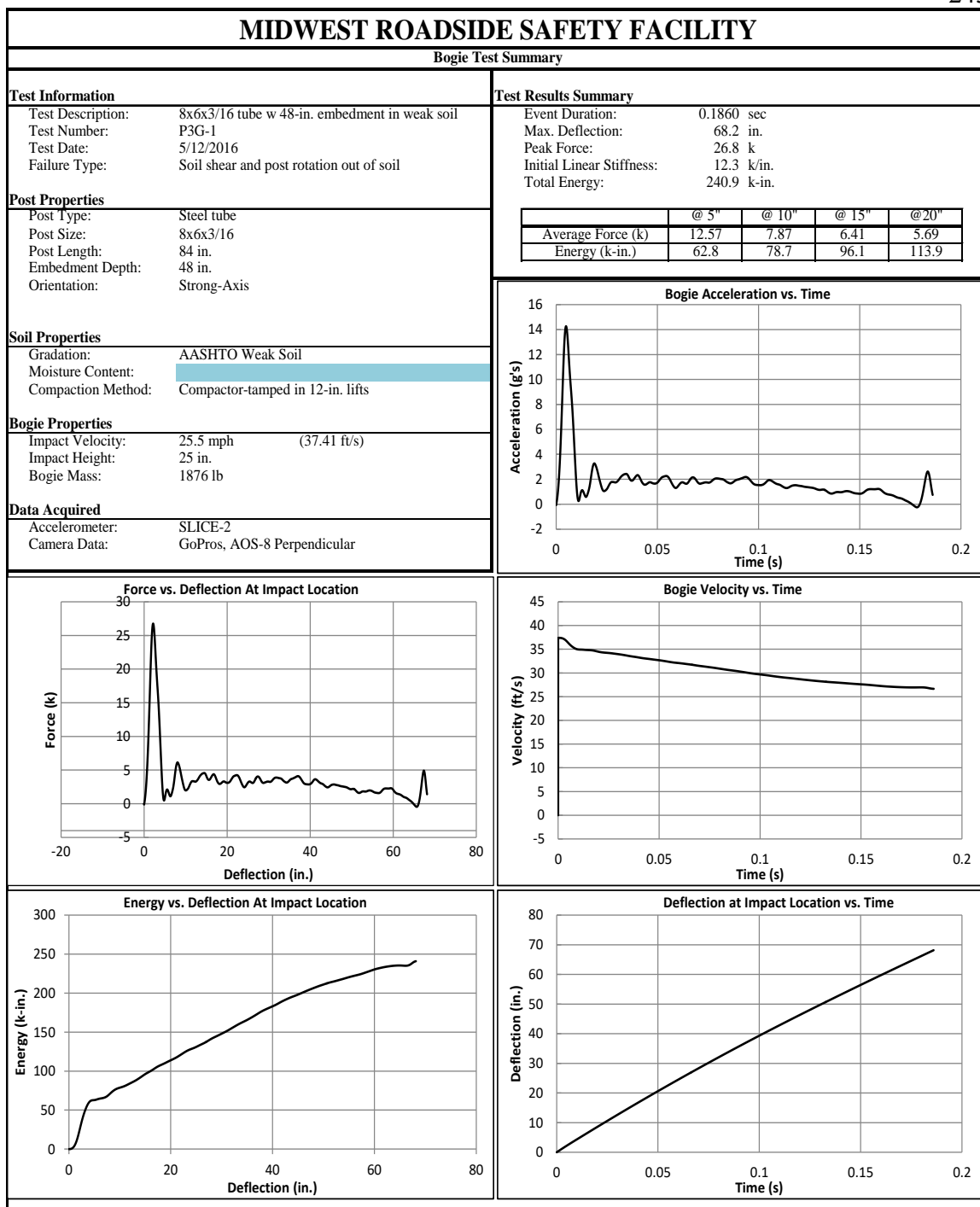


Figure H-2. Test No. P3G-1 Results (SLICE-2)

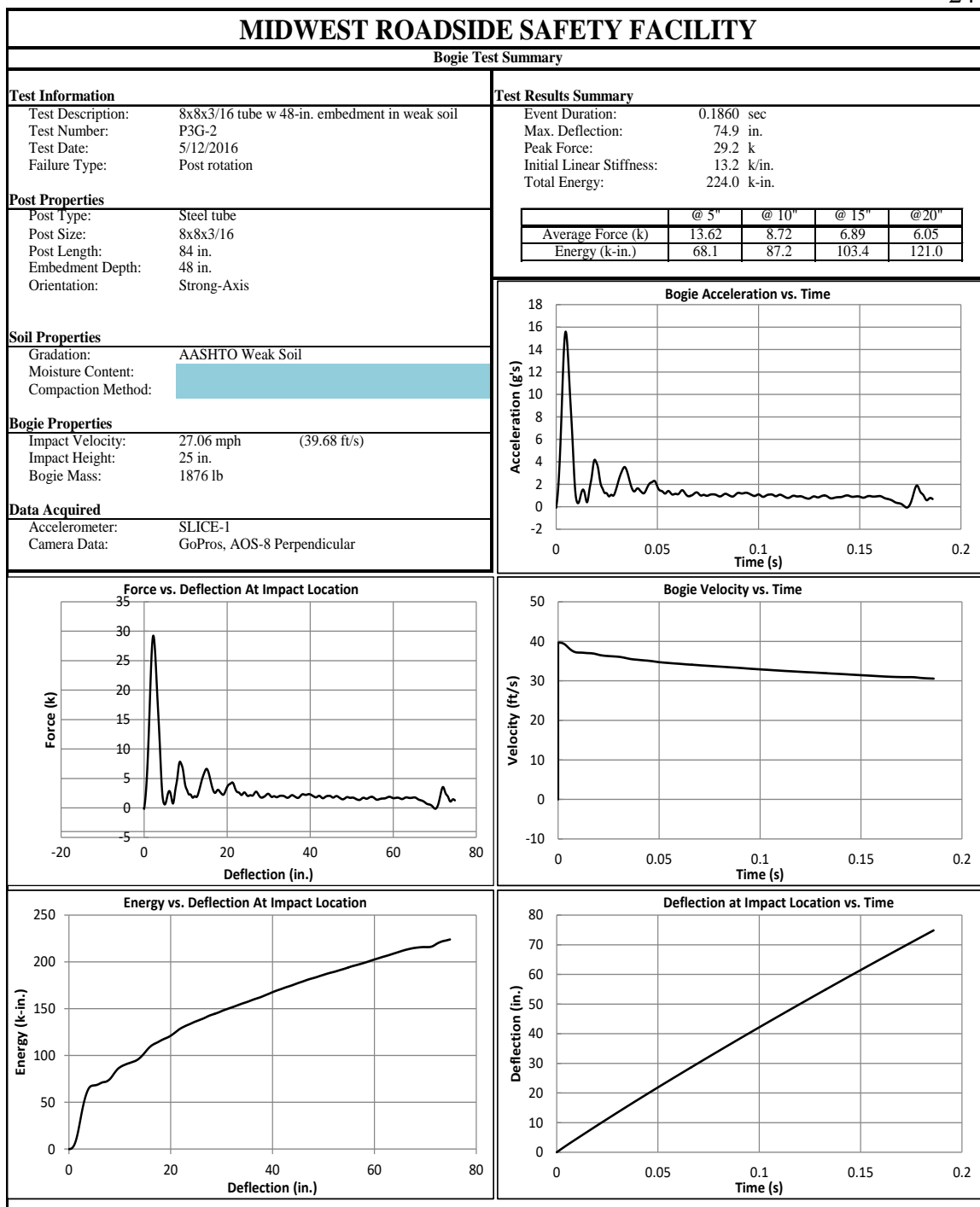


Figure H-3. Test No. P3G-2 Results (SLICE-1)

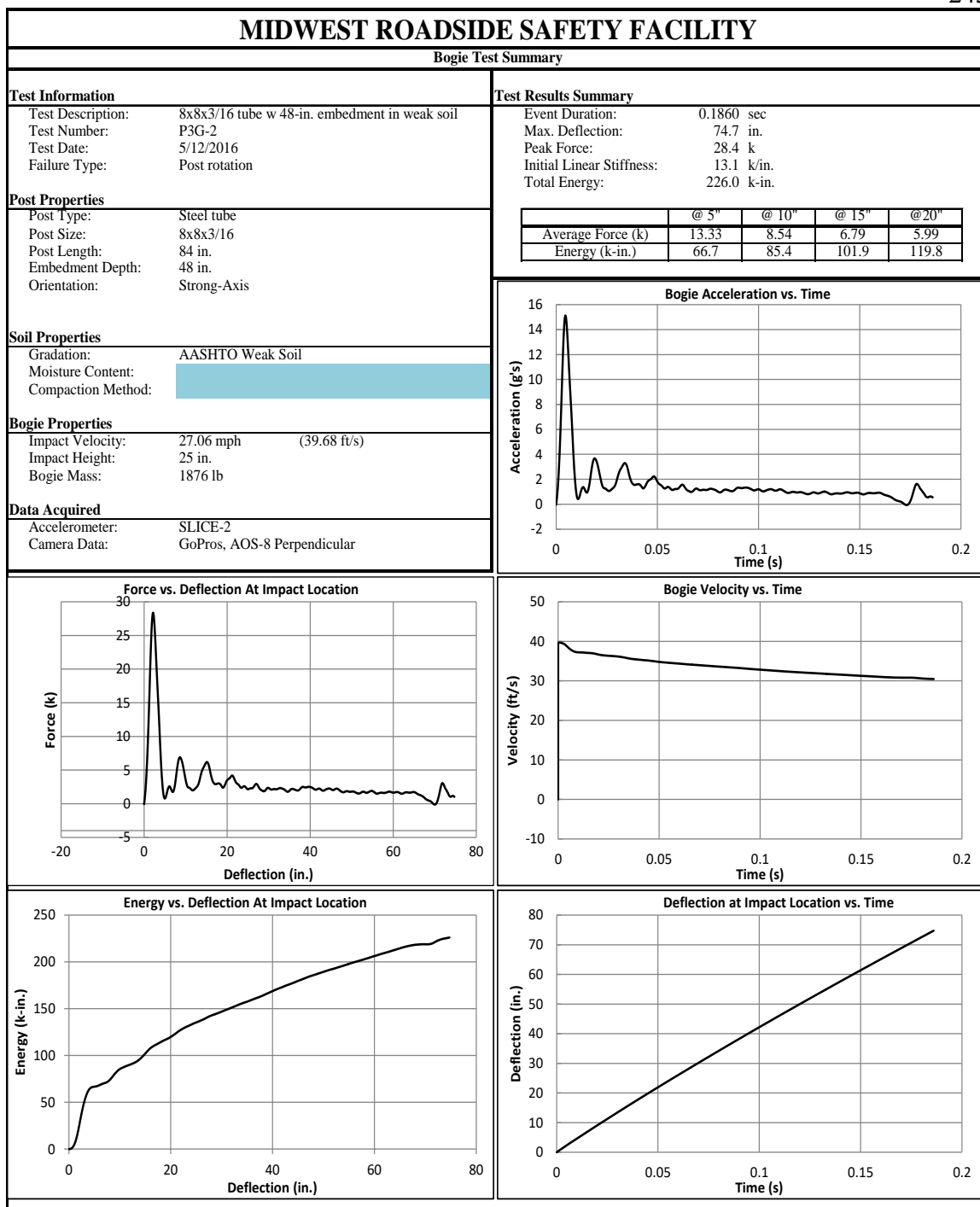


Figure H-4. Test No. P3G-2 Results (SLICE-2)

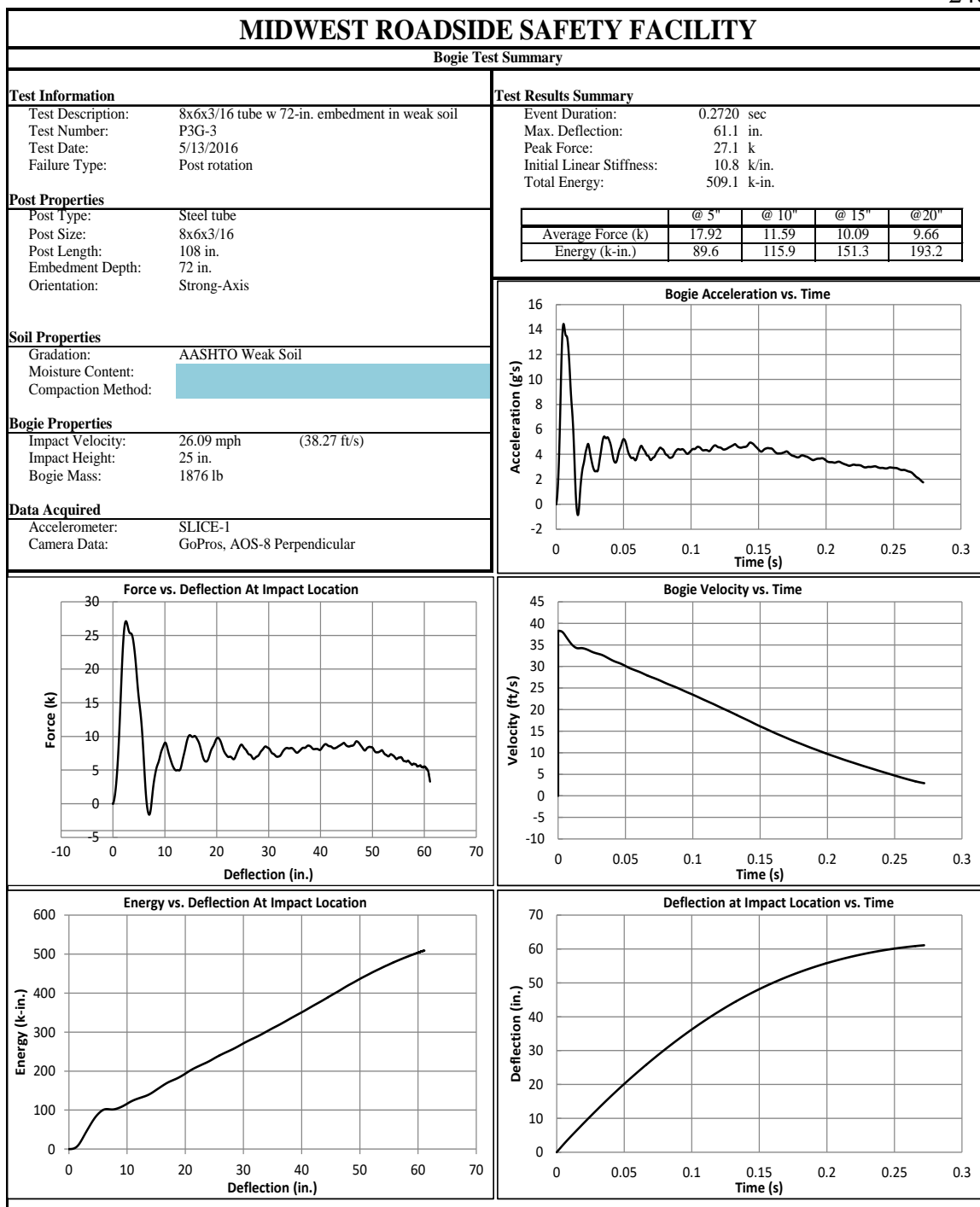


Figure H-5. Test No. P3G-3 Results (SLICE-1)

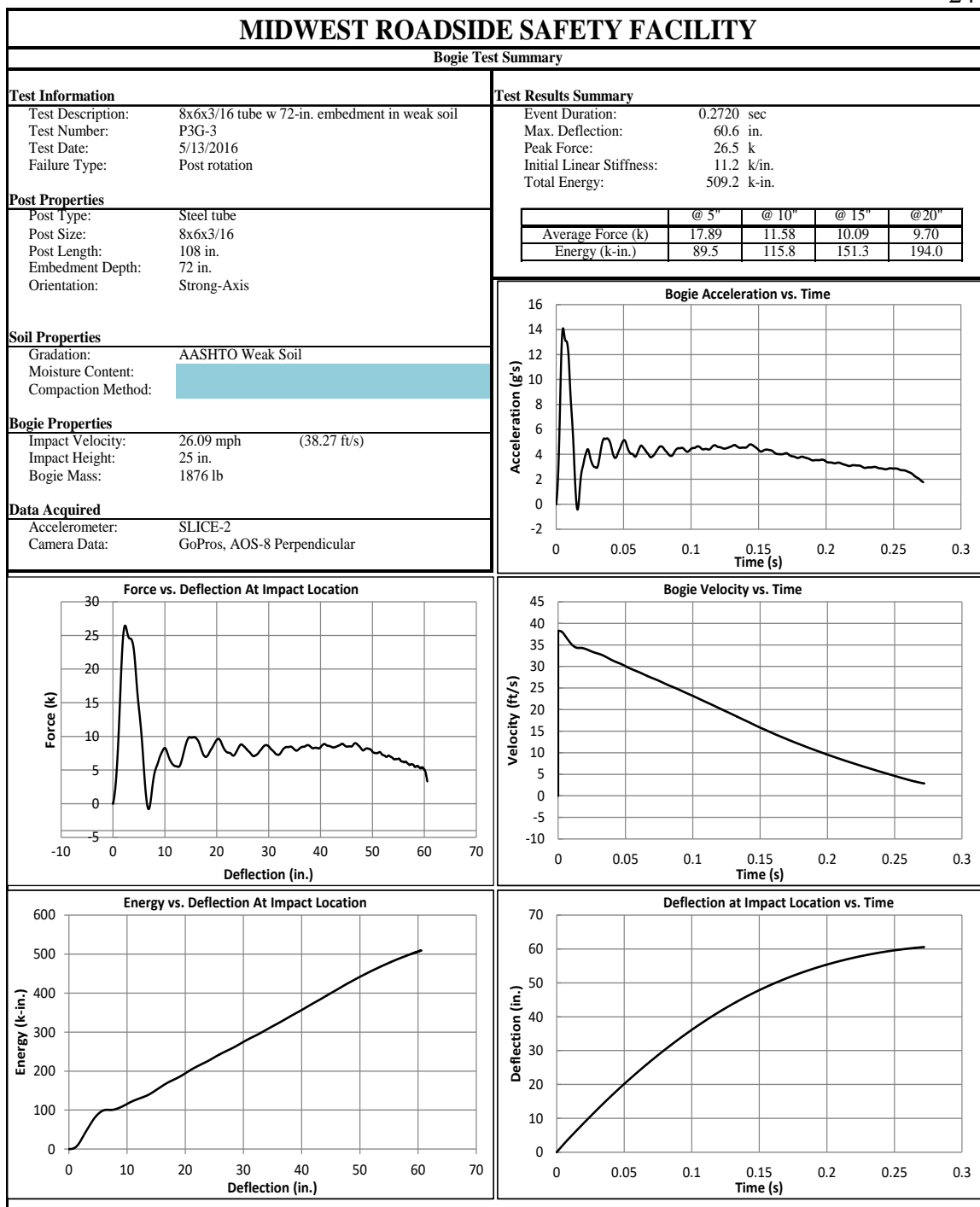


Figure H-6. Test No. P3G-3 Results (SLICE-2)

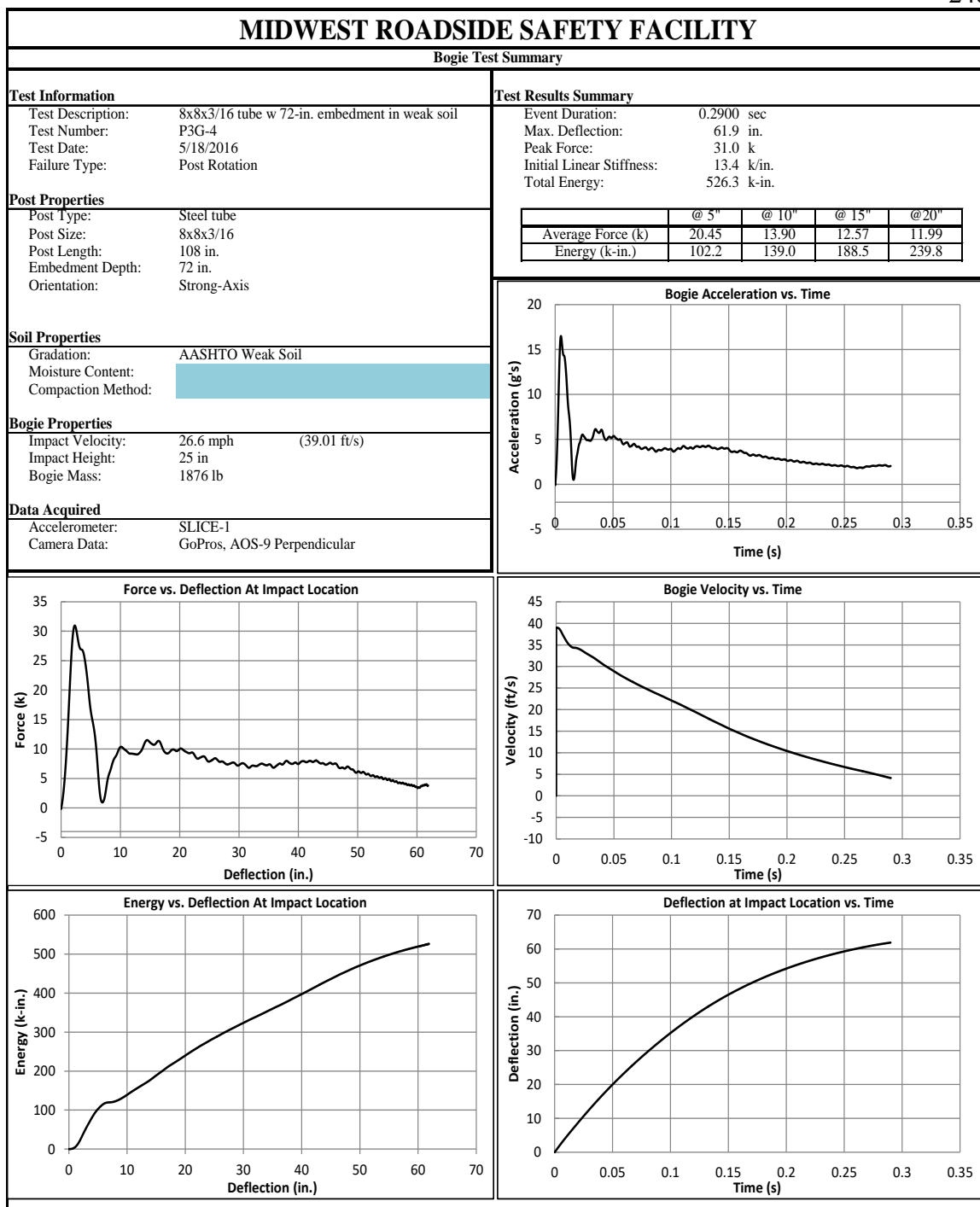


Figure H-7. Test No. P3G-4 Results (SLICE-1)



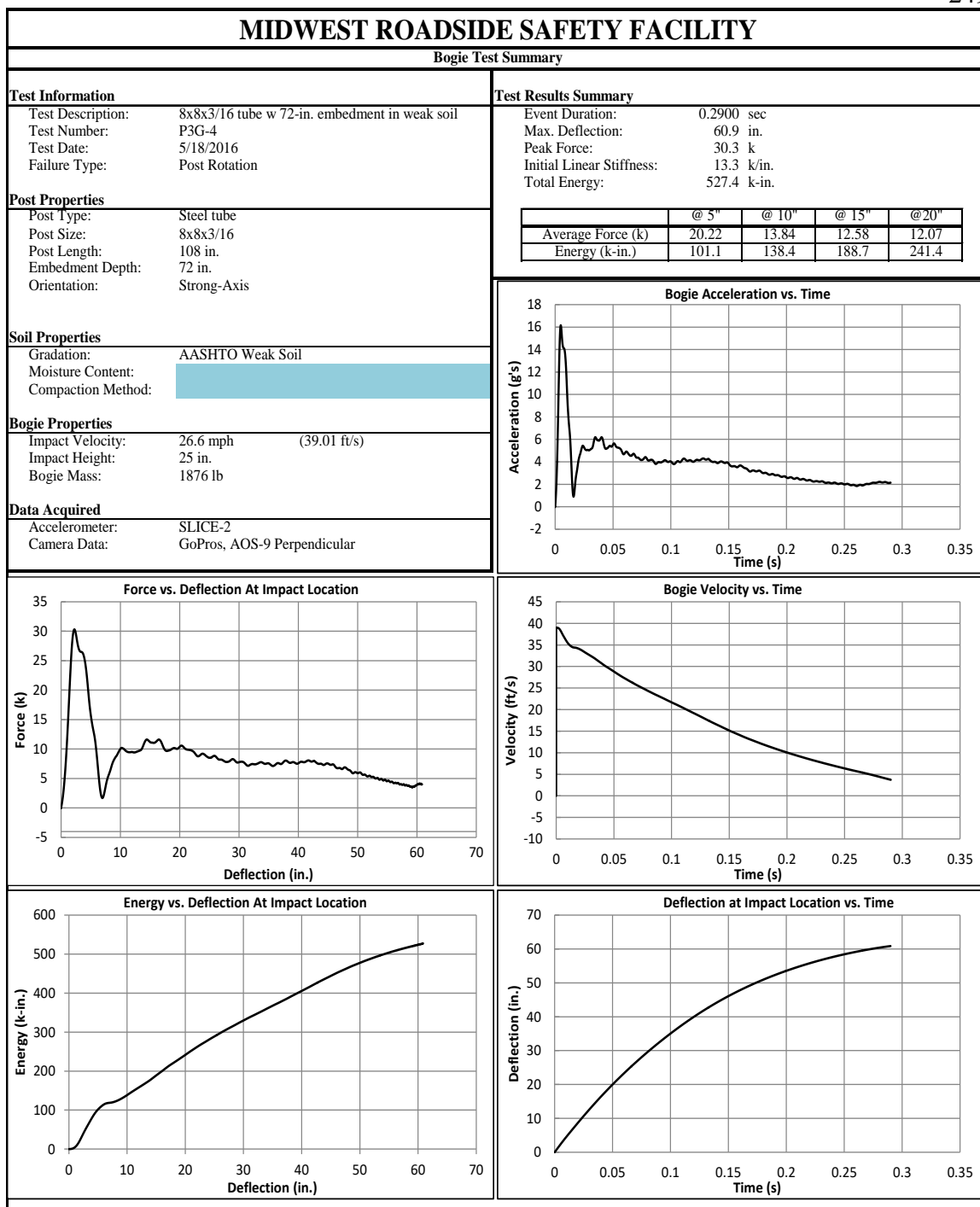


Figure H-8. Test No. P3G-4 Results (SLICE-2)

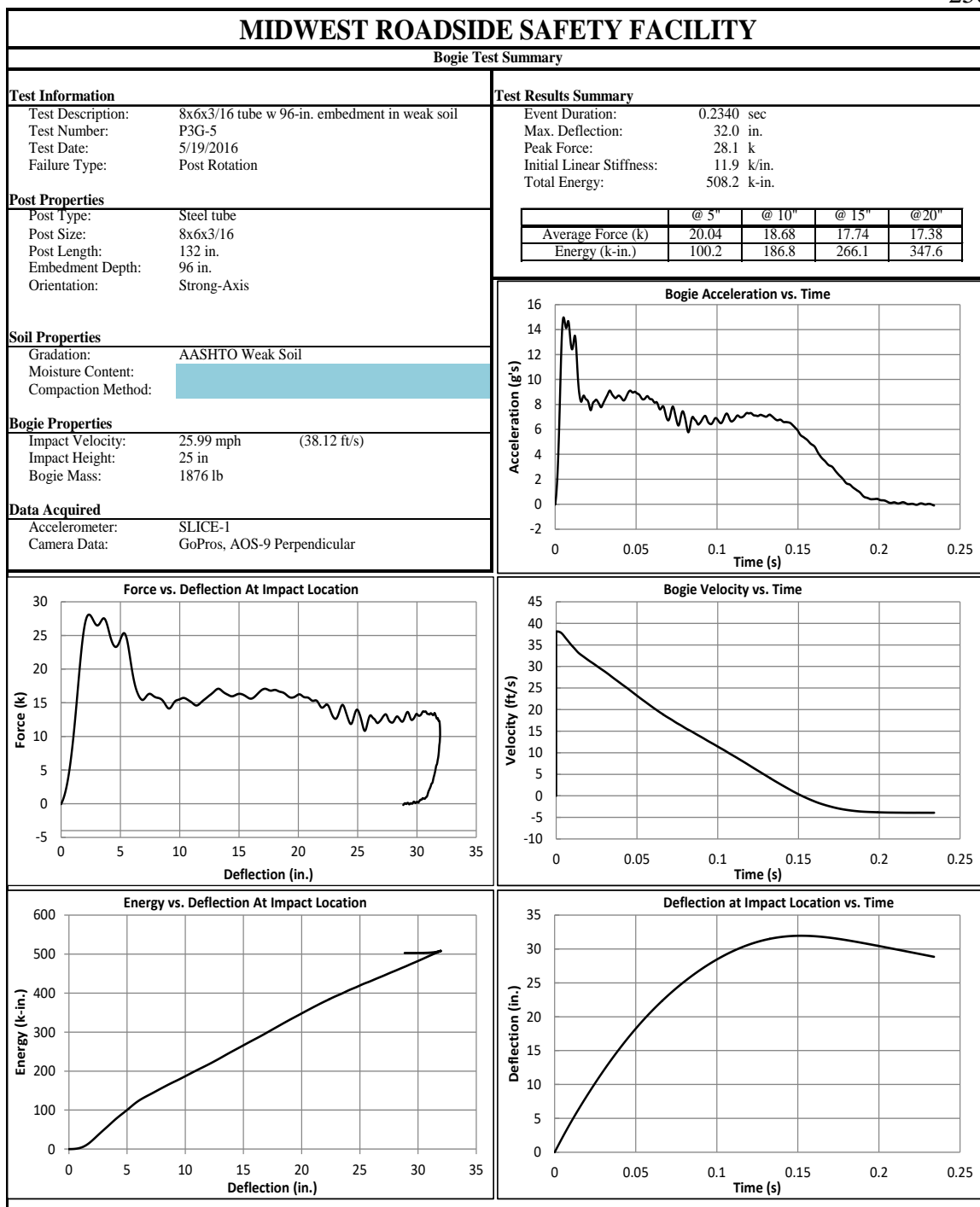


Figure H-9. Test No. P3G-5 Results (SLICE-1)

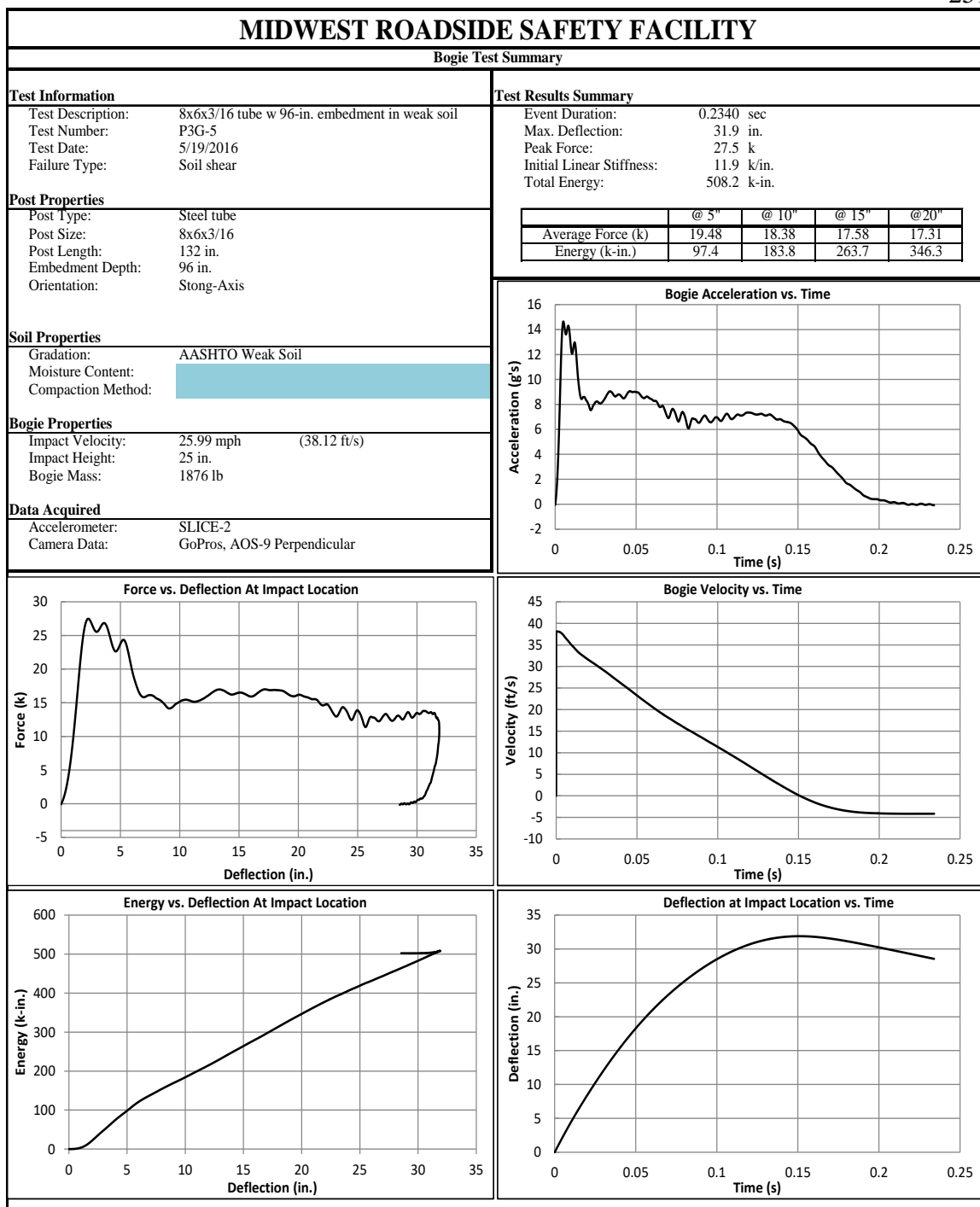


Figure H-10. Test No. P3G-5 Results (SLICE-2)

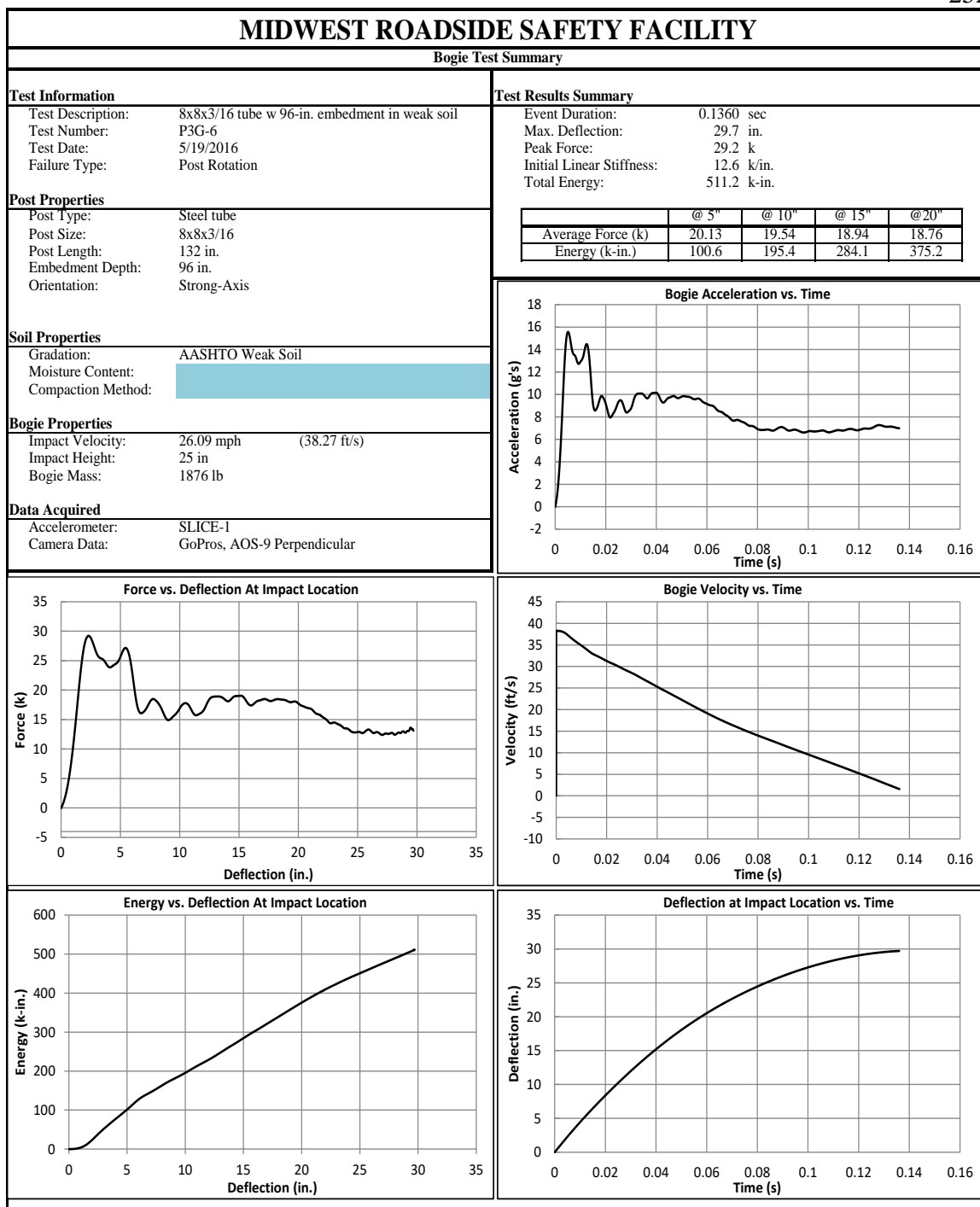


Figure H-11. Test No. P3G-6 Results (SLICE-1)

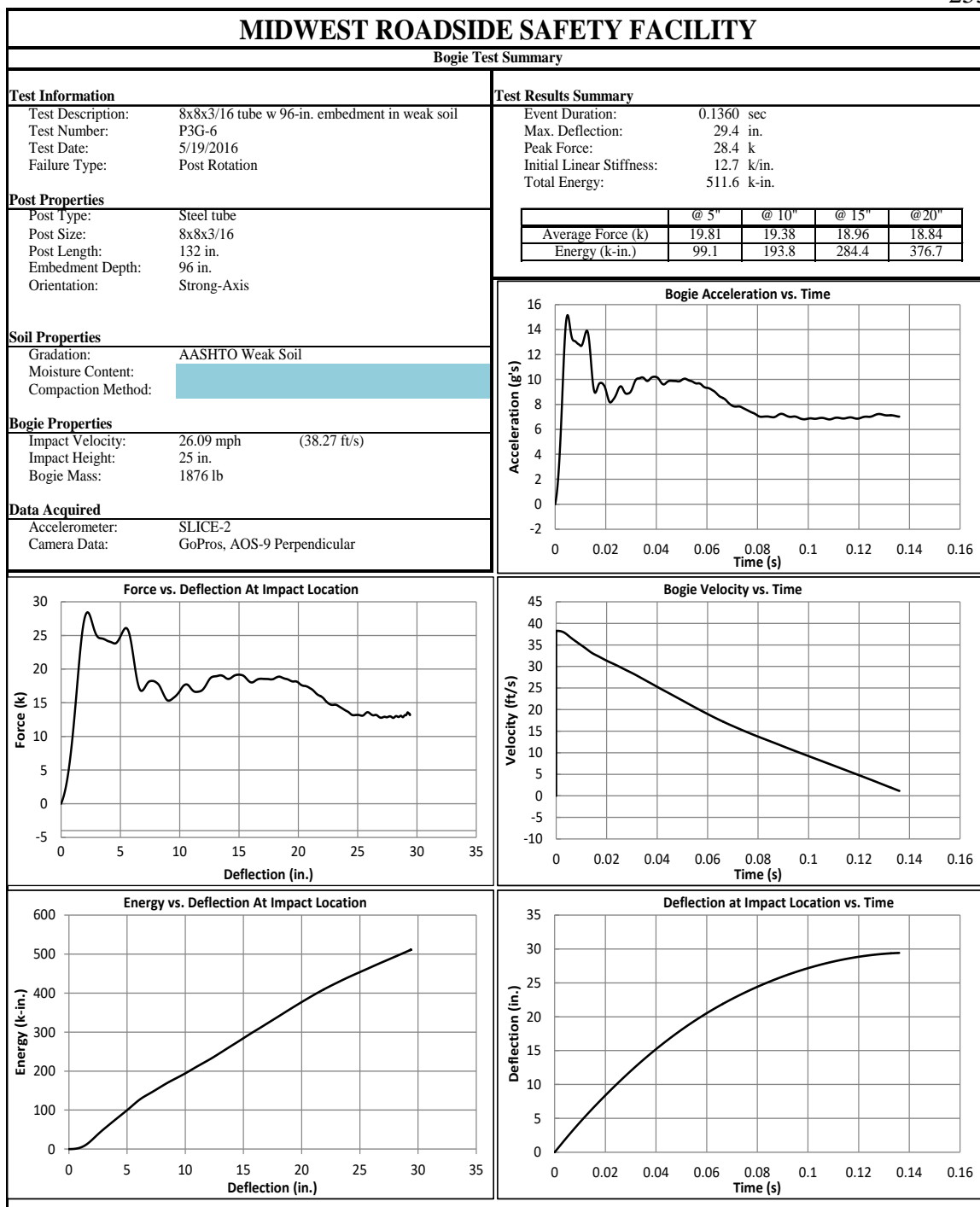


Figure H-12. Test No. P3G-6 Results (SLICE-2)

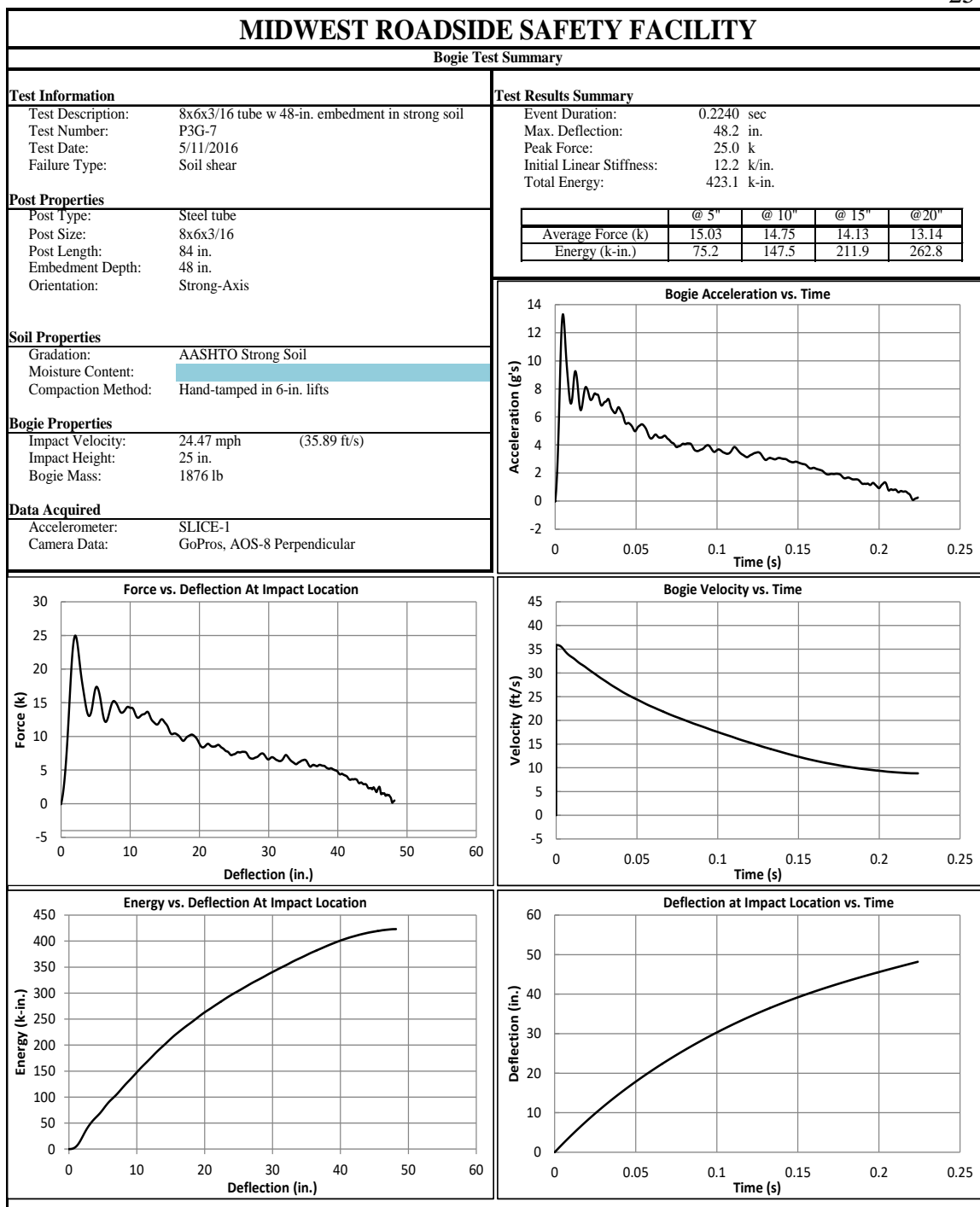


Figure H-13. Test No. P3G-7 Results (SLICE-1)

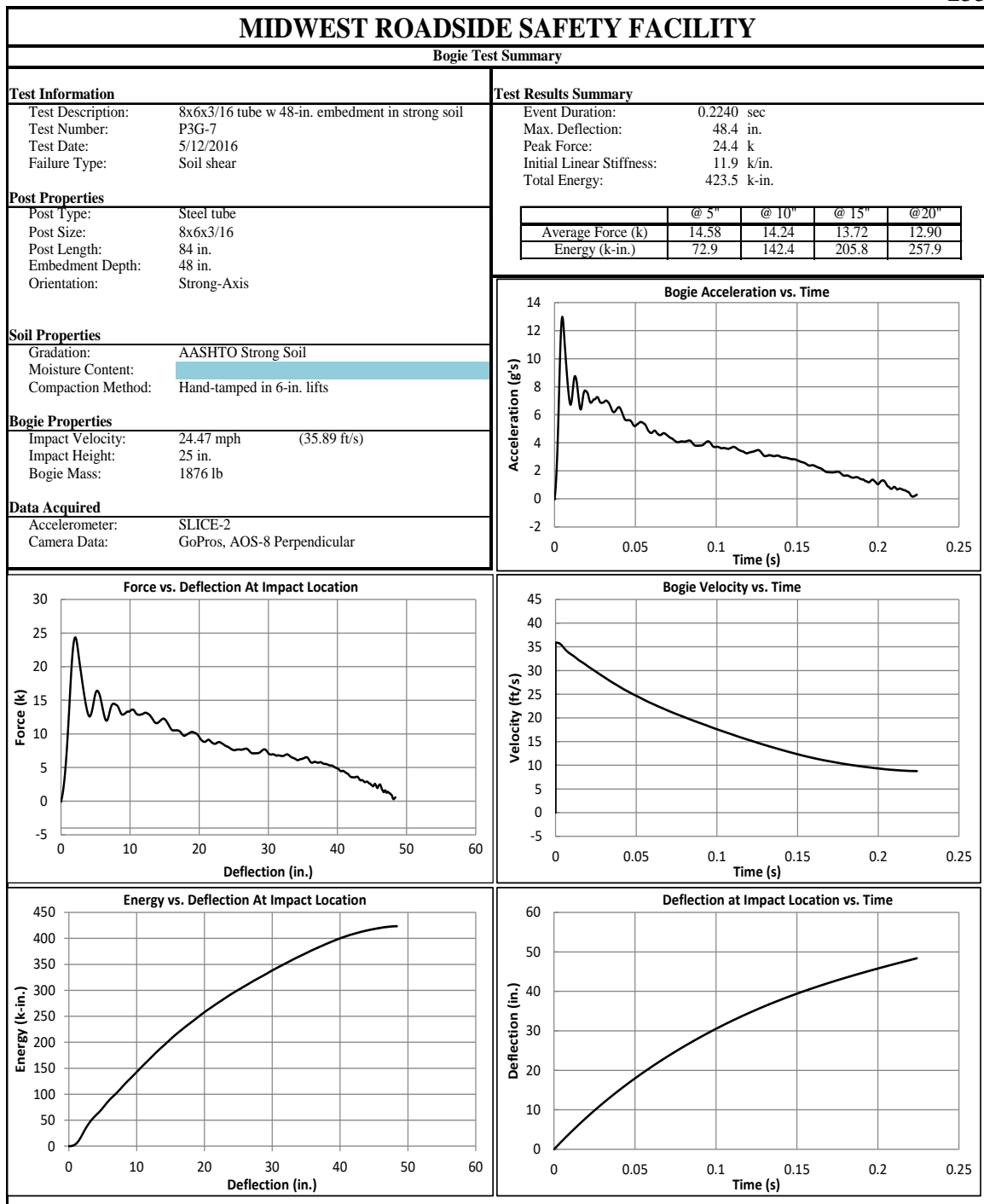


Figure H-14. Test No. P3G-7 Results (SLICE-2)

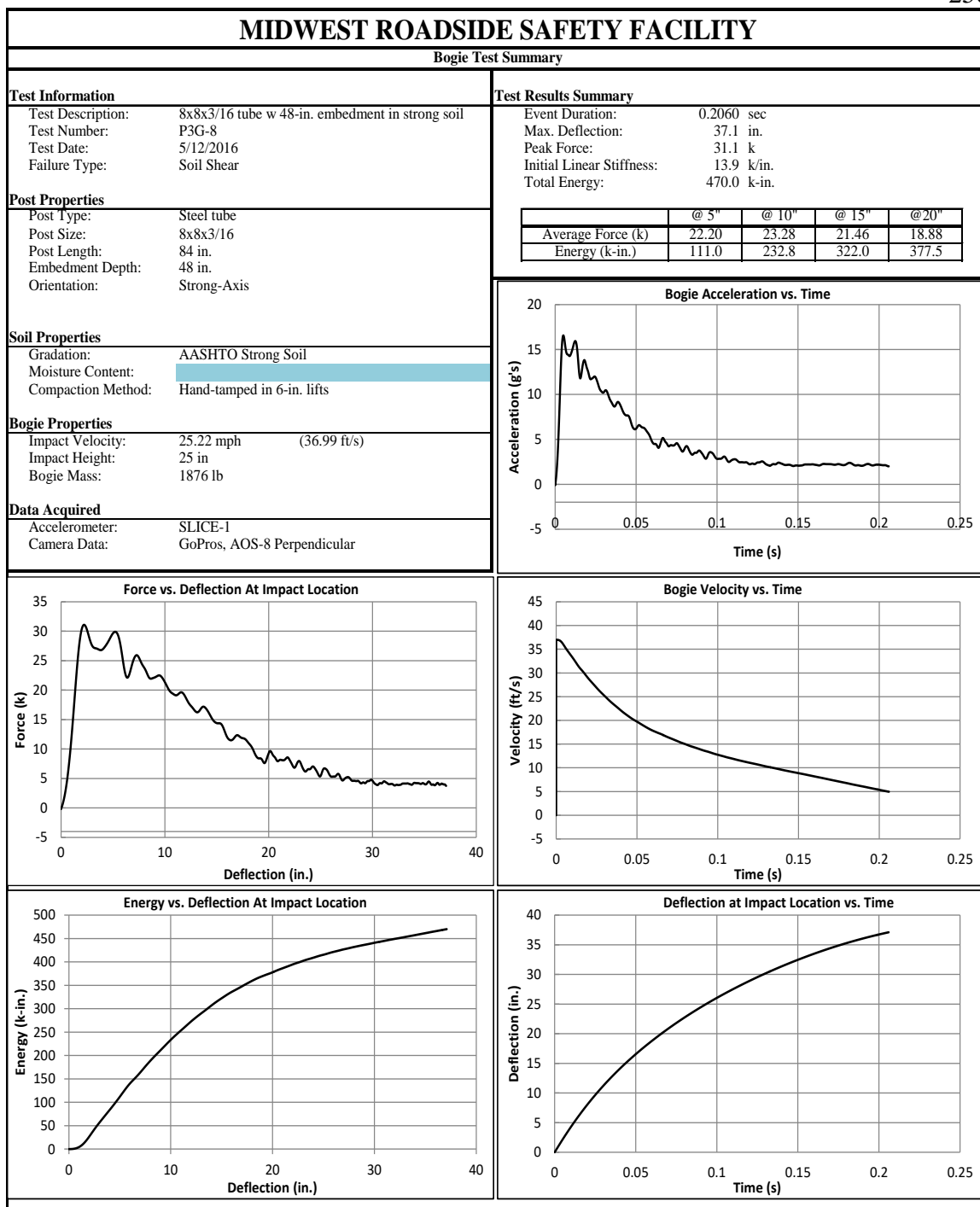


Figure H-15. Test No. P3G-8 Results (SLICE-1)



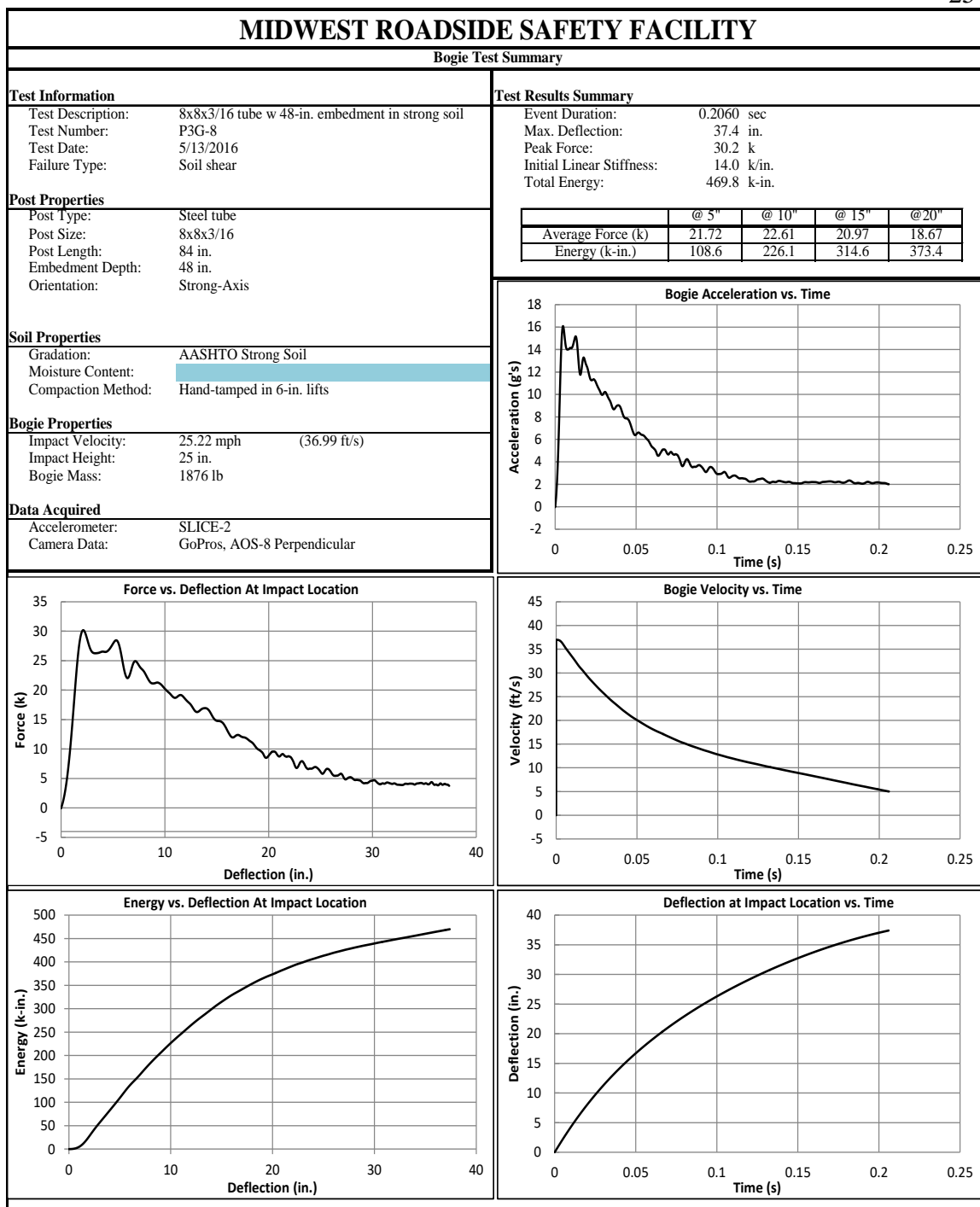


Figure H-16. Test No. P3G-8 Results (SLICE-2)

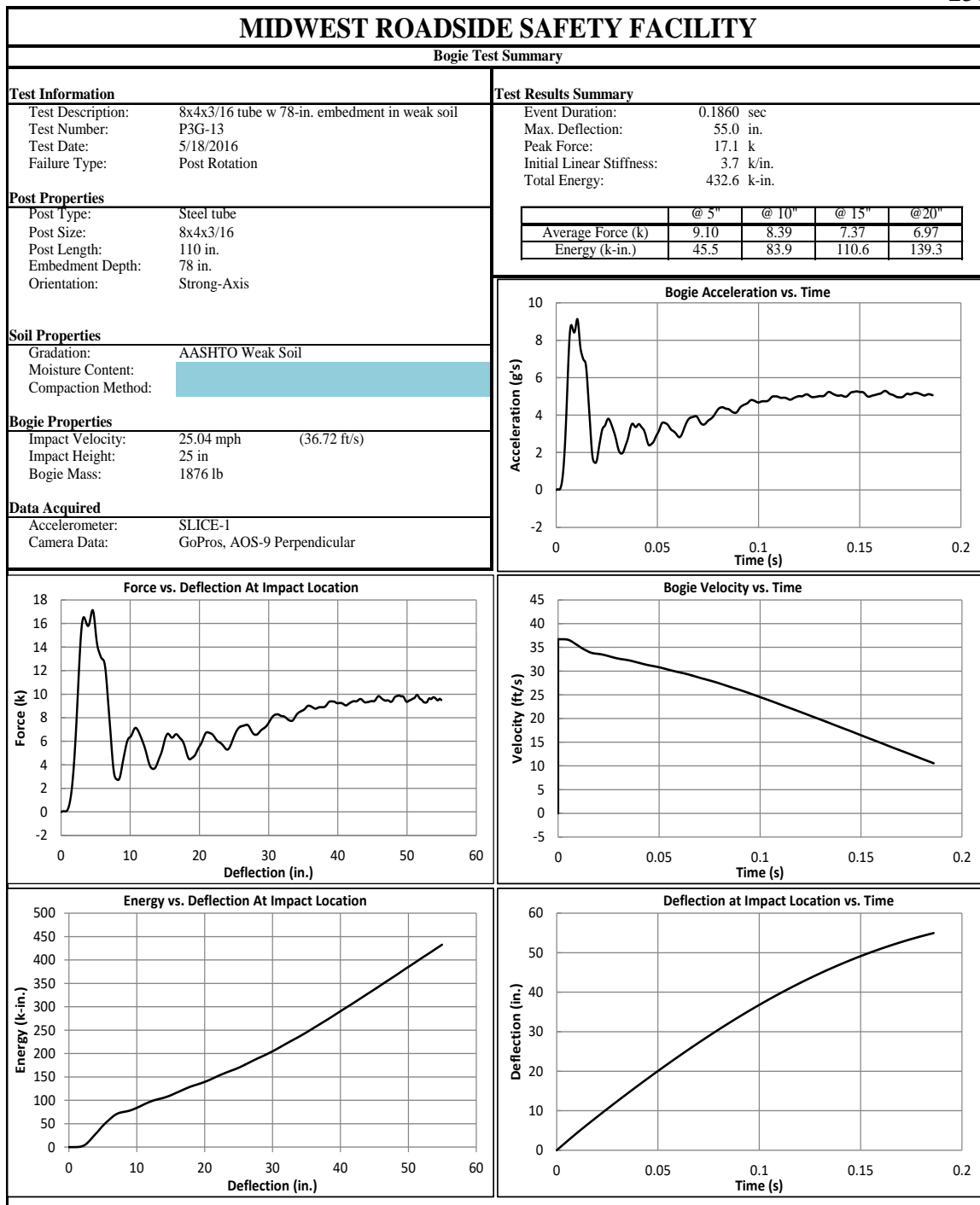


Figure H-17. Test No. P3G-13 Results (SLICE-1)

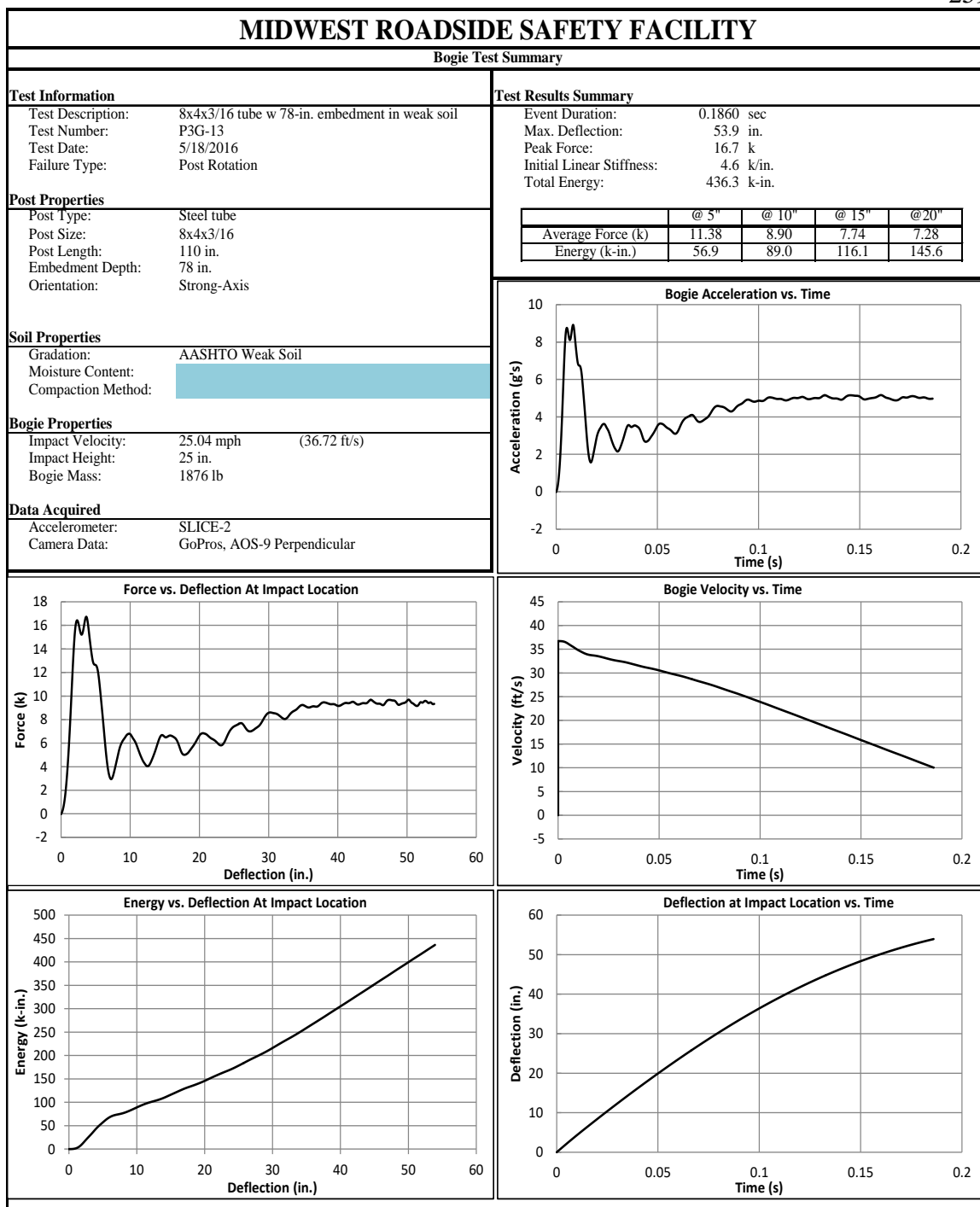


Figure H-18. Test No. P3G-13 Results (SLICE-2)

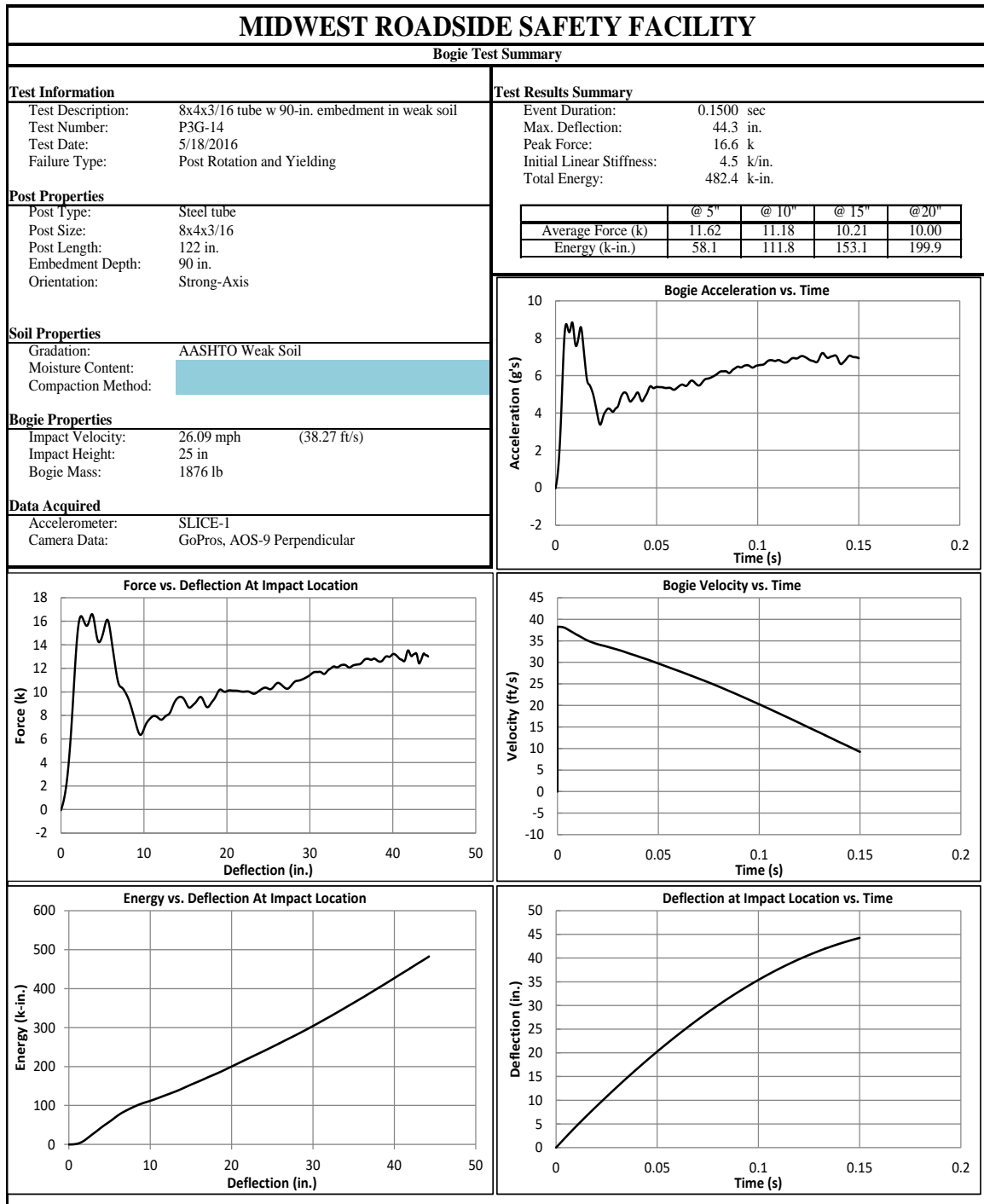


Figure H-19. Test No. P3G-14 Results (SLICE-1)

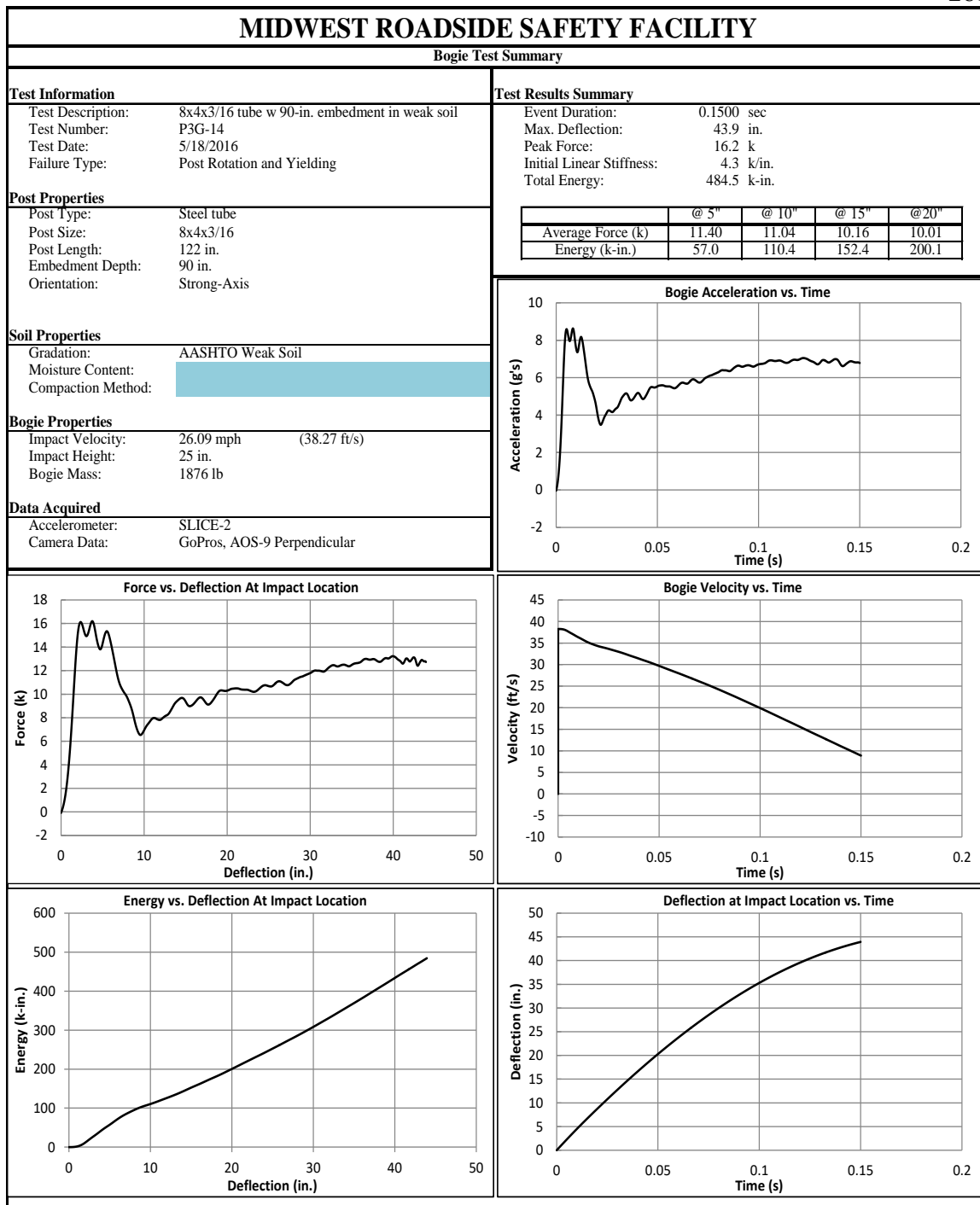


Figure H-20. Test No. P3G-14 Results (SLICE-2)

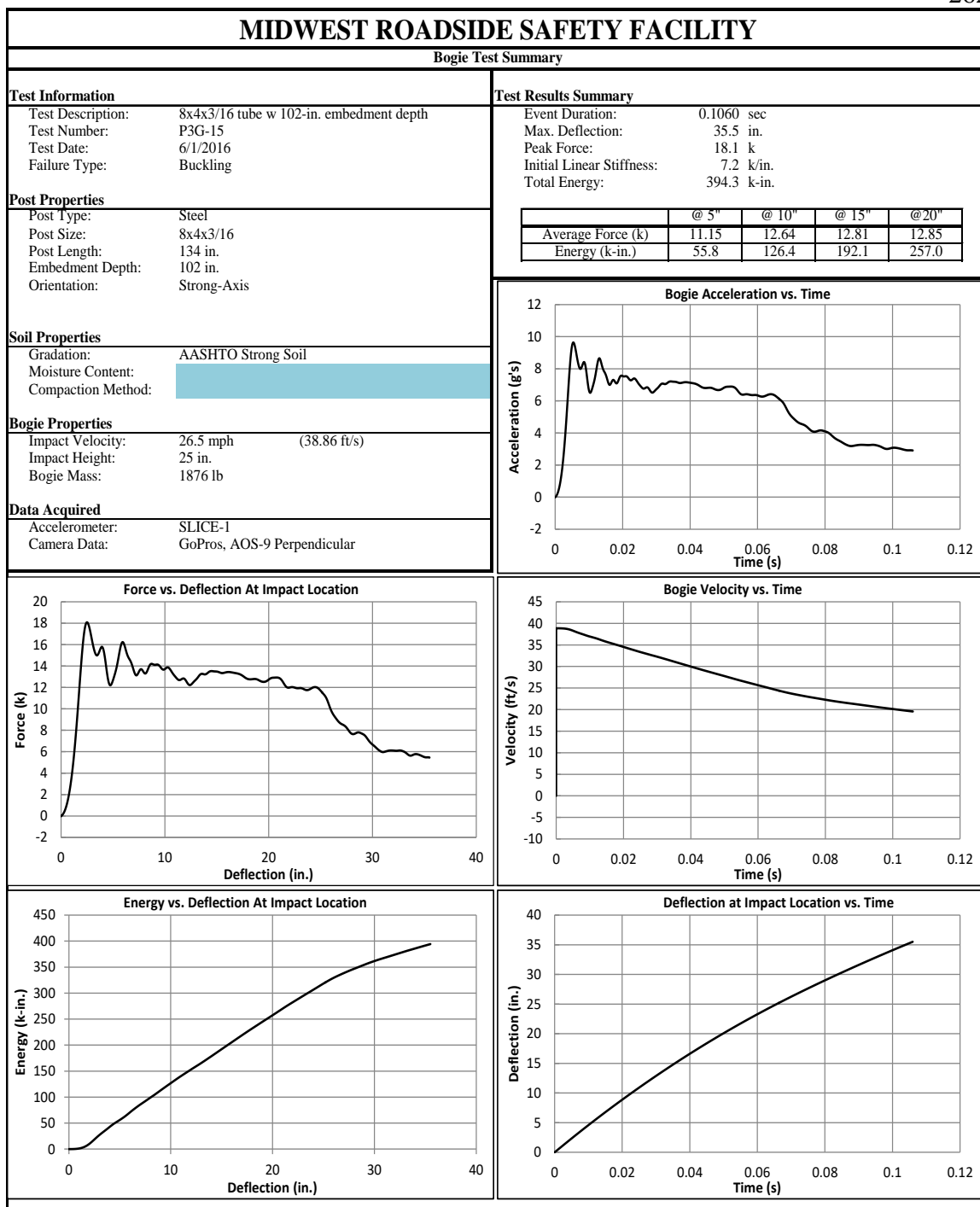


Figure H-21. Test No. P3G-15 Results (SLICE-1)

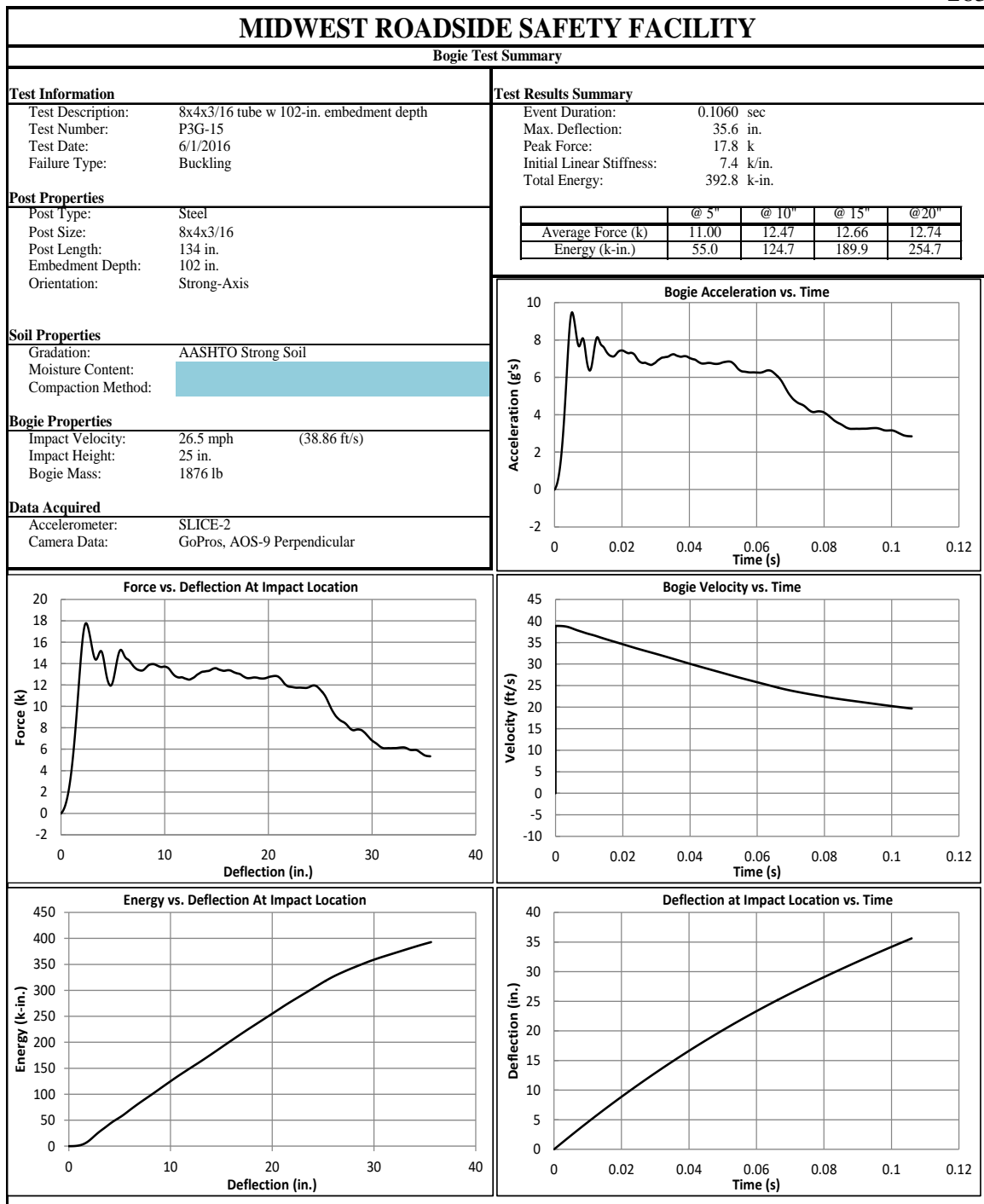


Figure H-22. Test No. P3G-15 Results (SLICE-2)

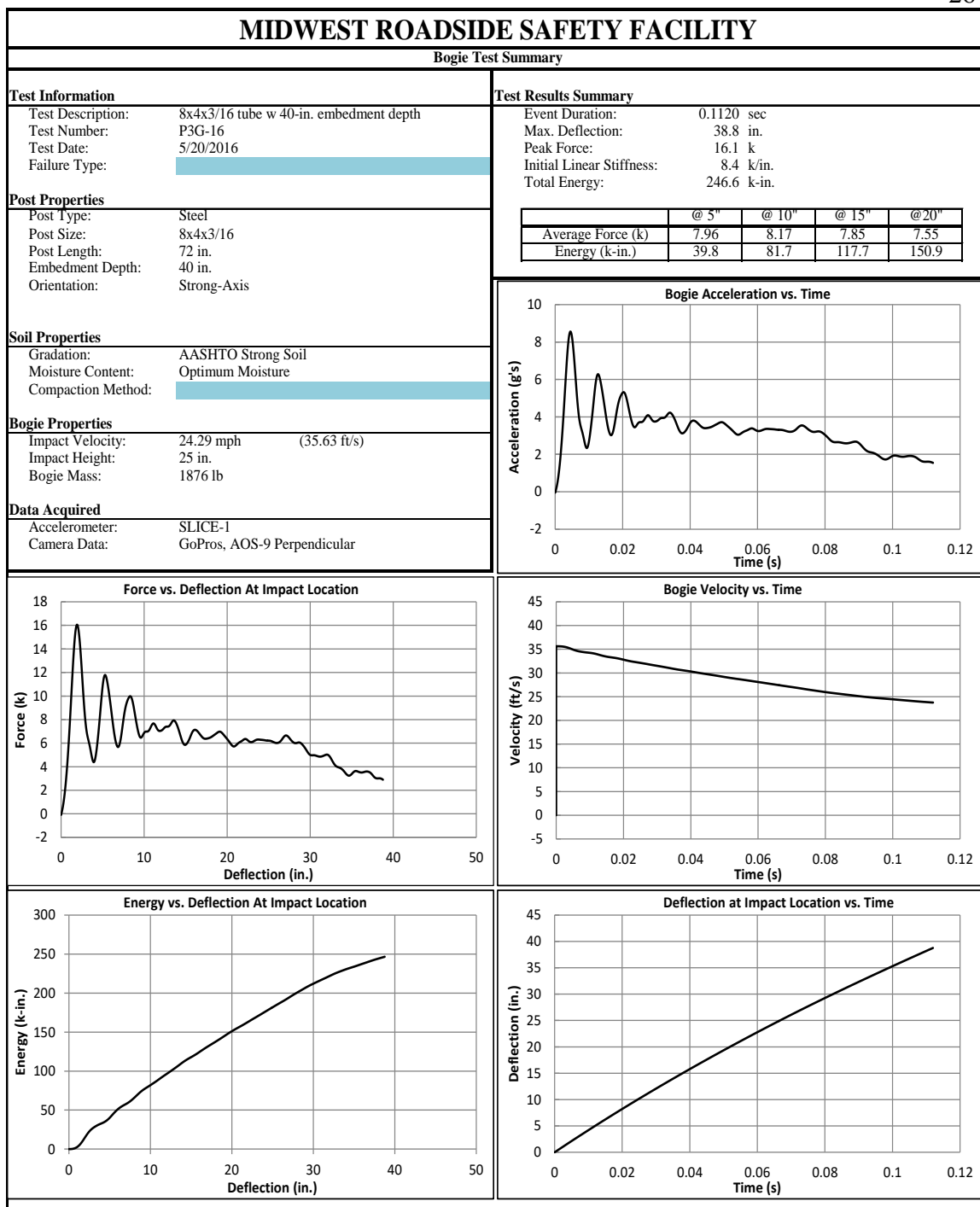


Figure H-23. Test No. P3G-16 Results (SLICE-1)



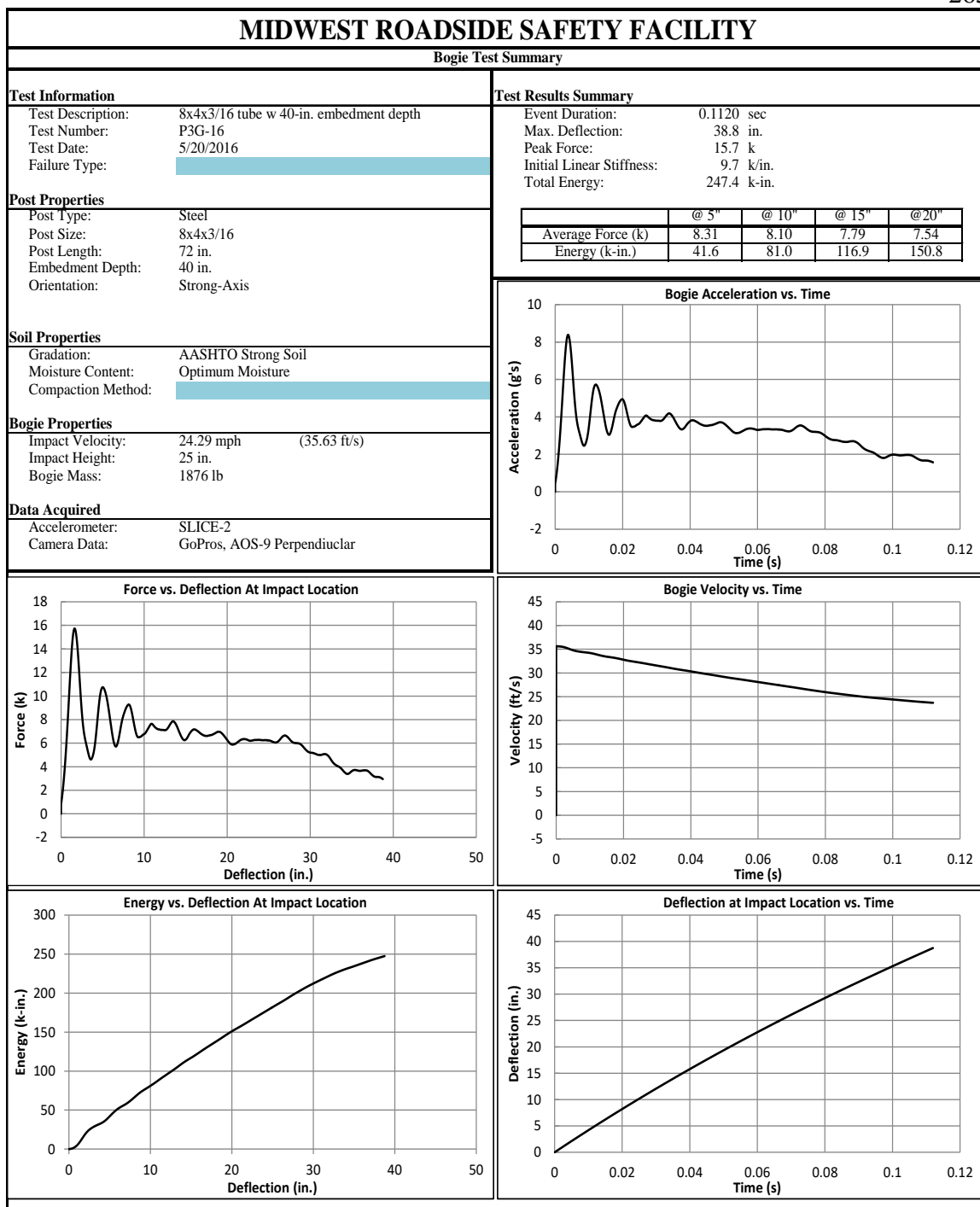


Figure H-24. Test No. P3G-16 Results (SLICE-2)

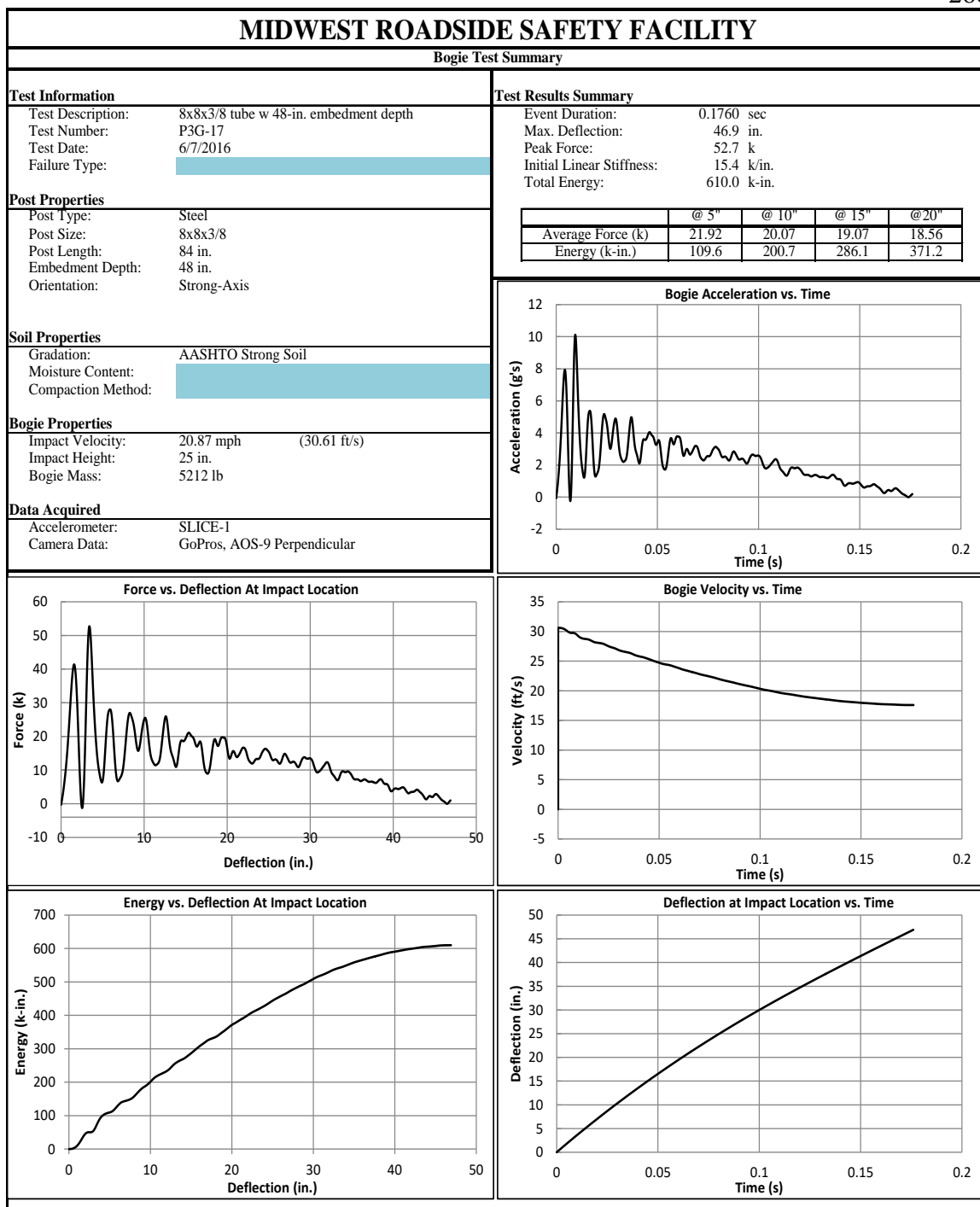


Figure H-25. Test No. P3G-17 Results (SLICE-1)

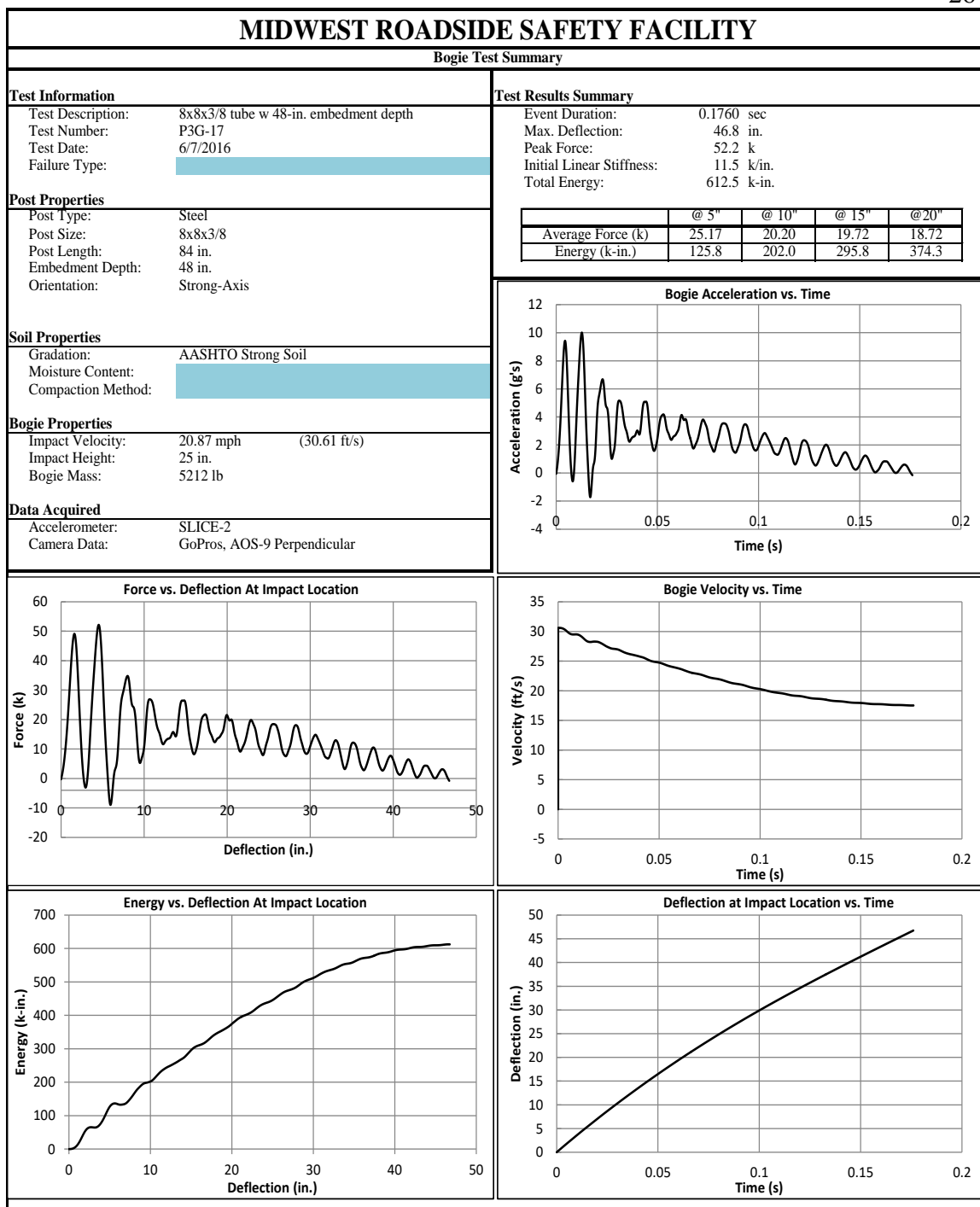


Figure H-26. Test No. P3G-17 Results (SLICE-2)

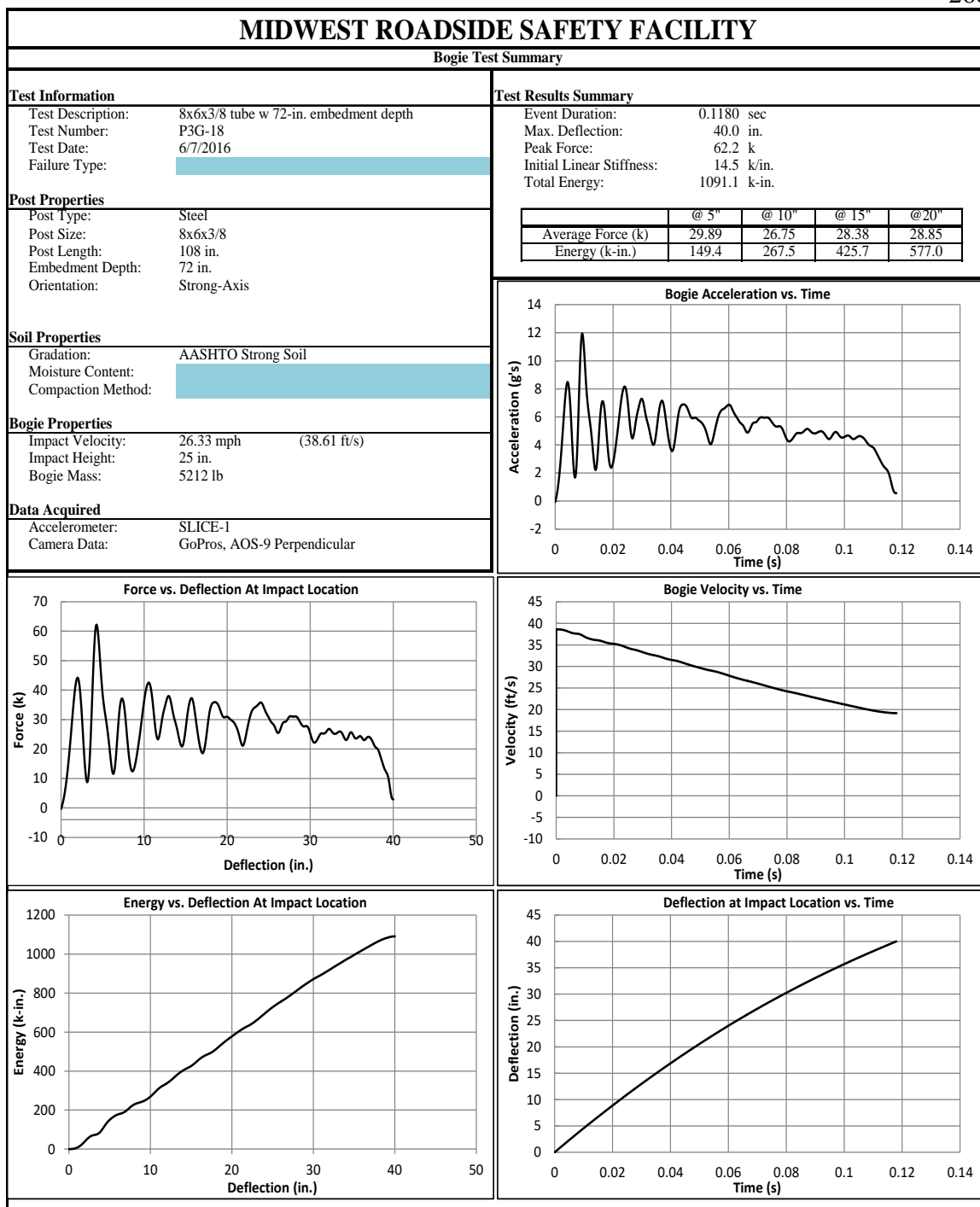


Figure H-27. Test No. P3G-18 Results (SLICE-1)

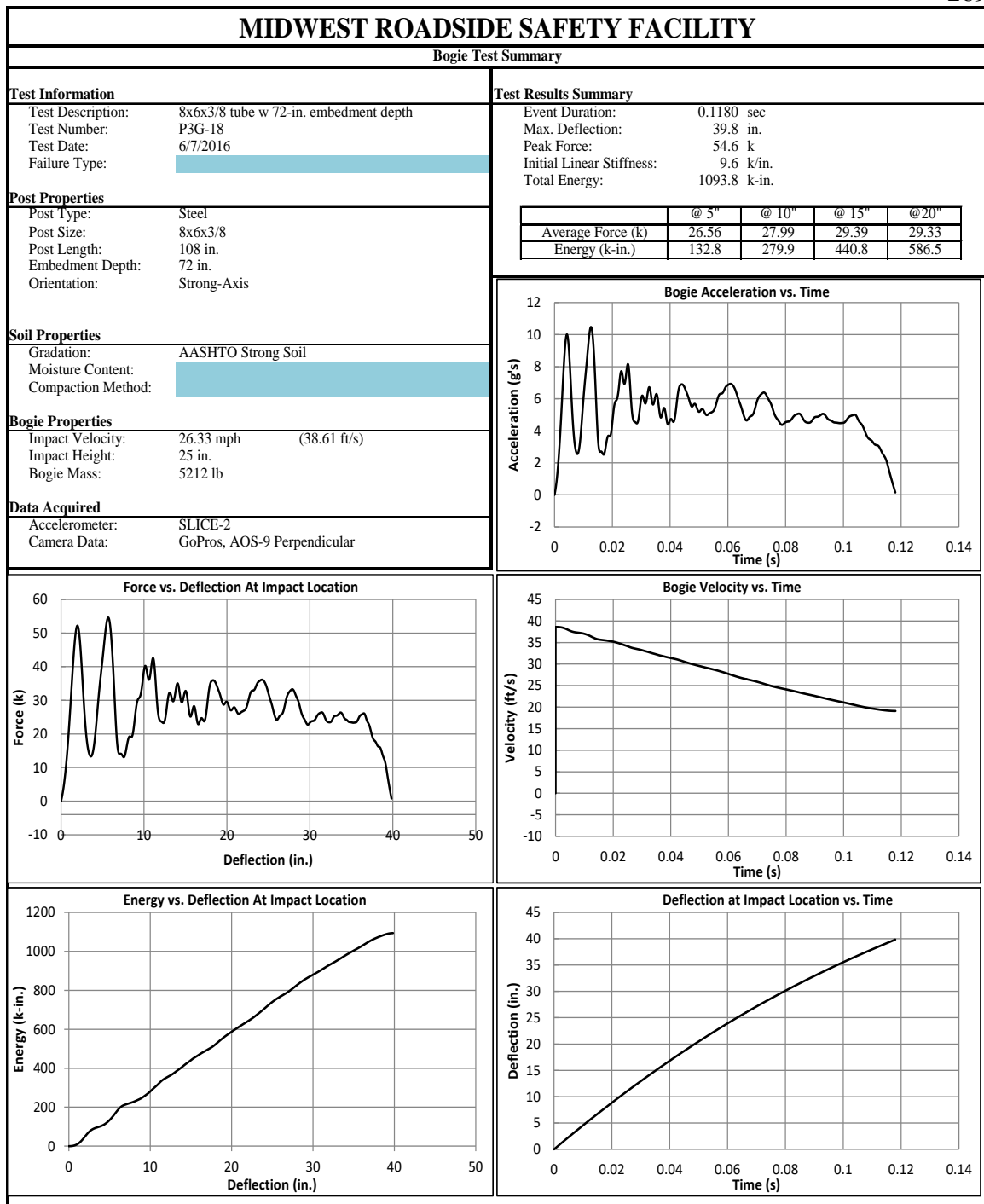


Figure H-28. Test No. P3G-18 Results (SLICE-2)

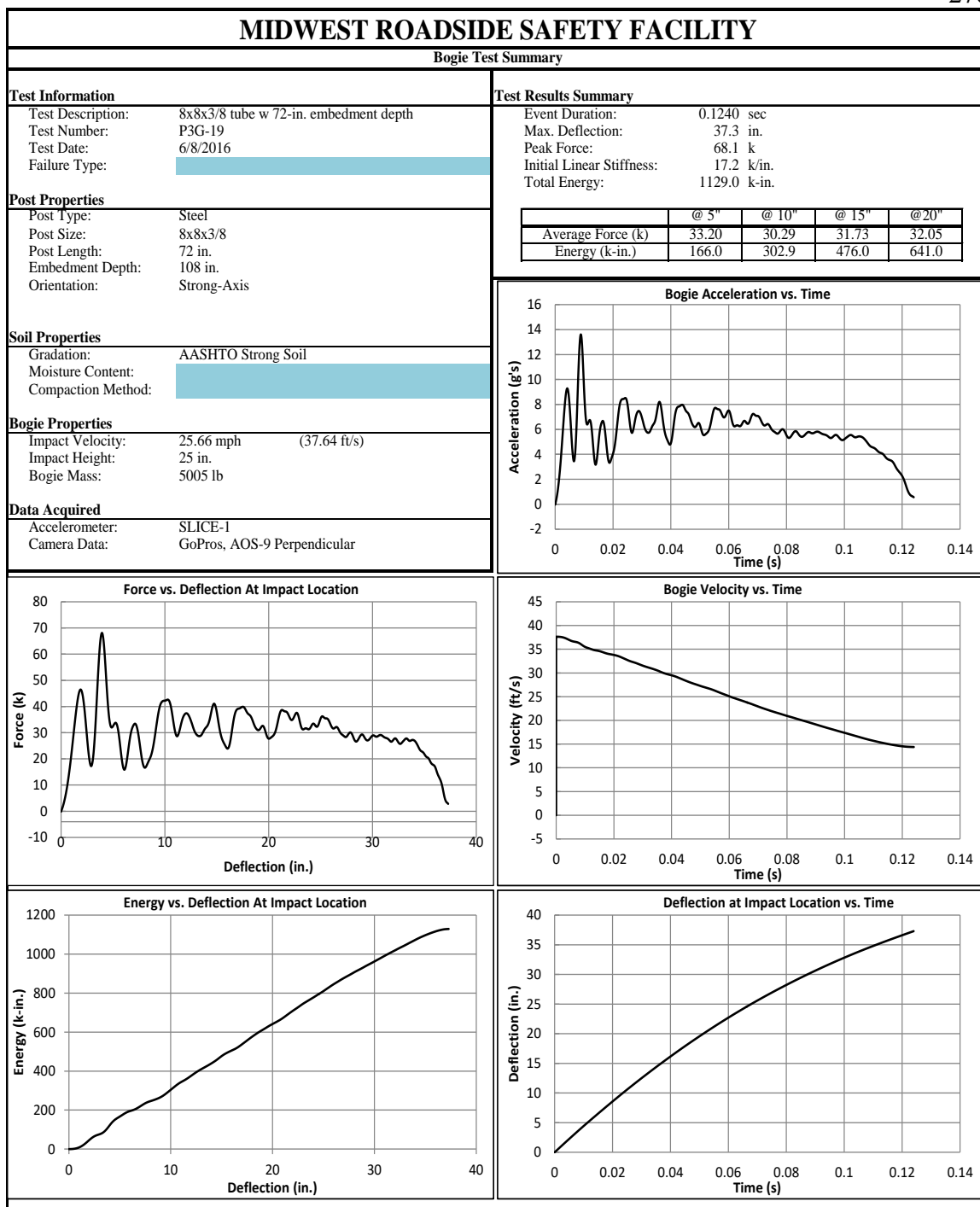


Figure H-29. Test No. P3G-19 Results (SLICE-1)

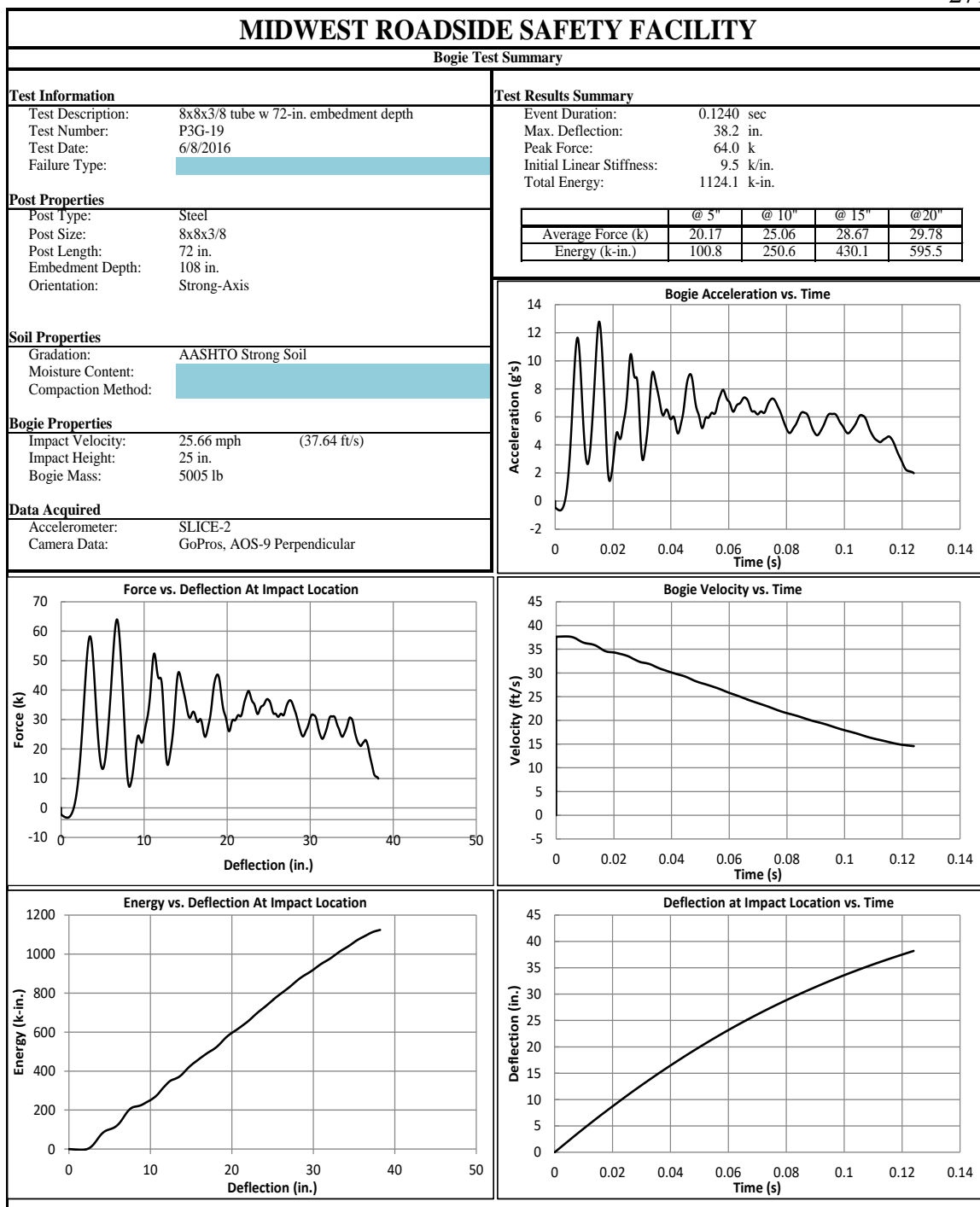


Figure H-30. Test No. P3G-19 Results (SLICE-2)

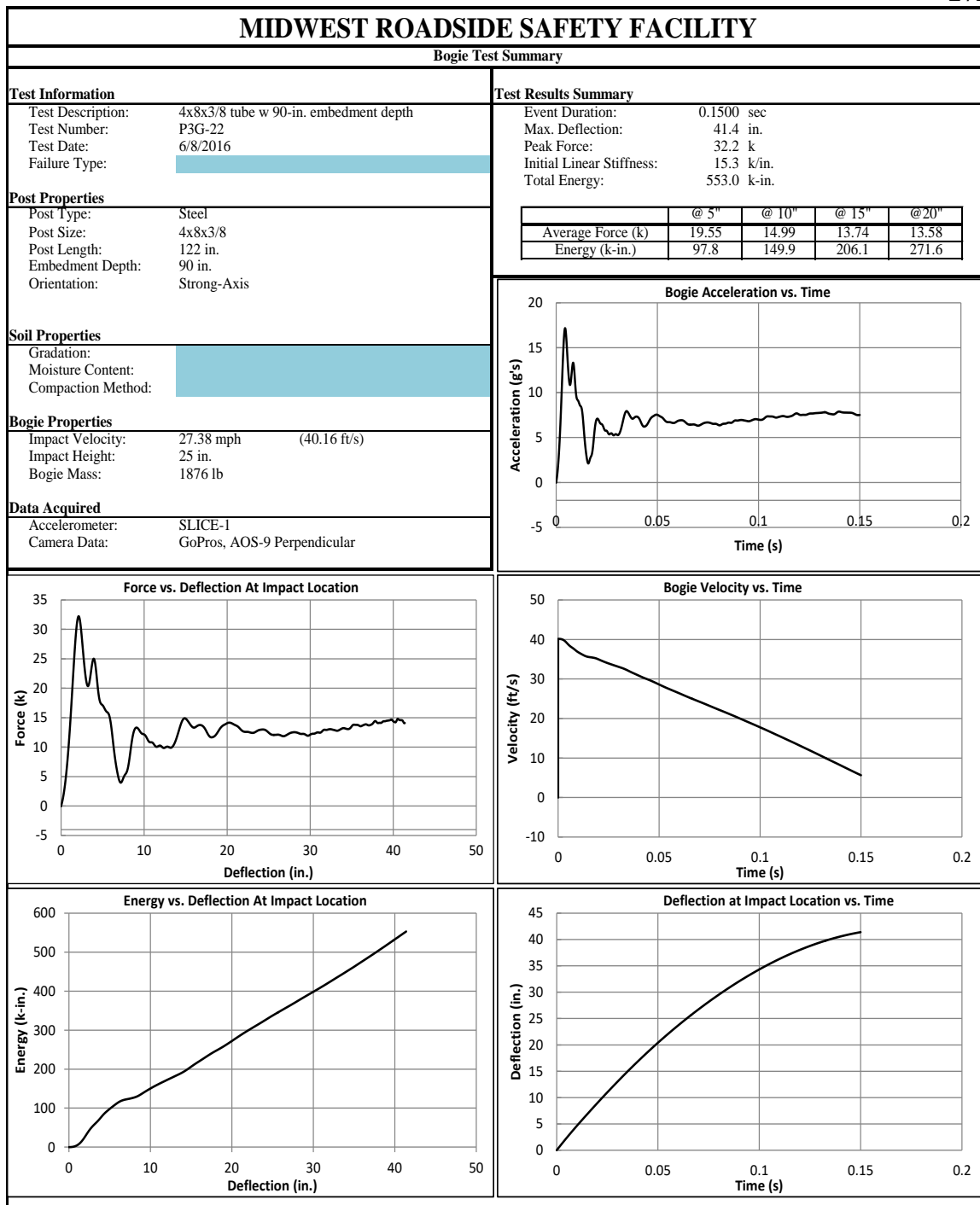


Figure H-31. Test No. P3G-22 Results (SLICE-1)



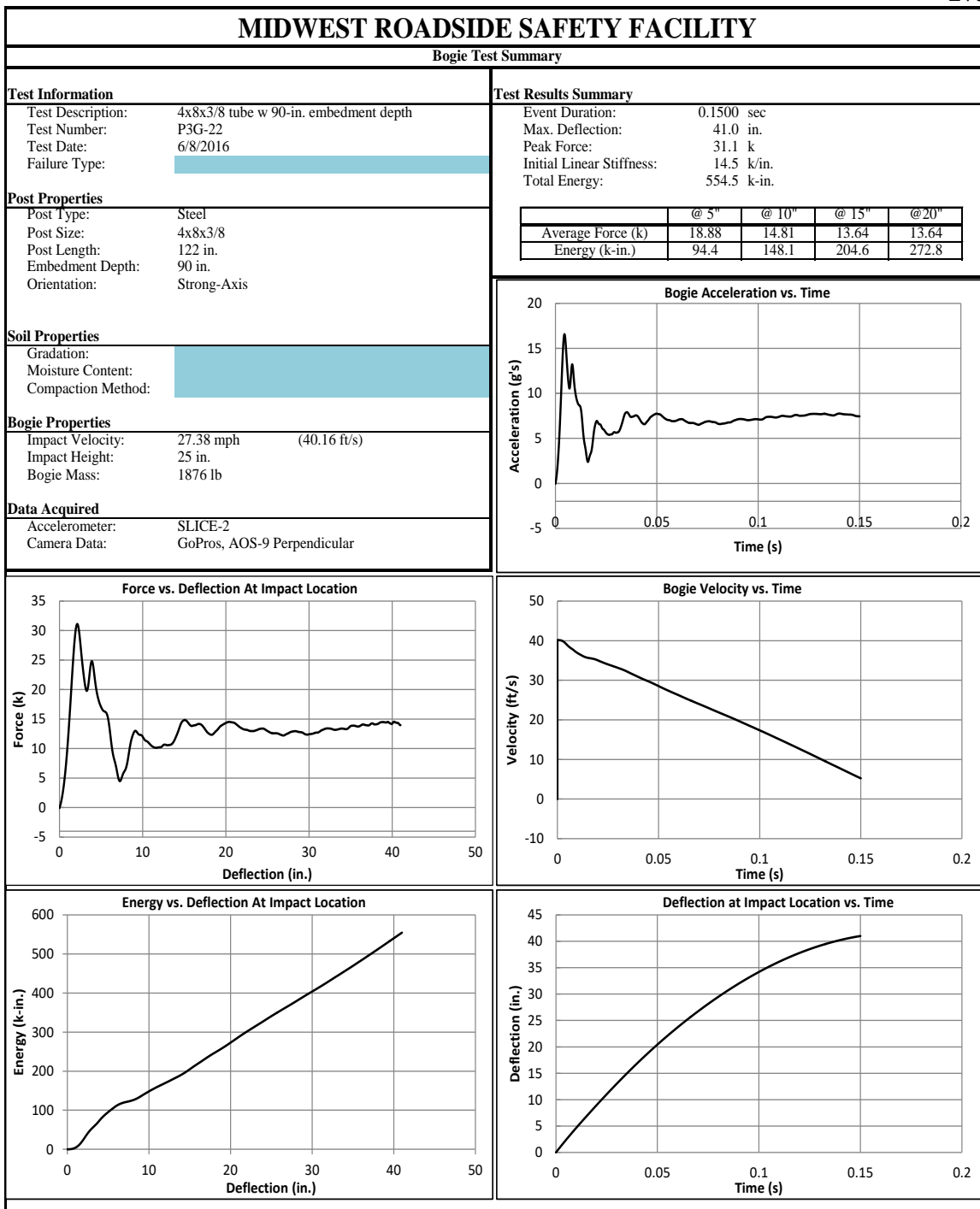


Figure H-32. Test No. P3G-22 Results (SLICE-2)

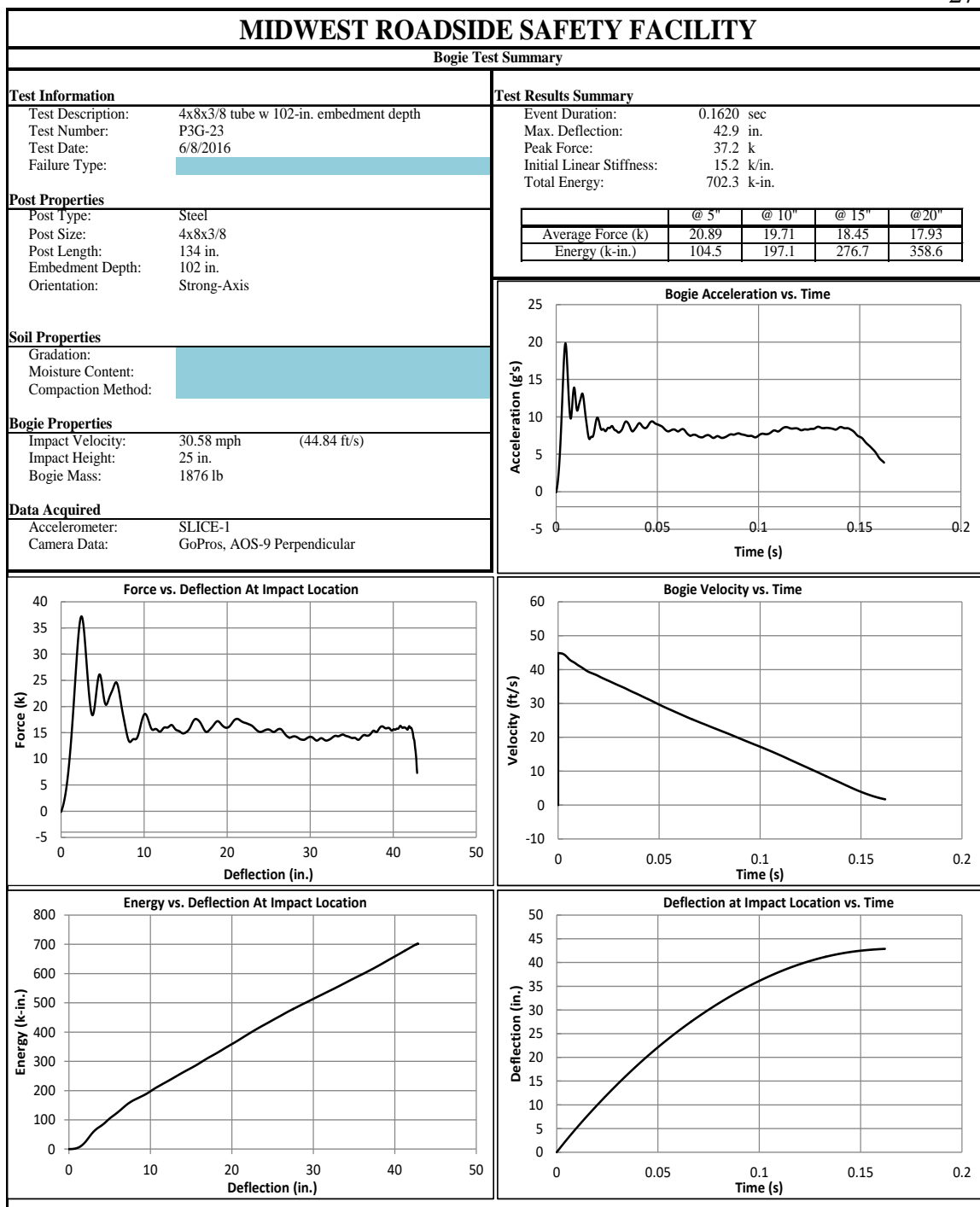


Figure H-33. Test No. P3G-23 Results (SLICE-1)

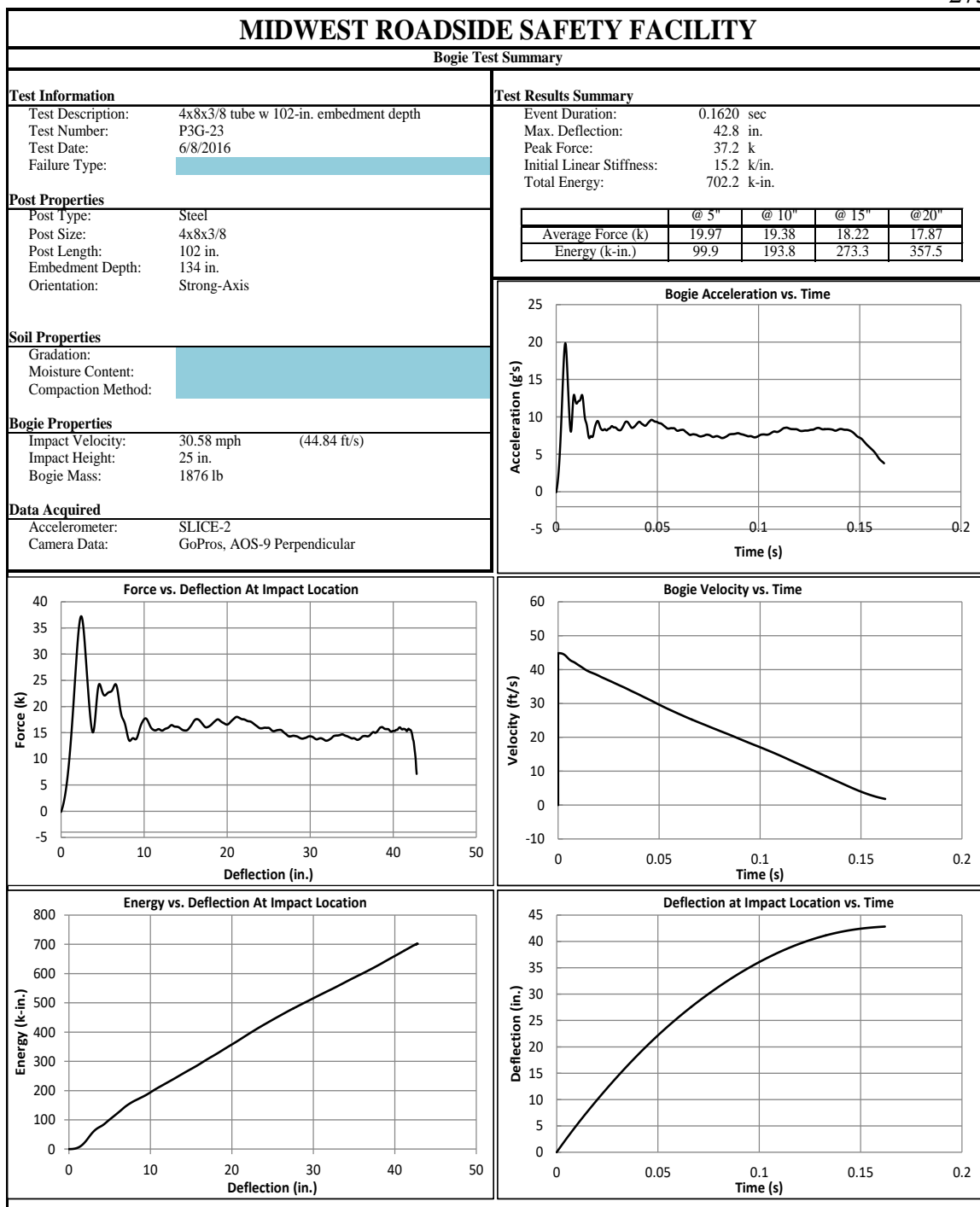


Figure H-34. Test No. P3G-23 Results (SLICE-2)

Appendix I. **Filtering Study**

### **11.1 Background**

The Society of Automotive Engineers (SAE) established guidelines for measuring and analyzing data for impact events in SAE J211 [37]. Two acceleration filters were used:

- To estimate forces, a CFC 60 filter is applied.
- To estimate vehicle and occupant displacements and injury risk, a CFC 180 filter is used.

Both filters are high pass filters, in which frequencies above the cutoff are attenuated significantly.

### **11.2 Research Objectives**

During an impact event, stress waves, part oscillations, harmonics and instrument noise can affect acceleration data. The SAE J211/1 recommendations for CFC 60 or CFC 180 filters may not be well suited for all impact test analysis. This study was completed to determine the limitations on filter representations of data shapes.

### **11.3 Scope**

Researchers evaluated the filter effects on data pulses for three wave forms and eight pulse durations:

- Square Waves
- Sawtooth Waves
- Triangle Waves
- 50, 25, 15, 10, 15, 7.5, 5, 2.5, 1 ms Durations

These waves and durations were inserted into the CFC 60 filter and a comparison was made between the raw and filtered output. This study looked at how changing the

duration of a burst pulse affected the output from the CFC 60 filter. A nominal sampling frequency of 10,000 Hz. was used to generate the raw data.

#### **11.4 Methods**

After the acceleration pulses were inserted into the digital filter, maxima were identified and recorded. The ratio of filter maxima to input data was also calculated and was displayed on the output graphs as: "Filter Max / Input Max". Researchers also calculated the peak slope of the filtered data as well, using linear approximation of peak-to-rise amplitude and time duration. Internal functions within excel were used to determine the slope from 0 to the maximum value and is displayed on the graphical outputs. For the square and triangle wave pulses the slope from the maximum value back to 0 is the negative version of the displayed value. The increase and decrease slopes for sawtooth waves are different and both of these values are displayed on the graphical outputs.

#### **11.5 Square Wave Pulses**

Square wave pulses ranging between 50 and 1 millisecond were input into the CFC 60 filter to determine the amount of attenuation and amplification that occurs. Square wave results are shown in the figures below and summarized in the table.

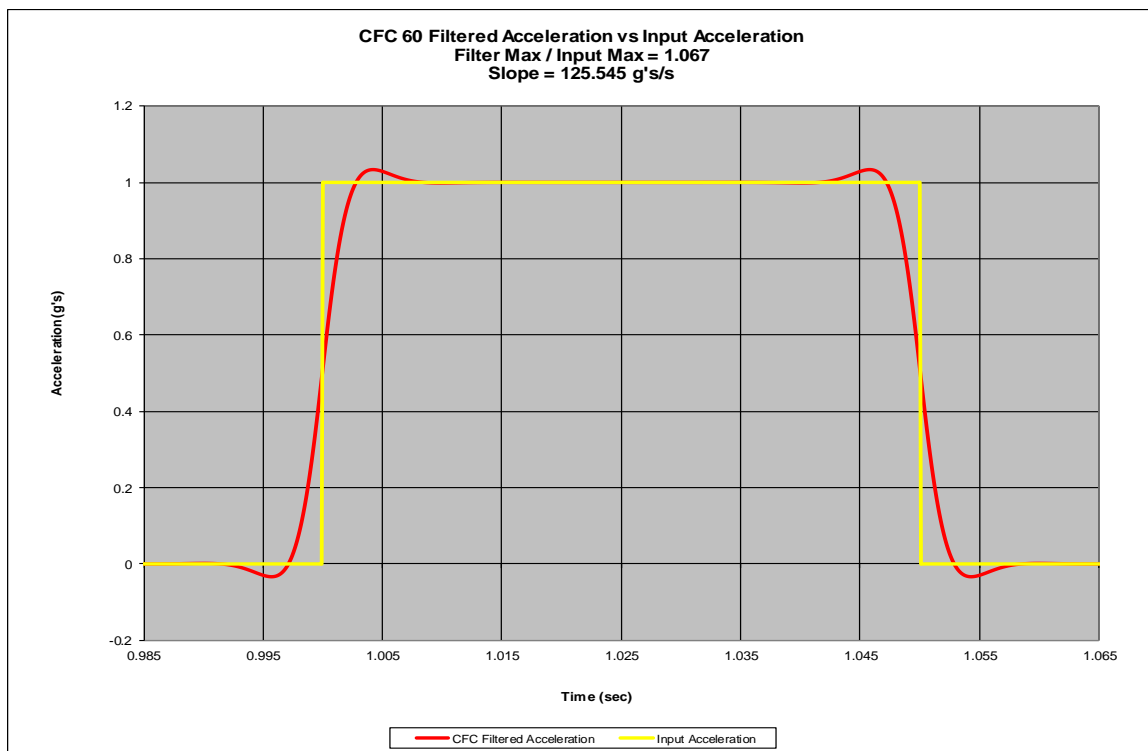


Figure I-1. 50 ms. Square Wave Pulse

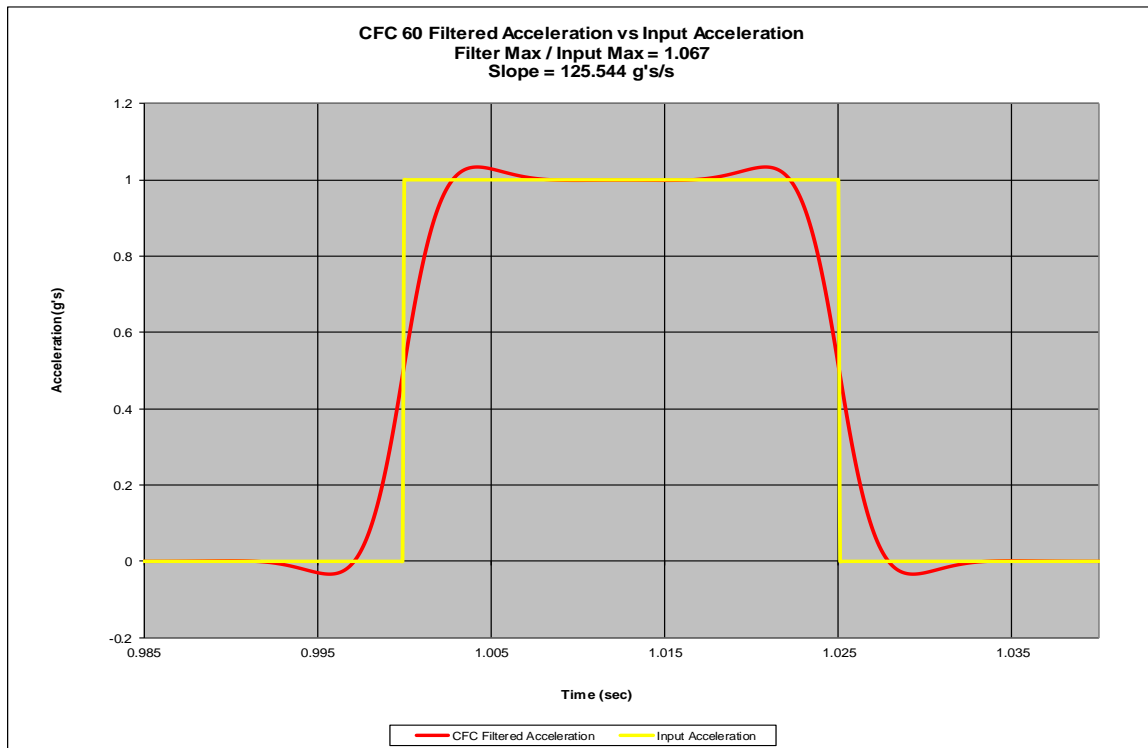


Figure I-2. . 25 ms. Square Wave Pulse

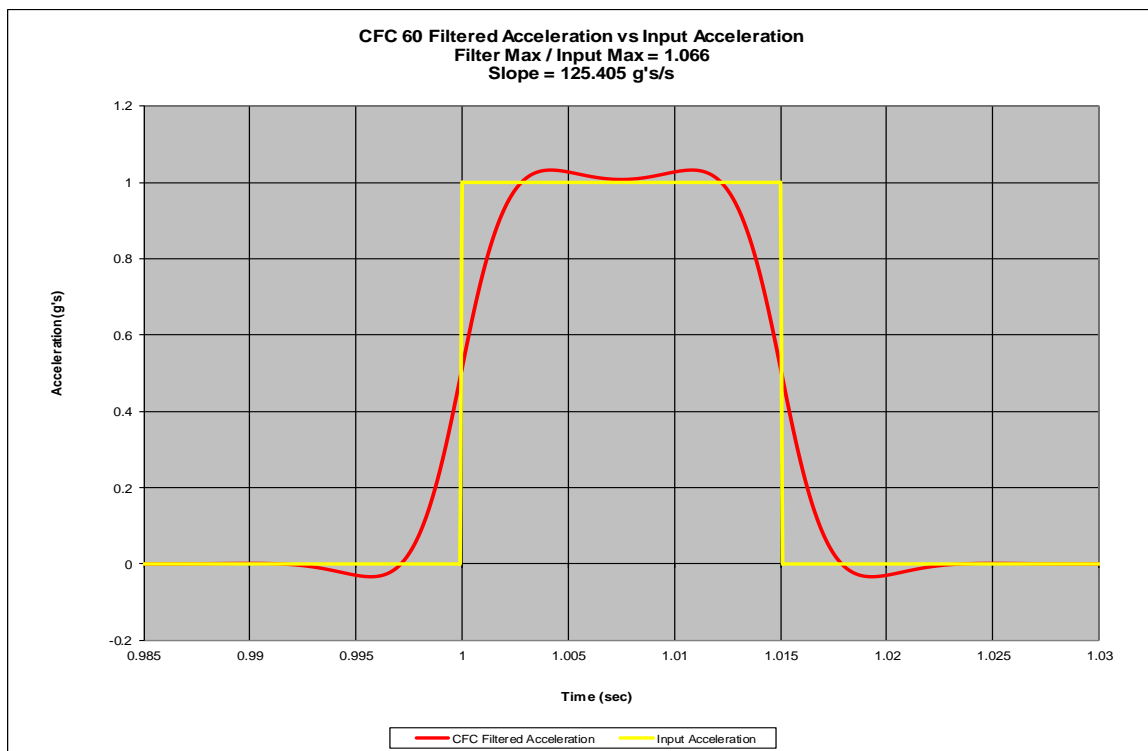


Figure I-3. 15 ms. Square Wave Pulse

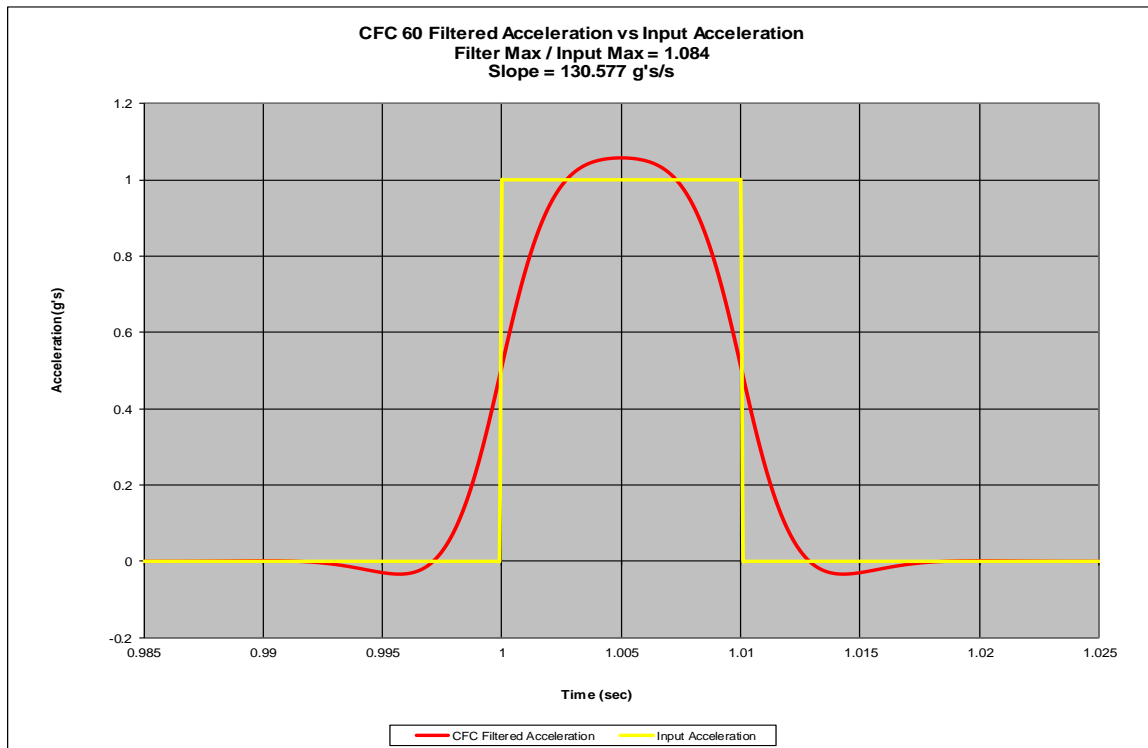


Figure I-4. 10 ms. Square Wave Pulse



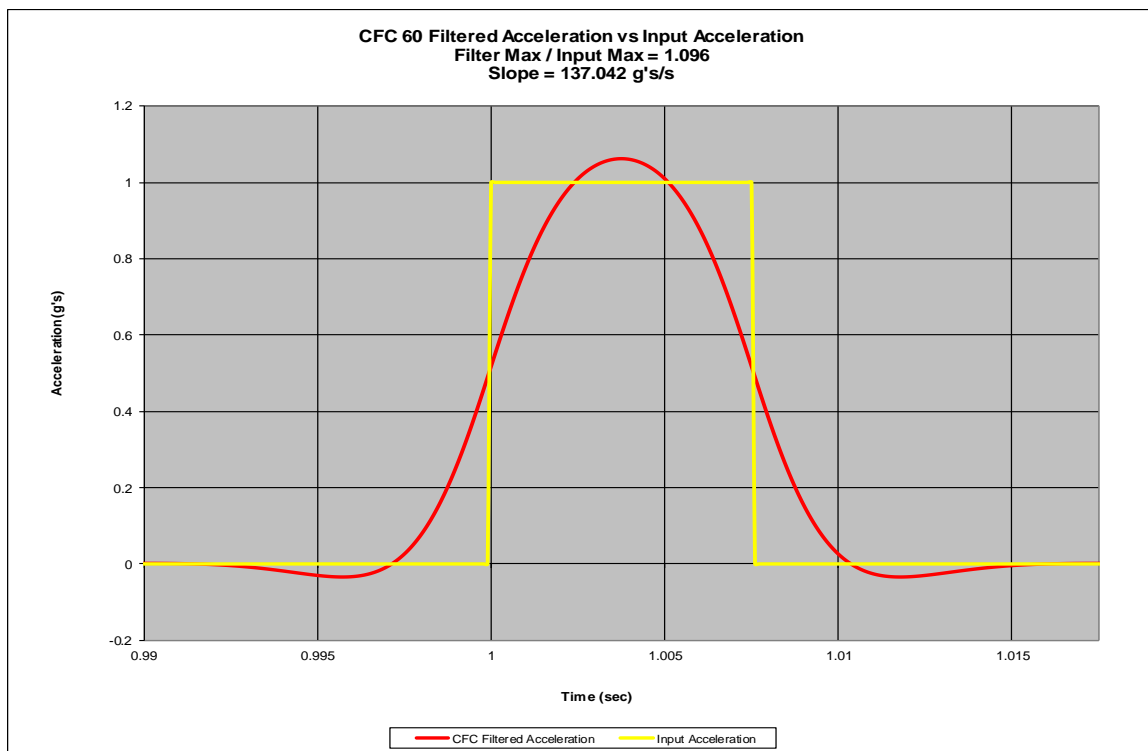


Figure I-5. 7.5 ms. Square Wave Pulse

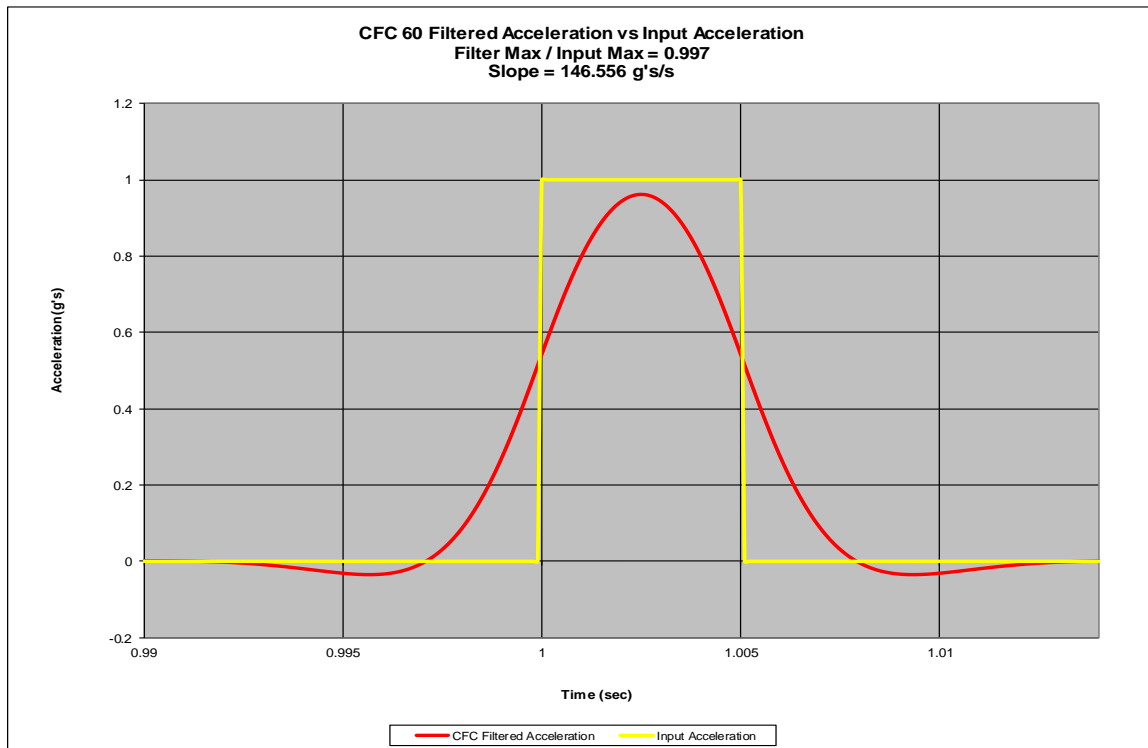


Figure I-6. 5 ms. Square Wave Pulse

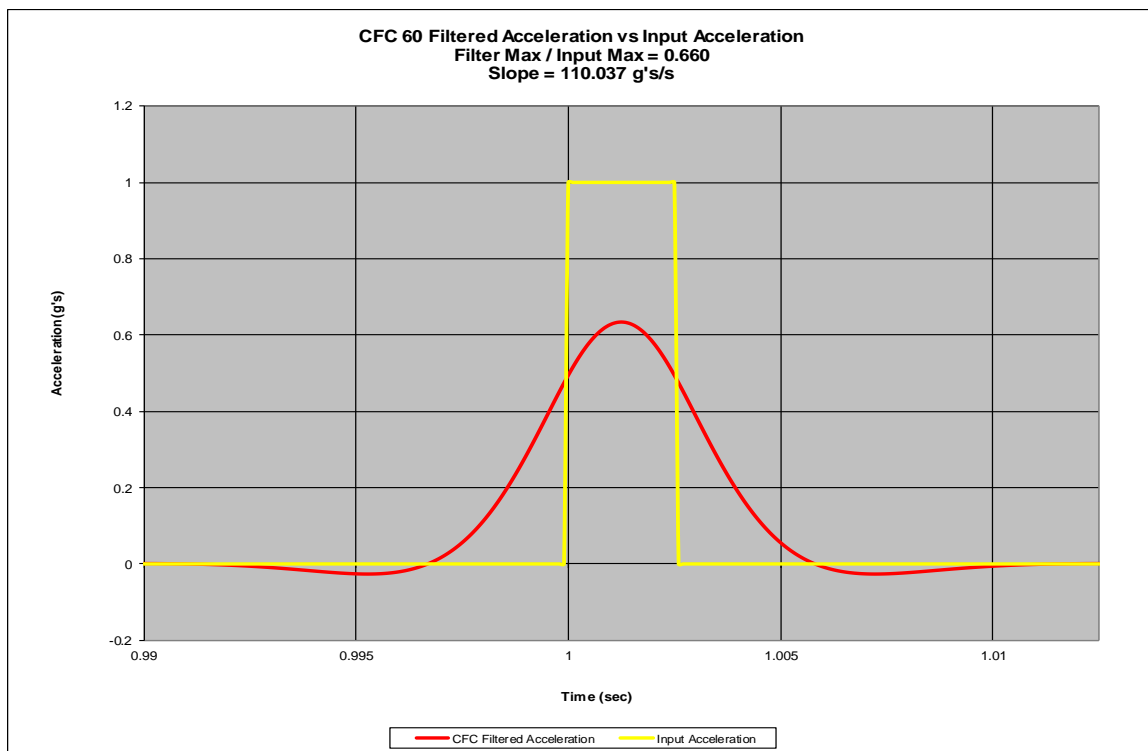


Figure I-7. 2.5 ms. Square Wave Pulse

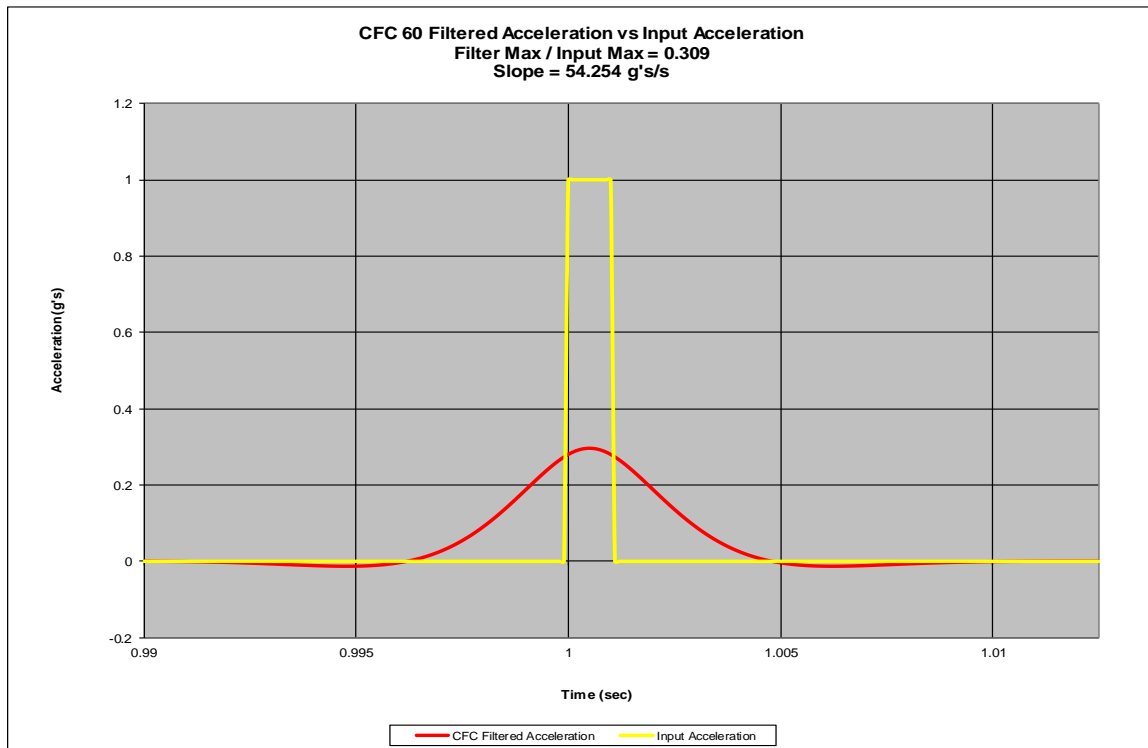


Figure I-8. 1 ms. Square Wave Pulse

Table 50. Filter Max / Input Max and Filter Slope for Square Waves

Pulse Length (ms)	Filter Max / Input Max	Slope (g's/s)
50	1.067	125.545
25	1.067	125.544
15	1.066	125.405
10	1.084	130.577
7.5	1.096	137.042
5	0.997	146.556
2.5	0.660	110.037
1	0.309	54.254

### 11.5.1 Square Wave Discussion

Pulses between 7.5 and 10 ms are slightly amplified near the center of the pulse but when the pulse is between 1 and 5 ms in length the data is attenuated to a very high degree. This suggests that impact events occurring between 7.5 and 10 ms will be slightly amplified in the resulting filtered acceleration but it appears that this amplification is minimal and pulse durations of this size will be accurately captured with the CFC 60 system. Even though data up until 7.5 ms is accurately represented, events occurring in less than 5 ms are being attenuated far too much and accelerations are not being represented in the correct way.

### 11.6 Sawtooth Wave Pulse

As mentioned previously a square wave is not the most realistic representation of an impact event because it takes a finite amount of time for the load to go from zero to some value. In an attempt to model an impact event more realistically sawtooth waves were inserted into the same CFC 60 filtration system that was used to test the square waves. Even though this model is more realistic than the square wave data it still has some problems. This is mainly due to the fact that the signal will not decrease instantaneously to zero, which is exactly how these waves are modeled. The output

graphs show the maximum output of the filtered data divided by the maximum input from the sawtooth wave signal at both the beginning and ending of the pulse and it also shows the slope of the signal as it increases from 0 to a maximum as well as the slope from the maximum value as it decreases back to zero, with the assumption that these slopes act linearly over the periods.

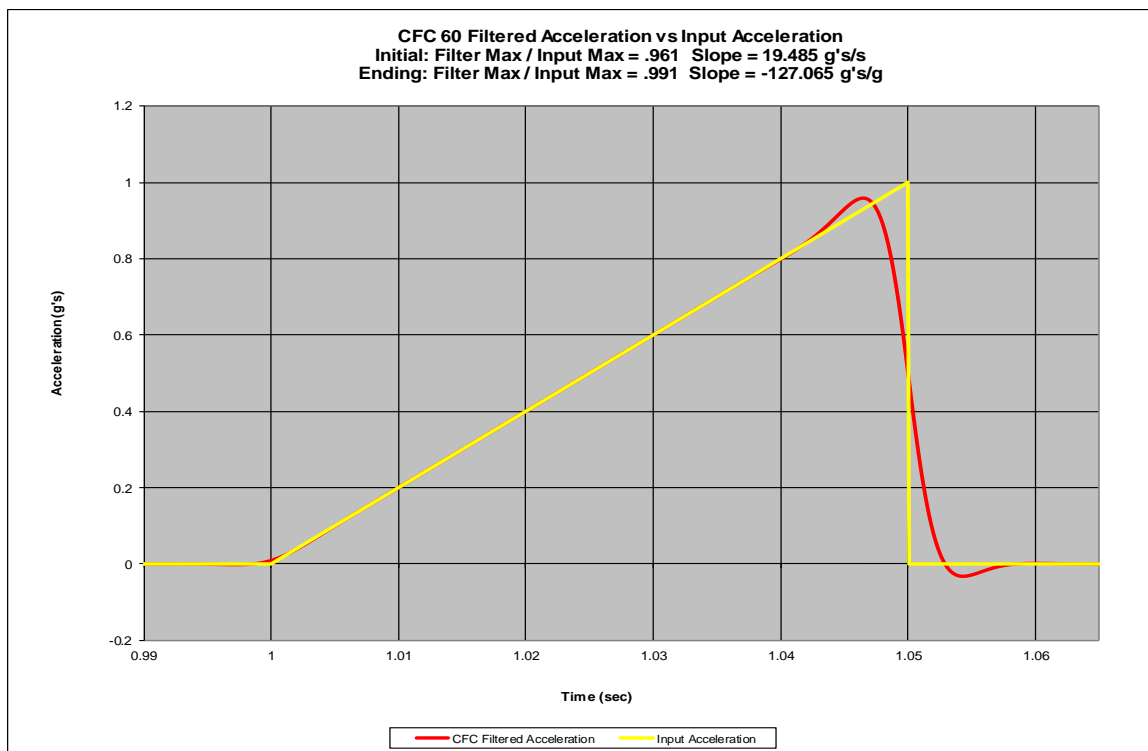


Figure I-9. 50 ms. Sawtooth Wave Pulse

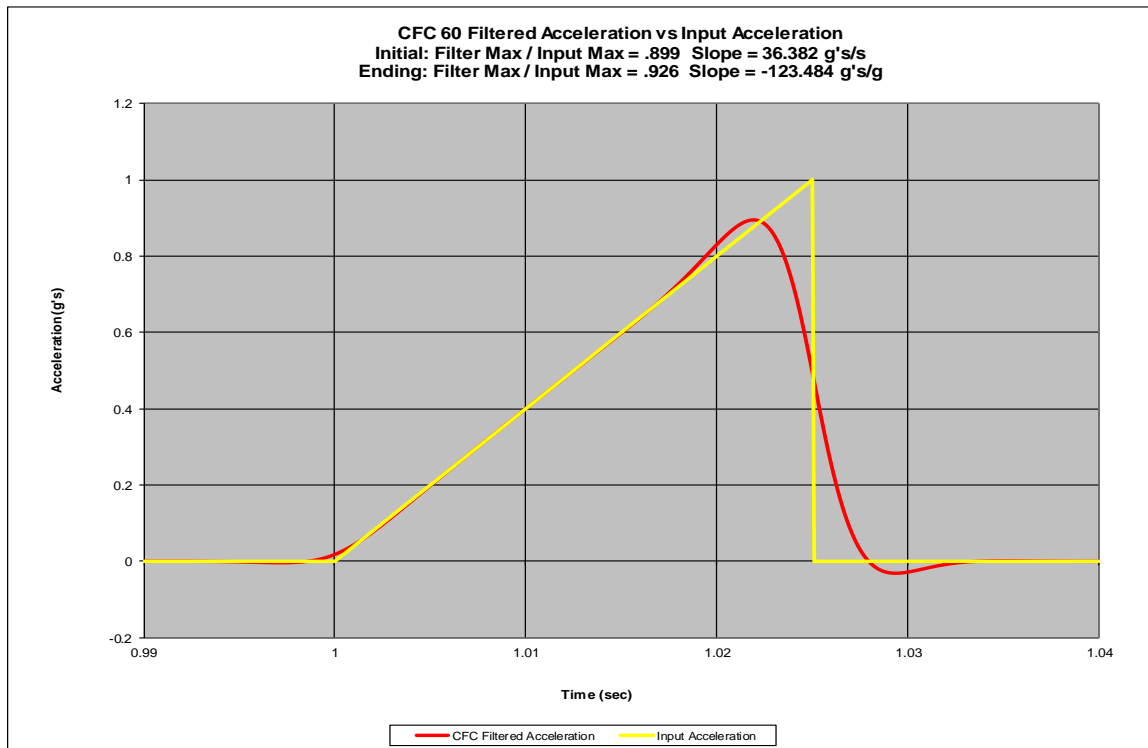


Figure I-10. 25 ms. Sawtooth Wave Pulse

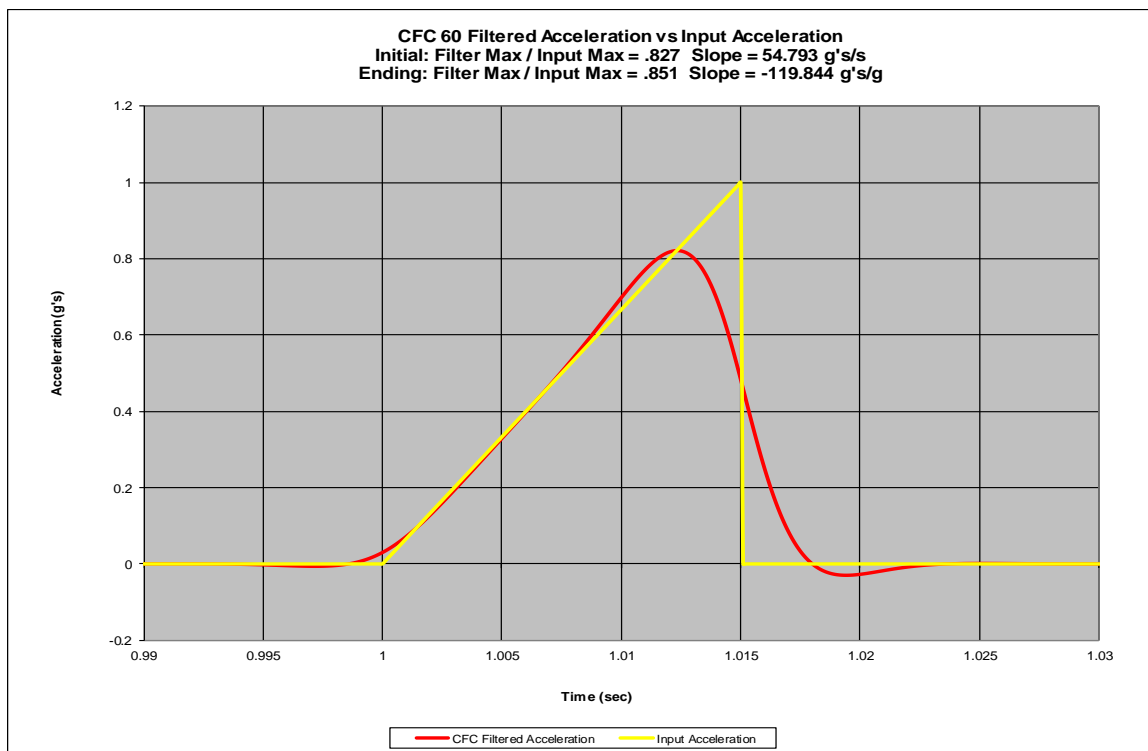


Figure I-11. 15 ms. Sawtooth Wave Pulse

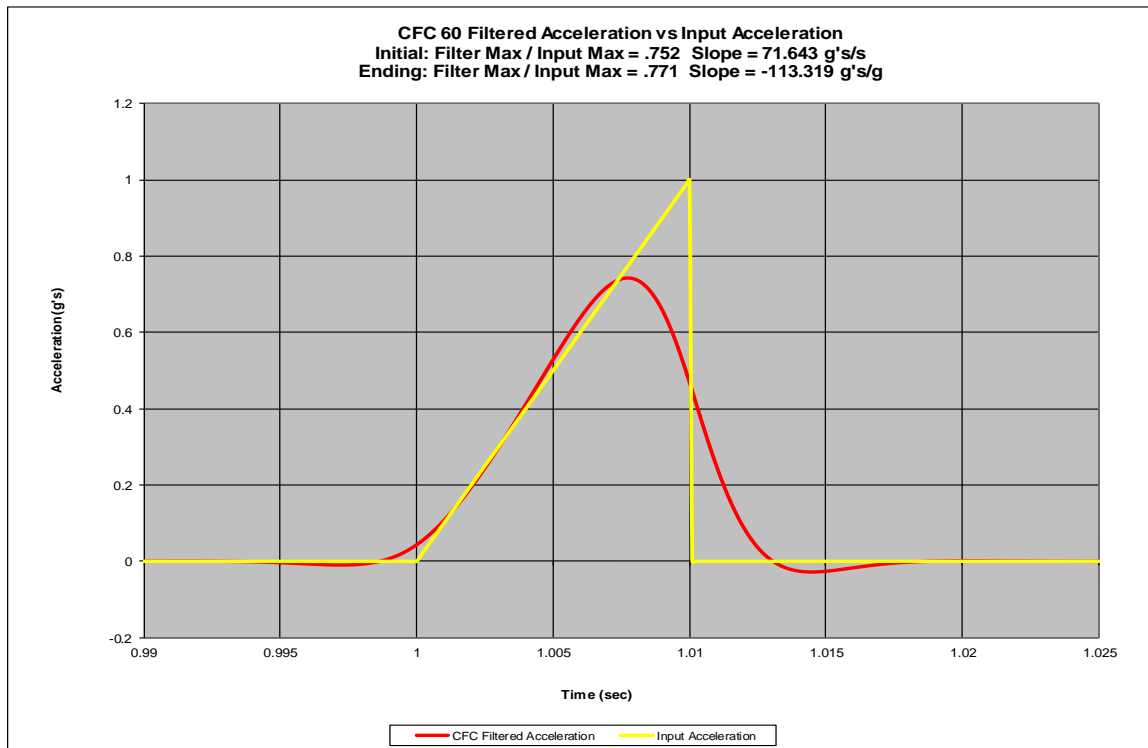


Figure I-12. 10 ms. Sawtooth Wave Pulse

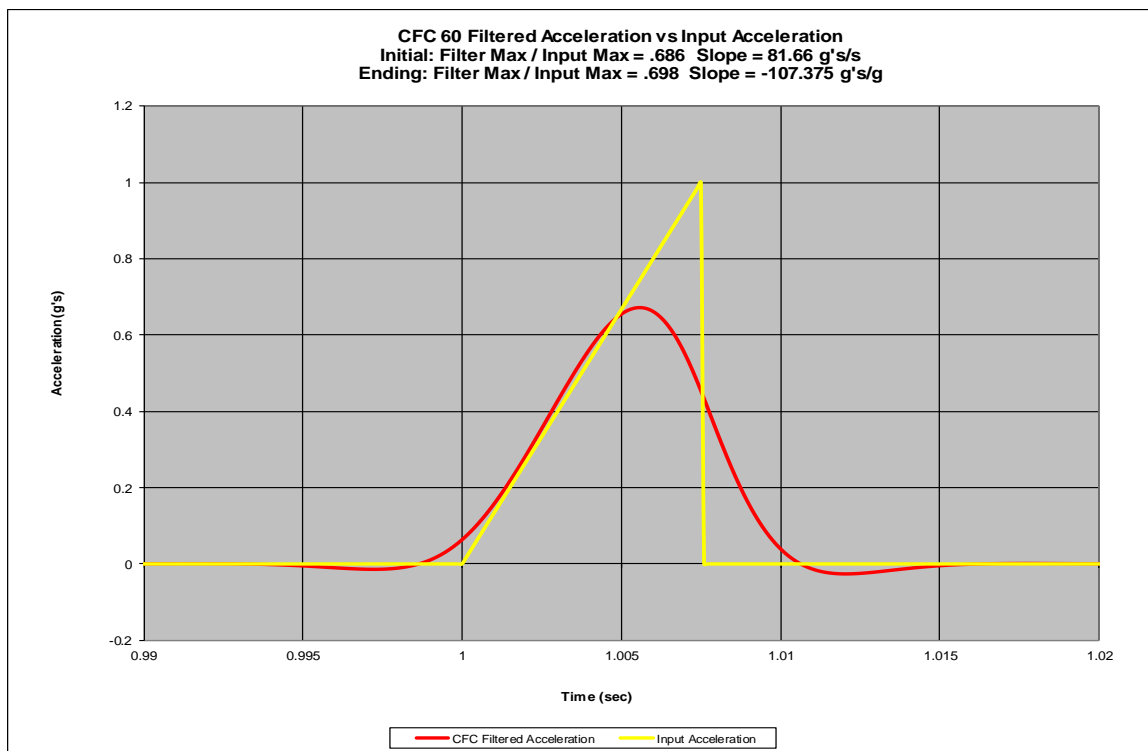


Figure I-13. 7.5 ms. Sawtooth Wave Pulse

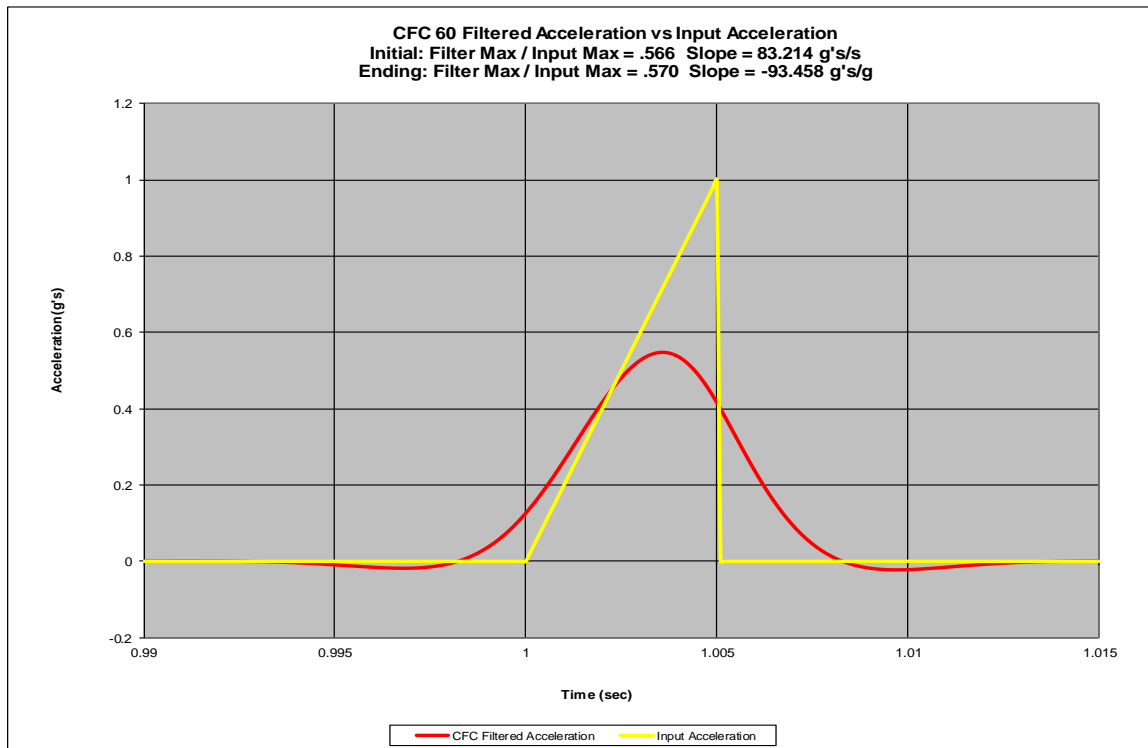


Figure I-14. 5 ms. Sawtooth Wave Pulse

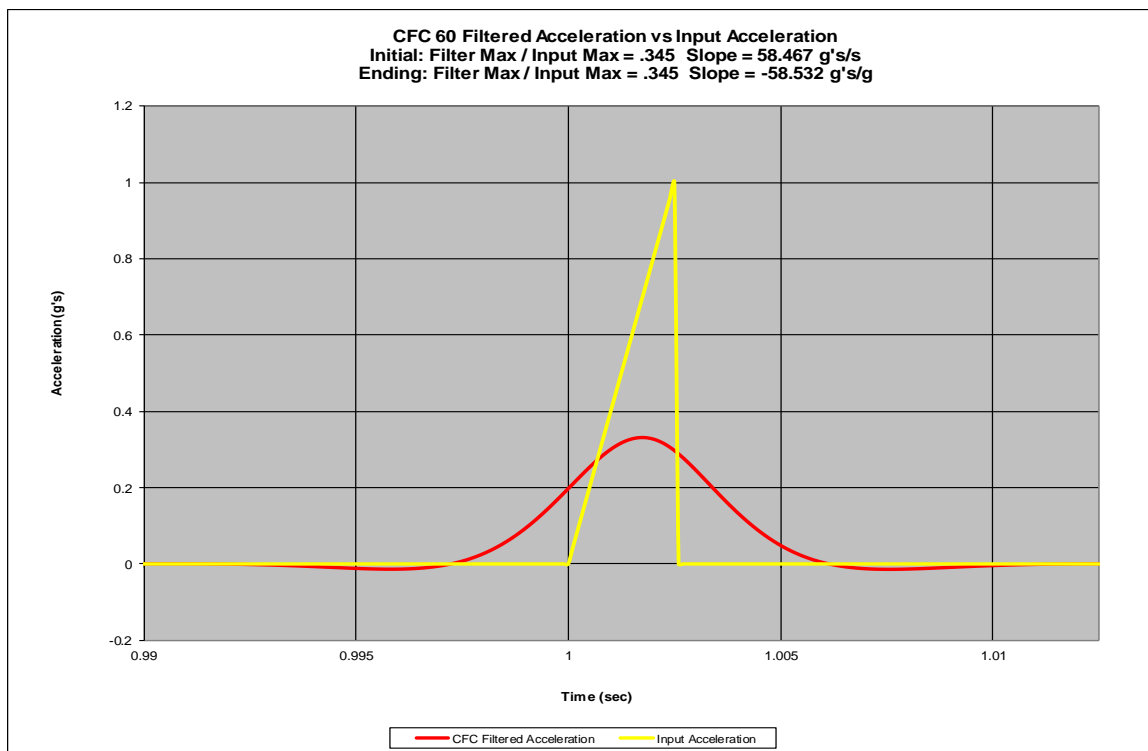


Figure I-15. 2.5 ms. Sawtooth Wave Pulse

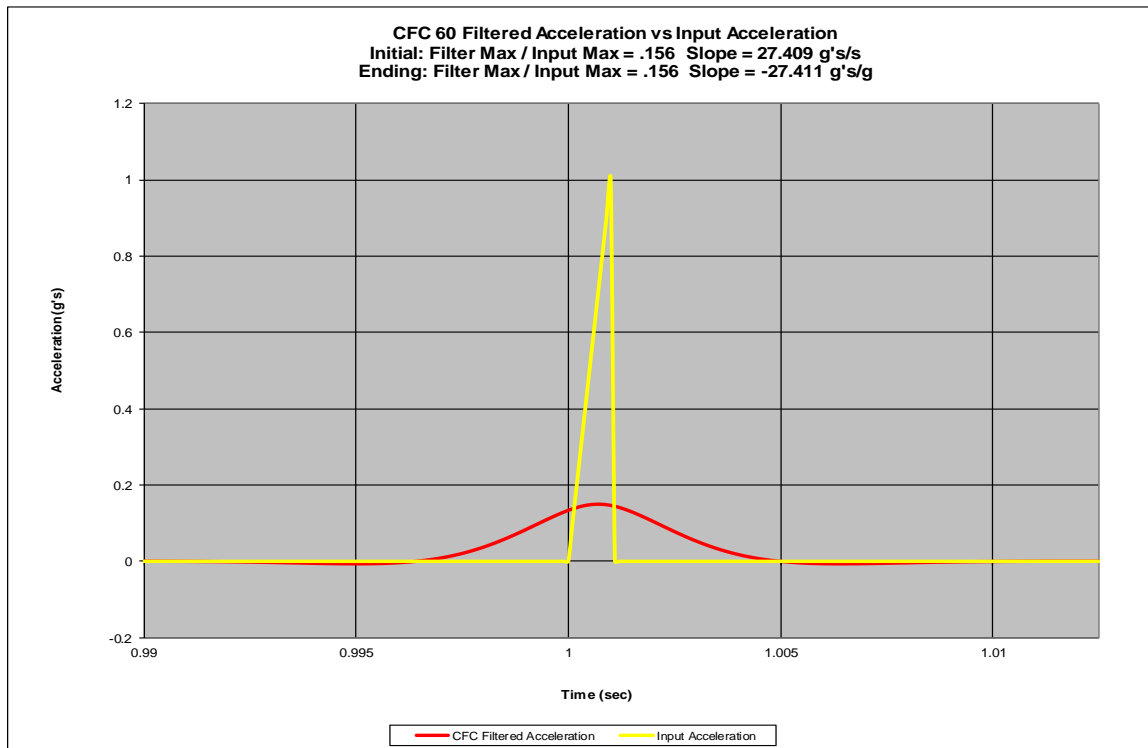


Figure I-16. 1 ms. Sawtooth Wave Pulse



Table I-1. Filter Max / Input Max and Filter Slope for Sawtooth Waves

Pulse Length (ms)	Initial Filter Max / Input Max	Initial Slope (g's/s)	Ending Filter Max / Input Max	Initial Slope (g's/s)
50	0.961	19.485	0.991	-127.065
25	0.899	36.382	0.926	-123.484
15	0.827	54.793	0.851	-119.844
10	0.752	71.643	0.771	-113.319
7.5	0.686	81.66	0.698	-107.375
5	0.566	83.214	0.570	-93.458
2.5	0.345	58.467	0.345	-58.532
1	0.156	27.409	0.156	-27.411

### 11.6.1 Sawtooth Wave Discussion

The resulting graphical outputs shown above suggest that when impacts are modeled as sawtooth waves and subjected to a CFC 60 filter the resulting output data is captured fairly well between 50 and 15 ms, but values less than 15 ms seem to experience attenuation levels that are quite severe and non-negligible. For example, when using a 5 ms pulse the acceleration profile is attenuated by around 40% when compared to the nonfiltered data. This sort of attenuation is too large and could easily result in the wrong decision being made when very fast impact events occur. This suggests that if impact events can be modeled as sawtooth waves the resulting acceleration and force plots for longer duration events are correctly represented but events that occur over very small durations of time are over attenuated.

### 11.7 Triangle Wave Pulses

Square and sawtooth waves are very simple ways of modeling an impact event but both of these waves experience a change in amplitude instantaneously which is obviously an unrealistic modeling technique. In an attempt to more correctly model an impact event triangle waves were inserted into the same CFC 60 filter that was used to test the square and triangle waves. Since these triangle waves contain both an initial and ending slope that occurs over a finite amount of time they should function as the best

model when compared against the square and sawtooth waves. The output graphs show the maximum output of the filtered data divided by the maximum input from the square wave signal and it also shows the slope of the signal as it increases from 0 to a maximum with the assumption that the slope acts linearly over this period.

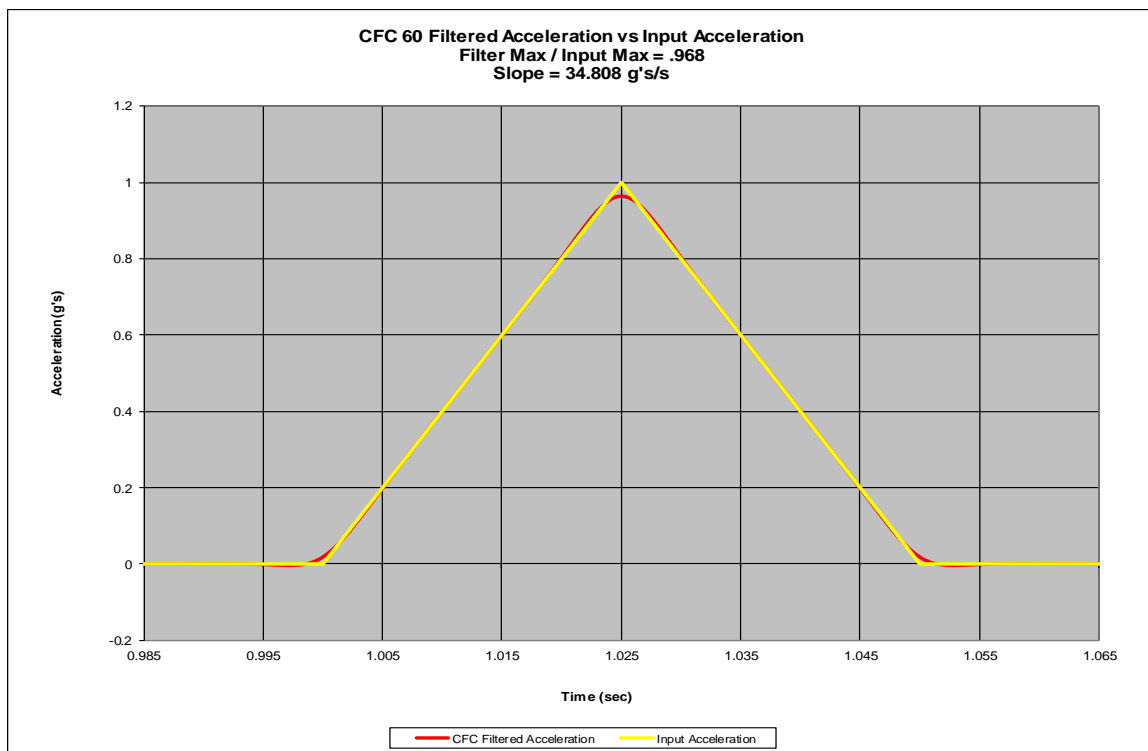


Figure I-17. 50 ms. Triangle Wave Pulse

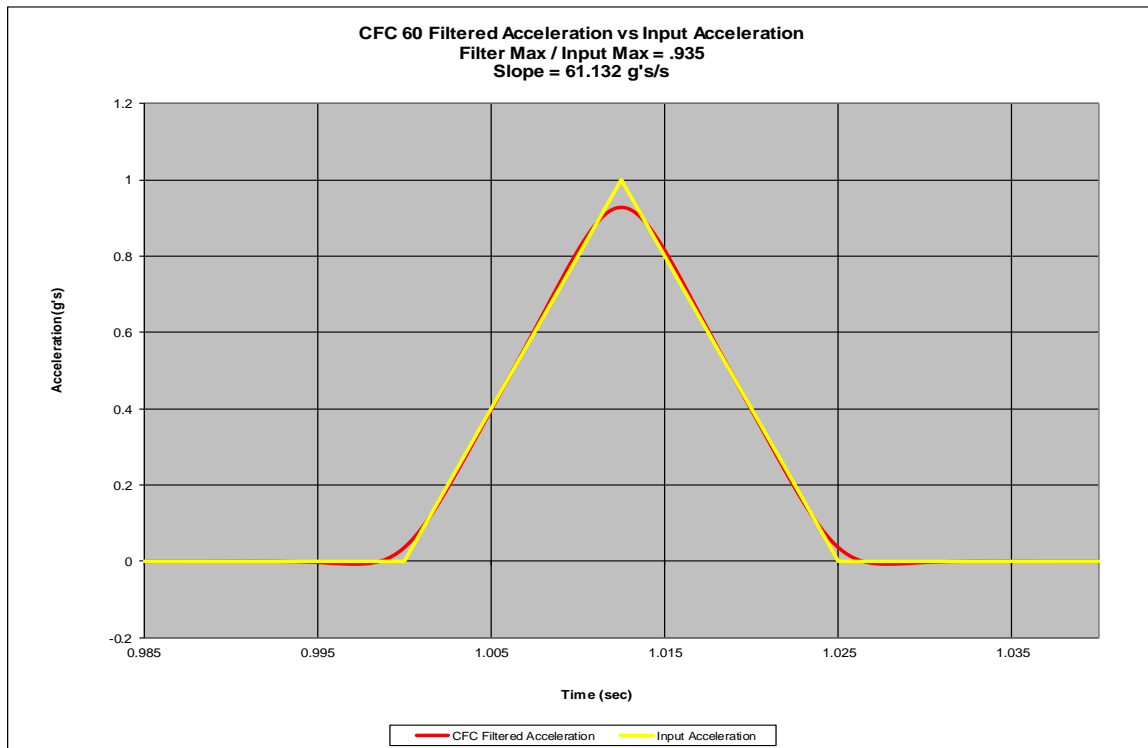


Figure I-18. 25 Triangle Wave Pulse

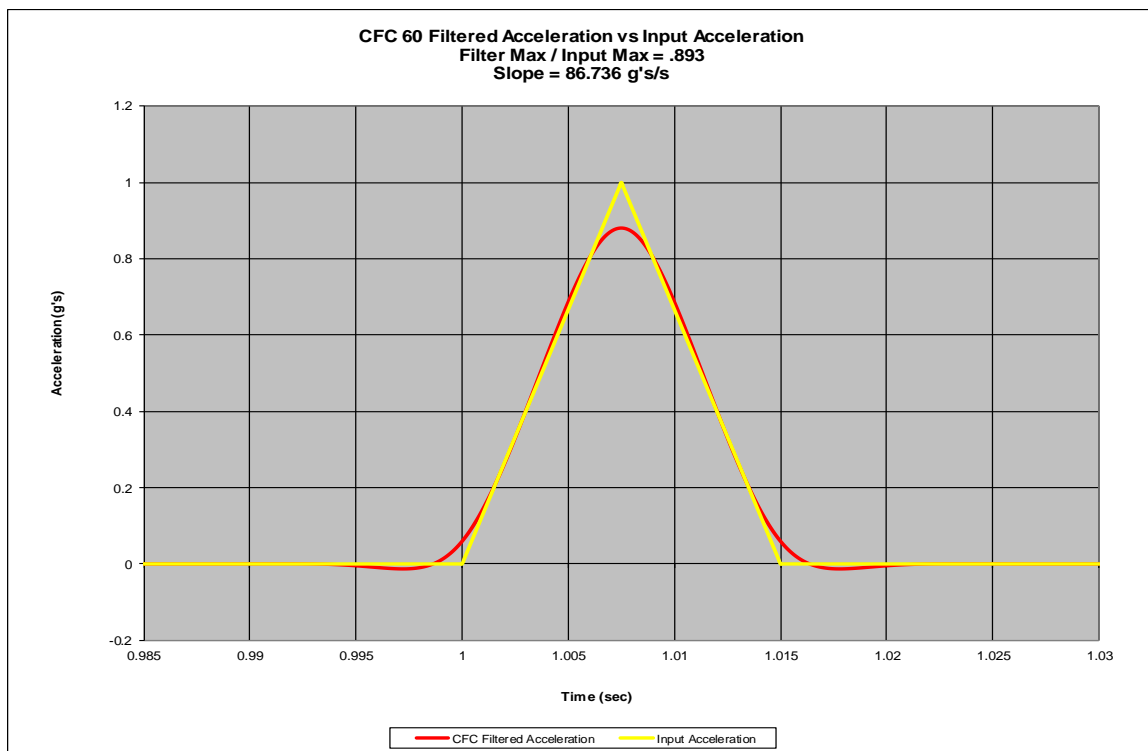


Figure I-19. 15 ms. Triangle Wave Pulse

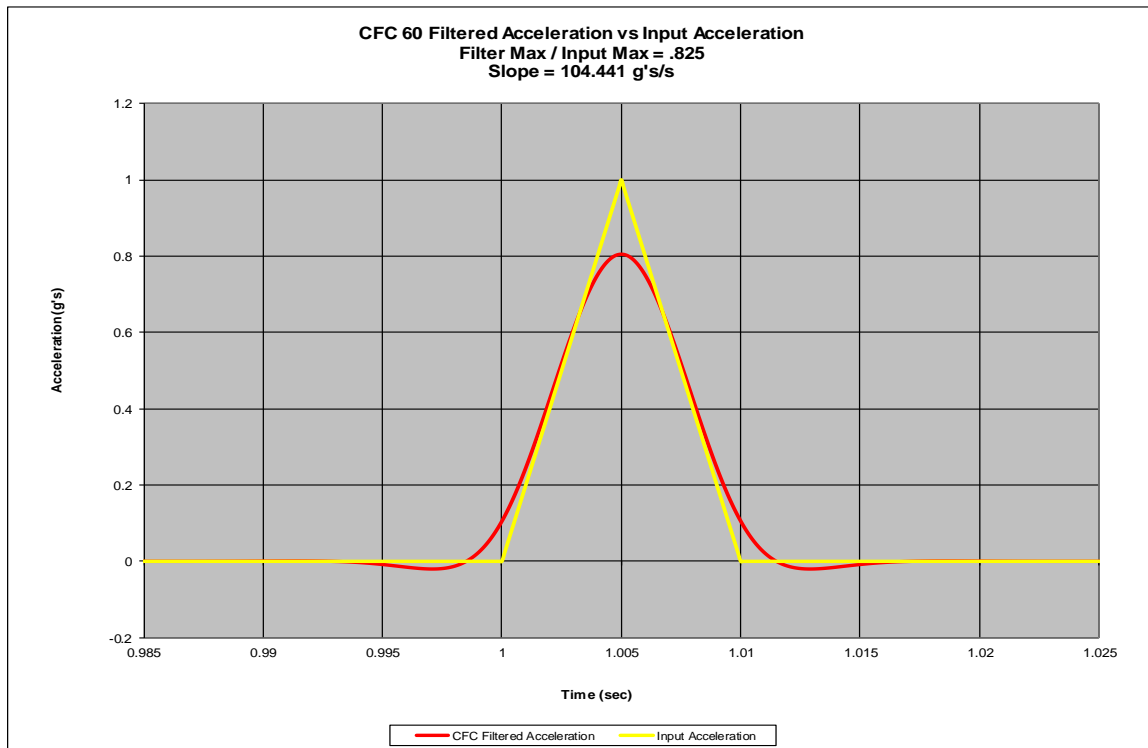


Figure I-20. 10 ms. Triangle Wave Pulse

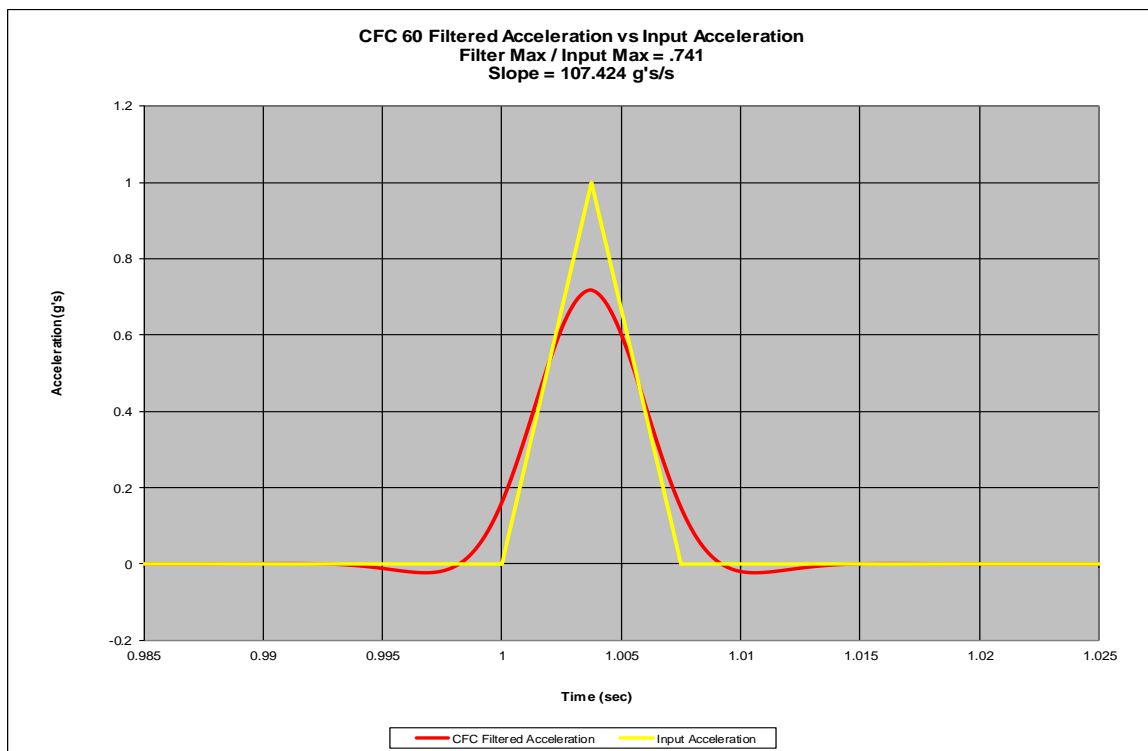


Figure I-21. 7.5 ms. Triangle Wave Pulse

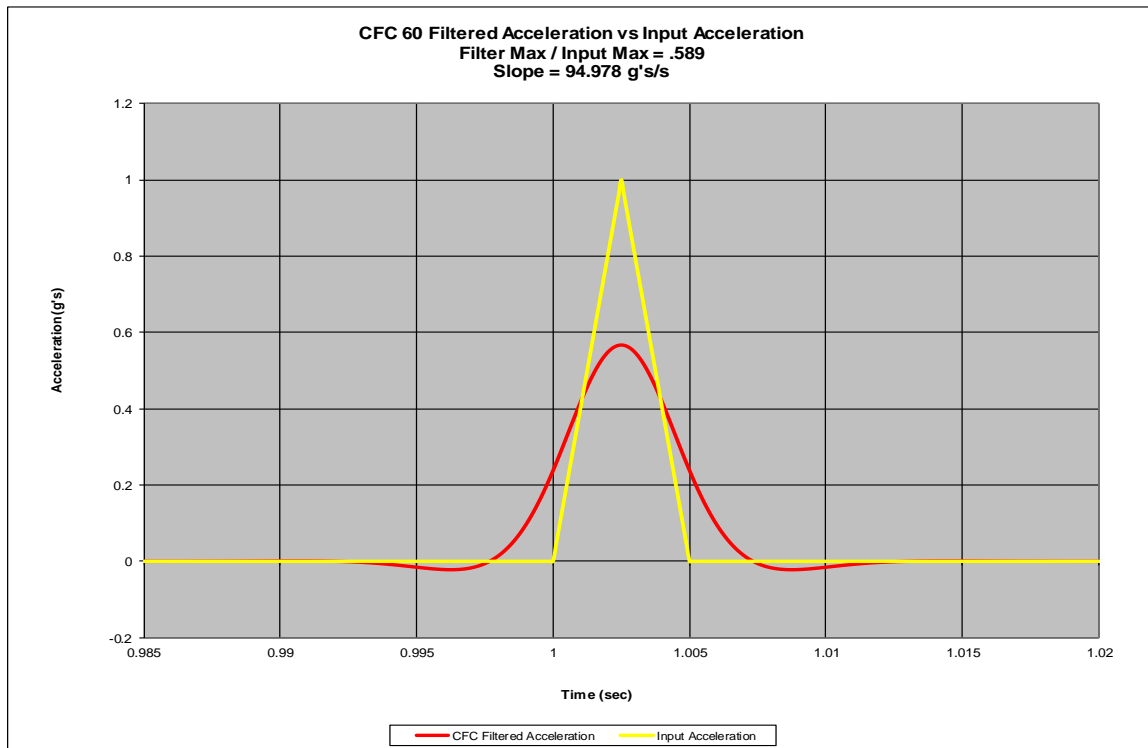


Figure I-22. 5 ms. Triangle Wave Pulse

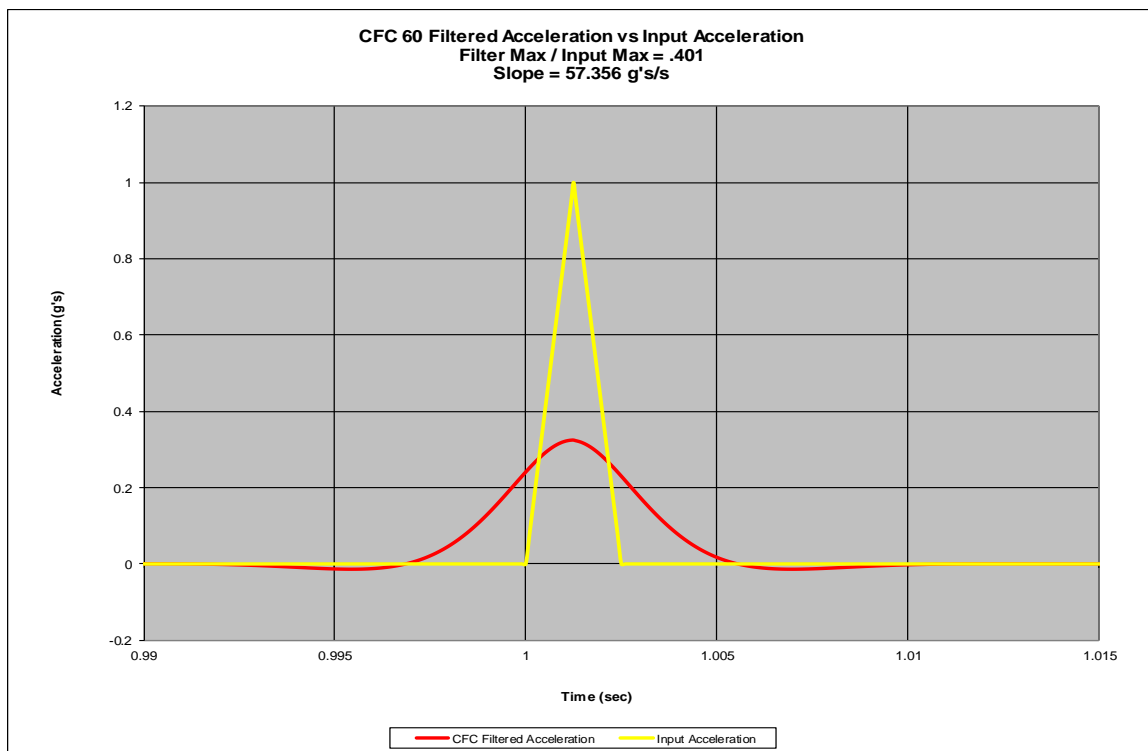


Figure I-23. 2.5 ms. Triangle Wave Pulse

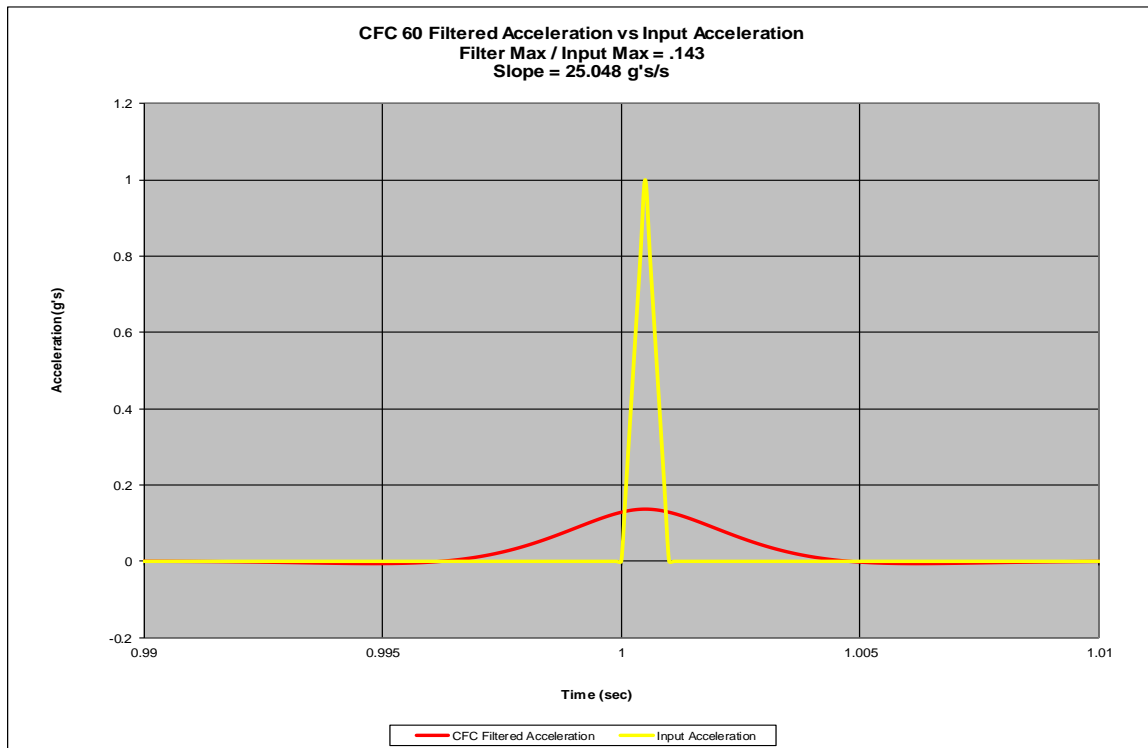


Figure I-24. 1 ms Triangle Wave Pulse

Table I-2. Filter Max / Input Max and Filter Slope for Triangle Waves

Pulse Length (ms)	Filter Max / Input Max	Slope (g's/s)
50	0.968	34.808
25	0.935	61.132
15	0.893	86.736
10	0.825	104.441
7.5	0.741	107.424
5	0.589	94.978
2.5	0.401	57.356
1	0.143	25.048

### 11.8 Triangle Wave Discussion

The resulting graphical outputs shown above suggest that when impacts are modeled as triangle waves and subjected to a CFC 60 filter they are, for the most part, represented well and do not experience very much attenuation or amplification until pulse lengths are less than 10 ms. Between 50 and 10 ms the amount of attenuation increases from about 4 to 18 percent and after 10 ms it quickly decreases down to unacceptable levels. This suggests that if an impact can be correctly modeled as a triangle wave adverse attenuation will most likely not occur until the pulse length is below 10 ms.